DOCTOR OF PHILOSOPHY

Investigating nutrient excess and endothelial dysfunction a role for BACE1 and amyloid?

Coull, Bethany Mae

Award date:
2020

Investigating nutrient excess and endothelial dysfunction: a role for BACE1 and amyloid?

Bethany Mae Coull

Thesis submitted for the degree of Doctor of Philosophy

University of Dundee

October 2020

Table of contents

List of figures

Chapter 1

Chapter 2

Chapter 3

Chapter 4

Chapter 5

Appendix

List of tables

Chapter 2

Chapter 4

Acknowledgements

First and foremost, I would like to thank my supervisor, Professor Mike Ashford, without whom this project would not have been possible. You have given me so many opportunities and have taught me so much.

Thank you to the Alzheimer's Society for funding this PhD project and to everyone at the Scotland DTC for their guidance and support, especially Josh, Heather, and Vanya. Thanks also to Dr. Dawn Thompson and Professor Mirela Delibegovic, and to Kat and Scott for supporting me ever since I was just a baby Honours student.

To all of the staff at the MSRU, thank you for providing excellent care for my mice. Thank you especially to Christie for her help with surgery, Joanne for taking extra special care of the experimental room, Lynsey for her help with ear notching, Kally for her endless generosity, and Ngaire for providing words of wisdom.

Thank you to Dr. Paul Meakin for teaching me all of the surgical techniques, to Dr. Andy Cassidy for his help with genomic analysis, to Oualid for his help with Seahorse, and to Professor Karen Horsburgh and Alessio for providing advice on vessel enrichment protocols. Special thanks to Dr. Alison McNeilly for endless advice about statistics and *in vivo* work. Thanks must also go to my summer student Adam Hetherington for his help with tissue processing and Western blotting.

I would like to extend my gratitude to every single person who has been a part of my time in MCM/Systems Medicine/what is it even called now? Thanks to Jen G, Lidy, Celine, Chandi, Annie, Jess, Holly, Suz, Fiona A, Fiona P, Lisa T, Richard, Holly-Ann, Jodi, Jamie T, Jamie O, and Omar. You have all made our department a very special place to work. Thanks must also go to Dr. Colin Henderson and Susan Simpson for giving me such wonderful public outreach and networking opportunities. Thanks also to my TMC, Dr. Colin Murdoch, Professor Faisel Khan, and Professor Roland Wolf for their moral support and uplifting words.

Thanks to Aimée, Nicola, Catriona, Mirren, Claire, and Calum for endless support and so many good times. Special thanks to my fellow student, flatmate, gym bro, and friend Conor for the many hours spent listening to me complain. I would also like to thank my fellow Ashford, Dr. Fiona McLean who performed all of the db/db genotyping and open-field tests. Thanks for your advice and support Fiona, you really kept me from going full on crazy towards the end.. even if you did unfortunately lose your own sanity when you found out that thing about kit-kats.

To the Ashfords been-and-gone, David and Daniella, thank you for being so welcoming from the beginning. Thank you for all your advice both in and out of the lab, for the laughs, the nights out, and the reunions.

Thank you to my best gals Heather and Meghan. You both have been such amazing friends to me, and I could not be more grateful. Every time I see an elf I will think of you two. You made the last few months of my PhD so special, but that's probably just because our birth charts are compatible.

I would like to say a very special thank you to Dr. Jennie Gabriel. Without you, I'm really not sure I would've made it to the end. Thank you for teaching me all things cell culture and gracing me with Señor Neuron, who kept me going on my darkest days. You started off as my labmate for life, but now you're a best friend for life.

Thank you to my wonderful friends Noor and Laura, to Robbie and Carrie, to my brother Johnny, and my sister Joanna, and the rest of the family for all of their support. A very special thanks to my best friend and partner Lee; without your positivity and encouragement this would not have been possible.

Finally, I would like to express my eternal gratitude to my amazing parents, John and Marjie. I would never have gotten to where I am today without your love and support. I do not know how I will ever repay you, but I hope I have made you proud.

Declarations

Student declaration

I hereby declare that all results described in this thesis, unless otherwise stated, are entirely my own work. I further state that the composition of the thesis was performed by myself and none of the material has been submitted for any other degree. Lastly, I verify that all of the sources have been appropriately cited. The work was carried out in the school of Medicine, University of Dundee, under the supervision of Professor M. L J. Ashford.

Bethany M. Coull

Supervisor declaration

I certify that Bethany M. Coull has completed 7 semesters of experimental research and has fulfilled the conditions of the Ordinance 39, University of Dundee, such that she is eligible to submit the following thesis in application for the degree of Doctor of Philosophy.

Professor Michael L. J. Ashford

Abbreviations

2-DG	2-deoxyglucose
2-PGA	2-phosphoglycerate
3-PGA	3-phosphoglycerate
Aβ	Amyloid beta
AA	Amino acid
ACAD	Acyl-Coa dehydrogenase
ACAT	Acyl-CoA:cholesterol acyltransferase
Acetyl-CoA	Acetyl coenzyme A
ACh	Acetylcholine
ACSL	Long-chain acyl-CoA synthetase
AD	Alzheimer's disease
ADP	Adenosine diphosphate
AGE	Advanced glycated endproducts
AgRP	Agouti related peptide
AH	Aconitase
ALDA	Aldolase
AMPK	Adenosine monophosphate activated kinase
ANS	Autonomic nervous system
ANT	Adenine nucleotide translocase
APP	Amyloid precursor protein
AR	Adrenoreceptor
ARC	Arcuate nucleus
ATP	Adenosine triphosphate
BACE1	Beta-site APP cleaving enzyme 1
BAE	Bovine aortic endothelial cells
BAT	Brown adipose tissue
BBB	Blood-brain barrier

BH_4	Tetrahydrobiopterin
BM	Basement membrane
BMI	Body mass index
BP	Blood pressure
BPG	1,3-bisphosphoglycerate
BSA	Bovine serum albumin
Ca^{2+}	Calcium
CAA	Cerebral amyloid angiopathy
CACT	Carnitine acylcarnitine translocase
cAMP	Cyclic adenosine monophosphate
CBF	Cerebral blood flow
cGMP	Cyclic guanosine monophosphate
COX	Cytochrome c oxidase
CPT1/2	Carnitine palmitoyl transferase 1/2
CRP	C-reactive peptide
CS	Citrate synthase
CVD	Cardiovascular disease
Cyt c	Cytochrome c
DAG	Diacylglycerol
DHA	Docosahexaenoic acid
DHAP	Dihydroxyacetone phosphate
DIOR	Diet-induced obesity resistance
DMEM	Dulbecco's modified essential media
DMH	Dorsomedial hypothalamus
Drp1	Dynamin-related protein 1
EA	Endothelial activation
EC	Endothelial cell
ECAR	Extracellular acidification rate
ECH	Enoyl-CoA hydratase
ED	Endothelial dysfunction
EM	Electron microscopy

ENO	Enoyl tranferase
eNOS	Endothelial nitric oxide synthase
EOAD	Early-onset Alzheimer's disease
ER	Endoplasmic reticulum
ERK	Extracellular signal-regulated kinase
ET-1	Endothelin-1
ETC	Electron transport chain
F6P	Fructose-6-phosphate
$FADH_2$	Flavin adenine dinucleotide
FAO	Fatty acid oxidation
FATP	FA transport proteins
FBP	Fructose 1,6-bisphosphate
FCCP	Carbonyl cyanide-4 (trifluoromethoxy) phenylhydrazone
FFA	Free fatty acid
FOXO	Forkhead box
FSS	Fluid shear stress
G6P	Glucose-6-phosphate
GAP	Glyceraldehyde 3-phosphate
GAPDH	Glyceraldehyde 3-phosphate dehydrogenase
GDP	Guanosine diphosphate
GFP	Green fluorescent protein
GHSR	Growth hormone secretagogue receptor
GL	Glycaemic load
Grb2	Growth factor receptor-bound protein 2
GSIS	Glucose stimulated insulin secretion
GSK	Glycogen synthase kinase
GTP	Guanosine triophosphate
GTT	Glucose tolerance test
H_2O_2	Hydrogen peroxide
HADH	3-hydroxyacyl-CoA dehydrogenase
HDL	High density lipoprotein

HeNe	Helium Neon
HFD	High fat diet
HG	High glucose
HK	Hexokinase
HMEC	Human microvascular endothelial cells
HSL	Hormone sensitive lipase
HSD	High saturated fat diet
HUVEC	Human umbilical vein endothelial cells
ICAM	Inducible cell adhesion molecule
icv	Intracerebroventricular
IDE	Insulin degrading enzyme
IDH	Isocitrate dehydrogenase
IKK	Inhibitor of nuclear factor kappa B kinase
IL-1β	Interleukin-1β
IL-6	Interleukin-6
IL1R2	Interleukin-1 receptor 2
IMM	Inner mitochondrial membrane
IMS	Intermembrane space
iNOS	Inducible nitric oxide synthase
IR	Insulin receptor
IRS1/2	Insulin receptor substrate 1/2
IRsol	Soluble insulin receptor
ITT	Insulin tolerance test
JNK	c-Jun N-terminal kinase
KLF2	Krüppel-like factor 2
L-arg	L-arginine
L-cit	L-citrulline
L-glut	L-glutamine
L-NAME	L-NG-arginine methylester
LDF	Laser Doppler flowmetry
LDH	Lactate dehydrogenase

LDI	Laser Doppler imaging
LDL	Low density lipoprotein
Lep-R/Ob-R	Leptin receptor
LG	Low glucose
LH	Lateral hypothalamus
LOAD	Late-onset Alzheimer's disease
LPS	Lipopolysaccharide
LRP	Lipoprotein receptor-related protein
MAPK	Mitogen activated protein kinase
MC4R	Melanocortin 4 receptor
MCP-1	Monocyte chemoattractant protein-1
MDH	Mitochondrial pyruvate carrier
MEF	Mouse embryonic fibroblast
Mff	Mitochondrial fission factor
Mfn1/2	Mitofusin 1/2
MIP	Macrophage inflammatory protein
MitoQ	Mitoquinone mesylate
MMP	Mitochondrial membrane potential
MnSOD	Manganese superoxide dismutase
MPC	Mitochondrial pyruvate carrier
mPTP	Mitochondrial permeability transition pore
mRNA	Messenger ribonucleic acid
mROS	Mitochondrial reactive oxygen species
MSRU	Medical school resource unit
mtDNA	Mitochondrial deoxyribonucleic acid
mTOR	Mammalian target of rapamycin
NADH	Nicotinamide adenine dinucleotide
NADPH	Nicotinamide adenine dinucleotide phosphate
$Na_v\beta_{1-4}$	Voltage-gated sodium channelβ_{1-4}
NC	Normal chow
NF-κB	Nuclear factor-kappa B

NFT	Neurofibrillary tangles
NHF	Normal human fibroblasts
NMDA	N-methyl-D-aspartate
NO	Nitric oxide
NO_2^-	Nitrite
NOX	NADPH oxidase
NPY	Neuropeptide Y
Nrf2	Nuclear factor erythroid 2-related factor 2
NVU	VE fraction unit
O_2^-	Superoxide
OCR	Oxygen consumption rate
OGDC	Alpha-ketoglutarate dehydrogenase
OMM	Outer mitochondrial membrane
$ONOO^-$	Peryoxynitrite
OPA1	Optic atrophy 1
OxLDL	Oxidise LDL
OXPHOS	Oxidative phosphorylation
PAGE	Polyacrylamide gel electrophoresis
PARP	Poly-ADP ribose polymerase
PBS	Phosphate buffered saline
PDBu	Phorbol dibutyrate
PDH	Pyruvate dehydrogenase
PDK1	Pyruvate dehydrogenase kinase 1
PE	Phenylephrine
PEP	Phosphoenolpyruvate
PFK	Phosphofructokinase
PGC1α	Peroxisome proliferator-activated receptor gamma activator 1 alpha
PGK	Phosphoglycerokinase
PGlyM	Phosphoglyceromutase
PGM	Phosphoglucomutase
P_i	Inorganic phosphate

PI3K	Phosphatidylinositol 3-kinase
PIP_2	Phosphatidylinositol 4,5-biphosphate
PIP_3	Phosphatidylinositol 4,5-triphosphate
PK	Pyruvate kinase
PKB	Protein kinase B
PKC	Protein kinase C
PKG	Protein kinase G
POMC	Proopiomelanocortin
PPAR-γ	Peroxisome proliferator-activated receptor gamma
PSGL-1	P-selectin glycoprotein ligand 1
PTM	Post translational modification
PTP1B	Protein tyrosine phosphatase 1B
PVN	Paraventricular nucleus
PyT	Pyruvate transporter
RAGE	Receptor for advanced glycated endproducts
RBC	Red blood cell
RET	Reverse electron transport
ROS	Reactive oxygen species
SAH	Subarachnoid haemorrhage
sAPPα	Soluble APP alpha
sAPPβ	Soluble APP beta
ScrP	Scrambled peptide
SDH	Succinate dehydrogenase
SDS	Sodium dodecyl sulfate
sGC	Soluble guanylate cyclase
Shc	Src homology and collagen
SNP	Sodium nitroprusside
SOD	Superoxide dismutase
SOS	Sons of Sevenless
STZ	streptozotocin
T1D	Type 1 diabetes/diabetics

T2D	Type 2 diabetes/diabetics
TBST	Tris buffered saline-tween
TCA	Tricarboxylic acid cycle
TEER	Transepithelial resistance
TG	Triglyceride
TJ	Tight junction
TLR2	Toll-like receptor 2
TNFα	Tumour necrosis factor alpha
TPI	Triose-phosphate isomerase
UCP	Uncoupling protein
UDP-GlcNAc	Uridine 5-diphosphate N-acetylglucosamine
UQ	Ubiquinone
VCAM	Vascular cell adhesion molecule
VD	Vascular dementia
VE	Vessel enriched
VLDL	Very low-density lipoprotein
VMH	Ventromedial hypothalamus
VSMC	Vascular smooth muscle cell
WSS	Wall shear stress
WT	Wild-type
α-MSH	Alpha-melanocyte stimulating hormone

Summary

Background: Endothelial dysfunction (ED) often occurs secondary to metabolic pathologies associated with nutrient excess, such as hyperglycaemia and dyslipidaemia. ED, characterised by reduced nitric oxide (NO) bioavailability and activity, and inflammation, is associated with cardiovascular diseases, stroke, and neurodegeneration.

Nutrient excess increases amyloid beta peptides (Aβ), which are produced in varying lengths by beta-site APP cleaving enzyme 1 (BACE1). Increased circulating $A\beta_{42}$ levels is reported to promote ED, by reducing NO bioavailability, suggesting a role for Aβ in the pathogenesis of ED, but the underlying mechanism is unclear.

One potential mechanism involves mitochondrial dysfunction, whereby mitochondria exhibit impaired bioenergetics, increased reactive oxygen species (ROS) production, and dysregulated mitochondrial dynamics. Functional mitochondria are key to endothelial cell health and impairments may lead to reduced ATP production and increased ROS generation, resulting in a decrease in NO bioavailability and activity. Furthermore, nutrient excess and Aβ peptides are reported to induce mitochondrial dysfunction.

Therefore, the work described herein sought to determine whether the early pathogenesis of ED, promoted by nutrient excess, is in part due to raised BACE1 activity and circulating Aβ levels. Further, it aimed to investigate the potential mechanistic role of mitochondrial dysfunction in this process.

Methods: Microvascular endothelial function was measured *in vivo* using laser Doppler imaging in several mouse models of nutrient excess and varying circulating Aβ levels. A 6-month old 10-week high-fat diet (HFD)-fed mouse (45% HFD) and an 8-week old db/db mouse were used as models of nutrient excess. A 10-12-week old, 10-week HFD-fed BACE1 knockout (BACE1KO) mouse was used to investigate the role of BACE1 and Aβ in the pathogenesis of ED. Two 10-12 week old, 10-week HFD-fed cohorts of mice, infused either centrally or peripherally with $A\beta_{42}$ peptides (3.36mg/kg/day) for 4 weeks were investigated as models of raised circulating Aβ levels. Finally, the APP23 mouse, a genetically engineered model of increased Aβ, was infused peripherally with a BACE1 inhibitor (10mg/kg/day) for 4 weeks to investigate the effects of reducing Aβ peptides on endothelial function.

Following *in vivo* investigation, proteins involved in mitochondrial dynamics were analysed using Western blot in tissues of interest (vessel enriched brain fraction, aorta) as a measure of mitochondrial function.

Results: Impaired endothelial function was observed *in vivo* in db/db mice, but not in the HFD-fed model. BACE1KO mice had improved endothelial function compared to wild-type and heterozygous littermates. Both cohorts infused with Aβ, as well as the APP23 mouse, exhibited reduced endothelial function, whilst treating the APP23 mouse with a BACE1 inhibitor and thereby reducing Aβ levels rescued the endothelial dysfunction phenotype. No significant findings were observed in relation to mitochondrial dynamics proteins in any of the models studied.

Conclusion: The data presented herein suggest a role for increased BACE1 activity and circulating Aβ, due to nutrient excess, in the early pathogenesis of ED. However, it is unlikely that this process involves altered mitochondrial dynamics processes. These studies highlight the possibility of repurposing BACE1 inhibitors for the treatment of ED and subsequent vascular diseases.

Chapter 1

Introduction

1.1 Nutrient excess and disease

The transition of global diet towards highly refined foods, carbohydrates with high glycaemic load (GL; how much a carbohydrate will increase plasma glucose levels), and foods rich in saturated fat, termed the 'nutrition transition' is becoming increasingly evident in the 21st century[1]. Nutrient excess and unhealthy diet composition can exert both immediate and/or long-term adverse implications on health[2]. The role of this 'Western diet' in the etiology of non-communicable diseases, that is diseases that cannot be transmitted, is well accepted. Indeed, excessive nutrient consumption, together with sedentary lifestyles and tobacco smoking, plays a major role in the development of obesity, diabetes, cardiovascular diseases, and neurodegenerative disorders[3,4] (Fig. 1.1).

1.2 Obesity

Obesity is described as having an excess of fat accumulation, which could potentially pose a risk to an individual's health. It occurs when an individual has a total energy intake that exceeds total energy output. It is clear therefore that dietary patterns are inextricably linked to the onset of obesity[5]. Obesity is associated with a number of pathologies, such as but not confined to inflammation[6], hypertension[7], dyslipidaemia, including hypercholesterolaemia[8], hyperglycaemia[9], insulin resistance[9], and poor cognitive function[10,11]. The standard method of measuring obesity is through body mass index (BMI), by which the person's weight (kg) is divided by the square of their height (metres). Those who have a BMI of between 25-30 kg/m^2 are overweight, whereas those with a BMI of over 30 kg/m^2 are considered obese. Some studies report variances in obesity prevalence across sex, socioeconomic class, ethnicity, and age[12,13]. However, it is clear that obesity is a growing epidemic worldwide. Particularly in developed regions, such as North America and Europe where the consumption of Western diet gained momentum in the 1970s, the prevalence of overweight and obese people has risen unmitigated over the last 50 years. Prevalence of obesity in the USA is reported as ~35% of all adults and ~30% of children between the ages of 2-19[14]. Scotland is not far behind, with ~29% of adults and ~13% of children being classed as obese[15]. As the prevalence of

obesity increases, so does the burden of its co-morbidities. Obesity poses a major risk to health and is an independent risk factor for many other diseases, including metabolic disorders (insulin resistance, type 2 diabetes [T2D]), liver disease, respiratory diseases, cardiovascular diseases (CVD), cancer, and as previously mentioned, neurodegenerative diseases[16,17]. Management of obesity focuses on weight loss, which is achieved by a negative energy balance – i.e. eating less and exercising more. Management options include, but are not limited to, diet therapy and physical activity, bariatric surgery and anti-obesity pharmacotherapy[18]. Despite these widely available treatment options, the prevalence of obesity still grows and places a massive strain on healthcare economy. Indeed, people with obesity struggle to adhere to diet/physical activity regimes and find it difficult to retain their weight loss, likely ending up heavier than they were before. This highlights the need for new treatment options.

1.3 Insulin resistance and type 2 diabetes

Type 2 diabetes mellitus (T2D) is characterised by deficiency in insulin action caused by pancreatic beta cell dysfunction and insulin resistance, resulting in hyperglycaemia. The aforementioned increase in obesity, due to physical inactivity and calorie-dense Western diets, has resulted in an unprecedented increase in the number of people presenting with T2D. Around 4.7 million people in the UK have diabetes, 90% of which have T2D[19]. T2D can commonly lead to amputation due to diabetic foot, CVD, stroke, kidney failure, and heart attack[19], and is associated with inflammation[20,21], dyslipidaemia[22], oxidative stress[23], and hypertension[24]. Front line therapies for T2D are lifestyle changes, insulin therapy, metformin, or sulphonylureas[25].

Insulin, a peptide hormone synthesised and secreted from pancreatic beta cells, is considered one of the main anabolic hormones and controls many aspects of metabolism and growth. Insulin action is heavily linked to diet, as its secretion from beta cells is triggered by an increase in plasma glucose (i.e. after eating). Insulin is then transported via the circulatory system to target insulin receptors (IR), present on many tissues. There are two major pathways in insulin signalling; the phosphoinositide 3-kinase (PI3K) pathway and Ras/extracellular signal-related kinase (ERK) pathway, a

schematic representation of which is shown in Figure 1.2[26]. Insulin plays many different roles depending on cell type. A very important role for insulin is regulating blood glucose homeostasis. For example, particularly in skeletal muscle, insulin is responsible for glucose uptake via GLUT4 translocation[27] as well as inhibiting hepatic glucose production by inducing the phosphorylation of forkhead box (FOXO) transcription factors[28]. Furthermore, insulin is known to act on the endothelium to cause vasodilation[29], in the hypothalamus anorexigenically[30], as well as the hippocampus to promote learning and memory[31]. Under certain conditions, peripheral insulin resistance can occur, and can be described as the continual release of insulin from pancreatic beta cells in response to increasing blood glucose levels, but a dampened cellular response upon insulin-IR binding in comparison to normal. The dampened cellular response results in continual high blood glucose levels (hyperglycaemia) coupled with increased pancreatic insulin release from pancreatic beta cells (hyperinsulinaemia) Eventually, pancreatic beta cells become exhausted, leading to a decline in insulin release, resulting in T2D. The mechanisms behind insulin resistance and type 2 diabetes are currently unknown, but it has been suggested that the impairment may be due to inflammation due to obesity[21], oxidative stress[23], mitochondrial dysfunction[32], a defective IR or a loss of affinity to insulin, or chronic dysregulation of normally adaptive feedback and feed-forward mechanisms that results in the attenuation of insulin signalling[33].

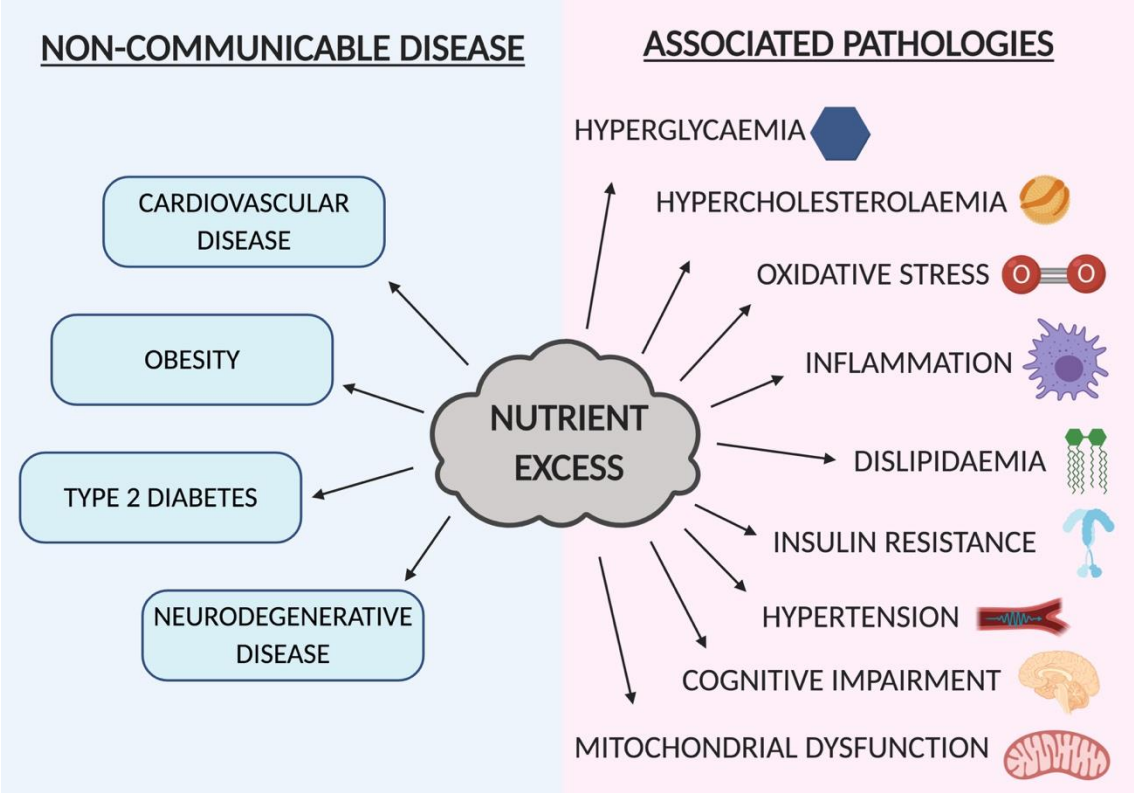

Figure 1.1 Nutrient excess and disease

Nutrient excess due to over consumption of highly processed foods, carbohydrates with high glycaemic load (GL), and foods containing high levels of saturated fats are a root cause of many non-communicable diseases, such CVD, obesity, T2D, and neurodegenerative disorders. These diseases are inextricably linked to one another. Indeed, there are parallels between their pathologies, some of which are associated with nutrient excess and are shown above. These are as follows; hyperglycaemia - high blood glucose levels; hypercholesterolaemia - high blood cholesterol levels (low-density lipoprotein, LDL); oxidative stress - imbalance in oxidants vs. antioxidants, resulting in increased reactive oxygen species; inflammation - physiological reaction presenting as increased immune cell recruitment, and increased cytokine, chemokine and chemoattractant expression; dyslipidaemia - dysregulation in blood lipid content, e.g. increased triglyceride levels, increased LDL and decreased high-density lipoprotein (HDL); insulin resistance - impaired cellular insulin signalling ; hypertension - high blood pressure; cognitive impairment - umbrella term describing a range of neurological deficits, including memory loss, behavioural changes, and problems with everyday decision making; mitochondrial dysfunction - mitochondria that are functioning inadequately resulting in loss of mitochondrial homeostasis and bioenergetic dysfunction.

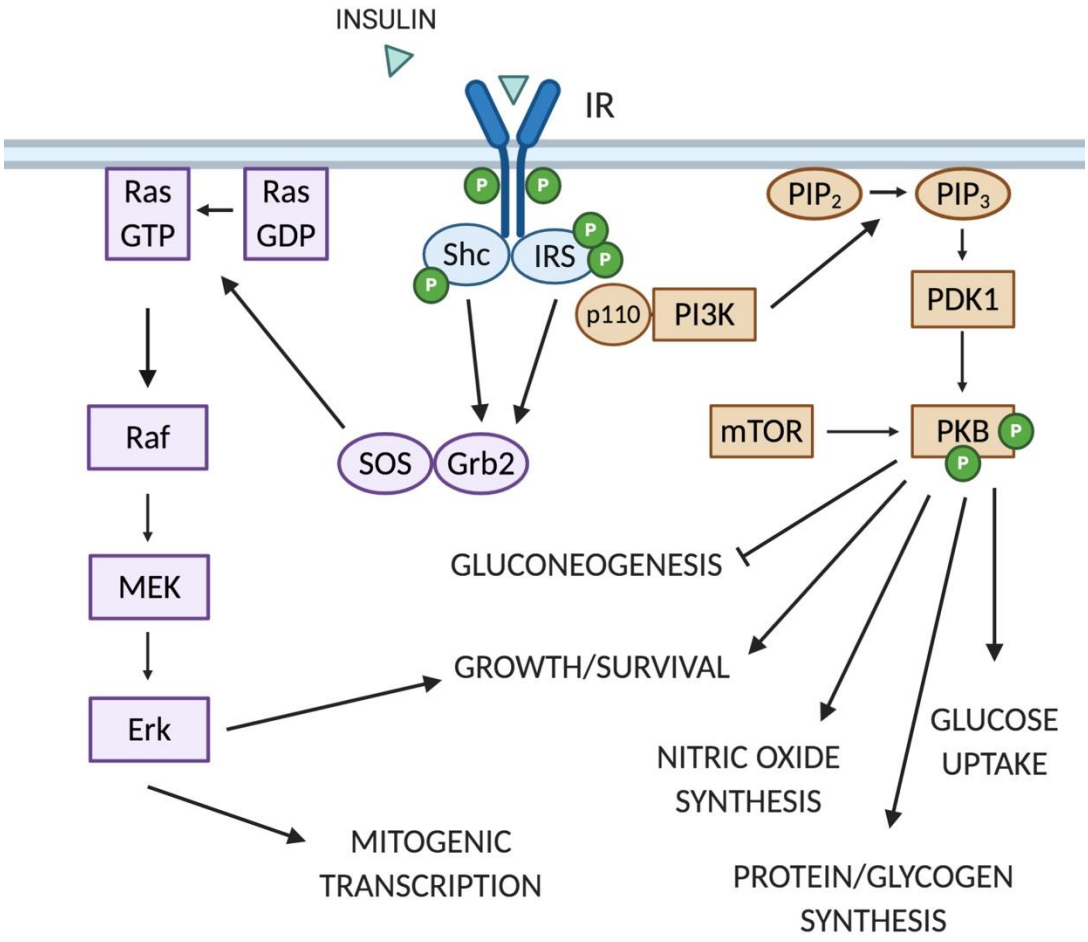

Figure 1.2 Cellular insulin signalling

Insulin binds the insulin receptor (IR) inducing autophosphorylation and recruitment and subsequent phosphorylation of substrates (mainly insulin receptor substrate 1 or 2 [IRS1/2]) required for further downstream signalling. Upon IRS phosphorylation, it associates regulatory subunits of PI3K, stimulating the transformation of membrane-bound lipoprotein PIP_2 in to PIP_3. PIP_3 recruits PDK1 to the plasma membrane, resulting in phosphorylation of PKB by PDK-1 at Thr308, which facilitates a second phosphorylation at Ser473 by mTOR. These phosphorylation events potentiate PKB activity seven-fold and induce full activation. PKB activation can produce a number of effects dependent on cell type. For example, PKB activation facilitates glucose uptake and nitric oxide synthesis. It also inhibits hepatic glucose production by phosphorylating FOXO transcription factors and is involved in regulating glycogen and protein synthesis, as well as cell growth and survival. IRS, as well as another secondary protein Shc, can facilitate the binding of Grb2 and SOS. This then induces the transformation of Ras GDP to Ras GTP, which activates the Raf/MEK/Erk pathway. This pathway is known to activate transcription factors involved in mitosis and survival.

1.4 Cardiovascular disease

The leading cause of death in Western countries is cardiovascular disease (CVD)[34], a term used to describe a range of disorders affecting the circulatory system including hypertension, atherosclerosis, and stroke. It is clear that poor nutrition is a root cause of CVD, with excessive intake of processed sugars and saturated fats, together with obesity, T2D, and tobacco smoking, being associated with the development of CVD[35,36]. Due to the large body of evidence that suggests that nutrition is one of the most preventative factors in CVD death[37] and alongside the fact that diet plays an important role in the management of CVD-associated pathologies such as hyperglycaemia, hypercholesterolaemia, and T2D, it is clear that the role of nutrient excess in the onset of CVD needs to be further investigated.

1.5 Dementia

'Dementia' is an umbrella term, which describes a range of cognitive symptoms such as memory loss, behavior and personality changes, issues with problem solving, and language impairments. There are many dementia-causing diseases, including Alzheimer's disease, vascular dementia, Parkinson's disease, and Huntington's disease. Dementia affects an estimated 47 million people worldwide; 850,000 of which reside in the UK. This number is rapidly growing due to the ageing population and the lack of disease therapeutics and is expected to reach more than 131 million worldwide and 2 million in the UK by 2050[38,39]. Despite scientific advances and an increase in research funding (£75 million in 2014 compared to £45 million in 2009[39]), the fact remains that there are no effective pharmacotherapeutic treatments for dementia-causing diseases[40]. Current treatment options focus on symptomatic improvements and mainly consist of neurotransmitter-balancing drugs such as cholinesterase inhibitors[41,42], the N-methyl-D-aspartate (NMDA) receptor antagonist memantine[43,44], and several antidepressants[45,46]. Many disease-modifying therapies have made it to clinical trials, but these are met with little to no success. Mehta and colleagues offer a concise perspective of dementia clinical trials active from 2010 to 2015, with suggestions as to why these trials may have failed[47]. With the increasing prevalence of dementia-causing

diseases, it is clear that further investigation into the pathophysiology of these diseases is required.

1.5.1 Alzheimer's disease

Alzheimer's disease (AD) is the most common form of dementia[48], accounting for approximately 80% of cases[49]. The majority of AD cases occur after the age of 65, constituting late-onset AD (LOAD), whilst cases that appear before the age of 65, early-onset AD (EOAD) are considerably rarer, constituting 5% of all AD cases[50]. There are two pathologies that were first described by Alois Alzheimer[51,52] that are associated with AD; amyloid plaques, extracellular deposits consisting of aggregates of the small peptide amyloid beta (Aβ) and neurofibrillary tangles (NFT), intracellular aggregates of hyperphosphorylated tau protein. The confirmation of the presence of these two abnormalities is still required for post-mortem diagnosis of the disease and it is often said these are the hallmark pathologies of the disease[53].

1.5.2 Vascular dementia

Vascular cognitive impairment (VCI) is an umbrella term used to describe a range of symptoms associated with decline in mental cognition caused by an abnormality of vascular origin. This might include ischaemic attacks or stroke[54], cerebral amyloid angiopathy (CAA)[55], microbleeds[56], or a reduction in global cerebral perfusion due to cardiac arrest[57]. The most severe form of VCI is vascular dementia, which is responsible for around 20% of dementia cases[58]. It is hard to pin down exactly how these pathologies then lead to VD, but at the heart of them all is the reduction in cerebral blood flow (CBF), be that acute yet severe (stroke) or chronic, discrete, and reoccurring (multi-infarct). A reduction in CBF to brain tissue results in a hypoxic and nutrient-deprived environment within the brain area affected, stressors which may lead to oxidative stress, cellular metabolic dysfunction, inflammation, and lasting tissue damage. Indeed, there is a general consensus that cognitive impairment results from brain dysfunction caused by multifactorial and cumulative tissue damage[58].

The development of dementia can be the result of both Alzheimer-pathology as well as a vascular contribution. Patients with VD may also present with amyloid accumulation[55], and likewise AD patients present with vascular abnormalities[59,60], meaning there is overlap between these diseases. It is likely that individuals living with dementia may experience varying levels of AD-related and vascular pathologies and no two cases will be the same. It is important that we do not look at these diseases in pure isolation if we are to better understand what is at the core of their development.

1.5.3 Metabolic risk factors for dementia

Interestingly, both VD and AD share common risk factors, largely related to poor nutrition, metabolic disorders, and vascular diseases. The biggest risk factor in developing dementia is age, with cardiometabolic disturbances such obesity, T2D, and hypertension also being implicated. The existing literature on the relationship between obesity and dementia is conflicting and contradictory. Most studies report an association between obesity in mid-life and increased dementia risk, as well as greater burden of Alzheimer's pathology[61–64]. It remains unclear whether obesity increases the risk of dementia independently or due to its co-pathologies. The pathophysiology of T2D and insulin resistance has been likened to the pathophysiology of AD, some reporting AD is a brain specific form of diabetes[65]. The connection between the two pathologies gained significant interest after the publishing of the Rotterdam Study, which found that those suffering from diabetes had an increased risk of developing dementia[66,67]. Since then, many epidemiological studies have further confirmed this[68–72]. Although precise mechanisms are unclear, there are known parallels between the two diseases that are heavily associated with poor diet. As previously stated, those with T2D suffer from a chronic low-grade inflammation as well as oxidative and metabolic stress, and these cellular impairments are also seen in AD and present as metabolic stress and neuroinflammation, as well as insulin resistance[73]. Both pathologies also present with amyloid aggregation, neurodegeneration, and cognitive decline[74,75].

1.5.4 Vascular risk factors for dementia

Systemic and cerebral atherosclerosis has been suggested to play a role in the development of dementia in the elderly[76]. Atherosclerosis is preceded by endothelial cell dysfunction, which kick-starts a cycle of inflammatory events. This disease, the development of which is summarised in Fig. 1.3, is characterised by fatty plaque deposition in the sub-endothelial space of arteries, often resulting in hardening of the vessels. Atherosclerosis can occur in both peripheral and cerebral arteries, but is especially common in ilio-femoral arteries in the leg, carotid arteries in the necks, and the basilar, posterior, and middle cerebral arteries in the brain[77,78]. Atherosclerotic plaques can remain stable for some time, but if the plaque suddenly ruptures, it may trigger platelet aggregation and thrombosis (blood clots) may occur. This can lead to ischaemic stroke, or further embolisms as the plaque may detach and travel through the blood stream to other vessels. Classical risk factors for developing atherosclerosis include poor nutrition[79], the presence of a metabolic disorder (obesity, insulin resistance, T2D)[80], tobacco smoking[81], hypertension[82], and genetic predisposition[83]. One of the main triggers for developing the disease is the presence of hypercholesterolaemia[79], usually stemming from an increased consumption of cholesterol in the diet or an inherited condition[83]. Hypercholesteraemia may influence disease development through cellular pathologies including inflammation, oxidative stress and mitochondrial dysfunction[80]. Several studies indicate a direct relationship between atherosclerosis and Alzheimer's pathology, thus implying Alzheimer's pathology is potentially rectifiable with the treatment of atherosclerosis. The effect of atherosclerosis on dementia may be attributable to its strong relation to cerebral infarcts and ischaemic stroke, or a common pathology such as ApoE variants[83]. However, Dolan and colleagues found that the risk of developing dementia greatly increased in the presence of intracranial atherosclerosis, independent of the incidence of cerebral infarcts[76]. Atherosclerosis and dementia are clearly linked, but the foundations of this relationship are presently unclear and need to be further investigated.

Hypertension, also known as high blood pressure (BP), is another known vascular risk factor for developing dementia. Blood pressure consists of both systolic blood pressure,

which is the pressure the blood exerts on the artery walls during a heartbeat, and diastolic, which is the pressure the blood exerts on the artery walls when the heart is at relaxed. The reading is given as systolic blood pressure/diastolic blood pressure in millimeters of mercury (mm Hg). Normal blood pressure is anything below or equal to 120/80 mmHg. Hypertension stage one is a blood pressure reading of 130-139/80-89 mmHg and stage 2 is >140/>90 mmHg. Several studies have established a link between elevated BP in mid-life and the development of dementia in later life. Chronically elevated BP exerting pressure on vessels[82], leading to vessel wall thickening and reduced microvessel diameter, is likely the cause of this increased risk[84]. Chronic hypertension is also associated with thickening of larger cerebral arteries and atherosclerotic plaque formation, which as previously stated can rupture and occlude blood flow. Of note is that although several studies have addressed the issue, only two studies have identified an association between late-life hypertension and dementia[85]. Interestingly, two clinical trials reported a positive effect of lowering blood pressure on the incidence of dementia, again suggesting dementia may be remediable with the treatment of hypertension[85].

1.6 Endothelial cells

Endothelial cells (ECs) exist as a monolayer, making up the inner lining of all blood vessels in the body. The vessels' job is to retrieve nutrients and oxygen from their site of uptake or production and deliver them around the body where they can be metabolised. They are also responsible for removal of waste products from these tissues. ECs play a key role in not only regulating blood flow and therefore nutrient and oxygen supply, but also transport of numerous molecules across their monolayer barrier.

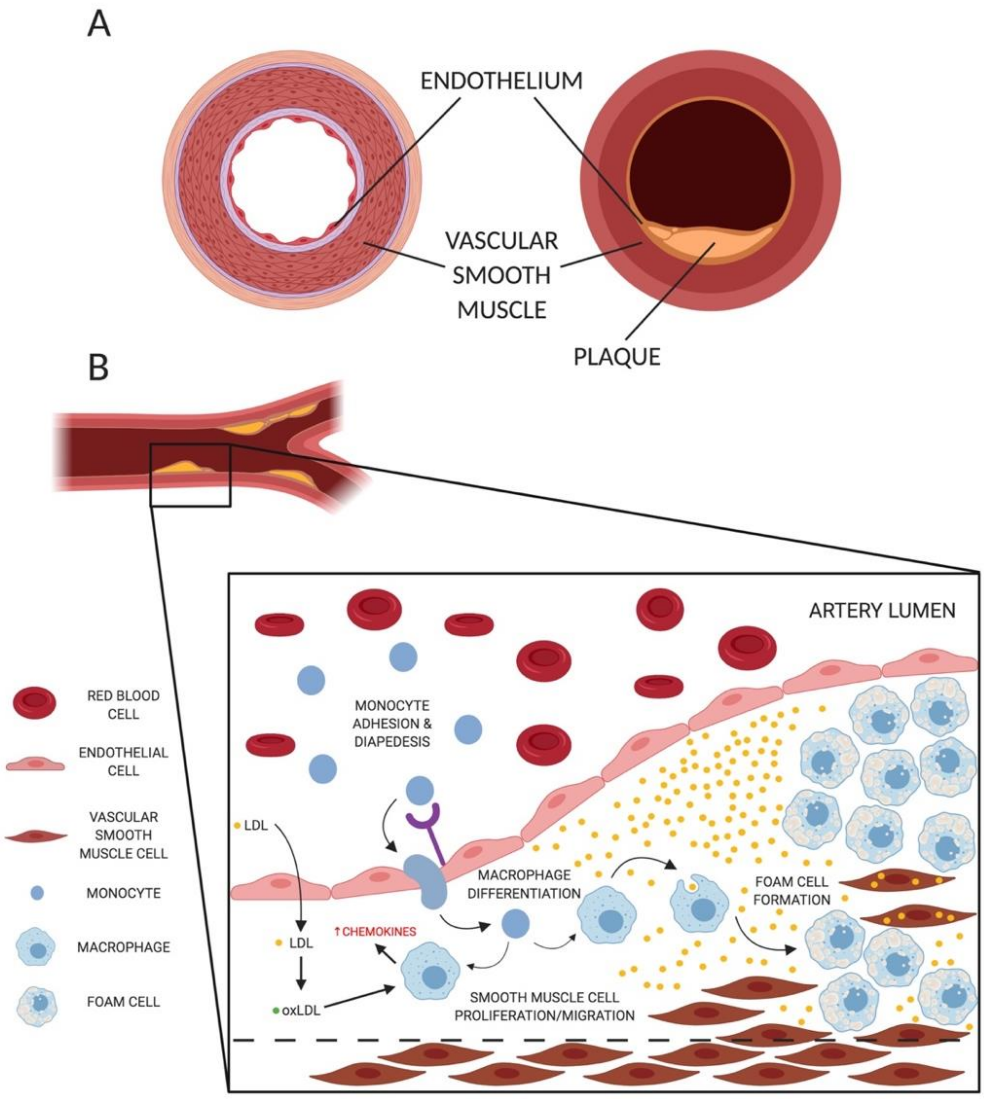

Figure 1.3 The development of atherosclerosis

(A) Cross sectional image of both a healthy and atherosclerotic artery. (B) Development of atherosclerosis. The first trigger is the increased expression of cell-surface adhesion molecules (shown in purple) on the endothelium such as VCAM, ICAM, and P-selectin, caused by various effectors, for example, chronic hypercholesterolaemia, hyperglycaemia, and dyslipidaemia. Monocytes adhere to the cell-surface adhesion molecules and begin to migrate through the endothelium (diapedesis). Once in the sub-endothelial space, they will differentiate into macrophages. Macrophages respond to this proinflammatory environment by secreting chemokines and chemoattractants, recruiting more monocytes to the lesion. The high levels of LDL become oxidised by free radicals, forming oxLDL, further activating the macrophages and exacerbating the proinflammatory environment. Macrophages develop into foam cells as they attempt to engulf the lipid present in the lesion. These processes are cyclical and eventually the lesion results in a fatty plaque in the sub-endothelial space. Smooth muscle cells migrate and begin to exhibit lipid deposits, which only acts to exacerbate the lesion. This plaque has the potential to impair blood flow at the lesion site, but also it may rupture, triggering platelet aggregation and thrombosis.

1.6.1 Nitric oxide signalling

One aspect of EC function is to control haemodynamics by releasing nitric oxide (NO). A schematic of NO signalling is shown in Fig. 1.4. Briefly, vasoactive agents (acetylcholine, insulin, bradykinin) that are present in the blood will act on their respective receptors on the luminal surface of ECs to induce a change in endothelial nitric oxide synthase (eNOS) activity. eNOS is an important enzyme that is involved in the oxidation of L-arginine (L-arg) to L-citrulline and NO. When eNOS is active, high concentrations of NO are produced, which can then diffuse into neighbouring vascular smooth muscle cells (VSMCs) and induce relaxation, ultimately causing vasodilation. If eNOS activity decreases, NO concentrations are reduced, which ultimately will cause vasoconstriction[86]. Therefore, NO bioavailability is a key regulator of haemodynamics. The production of NO from L-arg by eNOS requires the presence of 5 co-factors; tetrahydrobiopterin (BH_4), flavin adenine dinucleotide, flavin mononucleotide, calmodulin, and iron protoporphyrin IX (haem). eNOS is synthesised as a monomer but is required to exist as a dimer to bind BH_4 and L-arg and catalyse NO production. The monomers instead produce super oxide (O_2-), referred to as eNOS uncoupling. The activity and the coupling of eNOS are far more important than its expression in terms of NO production. Some vasoactive agonists such as acetylcholine and bradykinin increase eNOS activity through a calcium-dependent mechanism. They bind to their respective cell surface receptors, which activate downstream signalling pathways to increase intracellular calcium ion (Ca^{2+}) concentrations. Ca^{2+} then binds calmodulin, leading to the activation of the calmodulin-binding domain of eNOS and an electron flux from the reductase to the oxygenase domains of eNOS facilitating oxidation of L-arg and production of NO[87]. Although independent of Ca^{2+}, phosphorylation of eNOS on certain sites results in a similar electron flux from the reductase to the oxygenase domains, therefore increasing NO production. Phosphorylation at serine 1177 increases eNOS activity, whereas phosphorylation at threonine 495 reduces eNOS activity. Serine 1177 phosphorylation is also downstream of protein kinase B (PKB) signalling and AMPK signalling[86].

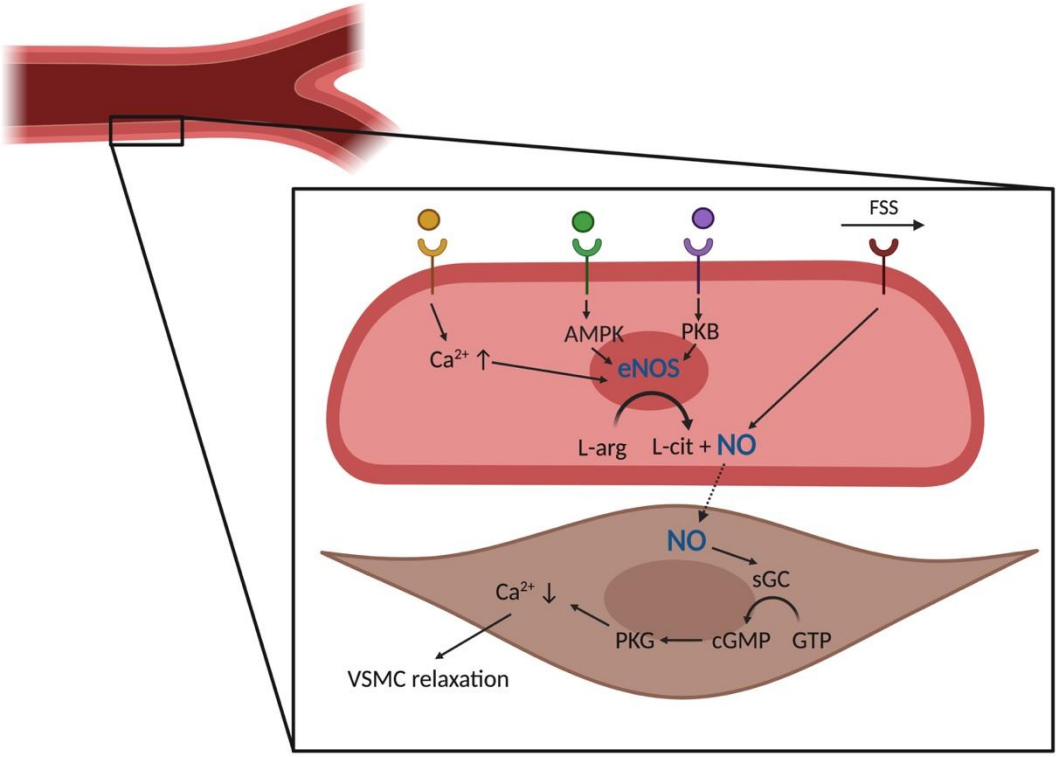

Figure 1.4 Nitric oxide signalling in healthy vasculature

Vasoactive agents from the blood act on the luminal surface of endothelial cells (pink) and stimulate downstream signalling pathways, resulting in an increase in NO bioavailability. Examples of vasomodulators are acetylcholine/bradykinin (yellow), histamine (green), insulin (purple), and fluid shear stress (red), which activate a range of signalling molecules including Ca^{2+}, AMPK and PKB. These signals can then go on to increase eNOS activity, either by phosphorylation or promoting coupling, resulting in enhanced NO production from L-arg. NO can diffuse into the neighbouring vascular smooth muscle cells (brown), and activates sGC, which in turn converts GTP to cGMP. cGMP induces activated of PKG, which is known to decrease cytosolic Ca^{2+}, resulting in muscle relaxation and vasodilation. In the event of reduced NO bioavailability, either as an adaptive response or in cases of endothelial dysfunction, PKG is no longer active and thus unable to minimise cytosolic Ca^{2+}, resulting in muscle contraction and vasoconstriction.

It is important to mention that ECs also respond to physical forces exerted upon them by blood flow. There are two main forces that the EC will experience; a frictional force of the blood moving parallel to the ECs called fluid shear stress (FSS) or wall shear stress (WSS), and the force of pulsatile blood pressure, which stretches the vessel wall. Mechanical stress on the vessel wall can influence NO signalling as well as increase the expression of Krüppel-like factor 2 (KLF2), a transcription factor with anti-inflammatory and antithrombotic downstream effects. A coherent model of how mechanostimulation initiates EC signalling is still to emerge. *In vitro* studies have implicated an array of shear-responsive kinases, GTPases, ion channels, and cilia. An excellent review of this topic is provided by Zhou and colleagues[88].

Once produced, NO diffuses into VSMCs and stimulates soluble guanylyl cyclase (sGC), resulting in the formation of cyclic guanosine monophosphate (cGMP) from guanosine triphosphate (GTP). cGMP activates protein kinase G, which promotes the uptake of cytosolic Ca^{2+} into the sarcoplasmic reticulum, the discharge of Ca^{2+} out of the cell, and the opening of Ca^{2+} dependent potassium channels. Intracellular Ca^{2+} concentration decreases and due to this, myosin phosphorylation is attenuated and VSMCs relax[89].

1.6.2 Endothelial cell dysfunction

Endothelial dysfunction (ED) can be described as the shift in EC phenotype toward that of one which exhibits a blunted response to vasodilatory agents and is generally proinflammatory and prothrombotic. As a general rule, if ED is present, NO bioavailability will be decreased, usually by a reduced response in the signalling that precedes NO production (reduced eNOS activity/coupling, reduced PKB or AMPK activity, reduced Ca^{2+} signalling)[90], or NO activity will be reduced.

ED is strongly associated with increased reactive oxygen species (ROS) production and there is a growing body of evidence to suggest that oxidative stress plays a causal role in the development of ED. NADPH oxidases (NOX) are the main contributor of ROS production in endothelial cells, although other sources such as the mitochondria do exist (see section mitochondrial ROS). Indeed, Doerries and colleagues showed that deletion

of the NOX subunit p47phox protected mice against ED[91]. Wenzel and colleagues described a role for mitochondrial ROS (mROS), when they reported that mice lacking one copy of the MnSOD gene, and that therefore exhibit increased mROS, presented with worsened age-related ED[92]. It is well established that one of the most abundant ROS, superoxide (O2-) can react with NO to inactivate it and form peroxynitrite (ONOO-), contributing to ED[93]. eNOS uncoupling is also associated with ED, potentially due to increased NOXs and ROS, leading to oxidation of BH4. In more detail, the product of the superoxide O2- and NO, ONOO- oxidises BH4 into the BH3- radical[94]. As previously mentioned, BH4 is a cofactor in the production of NO from L-arginine, thus a reduction in its availability will uncouple eNOS from NO production and instead eNOS will produce O2-. ONOO and H2O2 have also been shown to increase arginase activity and expression in ECs [95,96], resulting in less L-arginine to react with eNOS and lowering NO bioavailability.

Aside from NO bioavailabiliy/activity, NOXs can contribute to the development of ED in other ways. For example, NOX-derived ROS are involved in NF-kB activation and expression of adhesion molecules such as ICAM-1, thus facilitating an inflammatory state within the EC[97] (see section 1.6.3). Additionally, NOXs are potent activators of protein tyrosine phosphatases, such as protein tyrosine phosphatase 1B (PTP1B), which is an inhibitor of growth factor signaling[98], particularly insulin action. Activation of this phosphatase by NOXs may contribute to ED by blocking the vasodilatory action of insulin at the ECs.

Interestingly, ED has been associated with an increase in total eNOS expression, likely due to high concentrations of hydrogen peroxide (H_2O_2), the dismutation product of O_2- (produced by uncoupled eNOS). H_2O_2 can increase the production and extend the half-life of eNOS mRNA[94]. Indeed, H_2O_2 effects endothelial function in both positive and negative ways. H_2O_2 can induce vasorelaxation through increasing eNOS activity via PI3K and ERK1/2 but has also been reported to have vasoconstrictor capabilities[99]. H_2O_2 is also a hyperpolarising factor which can have a direct effect on potassium (K^+) channels on ECs, acting to decrease intracellular K^+ concentration and promote hyperpolarisation. Hyperpolarisation of ECs and release of K^+ into the subendothelial space allows for VSMC

K^+ channels which will further result in hyperpolarisation of VSMCs, promoting VSMC relaxation and thus vasodilation. Additionally, H_2O_2 can promote endothelial activation (see section 1.6.3), mediate vascular remodeling and angiogenesis[100], and induce apoptosis.

Another marker of ED is the powerful vasomodulator endothelin-1 (ET-1). ET-1 is produced in ECs and secreted preferentially to the basolateral side of the endothelium, acting on endothelin receptor ET_A on neighbouring VSMCs to induce constriction. Secreted ET-1 can also act in a paracrine manner on ET_B, which is present on neighbouring ECs and results in an increase in NO, suggesting that ET-1 is a complex modulator of haemodynamics, capable of inducing both vasodilation and vasoconstriction. However, since the discovery of ET-1, several studies have suggested a link between high circulating levels of ET-1 and CVDs such as atherosclerosis and hypertension. Raised ET-1 has also been associated with metabolic disorders (obesity and T2D) and neurodegenerative disorders, including AD[101]. Therefore, ET-1 remains a well-utilised marker of ED.

1.6.3 Endothelial cell activation

Another pathology that arises in metabolic and vascular diseases is endothelial activation (EA, Fig. 1.5). EA is defined as the increased expression of cell surface adhesion molecules on the luminal surface of ECs, typically caused by a proinflammatory response from the EC itself. As mentioned in 1.5.4, proinflammatory signalling molecules such as TNFα and IL-6 will induce an increase in the expression of cell-surface adhesion molecules such as vascular cell adhesion molecule-1 (VCAM-1), inducible cell adhesion molecule-1 (ICAM-1), endothelial leukocyte adhesion molecule (E-selectin), and P-selectin. EA facilitates the recruitment of circulating leukocytes, particularly monocytes, which can then migrate into the subendothelial space and begin differentiating to macrophages, which will secrete further proinflammatory chemokines and chemoattractants[102].

EA and ED are undeniably linked, but it is unclear which pathology arises first. Proinflammatory signalling molecules such as TNFα are known to be able to inhibit eNOS expression by reducing eNOS mRNA half-life, as well as reduce NO bioavailability through induction of ROS through mechanisms described earlier[102]. It has been shown that in the presence of hypercholesterolaemia (through giving atherogenic diet to rabbits), VCAM expression is rapid and possibly the first response in the endothelium[103]. However, when cytokines are absent, reduced NO bioavailability (through NO inhibition via L-NG-arginine methylester; L-NAME) can also rapidly induce VCAM expression and monocyte recruitment, indicating NO can protect against EA[104,105]. This is further supported by the fact that atherosclerotic lesions are more prevalent in areas of vascular branching that are exposed to turbulent rather than laminar flow and have reduced NO bioavailability[106], as well as the fact that genetically modified eNOS-deficient mice develop increased atherosclerosis and inflammation[107].

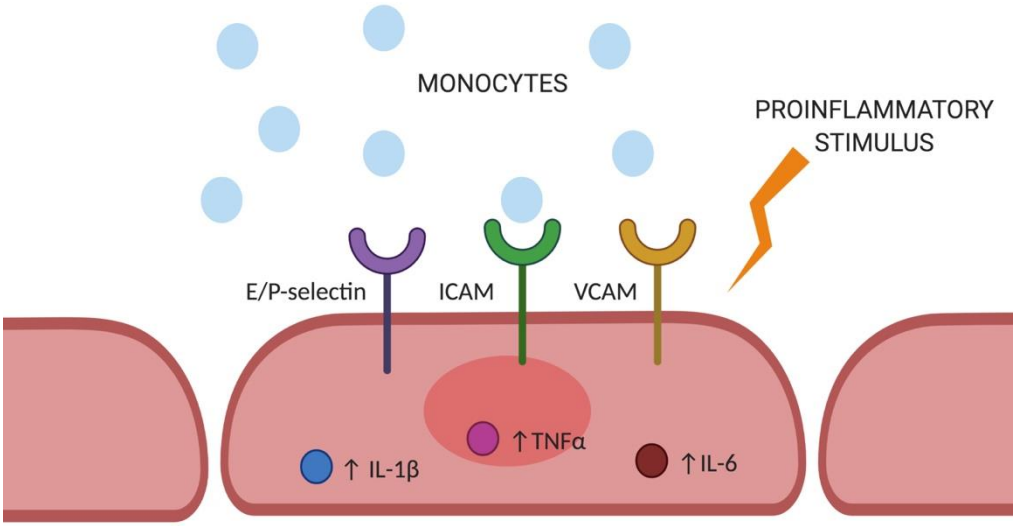

Figure 1.5 Schematic representation of endothelial activation

Endothelial activation is a proinflammatory state that the endothelial cell is experiencing due to a cyclical series of proinflammatory events. A proinflammatory stimulus (chronic dyslipidaemia, hypercholesterolaemia, hyperglycaemia) will induce an increase in the expression of cell-surface adhesion molecules such as VCAM, ICAM, E-selectin and P-selectin. This facilitates the recruitment of circulating leukocytes, particularly monocytes, which can then migrate into the subendothelial space and begin differentiating to macrophages, which will secrete further proinflammatory cytokines such as TNFα, IL-6 and IL-1β and chemoattractants such as MCP-1 and MIP.

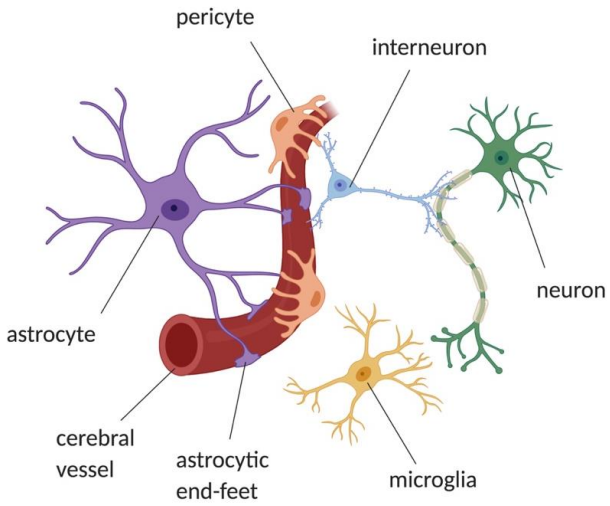

Figure 1.6 Schematic of the blood-brain barrier

The blood-brain barrier (BBB) is a barrier interface between the blood and the interstitial fluid of the brain. The physical barrier compromises of endothelial cells of cerebral vessels, and supporting cells such as pericytes, astrocytes, microglia, and neurons play a metabolic regulatory role in maintaining the integrity of the BBB.

1.7 The blood-brain barrier

The blood-brain barrier (BBB) is an "interface" barrier between the blood and the interstitial fluid of the brain. It is not a rigid structure, but rather a dynamic unit comprising several cell types, often referred to as the VE fraction unit (NVU; Fig. 1.6). ECs joined together by cell-cell junctions including tight junctions (TJs) and adherens junctions form the basic structure of the BBB[108], whilst pericytes and astrocytes may perform supporting and regulatory functions[109]. The BBB plays the important role of delivering essential nutrients to the brain and removing waste products. Indeed, entry of potentially damaging particles is severely restricted by the endothelium of the BBB and movement of molecules across the BBB depends on specialised transporters or carriers. Aside from barrier function, the endothelium of the BBB is also heavily involved in haemodynamics and regulation of cerebral blood flow (CBF). The integrity of the BBB is crucial to proper brain function, and when it is compromised, the damage that succeeds this may lead to neurodegenerative disorders such as dementia. EC dysfunction in the brain is linked to impaired cerebral blood flow and BBB opening[110]. BBB opening will allow entry of toxic blood-derived molecules into the brain and has been largely linked to neuroinflammation[111]. A pro-inflammatory environment at the BBB will act to exacerbate the damage; further impairing barrier integrity and dysregulating haemodynamics.

There is a growing list of pathologies that exhibit BBB dysfunction, including metabolic disorders such as obesity and T2D, as well as cardiovascular disorders such as hypertension. Furthermore, cerebrovascular integrity is altered during aging[112–114]; changes that can be accelerated by vascular pathologies such as cerebral amyloid angiopathy. Indeed, high-fat diet (HFD)-fed rats exhibit BBB dysfunction as early as 24-days post diet induction[115]. T2D-induced changes at the BBB include downregulation of TJ proteins including claudin-5 and occludin, and the TJ-associated protein ZO-1[116–120], promoting BBB opening[121,122]. Endothelial activation is also promoted, with upregulated protein expression of ICAM and VCAM[123]. Another aspect of BBB damage is basement membrane (BM) thickening, and this is seen in T2D[124–126], and can result in cell detachment from the BM as well as BBB opening. Systemic inflammation observed in

multiple metabolic disorders has also been shown to induce BBB opening and dysfunctional brain ECs. Indeed, lipopolysaccharide (LPS) challenge in mice induces BBB opening, a pathology that is dependent on reduced mitochondrial function[127]. Consequently, there is strong evidence to link nutrient excess, cerebral EC dysfunction, and loss of BBB integrity.

1.8 Effects of nutrient excess on endothelial cells

ED and EA are found in multiple diseases, including obesity[90,128–131], T2D[132–134], type 1 diabetes (T1D)[135], and dementias[84,136,137], and are indeed a main driver in the development of atherosclerosis and other CVDs. It is believed that pathologies succeeding nutrient excess, such as hyperglycaemia and dyslipidaemia, may drive ED and EA, contributing to the development of these diseases.

1.8.1 Animal dietary studies investigating endothelial cell function

EC function in relation to nutrient excess has been extensively studied in animal models. Noronha and colleagues found that HFD feeding (8 weeks duration) has the capacity to reduce insulin-mediated vasodilation in *ex vivo* murine aortae myograph studies, suggesting ED[138]. Interestingly, the authors observed no change in acetylcholine (ACh)-mediated aortic vasodilation in HFD-fed mice. This was attributed to the hyperpolarising capacity of increased ROS H_2O_2 levels, as in the presence of catalase (degrades H_2O_2) the response to ACh was indeed blunted in HFD-fed mice. The hyperpolarising effects of H_2O_2 in early ED may act as a compensatory mechanism. NO levels, measured by plasma nitrite concentration, were increased in HFD-fed mice[138], but this was attributed to increased inducible NOS (iNOS) expression, a potential inflammatory response to the nutrient excess. Other HFD rodent models (6-24 weeks on HFD) suggest similar findings in that HFD induces a blunted vasodilatory response in *ex vivo* aortae, indicating endothelial dysfunction[139–141]. We have reported that mice fed HFD (20 weeks) exhibit significantly reduced *in vivo* ACh-induced vasodilation when undergoing microvascular assessment using laser Doppler flowmetry (see section 2.5), as well as decreased aortic phospho-eNOS (S^{1177}), and increased plasma ET-1 levels, increased aortic ICAM protein

expression, and reduced plasma nitrite[142]. These data suggest nutrient excess caused by HFD consumption compromises endothelial response through reduced NO bioavailability, perhaps caused by blunted upstream signalling and/or a proinflammatory environment. It is unclear whether this dysfunction develops prior to the onset of obesity and T2D in the mouse. Indeed, we have previously observed marked reductions in *in* vivo vasodilatory response to ACh in HFD-fed mice as soon as 5 weeks on when blood glucose levels are likely higher than normal[142], but perhaps prior to the onset of a complete whole-body insulin resistance[143]. We did not observe any changes at 1 week of HFD and unfortunately do not possess data at this time investigating the effects of 2-4 weeks of HFD on ACh-induced vasodilation. It is certainly of interest whether endothelial function is compromised after a short duration of nutrient excess, or whether it is secondary to the onset of obesity and T2D. Da Silva Rocha and colleagues also investigated the effects of HFD-induced obesity on endothelial dysfunction via *ex vivo* aortic myograph experiments[144]. Interestingly, their model of obesity (HFD-induced, 20% of calories from fat, 27 weeks), whilst significantly heavier than regular chow controls, did not exhibit many classical pathologies of obesity including reduced glucose tolerance, hypercholesterolaemia, dyslipidaemia, or hyperinsulinaemia. Additionally, they observed no reduction in aortic dilatory response to ACh in obese mice, which is contradictory to previous studies. This suggests that HFD-induced endothelial dysfunction is dependent on obesity-related pathologies, including hyperglycaemia, dyslipidaemia and hypercholesterolaemia. In line with the notion that hypercholesterolaemia is a strong contributor to ED, Belch and colleagues reported that 4 weeks of high-cholesterol diet induced a potent reduction in *in vivo* skin perfusion response to ACh[145].

Studies focusing on nutrient excess and brain vasculature are contradictory. Zuloaga and colleagues reported that 6 months of HFD feeding in mice did not reduce CBF[146], whilst Bracko and colleagues observed no worsening of CBF in the Alzheimer's model APP/PS1 when they challenged the mice with a 15 month HFD[147]. However, acute HFD feeding has been reported to exacerbate brain ischaemic damage in middle cerebral artery occlusion stroke model[148], and chronic HFD (12 months) results in a reduction in CBF in

mice[149]. Furthermore, high cholesterol diet reduced *ex vivo* responsiveness of murine posterior cerebral artery to ACh[150].

1.8.2 Effects of hyperglycaemia on endothelial cell function

To further investigate how hyperglycaemia may affect EC function, we can look to both rodent and human studies on type 1 diabetes mellitus (T1D). Hyperglycaemia alone has been linked to atherosclerosis in people with T1D, which we can assume is an indicator of reduced EC function. Postmortem studies in T1Ds with favourable lipid profiles indicate that hyperglycaemia is an independent risk factor for atherosclerotic plaque development[151], whilst T1Ds also exhibit reduced CBF[152]. Genetic and streptozotocin (STZ)-induced T1 diabetic mouse models have also shed light on this topic. STZ mice exhibit reduced ACh-induced vasodilation in *ex vivo* aortic myograph studies[153,154], increased aortic superoxide expression[154], and increased serum TNFα[153]. Furthermore, when administered to a mouse model of atherosclerosis (ApoE KO mouse), STZ-induced chronic hyperglycaemia acted to further exacerbate the already-blunted ACh-mediated vasodilation (*ex vivo* myography) and increased eNOS mRNA[155]. Furthermore, on crossing a genetic model of T1D (Ins2 Akita mouse) with a genetic model of atherosclerosis (LDL receptor KO), Zhou and colleagues found that chronic hyperglycaemia exacerbated aortic atherosclerotic lesion area[156]. In these studies, inducing T1D in mouse models of atherosclerosis acted to further increase plasma very low-density lipoprotein (VLDL) LDL, HDL, and triglyceride levels, potentially due to impaired hepatic function and increased hepatic inflammation[156]. Therefore, it is presently unclear whether hyperglycaemia in these models is directly affecting EC function, or whether it is indirectly doing so via enhancing dyslipidaemia. In terms of brain vasculature, STZ mice exhibit profound reductions in CBF, which is associated with cognitive impairment and worsened performance in memory tasks[157]. Clinically, implementing tight glycaemic control in young T1Ds reduced microvascular complications in the initial follow-up period, and also reduced the number of CVD events (e.g. ischaemic attacks) in the 10-year follow-up[158]. Similarly, a similar trial undertaken in newly diagnosed T2 diabetics found that tight glycaemic control reduced the number

of CVD events in the 10-year follow-up[159]. However, glycaemic control in persons who are already high CVD risk did not exhibit any benefit[160,161]. These clinical trials data suggest that implementation of glycaemic control early following a diabetes diagnoses could be a protective measure in reducing CVD risk, but it is unclear whether it would be a beneficial course of action in those already at high risk. In

Some *in vitro* studies corroborate the role of hyperglycaemia in the development of ED. Exposing cells to high glucose (HG) concentrations is a tool for measuring the effect of HG on cellular function in the absence of other factors. Exposure to HG has been reported to reduce phospho-AMPK expression[154], reduce phospho-PKB expression[162–164], reduce phospho-eNOS expression[154,163], reduce NO levels[154,163], impair ERK activation[164], reduce mitochondrial bioenergetics[165,166] increase superoxide levels[154], induce apoptosis[162,167,168], increase cell permeability[169], increase ICAM/VCAM expression[162], enhance cell senescence[162,170], and impairs angiogenesis[163,164] in a number of endothelial cell line models including HUVECs, BAECs, and HMECs.

Studies investigating the effects of hyperglycaemia on brain ECs *in vitro* are limited. Most brain EC studies investigate BBB function and measure outcomes such as transepithelial resistance (TEER) as well as expression of tight junction proteins. In brain endothelial cell lines (hCMEC/d3, BMEC), acute and chronic exposure to HG both reduced TEER[171,172], increased permeability[118], elevated glycation of tight junction proteins[172], reduced expression of tight junction proteins[118], induced apoptosis[171,173], increased oxidative stress markers[171,173], increased VCAM expression[118], increased mitochondrial permeability transition pore (mPTP) expression[173], decreased mitochondrial membrane potential[173], increased Ca^{2+} levels[173], increased mitochondrial Drp1 (see 1.12.1) expression[173], reduced mitochondrial mass[173] and reduced mitochondrial biogenesis[173].

There are several hypotheses as to how hyperglycaemia impairs NO bioavailability in endothelium. A model was proposed by Michael Brownlee (summarised in Fig. 1.7), which suggests that hyperglycaemia increases ROS production, which then through activation of poly-ADP ribose polymerase (PARP) and subsequent inhibition of the glycolysis enzyme D-glyceraldehyde-3-phoshae dehydrogenase (GAPDH), results in an

accumulation of glycolysis intermediates (glucose, fructose-6-phosphate [F6P], glyceraldehyde [G6P]. Accumulation of G6P may lead to increased *de novo* synthesis of diacylglycerol (DAG)[174]. DAG is a known activator of PKC, which has been implicated previously in the development of ED due to its role in activating ET-1[175]. G6P can be converted into methylglyoxal, which is known to increase formation of intracellular advanced glycated end products (AGEs)[176], thus increasing inflammatory activation of ECs[177], promoting further oxidative stress[178], and inducing ED[179]. F6P can enter the hexosamine pathway to produce uridine 5'diphosphate N-acetylglucosamine (UDP-GlcNac). UDP-GlcNAc is a precursor for proteoglycans and O-linked GlcNac addition to proteins. O-GlcNAcylation of eNOS has been shown to compromise activity[180] and is associated with enhanced VCAM and ICAM expression[181]. Increased flux of glucose through the hexosamine pathway is also associated with insulin resistance[182]. The sorbitol pathway, by which glucose is converted to sorbitol by aldose reductase, is enhanced during hyperglycaemia. Aldose reductase inhibitors have been shown to improve endothelial responsiveness to ACh *in vivo*[183], and *in vitro* by reducing uric acid accumulation[184]. The model thus suggests that hyperglycaemia-induced ED may develop due to enhanced accumulation of glycolysis intermediates through oxidative stress-induced GAPDH inhibition. Indeed, pharmacological shunting of glycolysis intermediates down the pentose-phosphate pathway has been demonstrated to improve endothelial function[185]. This model depends on the ability of hyperglycaemia to induce ROS production, which is covered in section 1.12.4.

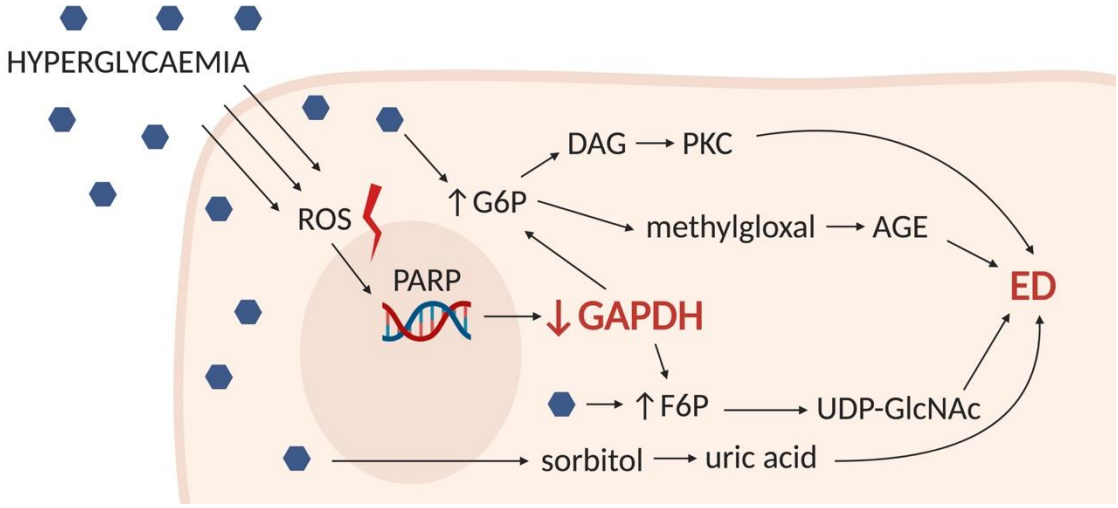

Figure 1.7 Mechanism of hyperglycaemia-induced ROS-dependent development of endothelial dysfunction

Blue hexagons represent glucose molecules. Hyperglycaemia increases intracellular ROS, which then through activation of PARP and subsequent inhibition of the glycolysis enzyme GAPDH results in an accumulation of glycolysis intermediates G6P and F6P. Accumulation of G6P leads to increased DAG levels and thus PKC activation, which has been implicated in the development of ED due to its role in promoting ET-1. G6P can be converted into methylglyoxal, which promotes formation of AGEs, known to increase inflammatory activation of ECs, promote further oxidative stress, and induce ED. F6P can enter the hexosamine pathway to produce UDP-GlcNAc, a precursor for proteoglycans and O-linked GlcNACylation. O-GlcNAcylation of eNOS has been shown to compromise activity and is associated with enhanced VCAM and ICAM expression. Increased flux of glucose through the hexosamine pathway is also associated with insulin resistance. Glucose flux through the sorbitol pathway (via aldose reductase) is enhanced during hyperglycaemia. Aldose reductase inhibitors have been shown to improve endothelial function *in vivo* and *in vitro* by reducing uric acid accumulation. The model thus suggests that hyperglycaemia-induced ED develops due to accumulation of glycolysis intermediates caused by oxidative stress-induced GAPDH inhibition.

1.8.3 Effects of dyslipidaemia on endothelial cell function

Dyslipidaemia is also associated with overnutrition and encompasses both hyperlipidaemia of saturated free fatty acids (FFA) and LDL due to a diet rich in animal products and saturated fats, as well as reduced unsaturated fatty acids (omega-3/-6) and HDL. It has long been accepted that FFA, from dietary intake or produced via the breakdown of stored triglycerides, are increased in subjects with obesity and T2D[186–188], and are a known risk factor in the development of CVD[188]. Elevation of FFA has been reported to induce insulin resistance, impair glucose uptake, and reduce the inhibition of hepatic gluconeogenesis. These findings are further corroborated by the finding that acipimox, a niacin derivative which inhibits lipolysis and thus reduces plasma FFA, can improve whole body glucose tolerance and insulin sensitivity in T2D humans[189]. Numerous animal and cell models of elevated FFAs have been associated with various EC pathologies including increased oxidative stress, reduced EC function, inflammation, and mitochondrial dysfunction.

Two of the most common FFAs found in human plasma are the long-chain saturated FFA palmitate (C16:0) and the monounsaturated oleate (C18:1). Palmitate is often used *in vitro* to simulate elevated FFA in cell culture models[190]. In peripheral EC lines including HUVEC, BAE, HMEC and EA.hy926, palmitate has been shown to induce oxidative stress[191–196], activate proinflammatory signalling pathways[195] (including Toll-like receptor [TLR2]/NF-κB[191,197], IL-6[191,197], IL-8[197]), induce apoptosis[191–193,196,198], increase ICAM expression[191,192,194,197,198], increase monocyte adhesion[194,197], increase receptor for AGE (RAGE) expression[196], promote endoplasmic reticulum stress[192], reduce insulin transcytosis[197], reduce insulin sensitivity[195], and dysregulate mitochondrial bioenergetics[194,198]. It has also been proposed that the detrimental effects of palmitate in ECs can be alleviated by oleate[192], highlighting the complex relationship between saturated and unsaturated lipids and how dyslipidaemia may lead to cellular dysfunction.

It is important to note that, similarly to studies into HG, the available literature on palmitate exposure in brain ECs is limited. Zhou and colleagues report that palmitate

exposure in human BMECs indeed, similarly to peripheral EC models, reduces cell viability through increased apoptosis and furthermore impairs mitochondrial membrane potential (MMP)[199].

Dyslipidaemia also encompasses hypercholesterolaemia (that is an increase in VLDL and LDL). The association between high LDL and reduced vascular function is well established, with LDL catabolism being significantly reduced in diseases with high CVD risk such as T2D. Treatment with statins (to increase LDL metabolism and thus lower plasma LDL) shows marked improvements in EC function in humans. Oxidised LDL (oxLDL) is a proinflammatory molecule that is produced when LDL reacts with free oxygen radicals and it is heavily associated with ED and EA. OxLDL is reported to impair eNOS activity and promote foam cell formation, thus exacerbating vascular lesions. Interestingly, another type of cholesterol HDL can reverse oxLDL-mediated eNOS inhibition. Decreased HDL levels are associated with diseases of overnutrition such as obesity and T2D. Furthermore, the two most widely used animal models of atherosclerosis are genetically manipulated to exhibit dysregulated cholesterol metabolism; LDL receptor KO mice ($LDLR^{-/-}$) have delayed clearance of VLDL and LDL, therefore have elevated plasma levels of these lipids, whilst Apolipoprotein E KO mice ($ApoE^{-/-}$) have impaired lipid uptake. This is because ApoE binds to lipids in the blood and transports them throughout the circulatory system. Without ApoE this process is dysfunctional, leading to dyslipidaemia and hypercholesterolaemia.

Native LDL has been shown to reduce endothelial cell viability[200], increase permeability[201], enhance monocyte adhesion[202], induce senescence[203,204], and promote oxidative stress[204] whereas glycated forms of LDL induce apoptosis, induce senescence, and reduce eNOS expression[205]. OxLDL has been reported to induce apoptosis[206–208], increase ICAM[206,209], VCAM[209], E-selectin[209] expression, decrease eNOS expression[206], induce inflammation (TLR4/NF-κB[207], TNFα[208,209], IL-1β[208–210], IL-8[209]), promote oxidative stress[208–210], enhance monocyte adherence[209,210], reduce ATP production[211], and reduce MMP[208].

More recent studies have investigated the effects of oxLDL on brain ECs and have reported that exposure to oxLDL can induce apoptosis[212–214], promote senescence[213], upregulate ICAM[213], VCAM[213,215], and E-selectin expression[215], enhance monocyte adherence[215], promote oxidative stress[213,214], and reduce NO production[213,214].

These results strongly indicate that nutrient excess-associated pathologies such as hyperglycaemia, dyslipidaemia, and hypercholesterolaemia, can alter healthy EC function. Of note is the strong link between nutrient excess and impairments in endothelial cellular respiration. However, in comparison to peripheral ECs, little is known about brain ECs and how they fare under nutrient excess. The current *in vivo* literature is contradictory, and the *in vitro* studies are few and far between, especially regarding nutrient excess. Considering the absolute importance of healthy brain EC function to multiple processes (including cerebral haemodynamics, BBB integrity, nutrient transport) and furthermore that neurological complications are secondary to many metabolic diseases, it is imperative that further research into nutrient excess and brain ECs is undertaken.

1.9 Endothelial cell metabolism

For a long time, EC metabolism was largely overlooked, as they were thought of only as an inert blood vessel lining material. However, study of EC function and metabolism has gained significant interest over the past 20 years, as researchers begin to realise the absolute importance of EC function in health and disease. Most research into EC metabolism and fuel utilisation has been in the field of angiogenesis and tumor vascularisation. Therefore, relatively little is known about the preferred metabolic pathways in cerebral ECs.

It has been reported extensively by Peter Carmeliet's lab that ECs prefer not to maximize ATP production by shunting all of their glucose into oxidative phosphorylation (OXPHOS, 1.10.4), but rely instead on glycolysis (1.10.1) for the vast majority of their ATP[216]. It was reported that coronary ECs anaerobically metabolise 99% of their available glucose (to produce lactate) and only 0.04% of their glucose was oxidized in the TCA cycle. Glucose shunting to aerobic respiration was increased only in glucose concentration lower than

1mM, a phenomenon known as the Crabtree/Warburg effect. Of note is that palmitate and lactate (substrates preferred by cardiac muscle) oxidation by coronary ECs are inhibited in the presence of glucose[216]. It is likely that FAs (1.10.3), as well as lactate (1.10.1), are transported through the coronary ECs to be used by cardiac muscle for fuel[217]. In HUVECs, others also found that glycolytic flux was estimated to be >200-fold higher than glucose oxidation flux[218]. These findings compliment studies that show mitochondrial content is significantly lower in ECs than other cell types; 5% in liver-derived ECs vs. 28% in hepatocytes[219], and that OXPHOS is not the main driver of ATP production in HUVECs[220].

The glycolytic nature of these peripheral ECs may be surprising, as one might assume ECs would make use of their close vicinity to oxygen in the blood. However, there are several benefits that ECs reap by using glycolysis over OXPHOS. Firstly, ROS production (often generated by OXPHOS) is kept to a minimum[221]. Secondly, the lactate produced by the anaerobic glycolysis can function as a pro-angiogenic signalling molecule[222,223]. Third, the oxygen that is not consumed by ECs can diffuse into perivascular oxygen-hungry tissues such as cardiac muscle. Furthermore, although glucose oxidation produces 10 times more ATP per molecule than glycolysis, ATP generation through glycolysis is far more rapid (when glucose is a nonlimiting factor)[224], which would enable sprouting vessels to proliferate during angiogenesis.

Fuel preference in cerebral endothelial cells has not been as extensively studied. Evidence suggests that brain endothelial cells harbor more mitochondria, indicating a higher capacity for OXPHOS[225,226]. Oldendorf and colleagues reported that mitochondrial volume accounted for 8-11% of total cytoplasmic volume in rat brain capillary ECs, which is 2-4 times the mitochondrial volume of peripheral ECs[227]. A study by Doll and colleagues investigated the role of mitochondria in brain EC function, particularly BBB permeability and effects on stroke[127]. The authors reported that inhibiting various parts of the electron transport chain (ETC, section 1.10.4) rapidly increased cell permeability in bEnd.3 cells, but did not induce cell death, indicating that mitochondrial respiration is key to healthy EC function. Wang and colleagues, who reported that rotenone (ETC inhibitor) exposure induced cell damage including

increased oxidative stress and increased lipid peroxidation, corroborated this data[228]. However, contrary to Doll and colleagues, the authors also reported increased apoptosis. Nevertheless, these studies give an insight into the importance of mitochondrial function in EC health, however it remains unclear what brain EC fuel preference is, in both health and disease, due to the lack of studies that directly compare them.

1.10 The hypothalamus

The hypothalamus can be thought of as the control centre of systemic metabolism, but is also involved in mediating circadian rhythm, cognition, hormonal regulation, and reproduction. In the hypothalamus, several groups of neurons communicate with one another to maintain metabolic homeostasis largely through appetite regulation and control of energy expenditure. Among them are the arcuate nucleus, (ARC), dorsomedial hypothalamus (DMH), ventromedial hypothalamus (VMH), paraventricular nucleus (PVN), and lateral hypothalamus (LH). In the ARC, an antagonistic interaction between neurons expressing agouti-related peptide (AgRP) and neuropeptide Y (NPY), and neurons expressing proopiomelanocortin (POMC) constitute the metabolic control centre (Fig. 1.8). Simply put, the AgRP/NPY neurons promote orexigenic behaviour through projections to the LH and PVN[229]. In addition, the Argp/NPY neurons participate in the control of energy expenditure by inhibiting thermogenesis of the brown adipose tissue[230]. The POMC neurons exert anorexigenic behaviour through connections to the PVN, LH, and VMH, and by releasing α-melanocyte-stimulating hormone (α-MSH), a processed protein product of POMC, to activate melanocortin receptors (MC4R) in the target neurons[231]. These processes are sensitive to hormonal signals from the periphery, including leptin, ghrelin, and insulin, as well as availability of nutrients like glucose and FAs. Due to its important role in regulating feeding behaviour and metabolic homeostasis, the ARC must be in close contact with the blood. For this reason, the capillaries comprising the BBB at the ARC are fenestrated, and evidence suggests that there are fewer cell-cell junctions between endothelial cells[232,233]. This allows for rapid diffusion of molecules that would not normally be able to pass through, meaning they can be detected by first order neurons in the hypothalamus that will then act

accordingly. The leakiness of the BBB at this site is obviously an advantage in terms of regulating metabolic homeostasis. However, it poses as a potential disadvantage as the hypothalamus is then vulnerable to the effects of pathologies associated with metabolic syndrome such as chronic hyperglycaemia, dyslipidaemia, and systemic inflammation. Therefore, the hypothalamus is an area of interest regarding nutrient excess and BBB leakiness.

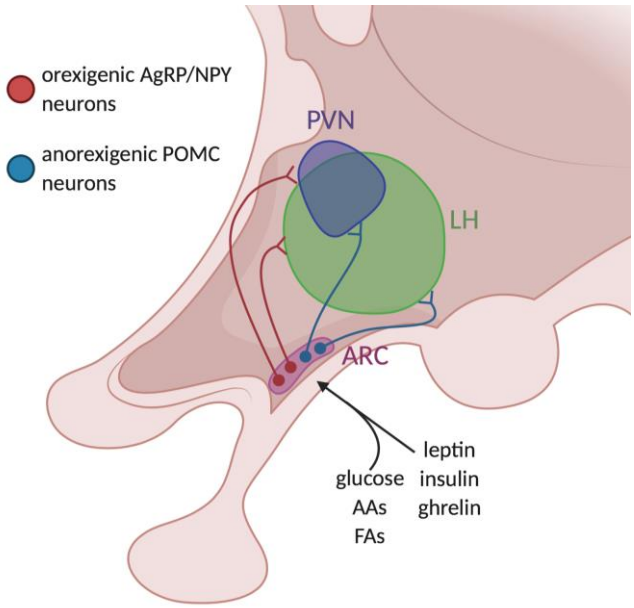

Figure 1.8 Schematic representation of the antagonistic actions of AgRP/NPY neurons and POMC neurons in the hypothalamus

AgRP/NPY neurons originating in the ARC promote feeding and reduce energy expenditure through projections to the LH and PVN. The POMC neurons decreased appetite and increase energy expenditure through connections to the PVN and LH by releasing α-melanocyte-stimulating hormone (α-MSH). These processes are sensitive to hormonal signals from the periphery, including leptin, ghrelin, and insulin, as well as nutrients such as glucose, amino acids (AAs), FAs.

1.11 Cellular respiration

Cells require energy in the form of adenine triphosphate (ATP). This energy is produced through respiration, where the cell utilises fuel (glucose, amino acids, fatty acids) to generate ATP. Healthy cellular respiration is key to the cell's functionality, and when respiration fails, cell stress and dysfunction is likely to occur.

1.11.1 Glycolysis

For a cell to use glucose as fuel, glucose must be converted to pyruvate via a process termed glycolysis (Fig. 1.9), which takes place in the cytosol. This process is anaerobic, meaning it does not require oxygen. Glycolysis produces a relatively low yield of ATP, with each 6-carbon molecule of glucose providing 2 molecules of pyruvate and 2 molecules of ATP. Pyruvate may be metabolised (1.11.2) in order to provide substrate for OXPHOS (1.11.4), or it may be reduced to lactate by lactate dehydrogenase (LDH).

1.11.2 Tricarboxylic acid cycle

Before pyruvate can be further metabolised, it must enter the mitochondria via the mitochondrial pyruvate carrier (MPC), where it is transformed to acetyl coenzyme A (acetyl-CoA) by pyruvate dehydrogenase (PDH). Acetyl-CoA then enters the tricarboxylic acid (TCA) cycle. The TCA cycle (Fig. 1.10) is an important mitochondrial process that generates reducing equivalents to supply the ETC (section 1.10.4).

1.11.3 Fatty acid oxidation

Glucose is not the only source of fuel, and in many cells is not the preferred substrate. FAs found in the plasma, or stored triglycerides (TG), can be broken down and used for fuel via a process known as fatty acid oxidation (FAO; Fig. 1.11). For stored TGs to be used for fuel, they must first be hydrolysed by hormone sensitive lipase (HSL) to become FAs, which can then enter the mitochondria of the same cell for FAO or can then enter the blood to be transported elsewhere for FAO. As FAs are transported across the plasma membrane, it is possible that they are rapidly converted to acyl-coA, due to the

known acyl-CoA synthetase activity of FA transport proteins (FATP) or can be converted by long-chain acyl-coA synthetases (ACSL). The mitochondrial membrane is impermeable to acyl-CoA; therefore, it must use the carnitine shuttle to gain entry. Carnitine palmitoyltransferase I (CPT1) converts acyl-CoA to acylcarnitine. Membrane-bound carnitine acylcarnitine translocase (CACT) exchanges acylcarnitiine for a carnitine molecule from inside the mitochondria, allowing acylcarnitine entry. Once inside, acylcarnitine is reconverted to acyl-CoA by CPT2 ready for FAO. During FAO, acyl-CoA is degraded to acetyl-coA by the process depicted in figure 1.5. Each cycle yields an acyl-CoA that is shortened by two carbons, an acetyl-CoA, one NADH, and one $FADH_2$. The shortened acyl-CoA will enter another round of FAO, acetyl-CoA will enter the TCA, and the electron carriers will deliver electrons to the ETC (see 1.10.4 Oxidative phosphorylation).

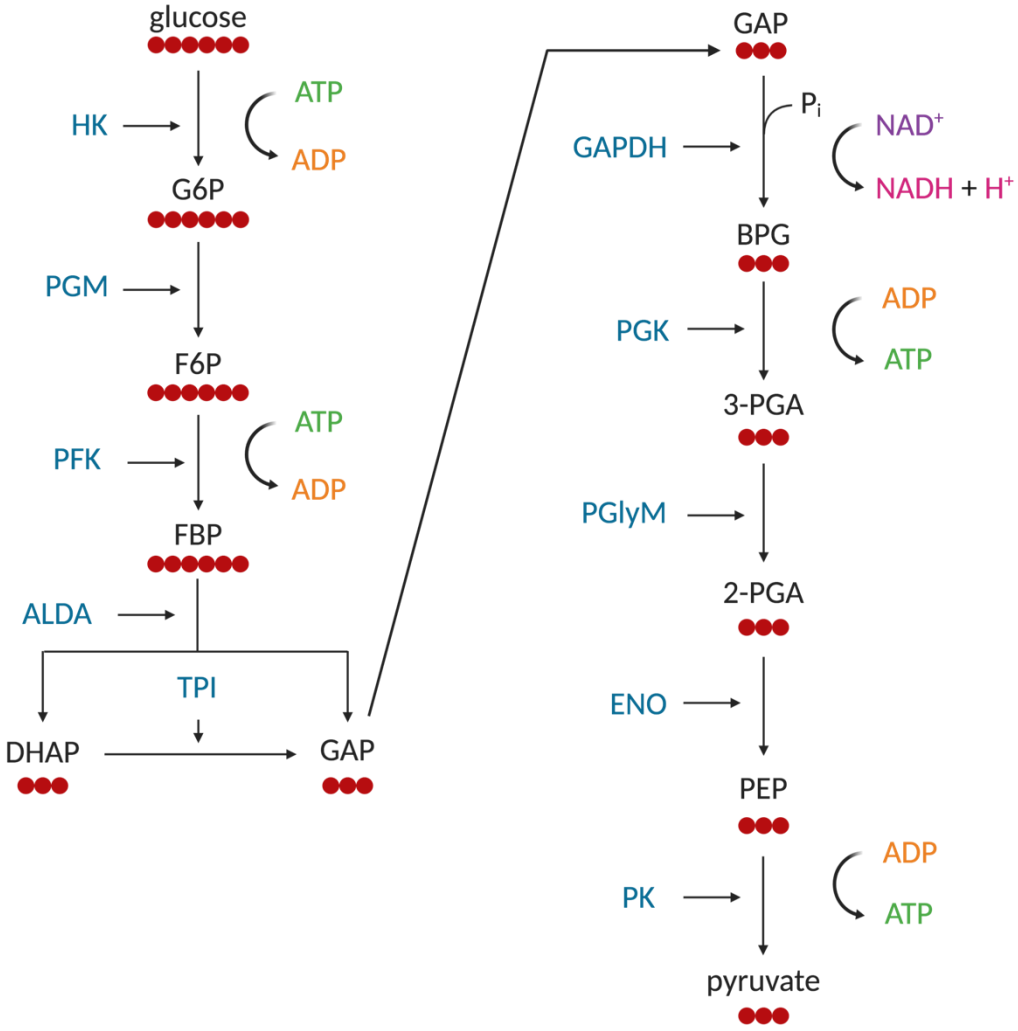

Figure 1.9 Anaerobic glycolysis

To produce ATP from glucose, glucose must undergo conversion into pyruvate via glycolysis in the cytosol. Hexokinase (HK) catalyses the transfer of ATP-derived P_i to glucose, which produces glucose 6-phosphate (G6P). Phosphoglucomutase (PGM) isomerises G6P into fructose 6-phosphate (F6P) before phosphofructokinase (PFK) transfers P_i from an ATP molecule to F6P, producing fructose 1,6-bisphosphate (FBP). FBP is split by aldolase (ALDA) into dihydroxyacetone phosphate (DHAP) and glyceraldehyde 3-phosphate (GAP), which are isomers of one another. DHAP is rapidly converted to GAP by the enzyme triose-phosphate isomerase (TPI). Glyceraldehyde 3-phosphate dehydrogenase (GAPDH) dehydrogenases GAP by transferring a hydrogen molecule to the oxidising agent nicotinamide adenine dinucleotide (NAD+) to form NADH + H^+ and phosphorylates GAP to form 1,3-bisphosphoglycerate (BPG). BPG is dephosphorylated to 3-phosphoglycerate (3-PGA) by phosphoglycerokinase (PGK), producing an ATP molecule. Phosphoglyceromutase (PGlyM) move P_i to the second carbon to form 2-phosphoglycerate (2-PGA). 2-PGA is dehydrated to form phosphoenolpyruvate (PEP) by enolase (ENO), which is then dephosphorylated by pyruvate kinase (PK) to produce pyruvate and ATP.

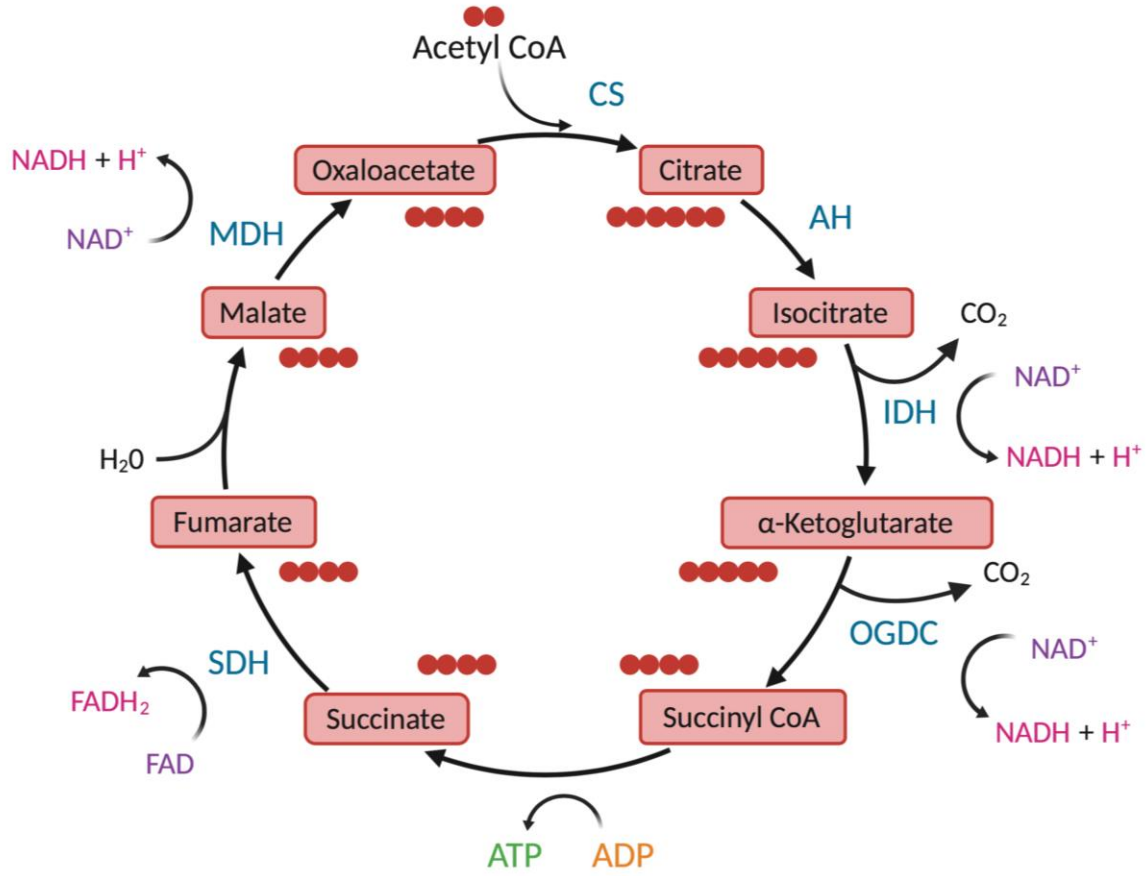

Figure 1.10 The TCA cycle

For pyruvate to be further metabolised for energy, it enters the mitochondria via the pyruvate transporter (PyT) and is transformed to acetyl-CoA by pyruvate dehydrogenase (PDH). Acetyl-CoA then enters the tricarboxylic acid (TCA) cycle. The TCA cycle is an important mitochondrial process that generates reducing equivalents to supply the ETC (see Fig. 1.11). The first step in the TCA cycle is the transfer of an acetate group from acetyl-CoA to oxaloacetate, producing citrate. This step is catalysed by citrate synthase (CS). Aconitase (AH) catalyses the isomerisation of citrate to isocitrate. Isocitrate is converted to alpha-ketoglutarate by isocitrate dehydrogenase (IDH), simultaneously releasing CO_2 a hydrogen molecule and transforming NAD^+ to NADH and H^+. Alpha-ketoglutarate dehydrogenase (OGDC) converts alpha-ketoglutarate to succinyl Co-A and produces CO_2 and NADH and H^+. Following this, succinyl Co-A releases its Co-A group to form succinate. Succinate dehydrogenase (SDH) is a unique enzyme that plays both an oxidation role in both the TCA cycle and OXPHOS. In the TCA cycle, SDH converts succinate to fumarate and reduces FADH to $FADH_2$. Fumarate is converted to malate, which is then oxidized by malate dehydrogenase, forming oxaloacetate alongside NADH and H^+. At the end of each TCA cycle, oxaloacetate is regenerated in order to begin the cycle again.

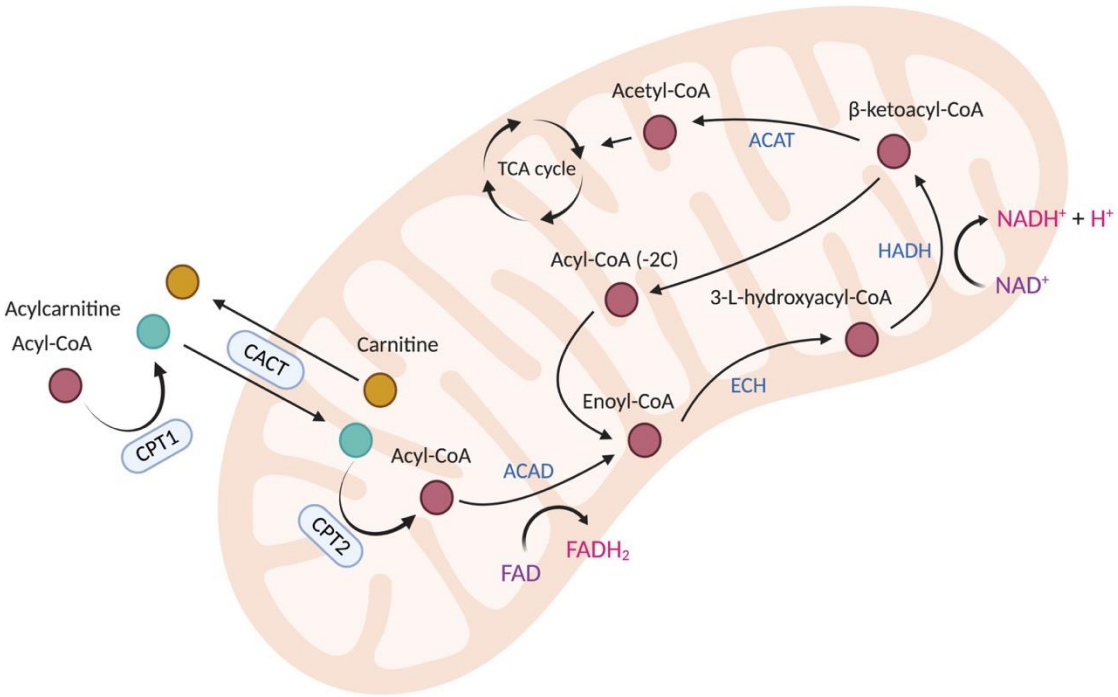

Figure 1.11 Fatty acid oxidation

FAs are converted to acyl-CoA by long-chain acyl-CoA synthetases (ACSL). The mitochondrial membrane is impermeable to acyl-CoA; therefore it must use the carnitine shuttle to gain entry. Carnitine palmitoyltransferase I (CPT1) converts acyl-CoA to acylcarnitine. Membrane-bound carnitine acylcarnitine translocase (CACT) exchanges acylcarnitine for a carnitine molecule from inside the mitochondria, allowing acylcarnitine entry. Once inside, acylcarnitine is reconverted to acyl-CoA by CTP2 ready for FAO. During FAO, acyl-CoA is dehydrogenated to enoyl-CoA by acyl-CoA dehydrogenase (ACAD), which is then hydrated to 3-L-hydroxyacyl-CoA by enoyl-CoA hydratase (ECH). This is then dehydrogenated to β-ketoacyl-coA by short chain 3-hydroxyacyl-CoA dehydrogenase (HADH), which undergoes cleavage by acyl-CoA:cholesterol acyltransferase (ACAT) to form another acyl-CoA molecule 2 carbons shorter than the original acyl-CoA, and acetyl-CoA, which can join the TCA cycle (see Fig. 1.10). The acyl-CoA (-2C) can continue undergoing FAO. Each cycle yields an acyl-CoA that is shortened by two carbons, an acetyl-CoA, one NADH molecule, and one $FADH_2$ molecule.

1.10.4 Oxidative phosphorylation

Oxidative phosphorylation (OXPHOS) is a highly utilised process that cells use to produce ATP as a result of the transfer of electrons from NADH or $FADH_2$ to O_2 by a series of electron carriers named the electron transport chain (ETC). The ETC (Fig. 1.12) consists of respiratory complexes I (NADH–ubiquinone oxidoreductase), II (succinate-ubiquinone oxidoreductase), III (ubiquinol-ferricytochrome *c* oxidoreductase) and IV (cytochrome *c* oxidoreductase; COX). The energy liberated during the oxidation of NADH and $FADH_2$ results in the movement of protons from the matrix to inter membrane space, forming an electrochemical proton gradient across the inner mitochondrial membrane (IMM). This membrane potential is utilised by ATP synthase (otherwise known as complex V) to produce ATP from ADP and one inorganic phosphate (P_i). Therefore OXPHOS can be thought of as an energy transduction system, which is coupled to (i) the substrate oxidation-driven electron transfer, (ii) the mitochondrial membrane potential (MMP), and (iii) ATP production[234]. However, not all energy generated by the ETC is used for ATP production. There exists an unavoidable diffusion of protons back across the IMM (referred to as proton leak) from the inter membrane space to the matrix, due to defects in the integrity of the IMM[235]. The extent of this proton leak indeed determines the coupling efficiency of OXPHOS to ATP production. In addition to proton leak, cells may induce proton leak through expression of uncoupling proteins (UCPs), which are proton ionophores and can pump protons across the IMM[236].

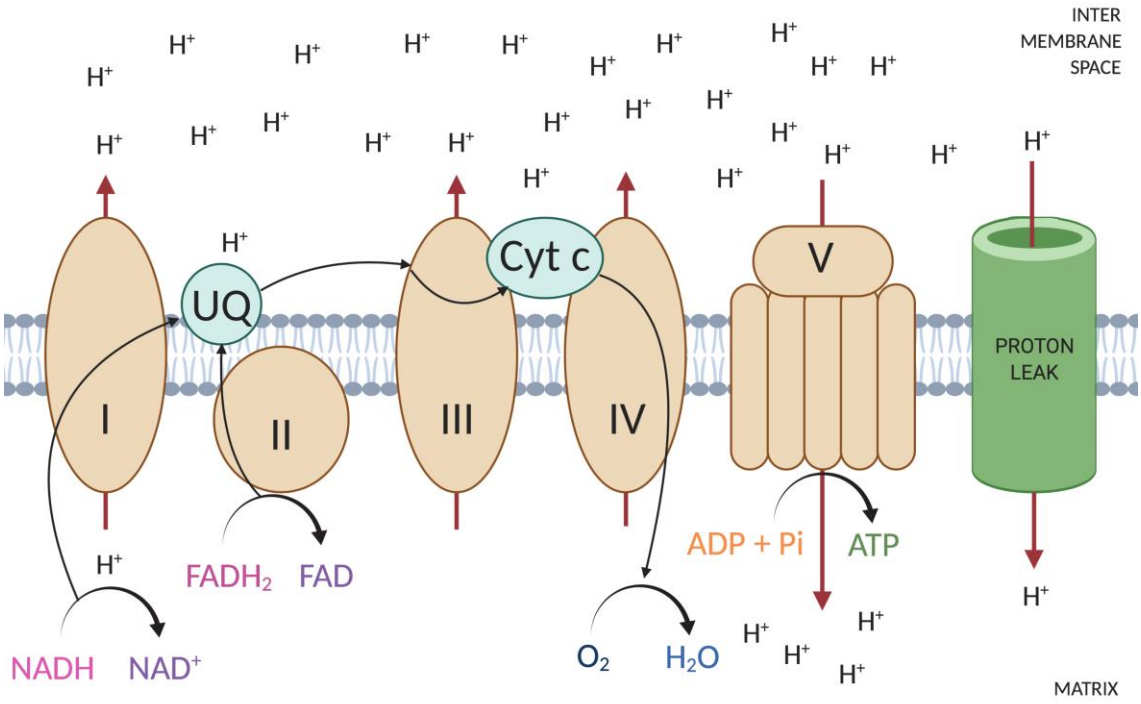

Figure 1.12 Oxidative phosphorylation

Oxidative phosphorylation (OXPHOS) takes place on the inner mitochondrial membrane (IMM). Reducing equivalents from the TCA cycle and FAO are oxidised by the respiratory complexes I and II. The produced electrons are transferred through the ETC. They enter at complexes I and II and are transferred to ubiquinone (UQ) then to complex III then to cytochrome *c* (Cyt c). They finally reach complex IV, where the electrons react with the final electron acceptor, O_2 to form H_2O. During the electron transferals, protons are pumped from the matrix into the inter membrane space through complex I, III, and IV. This results in an electrochemical gradient across the IMM, where the inter membrane space is more positively charged than the matrix. This is referred to as mitochondrial membrane potential (MMP). This electrochemical potential is used by complex V, ATP synthase, which pumps protons back to the matrix and with the energy acquired from that, undergoes a conformation change which facilitates the production of ATP from ADP + Pi. OXPHOS is incompletely coupled to ATP synthesis; protons can bypass ATP synthase and leak back into the matrix.

1.12 Mitochondria

Mitochondria are membrane bound organelles present in almost all eukaryotic cells with the exception of red blood cells. They are thought to have originated when primitive prokaryotic bacteria were engulfed by anaerobic eukaryotes, and then permanently integrated into their structure. This is supported by the fact they carry their own residual genome known as mitochondrial DNA (mtDNA) encoding 13 proteins involved in the ETC[237]. They comprise an inner and outer membrane that separate and maintain regions known as the intermembrane space and the matrix. Mitochondria contribute to many cellular processes such as contributing to providing energy as ATP for the cell (1.10.4 Oxidative phosphorylation), Ca^{2+} signalling, ROS production and signalling, biosynthesis of amino acids, nucleotides, and cholesterol, and cell cycle and apoptotic control[238]. Furthermore, mitochondria are dynamic organelles, and are capable of shifting their shape (dynamics) and positioning (motility) within the cell[239]. They undergo processes known as fission and fusion (mitochondrial dynamics), where mitochondria will separate into 2 or more daughter mitochondria, or 2 or more mitochondria will fuse to create one elongated mitochondrion respectively[239]. Mitochondria number is tightly controlled through this dynamic process, as well as by mitochondrial biogenesis and mitophagy, ensuring a relatively constant mitochondrial population under homeostasis[240]. In certain pathologies, mitochondria can become dysfunctional. This dysfunction may encompass respirational failure, dysregulated mitochondrial dynamics, imbalances in biogenesis/mitophagy, excessive ROS production, or altered Ca^{2+} signalling. Mitochondrial dysfunction has been associated with a number of diseases, especially age-related disorders and diseases of nutrient excess, such as obesity, T2D, CVD, and dementia[241].

1.12.1 Regulation of mitochondrial dynamics

As previously stated, mitochondria are dynamic organelles and the shape is largely dependent on a balance between fission and fusion. It is believed that mitochondrial bioenergetics (i.e. OXPHOS) is strongly dependent on mitochondrial morphology[239]. A number of different proteins have been proposed to contribute to mitochondrial

dynamics, including dynamin related protein 1 (Drp1), mitofusin 1/2 (Mfn1/2) and OPA1 (Fig. 1.13).

Drp1 is a GTPase that resides in the cytoplasm, which attaches and detaches mitochondria in cycles dependent on GTP availability, where high GTP induces recruitment of Drp1 to the outer mitochondrial membrane. Its assembly involves wrapping around the outer membrane of the mitochondria in a ring-like structure to facilitate fragmentation of the double membrane[242]. Some proteins have been suggested as docking receptors for Drp1, including Fis1 and mitochondrial fission factor (Mff), but the involvement of these proteins remains unclear. The role of Drp1 is absolute, however, in both mitochondrial morphology and in overall health; a study testing 4 different non-function mutations of Drp1 found that mitochondrial connectivity was greatly increased[243], with the mitochondria appearing highly hypertubulated. Additionally, a person born with a dominant-negative Drp1 allele presented with extensive metabolic defects as well as abnormal neural development and died 37 days after birth[244]. Furthermore, Drp1 knockout mice have severe developmental abnormalities and are embryonic lethal[245]. Interestingly, the assembly of Drp1 involves formation of helices that are smaller than the diameter of the average mitochondria, suggesting that additional factors are indeed required to constrict the organelle and perform the scission action[246].

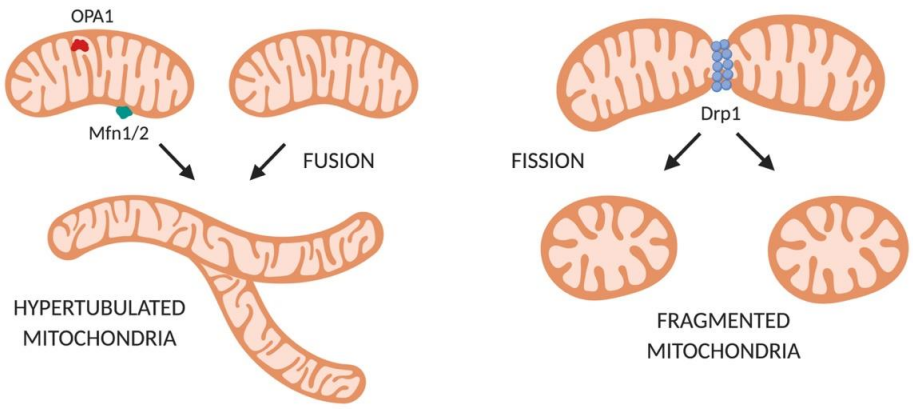

Figure 1.13 Mitochondrial dynamics

Mitochondria can undergo fusion or fission events to form hypertubulated or fragmented mitochondria respectively. OPA1 and Mfn1/2 are the primary modulators of fusion, whereas fission is regulated by Drp1.

Mitochondrial fusion requires fusion of both the inner and outer mitochondrial membranes in a two-step process. IMM fusion is controlled by Optic atrophy 1 (OPA1), a dynamin-like protein that resides in the inner mitochondrial membrane. A total of 8 isoforms of OPA1 are known, and it has been reported that homeostatic morphology of mitochondria is greatly dependent upon OPA1 cleavage and the balance of the long and short isoforms of OPA1[247]. Outer mitochondrial membrane (OMM) fusion is controlled by GTPases Mfn1 and 2. Genetic deletion experiments reveal that both Mfn1 and 2 are required for mitochondrial fusion[248], although tissues do show differing expression patterns. For example, Mfn2 is expressed more than Mfn1 in the brain, but the opposite is true for the heart[248]. It is thought that Mfn1/2 have a role in tethering mitochondrial membranes[249], but the exact mechanism as to how they control OMM fusion are unknown.

1.12.2 Functionality of mitochondrial dynamics

It has become apparent from numerous studies that the purpose of this tightly regulated fission/fusion process goes beyond the mere appearance of mitochondria and likely there is a functional role. Fission and fusion could be proposed as an inherent adaptive response that the mitochondria utilise to respond to cellular demand or stress. Healthy, normal cells respond to acute cellular stressors, partly by regulating mitochondrial dynamics, to restore cellular homeostasis. Issues arise when stress becomes chronic, leading to abnormal control of mitochondrial dynamics, resulting in mitochondria being ‘stuck’ in the fused state, or rendering them incapable of undergoing fusion at all. If fission is left unregulated, it may lead to a heterogeneous population of organelles with differing mtDNA distribution, as well as a reduced ability to produce ATP, increased mitochondrial ROS (mROS) production and increased apoptosis. If fusion is left unregulated, fused mitochondria can no longer expel their damaged parts, potentially leading to a reduced ability to produce ATP, as well as increased mROS production. It is clear, therefore, that fission and fusion work in concert to maintain the shape, size, number and overall health status of mitochondria.

One of the most important consequences of fusion is the mixing of mitochondrial content. The mixing of content of the inner matrix seems critical, as the mitochondrial defects studied in OPA1-null cells are as severe as Mfn-null cells. Thus even when some outer membrane fusion is preserved, this is not sufficient to preserve mitochondrial function, suggesting inner matrix fusion is crucial[250]. Interestingly, fusion assays have shown that content mixing can occur between mitochondria even when the duration of their fusion event is extremely short-lived; this has been termed 'kiss-and-run'[251]. This event has been observed to occur very frequently, highlighting its potential functional importance. Further studies need to be undertaken to elucidate this process; however, the model described below has been proposed by David Chan. Mitochondria have proteins that are encoded by their own mtDNA, but other important proteins that are required for mitochondrial function are imported from the cytosol. This means that individual mitochondria have the potential to act autonomously and have their own unique biochemical and functional profile, separate from other mitochondria. This would cause mitochondria to diverge. However, during fusion events contents of the mitochondria involved are briefly mixed and this may lead to more homogeneity between mitochondria, allowing them to function as a unit. Indeed, OPA-1-null and Mfn-null cells exhibit greater mitochondrial heterogeneity[252]. Content mixing may also allow dispersing of mutant mtDNA, meaning that mitochondria can share the load, and harbor mtDNA mutations without any functional consequence. When mitochondrial fusion is disrupted the reduction in content mixing may be partly responsible for functional defects, such as reduced respiratory capacity. A mouse model carrying an error-prone mtDNA polymerase cannot tolerate dysfunctional fusion, corroborating this hypothesis[253]. An alternative view is that fusion events in this setting may in fact be detrimental, allowing persistence and spread of mutant mtDNA[254]. OPA1-null and Mfn-null cells also exhibit reduced mtDNA nucleoid content, as well as defects in the distribution of mtDNA nucleoids throughout the mitochondrial population[253,255]. As mtDNA genome codes for crucial subunits of the ETC, nucleoid-lacking mitochondria are respiratory deficient. Indeed, reduced respiratory capacity has been observed in mouse embryonic fibroblasts[252], Purkinje cells[255], and skeletal[253] and cardiac myocytes[256] that lack either OPA1 or Mfn1/2. OPA1-null embryonic fibroblasts also exhibit severely abnormal cristae structure, which could potentially play a part in the respiratory defects.

Mitochondrial dynamics has also been implicated in mitochondrial-dependent apoptosis. For apoptosis to commence, mitochondria must release cytochrome *c*, amongst other pro-apoptotic factors, into the cytoplasm. Frank and colleagues have reported that mitochondria undergo increased fission and fragmentation close to the time of cytochrome *c* release and, interestingly, when Drp1 is inhibited, thus preventing mitochondrial fission, this prevents cytochrome c release, inhibiting cell death[257]. Other studies confirm this[258,259], whilst fusion has been reported to be anti-apoptotic[260,261]. The role for Drp1 in regulating apoptosis has however been disputed by studies involving the Drp1 KO mouse[262], amongst others[263,264]. Clearly, further investigation into the connection between fusion/fission and apoptosis needs to be performed.

1.12.3 Mitochondrial dysfunction due to nutrient excess

Mitochondrial dysfunction is associated with many metabolic and cardiovascular disorders. The capacity of an organism to adapt to different fuel availabilities is known as metabolic flexibility[265] . For example, a healthy cell should have the ability to switch from TG breakdown and FA metabolism in a fasted state, to suppression of FA oxidation and enhanced glucose oxidation and upon stimulation with insulin (post-prandial)[266]. Healthy mitochondria can adapt to acute nutrient overload and increase their function to burn excess metabolites, usually with a subsequent physiological increase in ROS[267]. However, when nutrient excess becomes chronic and persistent, the oxidative capacity of mitochondria may be unable to efficiently burn the excess nutrients, resulting in nutrient overload in the cell (Fig. 1.14). This may lead to impaired respiratory capacity and ATP production, increased mROS, dysregulated Ca2+ signalling, and potentially apoptosis.

Nutrient excess may cause mitochondrial dysfunction by saturating the TCA cycle and ETC, which would in turn reduce the capacity of the mitochondria to recycle electron acceptor molecules, highlighted in multiple HFD animal studies in varying tissues[268–271]. Furthermore, HFD has been shown to reduce MMP, thus affecting the rate of ATP generation[272]. Increased mROS production has been suggested as a major consequence of over-nutrition, with HFD and high-sucrose diet animal studies reporting increased

mitochondrial-derived H_2O_2 levels compared to controls[273]. Exposure to lard oil induced mitochondrial swelling in primary rabbit hepatocytes[274], whilst high saturated fat-feeding in mice decreased PPAR-γ coactivator 1-α (PGC1α) expression (potentially reducing mitochondrial biogenesis) and decreased enzymes associated with fatty acid oxidation and with the TCA cycle in epididymal white adipose tissue, indicating impaired mitochondrial function[275]. A study investigating high-saturated fat diet (HSD) on hepatic mitochondrial function in rats reported that HSD reduced mitochondrial respiratory capacity and increased ROS production[276]. *In vitro* studies have also furthered the understanding of how nutrient excess may lead to mitochondrial dysfunction. Palmitate exposure in both rat and human myoblasts impaired ATP production and furthermore altered how this ATP was used to fuel ATP-consuming processes, such as *de novo* protein synthesis, sodium pump activity, and DNA/RNA synthesis[277]. In a similar study, palmitate exposure in differentiated rat and human myotubes enhanced proinflammatory signalling pathways, promoted ROS generation, reduced mitochondrial respiratory capacity, reduced protein and mRNA expression of proteins key to mitochondrial function (e.g. PGC1α), and an increase in mitophagic particles[278]. Interestingly, however, palmitate was only able to induce these effects when glucose was present. When glucose was absent (either absent from the media or by using 2-deoxyglucose [2-DG]), it seemed that the cells were metabolically flexible enough to switch to using palmitate as fuel. These data suggest that the nutrient oversupply with both glucose and palmitate together poses a major substrate burden on mitochondria. It has been previously suggested that FAs not undergoing oxidation will accumulate as FA derivatives such as diacylglycerols and ceramide. These substances have been shown to further suppress mitochondrial activity.

Indeed, mitochondrial exhaustion due to nutrient burden has been reported in many cell types and tissues, ranging from hepatocytes[274], to neurons[279], to skeletal muscle cells[277]. Some researchers report similar findings in ECs. Cultured peripheral ECs grown in HG (25mM) exhibited reduced basal mitochondrial respiration compared to ECs grown in LG (5mM), which further decreased as duration exposed to HG conditions increased[280]. Interestingly, chronic HG exposure seems to reduce carbohydrate oxidation (pyruvate, glucose), but enhance lipid and amino acid oxidation (glutamine,

palmitate), suggesting a switch in metabolic preference in HG conditions. Indeed, the authors report that they observed a shuttling of glucose toward anaerobic glycolysis rather than oxidation. Switching oxygen usage toward glutamine and fatty acid oxidation may be a mechanism to increase anaplerosis and replenish TCA intermediates. The chronic HG exposure in these cells also induced oxidative stress. Peripheral ECs cultured for 6 days in physiologically normal palmitate concentrations (100-150µM) exhibited reduced mitochondrial capacity compared to control, as well as increased ICAM expression and increased superoxide production[198]

Mitochondrial dynamics is also vulnerable to nutrient excess. Cells exposed to nutrient rich environments tend to exhibit more fragmented mitochondria, and nutrient-starved cells tend to remain in their fused state for longer[281,282]. HSD feeding in rats also promoted fission over fusion by reducing Mfn2 and OPA1, and increasing Drp1 protein expression[276]. Nisr and colleagues also reported that exposure to nutrient overload (glucose and palmitate together) in rat myotubes resulted in a higher percentage of fragmented mitochondria, measured via confocal microscopy, which was accompanied by a modest increase in Drp1 and a modest decrease in Mfn2 protein expression[278]. These data, suggesting nutrient excess leads to mitochondrial fission, has been corroborated by others[283,284].

1.12.4 ROS production

Mitochondria are an important site for ROS production. The main species produced by mitochondria is the superoxide anion (O_2^-), which is formed when O_2 undergoes a one-electron reduction. This reduction usually takes place at a redox-active center of a contributing protein (flavin mononucleotide, FeS center), or when electron donors (such as reduced coenzyme Q $CoQH_2$) are bound to proteins, such as mitochondrial respiratory complexes[285]. Complex I is thought to contribute significantly to superoxide production[286], but only under conditions which result in reverse electron transport (RET, Fig. 1.15). This occurs when electrons are transferred backwards from complex II to complex I through coenzyme Q, reducing NAD+ to NADH. It has been shown that this backwards movement of electrons produces high levels of O_2^-, due to coenzyme Q

(ubiquinone) becoming oversaturated in its reduction ability[287]. Electrons will then be transferred to O_2. An oversupply of substrates to the ETC (hyperglycaemia, hyperlipidaemia), coupled with no complimentary increase in cellular ATP demand, may result in increased movement of electrons through the ETC, a high electrochemical mitochondrial membrane potential, increased RET, and therefore increased O_2^- production[287].

Interestingly, induction of uncoupling of mitochondria (by UCPs for example), which will dissipate the high membrane potential, is protective against O_2^- production[286,288]. Additionally, Dikalov and colleagues have shown that endothelial mitochondrial $O_2^{\cdot-}$ production may be dependent on NOX (Nox2 isoform in endothelial cells) activation, leading to the activation of RET[289]. Nutrient excess has also been linked to increased Nox2 activity[290].

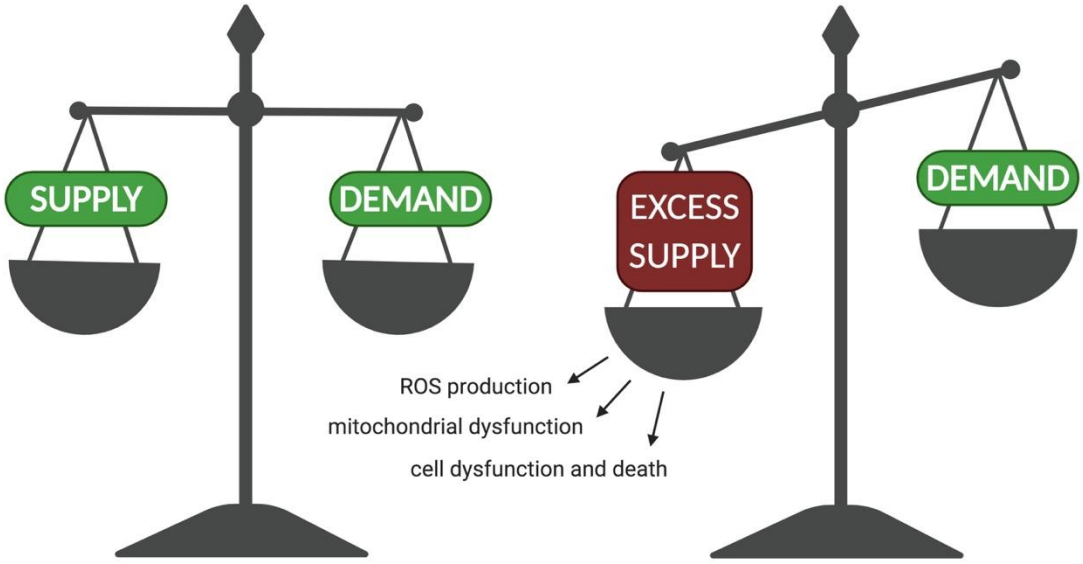

Figure 1.14 Regulation of cellular bioenergetics – supply and demand model

In a balanced/healthy state, the **'supply'** of nutrients is generally sufficient to sustain cellular **'demand'**. Nutrient excess characterised here as **'excess supply'** in the absence of an increased cellular **'demand'** results in a fuel-associated burden on the cell. The mitochondria can adapt to begin with, upregulating uncoupled mitochondrial respiration, i.e. inefficient waste of fuel in the form of heat. However, if the nutrient excess is chronic, the mitochondria will eventually become overwhelmed. Fuel that is not being used (to create ATP for cellular 'demand' or to waste energy as heat) may accumulate, leading to ROS production, mitochondrial dysfunction, and eventually cellular dysfunction and apoptosis.

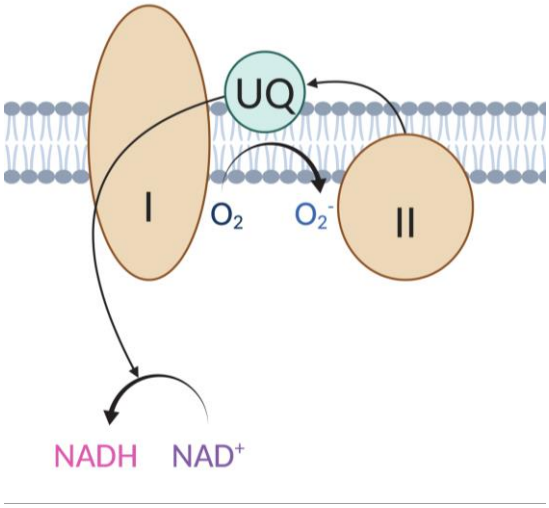

Figure 1.15 Mechanism of reverse electron transport and superoxide production

RET occurs when electrons are transferred backwards from complex II to complex I through ubiquinone, reducing NAD+ to NADH. Ubiquinone can become overwhelmed in its reduction ability, meaning electrons will then be transferred to O_2, producing high levels of O_2^-. An oversupply of substrates to the ETC, accompanied by no increase in cellular energy demand, may result in increased movement of electrons through the ETC, a high electrochemical mitochondrial membrane potential, increased RET, and therefore increased O_2^- production.

1.13 BACE1

Beta-site APP cleaving enzyme 1 (BACE1) is a membrane-associated aspartic protease, recognised as the β-secretase responsible for cleaving amyloid precursor protein (APP) in the amyloidogenic pathway[291]. BACE1 activity is thought to be highest in neurons, however BACE1 is expressed in multiple other tissues, including adipose tissue, endothelium, and muscle. BACE1 structurally consists of an N-terminal signal peptide sequence, a propeptide, a catalytic domain, a transmembrane domain and a cytoplasmic carboxy-terminal[291]. Importantly, BACE1 is subject to various post-translational modifications including cleavage to become mature BACE1, as well as palmitoylation and glycosylation. Indeed, an immature form of BACE1; pro-BACE1, with a molecular weight of approximately 58kDa is synthesised in the endoplasmic reticulum ER, which rapidly undergoes maturation in the golgi apparatus[292]. This stable and mature form of BACE1 runs during gel electrophoresis at approximately 70kDa, which is a greater mass than predicted for the protein suggesting BACE1 undergoes glycosylation[293]. BACE1 is most widely known for its role in cleaving APP but it is a promiscuous enzyme, which has been suggested to have at least 68 substrates[294]. Validated BACE1 substrates include the transmembrane proteins LDL receptor-related protein (LRP)[295], neuregulins 1 and 3[296], P-selectin glycoprotein ligand-1 (PSGL-1)[297], voltage-gated sodium channel β1-4 ($Na_v\beta_{1\text{-}4}$)[298], and IL-1 type II receptor (IL1R2)[299]. These proteins have been implicated in lipid metabolism, myelination, leukocyte recruitment, neuronal excitability, and inflammatory responses respectively. We have also identified the insulin receptor as a potential substrate for BACE1[300]. These data suggest a role for BACE1, independent of amyloid, in both general regulatory physiology as well as pathophysiology of a range of neurological and metabolic disorders.

1.13.1 APP processing

The Alzheimer's-related protein Aβ is produced by the cleavage of its parental amyloid precursor protein (APP), carried out by the enzyme complexes β- and γ-secretase. There is another secretase, denoted α-secretase, that can also cleave APP. ADAM10 is likely to be the main α-secretase in the brain. BACE1 has been identified as the primary β-

secretase[19], and the γ-secretase is a protein complex consisting of presenilin 1 and 2 (PS1/PS2), nicastrin, anterior-pharynx defective1 (aph1) and presenlin enhancer 2 (Pen-2).

APP processing can be either non-amyloidogenic or amyloidogenic (Fig. 1.16), existing in a ratio of approximately 9:1 non-amyloidogenic:amyloidogenic. In the preferred non-amyloidogenic pathway, α-secretase cleaves APP at a site 83 amino acids from the C-terminus. It is important to recognise that at this step the α-secretase cleaves APP in such a way that the production of toxic Aβ from APP is not possible. This cleavage results in the release of the ectodomain termed soluble-APP α (sAPPα) into the extracellular space and the retention of membrane-bound C83, which is subsequently cleaved by γ-secretase to produce the short p3 fragment. During amyloidogenic processing, APP is cleaved by β-secretase (i.e. BACE1) at a site 99 amino acids away from the C-terminus. This releases soluble-APP β (sAPPβ) and a peptide termed C99 is retained in the membrane. γ-secretase then cleaves C99 at varying sites, resulting in the production of Aβ peptides of different lengths, most notably $A\beta_{1\text{-}40}$ or $A\beta_{1\text{-}42}$[301]. Indeed, C-terminal truncation of Aβ is determined by where the γ-secretase cleaves. A number of different forms of Aβ can be produced at this step. For example, a significant proportion of the Aβ found in the human AD brain consists of $A\beta_{x\text{-}40}$, where x is anything from 2-11[302]. N-terminal truncated Aβ is thought to be produced as degraded product but emerging evidence suggests BACE1 may cleave APP at different sites depending on its location in the cell (ER, golgi body). Furthermore, Aβ species can be pyroglutamated ($A\beta_{pE3}$) at the N-terminus[303] and this form of Aβ has been reported to be present in high abundance in AD brains[302]. However, the fact remains that $A\beta_{1\text{-}40}$ and $_{1\text{-}42}$ are considered the most relevant; although only approximately 10% of Aβ produced consists of $A\beta_{1\text{-}42}$, it is more prone to fibril formation and is the predominant form found in senile plaques.

Amyloidogenic processing can be considered a stress response. Under certain stressors and disease states, there is a shift in APP processing toward the amyloidogenic pathway. Amyloidogenic processing of APP has been reported to increase during ageing[304] and in the presence of metabolic disorders[305–311]. Indeed, BACE1 expression and activity increase in response to oxidative stress[312], hypoxia[313], nutrient excess,[306,308], and

inflammation[314], pathologies that are known to be associated with not only metabolic disorders, but also neurodegenerative diseases. This concept is further elaborated on in section 1.13.2.

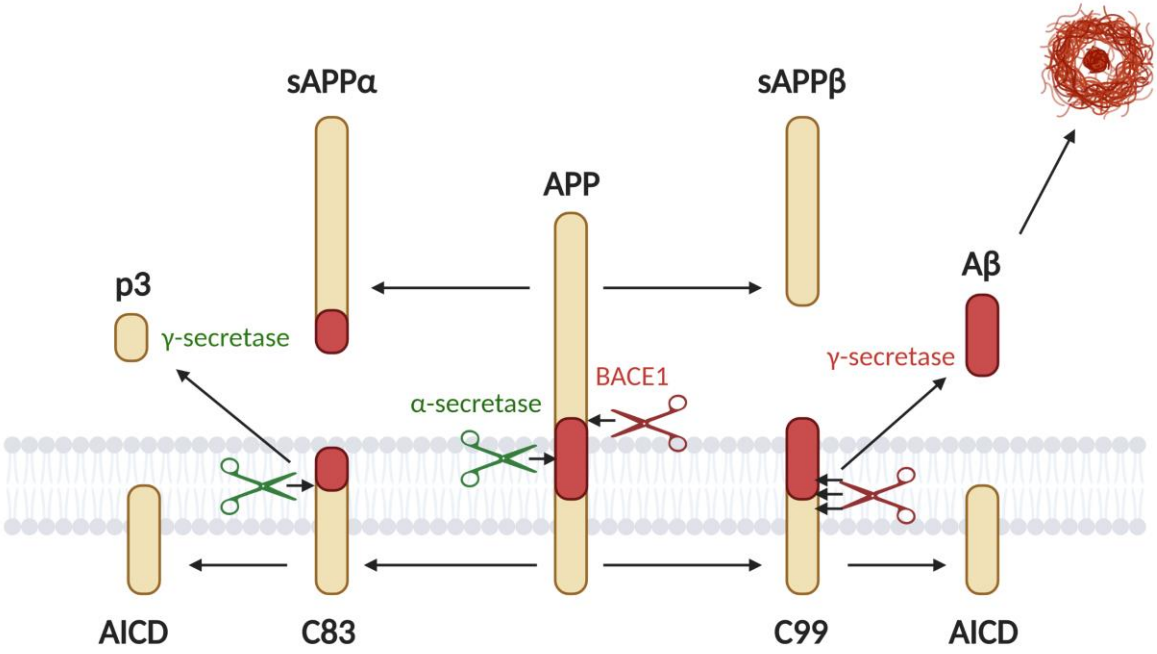

Figure 1.16 APP processing

APP can follow either an amyloidogenic pathway or a non-amyloidogenic pathway. In the non-amyloidogenic pathway, APP is cleaved by an α-secretase to form sAPPα and a membrane bound fragment C83. C83 is cleaved by γ-secretase to form a membrane bound fragment AICD, and an extracellular fragment p3. In the amyloidogenic pathway, APP is cleaved by BACE1 (at a different site than α-secretase) to form sAPPβ and the membrane bound fragment C99. C99 is cleaved by γ-secretase at varying sites to form the membrane bound fragment AICD and Aβ peptides of varying length. Of note is that α-secretase cleave APP at a site (shown in red) that makes it impossible for Aβ peptides to be produce, hence 'non-amyloidogenic'.

1.13.2 APP, BACE1, Aβ, and nutrient excess

Numerous studies have indicated that nutrient excess can influence BACE1 expression and activity. We have shown that BACE1 protein expression is increased by exposure to palmitate, and its derivative ceramide in differentiated C_2C_{12} myotubes[306], and that HFD-feeding in mice significantly increases hypothalamic BACE1 mRNA and protein[308], as well as BACE1 protein in adipose tissue[315]. HFD-feeding in these mice also increased hypothalamic sAPPβ and $Aβ_{42}$ protein levels, indicating increased BACE1 activity. Our collaborators corroborate these data, showing a HFD-dependent increase in BACE1 protein and mRNA in murine muscle tissue[307]. BACE1 levels are also increased in the livers of the diabetic mouse model db/db[300]. Most recently, we reported that HFD feeding increases aorta and plasma $Aβ_{42}$ in mice[316]. We also observed that in humans, BACE1 mRNA is increased in mammary arteries and adipose tissue of obese individuals, and $Aβ_{42}$ is increased in plasma from people with T2D, and this increase correlates with HbA1c. (Botteri and colleagues further report increased BACE1 levels in adipose tissue and increased sAPPβ in plasma from people with T2D[307].

In terms of animal models of metabolic disorders, APP, BACE1, and Aβ have all been proposed as potential mechanisms of disease progression. We first reported in 2012 that mice genetically void of BACE1 (BACE KO) are protected against HFD-induced obesity, have improved glucose tolerance, and improved insulin sensitivity[317], which is partly dependent upon adipocyte-BACE1 (unpublished data). The APP(SWE)/PSEN1 mouse model of AD, which presents with increased Aβ deposits in brain tissue, exhibits impaired glucose tolerance even when fed a normal chow diet[310]. Short-term HFD (8 weeks duration) led to hypervulnerability to diet-induced weight gain, fasting hyperglycaemia, and reduced glucose tolerance in APP(SWE)/PSEN1 mice compared to controls[310]. Neuronal knock-in of BACE1 induces systemic diabetes, in that it causes impaired glucose tolerance and increased adiposity, alongside a fatty liver phenotype[309,311]. We reported in 2018 a role for BACE1 and Aβ in the development of obesity. We found that BACE1 KO mice are protected against diet-induced leptin resistance, in that the leptin-induced reduction in food intake is retained in these mice, with reduced hypothalamic NPY and AgRP expression, and increased POMC and CART

expression[308]. Furthermore, pharmacological inhibition of BACE1 rescued diet-induced leptin resistance. Due to our findings that $A\beta_{42}$ was increased in hypothalamic tissue, we intracerebroventricularly (icv) infused HFD-fed mice (6 weeks on diet) with $A\beta_{42}$ versus scrambled peptide (ScrP) control and showed that $A\beta_{42}$ infusion caused hypervulnerability to HFD-induce leptin resistance, with mice gaining more weight and being hyperphagic[308]. Our collaborators have also shown that injecting mice with sAPPβ intraperitoneally reduces insulin sensitivity[307]. Additionally, Franck Peiretti's group exhibited a role for BACE1 in cleaving the insulin receptor, resulting in blunted insulin signalling[300]. Indeed, both BACE1 expression and plasma concentrations of cleaved insulin receptor (IRsol) are increased in db/db mice, whilst BACE1 KO mice exhibited reduced levels of IRsol.

Aside from metabolic dysfunction, APP, BACE1, and Aβ have been implicated in the development of vascular disorders. BACE1 is expressed in both peripheral[318], and brain endothelium[319], and its expression and activity is susceptible to stress such as endothelial cell senescence[318]. As previously mentioned, we have also confirmed the expression of BACE1 in mouse aortic and human temporal arterial ECs[316] and have further exhibited that BACE1 expression is increased by HFD-feeding (mice) and in obesity[305,307,317]. When we investigated endothelial function in our $BACE1^{-/-}$ mouse, we found that HFD-induced reductions in *in vivo* endothelial function were not as pronounced in $BACE1^{-/-}$ mice and furthermore mice lacking BACE1 exhibited increased aortic phospho-eNOS and phospho-PKB protein expression, and decreased ICAM expression[316]. Others report that overexpression of APP in mice resulted in a profound defect in neurovascular coupling, with a reduction in response of CBF to a somatosensory stimulus (whisker stimulation)[320]. *In vivo* CBF studies report that $A\beta_{1\text{-}40}$, but not $A\beta_{1\text{-}42}$ can impair neurovascular coupling (induced by whisker stimulation)[320] and induce vasoconstriction in cerebral arteries independently, an effect that can be partly rescued by superoxide scavenging agents SOD and MnTBAP[321] and NADPH-oxidase inhibition[322]. Further studies reported that the Aβ-dependent reduction in CBF was associated with reduced glucose utilisation[323]. This study was completed in a mouse model of cerebral amyloid pathology, but at a time point prior to plaque formation, suggesting that impairments to CBF and glucose metabolism due to smaller Aβ species

may be an early event in dementia progression. Park and colleagues corroborated this using the Tg-SwDI mouse model of amyloid. At 3 months of age when no amyloid deposition is present, mice still exhibited marked reductions in endothelium-dependent CBF regulation, a pathology that worsened with age[324]. These data highlight that endothelial dysfunction, due to increases in small Aβ species, may precede multiple dementia-causing diseases. However, it is important to note that many studies involving Aβ use knock-in animal models with extremely high levels of Aβ peptides that are not seen in human disease, or they use very high supraphysiological concentrations of Aβ (up to 10μM) that are topically applied directly to the cortex 30 minutes before CBF measurement, which is not physiological. A more useful study would be a chronic infusion of a physiological concentration of Aβ peptides and investigate *in vivo* how this may affect endothelial function. We undertook this investigation, and found that chronic peripheral $A\beta_{42}$ infusion at physiological concentrations on a HFD-fed background (1 week diet, 4 weeks further infusion and diet) reduced endothelial-dependent vasodilation *in vivo*, and reduced aortic phospho-eNOS and phospho-PKB expression and promoted ICAM expression when compared to ScrP control mice[316]. The physiological concentration of Aβ for these infusion studies was determined by the level that is found in murine plasma after 20 weeks HFD[316].

Perhaps paradoxically, Austin and colleagues reported that it is in fact the ED that precedes increased Aβ[325]. eNOS KO mice displayed increased brain APP and BACE1 expression, and $A\beta_{40}$ and $A\beta_{42}$ production compared to control. This is unsurprising, considered APP and BACE1 protein levels are reported to increase under many cellular stresses, including oxidative stress[326]. Indeed, lack of eNOS or eNOS function is associated with increased oxidative stress[327,328], and it may be that the elevated brain APP and BACE1 expression, and $A\beta_{40}$ and $A\beta_{42}$ production compared is due to the oxidative stress phenotype. However, it must be considered that there may exist a feed-forward mechanism, in that raised BACE1 activity and Aβ production due to nutrient excess reduced eNOS activity, which can in turn further induce BACE1 activity.

1.13.3 APP, BACE1, Aβ, and mitochondria

APP processing has been implicated in regulating mitochondrial function. APP is localised to the mitochondrial outer membrane in AD human brains[329], and mitochondrial Aβ accumulation is seen in AD human and transgenic AD mouse model brain tissue[245,330]. Of interest, mitochondrial Aβ accumulation in AD mouse models was seen prior to Aβ plaque deposits, again suggesting that Aβ-dependent metabolic dysfunction might precede disease onset[331].

Multiple animal APP transgenic studies have demonstrated a role for APP processing in mitochondria dysfunction. Hauptmann and colleagues reported reduced mitochondrial capacity, reduced MMP, and reduced ATP production in isolated brain mitochondria from Thy-1 APP mice, a double Swedish and London mutant APP transgenic mouse[332]. This data was corroborated by Keil and colleagues, who used the same mouse model and demonstrated reduced ATP levels and MMP in brain tissue[333]. In addition, Caspersen and colleagues observed, in a human mutant APP mouse, reduced oxygen consumption and reduced enzymatic activity of proteins involved in OXPHOS[331]. *In vitro*, APPswe overexpression in a neuronal cell line increased ROS production, decreased MMP, and reduced ATP production[334]. Aside from respiratory function, APPswe overexpression has been observed to impair mitochondrial morphology and distribution. Indeed, Wang and colleagues demonstrated a higher percentage of fragmented mitochondria via electron microscopy in cells overexpressing APPswe, as well as a reduction in OPA1, Mfn1/2, and an increase in Fis1 protein expression[334]. These defects were rescued through BACE1 inhibition, indicating the detrimental effects caused by APP overexpression may be dependent on sAPPβ or Aβ. The authors also report a positive correlation between the concentration of Aβ in cellular media and the percentage of cells that exhibited extensive fragmented mitochondria. It has been demonstrated that BACE1 overexpression in cultured skeletal muscle myotubes impairs glucose metabolism and reduced mitochondrial oxygen consumption, an effect that can be rescued by BACE1 inhibition[306]. BACE1 overexpression in neuronal SH-SY5Y cells also altered glucose metabolism, by inhibiting glucose oxidation, and compensating by

increasing glycolysis[335]. BACE1 overexpression also reduces alpha-ketoglutarate dehydrogenase and isocitrate dehydrogenase, indicating BACE1-dependent lesions in TCA cycle activity. Furthermore, BACE1 overexpression lead to a reduction in PDH, thus uncoupling glycolysis from OXPHOS. In our BACE1$^{-/-}$ model, we also observed increases in UCP2 and UCP3, indicating reduced metabolic efficiency[317]. These data suggest that in the present of raised BACE1, mitochondria have a reduced capacity to cope with metabolic stressors, resulting in mitochondrial dysfunction.

The literature is lacking in terms of amyloid and endothelial mitochondrial function. Vessels exhibiting CAA exhibit reduced haemodynamics and integrity, however it is unclear the extent to which mitochondria contribute to this. One study investigated the effects of Aβ40-Q22 (form of Aβ peptide produced with the Dutch mutation) on cultured ECs. Aβ40-Q22 incubation at 50μM induced apoptosis, reduced MMP, promoted oxidative stress, and reduced mitochondrial Ca^{2+} concentrations[336]. However, the study does not report any real-time mitochondrial physiological data, and utilises extremely supraphysiological concentrations of Aβ, and thus the effect of Aβ on this aspect of mitochondrial function remains unknown.

1.14 Project aims and hypotheses

Taken together, there is a potential role for nutrient excess-induced mitochondrial dysfunction in the development of ED. ED is a common pathology for non-communicable diseases such as obesity, T2D, CVDs and dementias. Specifically, nutrient excess may induce impairments in mitochondrial dynamics, leading to reduced mitochondrial function and thus ED. Nutrient excess is associated with increases BACE1 activity and increased Aβ levels. We have shown previously that increased $Aβ_{42}$ can induce dysfunction in peripheral ECs, but it is unknown whether this is also true of brain ECs.

Therefore, the main objective of this project was to investigate the contribution of nutrient-excess induce raised BACE1 activity, and thus $Aβ_{42}$ production on the onset of

endothelial dysfunction. Furthermore, the project sought to investigate the underlying molecular mechanism of this process by investigating endothelial mitochondrial dysfunction.

The knowledge gained from this research project may provide potential mitochondrial-related therapeutic targets in the treatment of EC dysfunction, perhaps slowing the progress of multiple diseases associated with this pathology, including dementia-causing diseases.

1.15 Objectives

1) To investigate whether endothelial function is impaired in animal models of nutrient excess and determine whether any effects seen are associated with impaired mitochondrial dynamics.

- Using two models of nutrient excess (6-month old short-term HFD-fed and db/db mice)*, in vivo* endothelial function will be measured.
- Tissues of interest (aorta, VE fraction unit, hypothalamus) will be examined to investigate whether mitochondrial dynamics are altered in these models of nutrient excess.

2) To investigate the role of BACE1 and $A\beta_{42}$ in endothelial function *in vivo* and determine whether any effects seen are associated with impaired mitochondrial dynamics.

- Using models of varied BACE1 activity (BACE1KO, APP23, and HFD-fed $A\beta_{42}$ icvly-infused)*, in vivo* endothelial function will be measure in these models.
- Tissues of interest (aorta, VE fraction unit, hypothalamus) will again be examined to investigate whether mitochondrial dynamics is altered in these models.

3) To investigate the effects of both nutrient excess and increased $A\beta_{42}$ levels on mitochondrial function in a brain endothelial cell line.

- A brain endothelial cell line cultured in a high glucose and high palmitate environment will be examined to investigate how nutrient excess affects mitochondrial function using extracellular flux analysis.
- The effects of chronic exposure of cells to $A\beta_{42}$ will be examined to help determine whether any changes in mitochondrial function due to high glucose/high palmitate are exacerbated by the presence of $A\beta_{42}$.

Chapter 2

Materials and methods

2.1 General

2.1.1 Chemicals, reagents, and materials

All chemicals and commonly used lab reagents were purchased from Sigma Aldrich or Invitrogen (ThermoFisher) unless otherwise stated. Chloroform, methanol, ethanol and Moxi cell counting strips were purchased from VWR. Isopropanol was purchased from ThermoFisher. Cell culture plastic-ware were purchased from Nunc (ThermoFisher), as were all Taqman probes. Acrylamide solution was purchased from National Diagnostics. EDTA-coated tubes were purchased from Sai Infusion Technologies. Minipumps were purchased from Alzet. Amyloid beta $_{1\text{-}42}$ ($A\beta_{42}$) and scrambled peptide were purchased from Bachem. Anti-body manufacturers are given in Table 2.7.

2.1.2 Statistical analysis

All data are expressed as mean ± standard error of the mean. Statistical analysis was carried out using GraphPad Prism 8. Statistical tests are stated in figure legends. A p value ≤0.05 was considered statistically significant, with levels of significance denoted at * = p≤0.05, **, = p≤0.01, *** = p≤0.001. In some instances, # and $ are also used to denote significance. Data were proved to follow normal distribution by using the Shapiro Wilk's test. Unpaired t-tests with Welch's correction were used for data sets with only two groups, Welch's ANOVA was used for data sets with 3 or more groups (post hoc Dunnett's), and for two factorial analysis, two-way ANOVA was used. Post-hoc tests (Bonferroni) were conducted when Welch's or two-way ANOVAs were significant ($p < 0.05$) to compared differences between groups. It should be noted that the non-parametric tests Kruskal Wallis and Mann Whitney were considered for the data herein due to the small sample sizes as well as the fact some data is normalised as fold change. However, these tests assume equal variances between groups and thus utilise a pooled standard deviation. For the data sets herein, the sample size is too small for the variances between groups to be equal. Thus, Welch's corrections need to be performed hence the use of the afore-mentioned tests.

2.1.3 Power calculations

Power calculations are performed in order to estimate the required sample size for an experiment, given a desired significance level (usually 0.05), effect size (difference between group means), and statistical power (usually 0.8). The sample sizes used here were based on previous power calculations performed by Dr. Paul Meakin. However, it became clear that the studies performed for this PhD project were underpowered and thus post-hoc power calculations were performed. Herein, post-hoc power calculations were mostly used to estimate sample size required to test significance sufficiently for the studies herein that exhibited a trend (estimated by graph appearance or by $p < 0.1$)[337]. Further, for pilot studies such as the *in vitro* real-time mitochondrial respiration studies found in Chapter 5, power calculations were performed on these data to estimate sample size for follow-up studies. The following formula was used to calculate sample size:

$$n_A = \kappa n_B \quad \text{and} \quad n_B = \left(1 + \frac{1}{\kappa}\right)\left(\sigma \frac{z_{1-\alpha/2} + z_{1-\beta}}{\mu_A - \mu_B}\right)^2$$

$$1 - \beta = \Phi\left(z - z_{1-\alpha/2}\right) + \Phi\left(-z - z_{1-\alpha/2}\right) \quad , \quad z = \frac{\mu_A - \mu_B}{\sigma\sqrt{\frac{1}{n_A} + \frac{1}{n_B}}}$$

where

μ_A is the mean of one group and μ_B is the mean of the second group

$\kappa = nA/nB$ is the matching ratio

σ is standard deviation

Φ is the standard normal distribution function

Φ^{-1} is the standard normal quantile function

α is the Type I error

β is Type II error

thus $1 - \beta$ is power

2.2 Animals studies

Animal procedures were performed in accordance with Home Office guidelines with project licences PPL 70/9068 (September 2016 – February 2018) and PLL P0A1F4C5 (February 2018 onwards) held by Professor Michael LJ Ashford, personal license PIL ID046E63B held by Bethany Mae Coull and personal license PIL I6174C440 held by Dr Paul Meakin. All procedures were approved by the local ethics board and the Dundee University Named Veterinary Surgeon, Ngaire Dennison.

2.2.1 Maintenance of animal lines

All animals were maintained on a 12-hr light/dark cycle at constant temperature and provided with *ad libitum* access to food (normal chow [NC]: 7.5% fat, 17.5% protein and 75% carbohydrate by energy) and water. For mice on high fat diet (HFD) studies, mice were initially provided with a 50/50 NC/HFD for 1 week before switching to 100% HFD (45% fat, 20% protein, 35% carbohydrate by energy) for the remainder of the study. Details of animal studies are given in introduction sections of the individual results chapters.

2.2.2 Tissue harvest

At the end of studies, mice were sacrificed by cervical dislocation and subsequent severance of a major artery. Tissues were excised and dissected as necessary. Tissue for mRNA and protein analysis were snap frozen in liquid nitrogen. Hemi-brains for vessel enriched fractions were processed using the procedure described in Methods 2.6.1. Blood was collected in an EDTA-coated tube (Sai Infusion Technologies, PMTP-E-1.3) and centrifuged at 2500g for 10 minutes at 4°C to separate plasma. Plasma supernatant was removed and snap frozen in liquid nitrogen in a 1.5ml Eppendorf™™.

2.2.3 Creation of the BACE1 knockout mouse

BACE1 KO mice were generated by GlaxoSmithKline on a C57BL6/J background and maintained in-house at the Medical Science Resource Unit (MSRU), Ninewells Hospital

& Medical School, University of Dundee. Mice were produced by the insertion of the LacZ reporter gene in place of exon 1 of BACE1 gene[338]. Mice were bred in-house het x het in order to produce WT, heterozygous, and BACE1 KO mice.

2.2.4 Diabetic (db/db) mouse model

The db/db mouse was first described by Hummel *et al*.[339]. Mice homozygous for a spontaneous single point mutation (G → T, intron 18) in the leptin receptor gene exhibit morbid obesity, hyperglycaemia and pancreatic β cell dysfunction. Obesity starts at 3-4 weeks of age, with elevated plasma insulin appearing at around 10-14 days and elevated blood sugar at 4-8 weeks. The point mutation produces a Gly to Thr mutation in the leptin receptor gene on chromosome 4, resulting in abnormal mRNA splicing and the subsequent production of a non-functioning Ob-Rb (LepR long-form) protein and thus, dysfunctional Ob-Rb signalling. 4 male and 4 female mice heterozygous for the mutation were purchased from Jackson Laboratories (BKS.Cg-*Dock7^{m} +/+ Lepr^{db}/J;* #00062) to initiate a breeding colony. Mice were bred het x het in order to obtain wt/wt, wt/db, and db/db mice.

2.2.3 DNA extraction from ear notches

Ear notches were taken from mice and placed into a 1.5ml Eppendorf™ tube. A master mix containing 100µl extraction buffer (Sigma Aldrich; E7526) and 25µl tissue preparation solution (Sigma Aldrich; T3073) per sample was made and 125µl added to each notch. The samples were incubated at room temperature for 10 minutes and then heated for 3 minutes at 95°c in a bench-top heat block, after which 100µl neutralization buffer (Sigma Aldrich; N3910) was added to each sample. Samples were kept at -20°c until required.

2.2.4 Genotyping the BACE1 knockout mouse

BACE1$^{-/-}$ mice were genotyped using PCR amplification of both BACE1 and LacZ genes using KOD hot start DNA polymerase in two separate reactions. BACE1 was detected using the forward primer 5'-CGC TGC ACT GGC TCC TGC TAT GGG-3' and the reverse

primer 5'-TCT CCA CAT AGT CCT GGC CGG-3'. LacZ was detected using the forward primer 5'-GAC CAG CCC TTC CCG GCT GTG CCG-3' and the reverse primer 5'-GCC GAC CAC GGG TTG CCG TTT TCA-3'. Contents of the PCR reactions contained 1x KOD buffer, 1.5mM $MgSO_4$, 0.2mM dNTPs, 0.02U/µl KOD hot start DNA polymerase and 0.15µM forward and reverse primers. Reactions used 2.5µl of DNA template from ear notches and were made up to 25µl total reaction volume using sterile nuclease-free H_20. PCR was completed using a Veriti Thermal Cycler (Applied Biosystems, 4375786) in the thermocycler conditions listed in Table 2.1.

Once the PCR amplification was completed, 5µl of 6X Blue/Orange loading dye (Promega, G2101) was added; final concentration 1X. 10µl of PCR product was loaded on to a 1% w/v agarose/1X TAE buffer gel containing 0.01% v/v SYBR Safe DNA Gel Stain (Invitrogen, SS33102). One well contained 5µl of 100bp DNA ladder (Promega, G2101). Gels were subjected to 110V for 35-40 minutes in 1X TAE buffer (Sigma, T9650) and visualised with UV light using a Bio-Rad ChemiDoc MP Imaging System. BACE1 and LacZ bands are present at 200bp and 299bp respectively. WT mice exhibit the BACE1 band. Heterozygous mice exhibit a band for both genes. $BACE1^{-/-}$ mice lack the band for BACE1 but express the LacZ band. Fig. 2.1 shows an example gel of BACE1 genotyping.

2.2.5 Genotyping the db/db mouse

All db/db genotyping was optimised and performed by Dr Fiona McLean using a modified protocol from Peng and colleagues[340]. Single point mutations are historically difficult to genotype for. The technique the authors developed for db/db genotyping is referred to as tetra-primer amplification refractory mutation system-polymerase chain reaction (ARMS-PCR). Tetra-primer amplification exploits the use of four primers. There are two outer primers (forward and reverse, FO and RO) that bind a site outside the target DNA and act as an internal control. There are also two inner primers (a forward WT primer and reverse mutant primer) that bind the target DNA site, which is the site of the single point mutation herein. The primer sequences are as follows:

Step	Temperature (°C)	Duration
1. Polymerase activation	95	2 minutes
2. Denaturation	95	20 seconds
3. Annealing	62	15 seconds
4. Extension	70	7 seconds
Repeat steps 2-4 x 35 cycles		
Hold at 4°C		

FO: TTGTTCCCTTGTTCTTATACCTATTCTGA
RO: CTGTAACAAAATAGGTTCTGACAGCAAC
WT: ATTAGAAGATGTTTACATTTTGATGGA**A**GG
mutant: GTCATTCAAACCATAGTTTAGGTTTGT**C**TA

Table 2.1 Thermocycler conditions for BACE1 genotyping

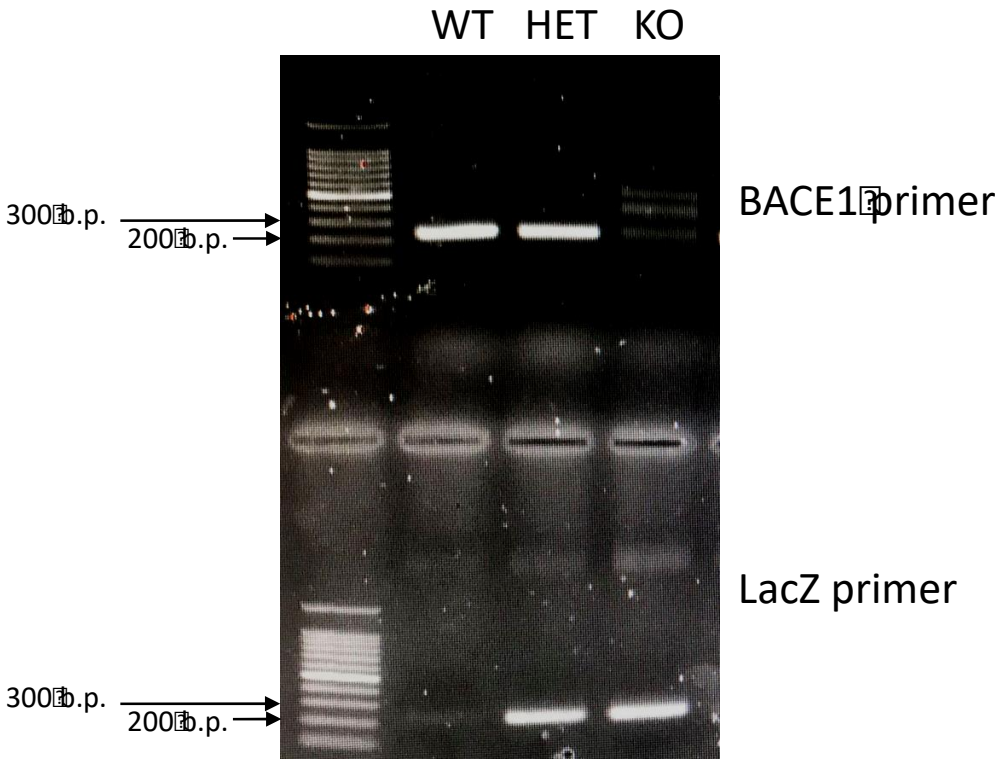

Figure 2.1 Representative genotyping gel for BACE1 KO mouse line

An ear notch was taken from each mouse and the DNA was extracted as described in section 2.2.3. Genotyping was performed as described in section 2.2.4. The figure shows an agarose gel exhibiting the relevant PCR products. BACE1 primers and LacZ primers were used to identify the genotype of each mouse. WT mice will express the BACE1 gene and no LacZ gene, HET mice will express a copy of each, and BACE1KO mice will express no BACE1 gene, but will express the LacZ gene.

The forward WT primer matches the WT target gene, whereas the reverse mutant primer sequence does not. Taq polymerase lacks proofreading activity and therefore cannot correct this mismatch. This means that when the Taq polymerase is amplifying the WT target DNA using the forward WT primer template in combination with the reverse outer primer, the DNA is amplified. However, when it tries to amplify the WT target sequence using the reverse mutant primer in combination with the forward outer primer, it gives up when it reaches the single point mutation. The opposite is true when the Taq polymerase attempts to amplify the mutant primer sequence. The PCR thus results in 3 potential products: the common amplicon targeted by the outer primers (610 b.p.), the WT amplicon targeted by the forward WT and reverse outer primers (264 b.p.), and the mutant amplicon targeted by the reverse mutant and the forward outer primers (406 b.p.). Contents of the PCR reactions contained 12.5µl of Promega PCR Master Mix (Promega, M75020, 0.5µl of 10mM FO-1, 0.5µl of 10mM RO-1, 0.5µl of 10mM FI-1, 0.5µl of 10mM RI-1, 9.5µl nuclease-free water, and 1µl extracted template DNA. PCR was completed using a Veriti Thermal Cycler in the thermocycler conditions listed in table 2.2. Once the PCR amplification was completed, 5µl of 6X Blue/Orange loading dye to produce a final concentration of 1X. 10µl of PCR product was loaded on to a 1% w/v agarose/1X TAE buffer gel containing 0.01% v/v SYBR Safe DNA Gel Stain, with one well containing 5µl of 100bp DNA ladder. Gels were subjected to 120V for 50 minutes in 1X TAE buffer and visualised with UV light using a Bio-Rad ChemiDoc MP Imaging System. A representative genotyping gel is shown in Fig. 2.2.

Step	Temperature (°C)	Duration
1. Polymerase activation	94	5 minutes
2. Denaturation	95	30 seconds
3. Annealing	55	30 seconds
4. Extension	68	1 minute
Repeat steps 2-4 x 40 cycles		
Hold at 4°C		

Table 2.2 Thermocycler conditions for db/db genotyping

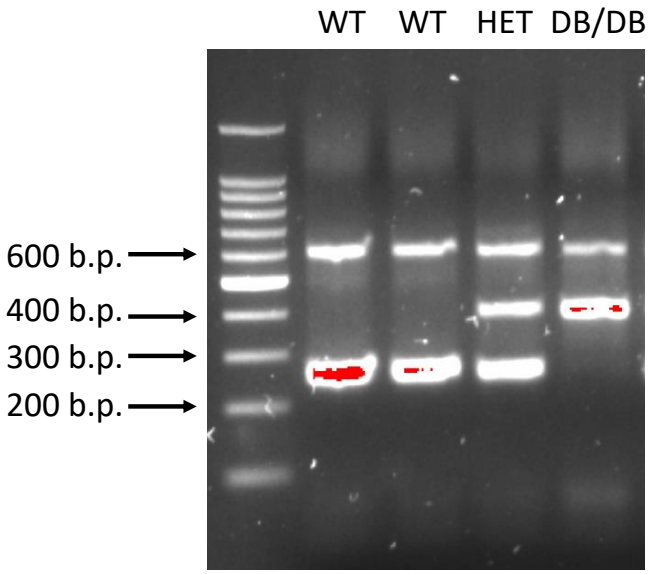

Figure 2.1 Representative db/db genotyping gel

An ear notch was taken from each mouse and the DNA was extracted as described in section 2.2.3. Genotyping was performed as described in section 2.2.5. The figure shows an agarose gel exhibiting the relevant PCR products. All mice will express the common amplicon at 610 b.p, wt mice will express the WT amplicon at 264 b.p., db/db mice will express the mutant amplicon at 406 b.p., and heterozygous wt/db mice will express both.

2.2.6 APP23 mice

APP23 mice are a genetic model normally used for studying AD. Indeed, mutations in the *App* gene are linked to familial AD and APP23 mice in particular express, under the Thy1 promoter, the human isoform 751 of APP harbouring the Swedish double mutation (APP_{751}*K670N/M671). These mice exhibit extensive β-amyloid pathology at 3-6 months of age[341]. 16 10-week old male hemizygote APP23 mice were purchased from Jackson Laboratories (Jax#030504) and were allowed two weeks to habituate to their new environment. Within this time, 4 APP23 mice were found dead, leaving 12 to undergo peripheral minipump surgery (2.4.2). Post-surgery, a further 4 APP23 mice were found dead/had to be euthanised, leaving a total of 8 (4 per treatment).

2.3 Metabolic phenotyping

2.3.1 Glucose tolerance test

Glucose tolerance tests are used to study the physiological ability of the mouse to dispose of a bolus of glucose. Mice were fasted for 16 hours prior to glucose tolerance testing. Blood was extracted via a small tail nick at the tip of the tail. Blood glucose (whole blood) measurements were made using a glucometer (Contour, Bayer, 83785579) and glucose test strips (Contour, Bayer, 85723154). Mice were injected intraperitoneally (i.p.) with 2mg/kg D-glucose (dissolved in PBS) with blood glucose levels assessed pre-injection and then 15, 30, 45, 60, and 120 minutes post-injection.

2.3.2 Insulin tolerance test

Insulin tolerance tests are used to study the insulin sensitivity (measured by disappearance of glucose from the blood) of the mouse. Mice were fasted for 4 hours prior to insulin tolerance testing. Blood was extracted via a small nick at the tip of the tail. Blood glucose (whole blood) measurements were made using a glucometer (Contour, Bayer, 83785579) and glucose test strips (Contour, Bayer, 85723154). Mice were injected i.p. with 0.75U/kg insulin (Actrapid) diluted in PBS with blood glucose levels assessed pre-injection and then 15, 30, 60, 90, and 120 minutes post-injection.

2.4 Surgery

All surgeries were performed using aseptic technique. All subcutaneous mini-pump and icv mini-pump surgeries were performed by Bethany Mae Coull. Surgical assistance was given by Dr Fiona McLean (subcutaneous) and Christie Hancock (icv).

2.4.1 Anaesthesia

Using anaesthetic apparatus (Vettech, AN002A) mice were anaesthetised by a mix of 3.5% isoflurane (Covetrus, 1169567761) and oxygen (compressed oxygen cylinder size E, BOC Medical) delivered at a flow rate of 1-1.5 litres per minute. Mice were maintained at a steady depth of anaesthesia, detected by a toe pinch reflex test and observation of breathing (optimal = ~55-60 breaths per minute), using a mix of 1-1.5% isoflurane and oxygen delivered at 1-1.5 litres per minute.

2.4.2 Peripheral mini-pump surgery

Under anaesthesia, mice were shaved with an electric razor (Wella Contura) to remove the fur from the base of the neck and across the upper back. Mice were placed on a heat mat for the duration of the surgery in order to help maintain body temperature. Mice were injected subcutaneously with 1ml/kg of the analgesic agent Rimadyl (Covetrus, 6451506845), which had previously been diluted 1:10 with sterile medical saline. The skin was sterilised using 1% betadine and 70% ethanol. An incision of around 4 cm was made across the upper back. Using blunt dissection, a small pocket was made under the skin on the left flank. A subcutaneous minipump (Alzet, 0000298), containing either a solution of 3.36µg/kg $A\beta_{42}$ (Bachem, 4035885.05) or ScrP (Bachem, 4064835.05) was placed into the pocket. This $A\beta_{42}$ concentration was chosen as when it is infused for the stated length (4 weeks) of time it results in similar circulating $A\beta_{42}$ concentrations to DIO-induced circulating amyloid concentrations[316]. For APP23 inhibitor studies, BACE1 inhibitor M-3 was delivered at 10 mg/kg/day, or vehicle control (50:50 DMSO:PBS). We have previously reported that this concentration of M-3 is sufficient to reduce BACE1 activity and produce a functional output in BACE1-regulated processes, such as

hypothalamic leptin action and food intake[305]. Skin was then glued using the veterinary topical adhesive GLUture (ThermoFisher, NC0632797). Mice were placed in baby incubators at 37°c to recover for around 30-60 minutes and were monitored closely the following week post-surgery. Mouse welfare was monitored using conventional body condition scores as well as food/water intake and weight measurements[342].

2.4.3 Intracerebroventricular mini pump surgery

Under anaesthesia, mice were shaved with an electric razor to remove the fur from their heads and necks. Mice were placed on a heat mat for the duration of the surgery and were placed in a stereotaxic frame, secured via a tooth bar and ear bars. Mice were injected subcutaneously with 1ml/kg of the analgesic agent Rimadyl which had previously been diluted 1:10 with sterile PBS. The skin was sterilised using 1% betadine and 70% ethanol. An incision of around 5cm was made from between the eyes to the base of the neck to expose the skull. The skin was pulled to either side and clipped back to ensure the skull would stay exposed. Using blunt dissection, a small pocket was made under the skin on the left flank. A subcutaneous minipump containing either a solution of $A\beta_{42}$ or ScrP (3.36ug/kg) was placed into the pocket. This concentration was chosen as, when infused for the stated length of time (4 weeks), it results in similar hypothalamic $A\beta_{42}$ concentrations to DIO-induced hypothalamic amyloid concentrations[305]. The intracerebroventricular (icv) catheter was placed in the stereotaxic frame and was inserted through the skull into the right lateral ventricle using stereotaxic coordinates: -0.46 anterior/posterior, +1 lateral. The cap was adhered to the skull using super glue and the wound then glued using the veterinary topical adhesive GLUture. Mice were placed in baby incubators at 37°c to recover for around 2 hours and were monitored closely the following week post-surgery. Mouse welfare was monitored using conventional body condition scores as well as food/water intake and weight measurements.

2.5 Laser Doppler flowmetry

Cutaneous microvasculature is an easily accessible vascular bed for the assessment of vascular function *in vivo* in both humans and rodents. Dysfunctional microvasculature has been associated with the development of CVD[343–345], and has been reported to be a good predictor of cerebrovascular dysfunction[346], and white matter lesions and cognitive impairment[347]. Therefore, assessing the microvasculature to measure vascular dysfunction is a good method for studying animal models of CVD, and may be a useful tool in researching the link between peripheral vascular disturbances and cerebrovascular impairments. However, it should be noted that peripheral ECs and brain ECs do differ from one another in terms of structure and function, and the peripheral microvasculature is not an absolute measure of cerebral microvasculature.

Since the commercialisation of the technique in the 1980s, laser Doppler flowmetry (LDF) has become one of the most widely used methods to study microcirculation *in vivo*. LDF adopts the use of a light source (in our case a helium-neon [HeNE] laser beam) that is directed at the area of interest on the skin. Consistent with the Doppler theory, the laser beam will undergo scattering when reflected off moving red blood cells (RBCs) in the microvasculature. The magnitude of this scattering can then be related to the number and the velocity of the RBCs providing a measure of blood flow. Scattered light from RBCs beam is received by a photodetector and converted into an electrical signal proportional to the Doppler shift. LDF only allows for single-point perfusion analysis, but laser Doppler imaging (LDI) measures blood flow over a larger area, thus helping dampen the heterogenous and variable signals obtains from blood flow measurements.

The method used herein is LDI, which adopts the use of a scanning HeNe laser beam and produces a measurement of skin perfusion over a given area. Using this technique, a colour-coded skin perfusion map relating to Doppler shift and therefore blood flow is produced (Fig. 2.3). Each pixel on the skin perfusion map corresponds to a ‘flux’ value, ranging from 0-1000 (AU). Low flow is represented by blue/purple colours on the skin perfusion map, corresponding to a lower flux value (0-250 AU). Larger flow is represented by green, yellow and red and corresponds to a higher flux value (300-1000 AU).

2.5.1 Iontophoresis

Assessment of endothelium-dependent vasodilation and non-endothelium dependent vasoresponsiveness can be assessed by coupling laser Doppler imaging (LDI) technology with iontophoresis of vasoactive agents, such as phenylephrine (PE), ACh, or sodium nitroprusside (SNP). Section 1.6.1 provides a detailed response of endothelial cell signalling in regard to vasoresponsiveness. Iontophoresis is the unidirectional transport of ions in a solution across the epidermal layer by a continuous applied current (Fig. 2.4). Ion movement is determined by polarity. The negatively charged electrode (cathode) repels negatively charged ions and attracts positively charged ions. A positively charged electrode (anode) repels positively charged ions and attracts negatively charged ions. By utilising iontophoresis technology *in vivo*, polarised vasoactive agents can migrate across the epidermis into the microvasculature and exert effects, which can be detected by laser Doppler imaging.

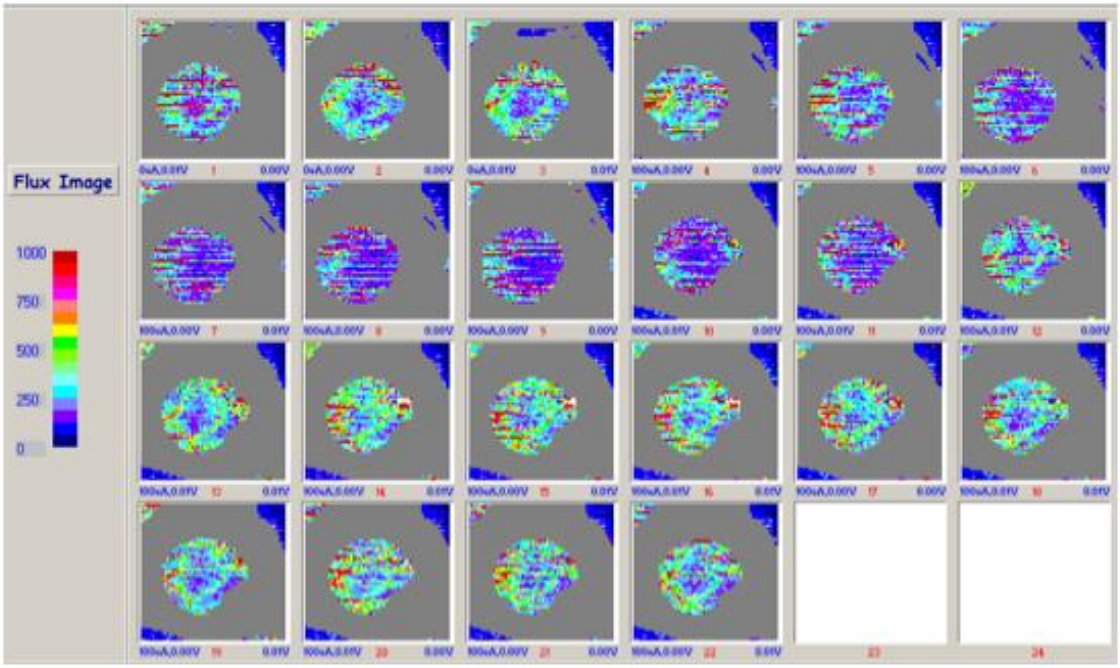

Figure 2.3 Example laser Doppler scan

LDI scan of an 8-week old WT NC-fed female mouse. Scans 1-3: baseline (dH_20), scans 4-9: PE-induced scans, scans 10-22: ACh-induced scans. Purple-blue: constricted microvasculature, green-red: dilated microvasculature.

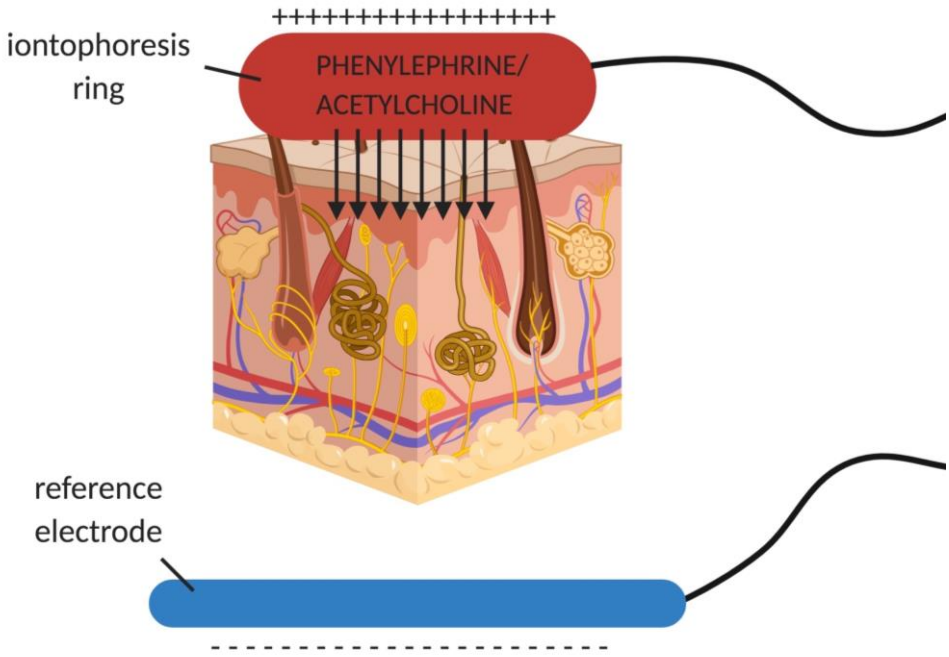

Figure 2.4 Schematic representation of the principles of iontophoresis in laser Doppler imaging

The iontophoresis ring is attached to the skin and, in its chamber, it houses the vasoactive agent dissolved in dH_20. The reference electrode is placed on another area of skin. Through the iontophoresis controller, which is connected both to the iontophoresis ring and the reference electrode, a current is applied to the skin. Due to this current, the iontophoresis ring becomes positively charged, and the electrode becomes negatively charged. Positively charged molecules (PE, ACh) are repulsed by the ring and attracted to the electrode, and thus move toward the electrode through the skin and into the microvasculature where they can take effect on endothelial cell signalling.

2.5.2 Anaesthesia

Using anaesthetic apparatus mice were anaesthetised by a mix of 3.5% isoflurane and oxygen (compressed oxygen cylinder size E, BOC Medical) delivered at a flow rate of 1-1.5 litres per minute. Mice were maintained at a steady depth of anaesthesia using a mix of 1-1.5% isoflurane and oxygen delivered at 1-1.5 litres per minute.

2.5.3 Animal preparation

An electric razor was used to shave both flanks of the animal (Fig. 2.5A, B). Gentle application of depilatory cream (Veet) was used to entirely remove the fur from one flank of the animal, followed by a thorough cleaning with warm H_20 to ensure removal of any residual cream (Fig. 2.5A). Skin must be exposed as the laser beam cannot penetrate through fur. A reference electrode (Moor Instruments Ltd, MIC2) was placed underneath the animal on the patch of shaved skin (Fig. 2.5C). The iontophoresis electrode ring (Moor Instruments Ltd, MIC2) was attached to the Veeted skin via double-sided adhesive tape (Fig. 2.5C). The ring was filled with approximately 2ml of dH_20 and a lid was placed on the ring to ensure there was no spillage of the liquid. There must be no air bubbles present in the liquid, as this will result in a false signal. The ring was placed at a 35° angle from the laser beam to allow accurate measurement and minimise direct reflection of the laser beam (Fig. 2.5C).

2.5.4 Experimental set-up

The laser (Moor Instruments Ltd, MLDI 5082) was positioned 50cm above the animal, with the bottom of laser hood being 32cm above tissue (Fig. 2.7A, B). Using Moor propriety software (Moor Instruments Ltd, Version 5.3), laser acquisition parameters were set as below:

Scan resolution: X=60, Y=60

Scan speed: 10ms/pixel

Average scan time: 49 seconds

Time between scans: 5 seconds

Total scan time: 55 seconds

To investigate endothelium-dependent vasodilation, iontophoresis of both phenylephrine (PE) and acetylcholine (ACh) was used. Since PE and ACh are positively charged molecules, they migrate toward the reference electrode when it is negatively charged and will be repelled from the iontophoresis ring when it is positively charged. Three 'baseline' scans were first completed with dH_20 before iontophoresis of vasoactive agents. To standardise baseline perfusion, vessels were preconstricted with 1% (w/v) phenylephrine (current = 100µA) and 6 scans were performed. To measure endothelium-dependent vasodilation, 2% (w/v) ACh was applied for 13 scans. To measure endothelium-independent vasodilation, vessels were preconstricted with 1% (w/v) phenylephrine, and then stimulated with 2% (w/v) sodium nitroprusside (SNP), an NO donor that can induce smooth muscle cell relaxation independently of endothelium-derived NO. SNP is negatively charged, therefore the charges on the reference electrode and iontophoresis ring must be swapped, making the reference electrode an anode, and the iontophoresis ring a cathode.

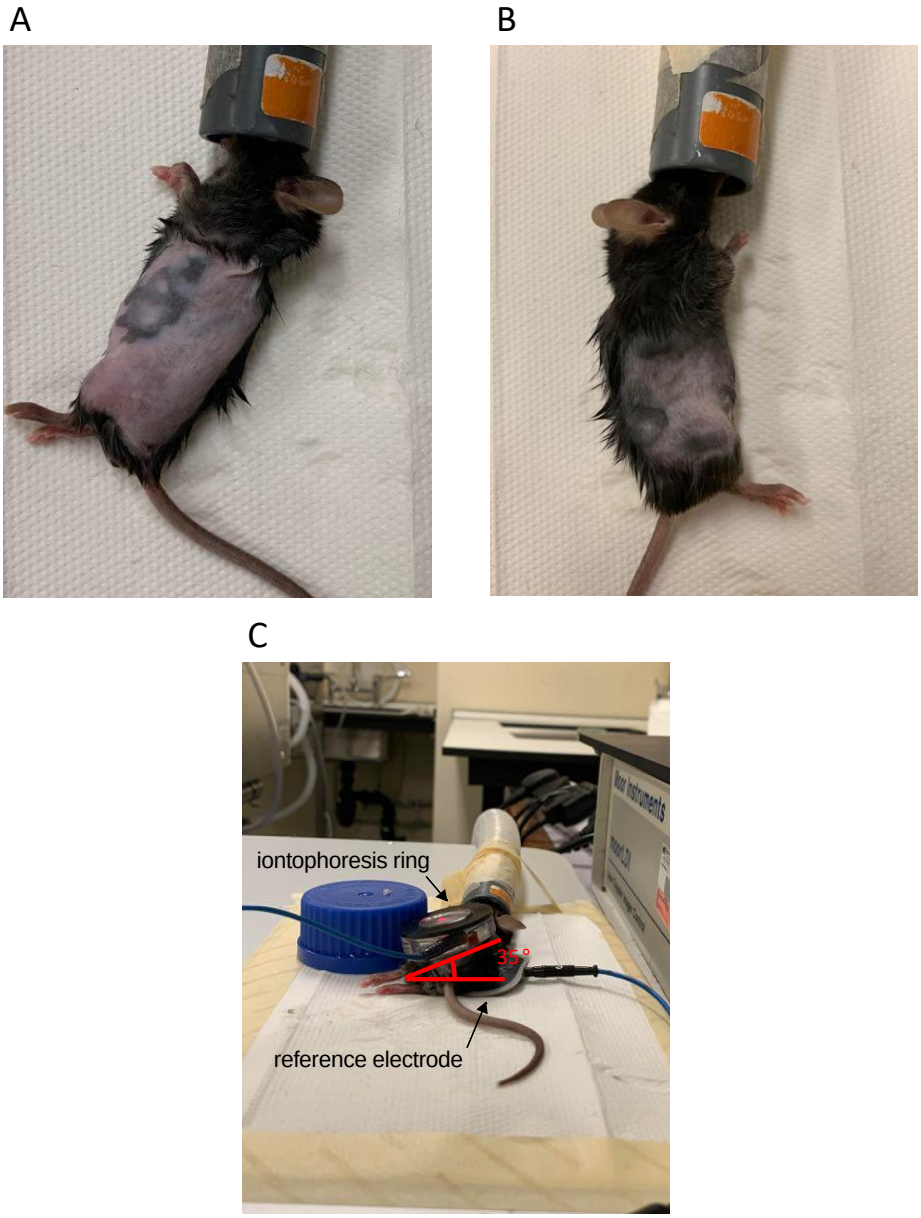

Figure 2.5 Animal preparation for laser Doppler imaging

Under anaesthesia, both flanks of the mouse were shaved using an electric razor. (A) The fur on one side was completely removed using depilatory cream (Veeted) and cleaned with warm H_20. (B) The fur on the other side was shaved, but depilatory cream was not applied. (C) On the flank that no fur was present, the iontophoresis ring was attached using double-sided adhesive ring-tape. The reference electrode was placed underneath the mouse on the shaved flank. The ring was placed at a 35° angle so as not to directly reflect the beam. Prior to the start of the scanning period, H_20 was placed in the iontophoresis chamber and the lid placed on top to assess whether any leaks were present

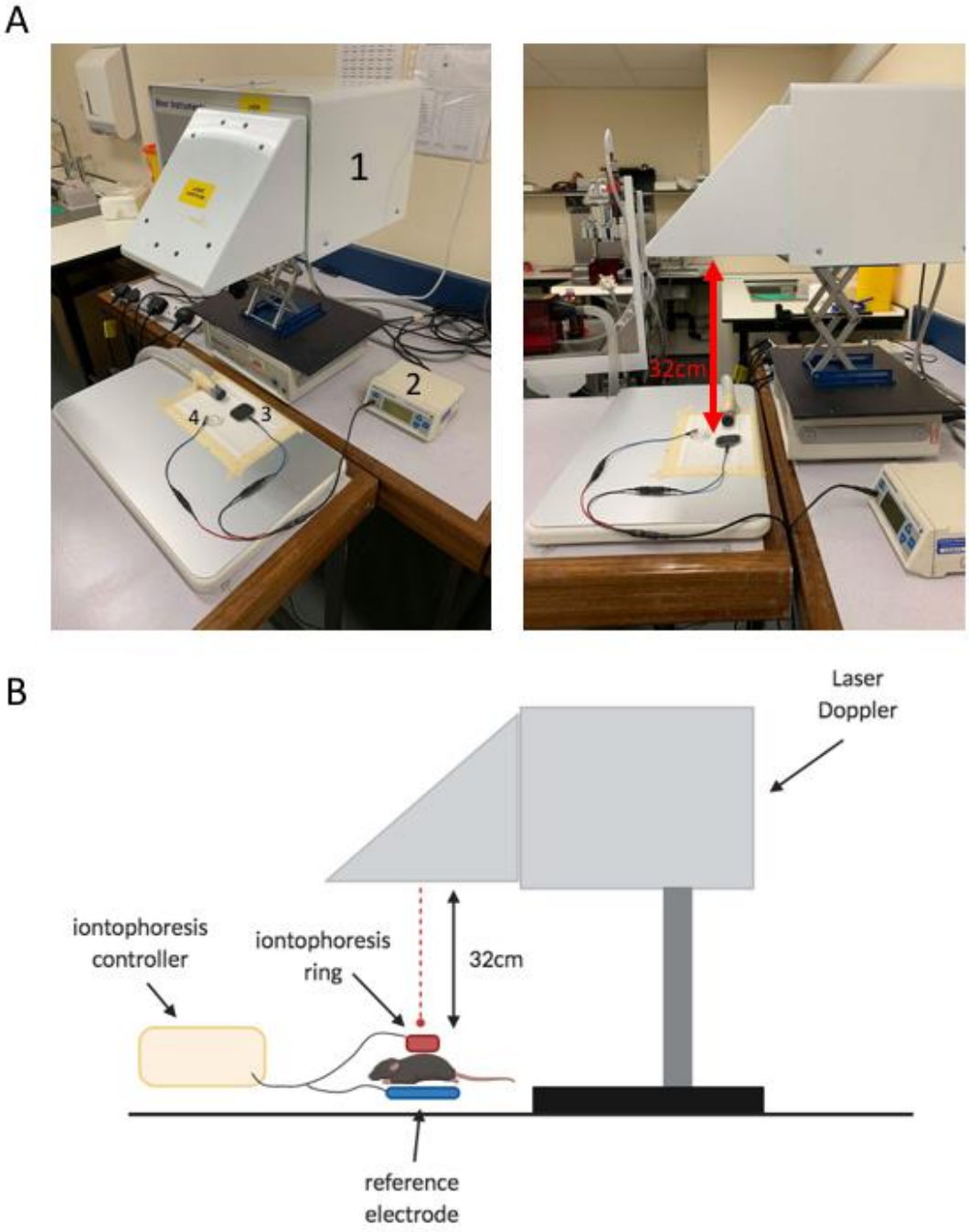

Figure 2.6 Laser Doppler imaging set-up

(A) Photographs of the laser Doppler imaging set-up, where 1 = laser, 2 = iontophoresis controller, 3 = reference electrode, and 4 = iontophoresis electrode ring. (B) Representative schematic of the laser Doppler imaging set up.

2.5.6 Perfusion analysis

Perfusion images (Fig. 2.3) were analyzed using propriety software (Moor Instruments, Version 5.3). Each coloured pixel on the image corresponds to a numerical value of flux, ranging from 0-1000 (AU). The median of these values is taken for further analysis (Fig. 2.7). Data are expressed in four ways: (1) baseline flux (AU) which is an average of the 3 baseline values (green circles in Fig. 2.7A), (2) peak flux in response to ACh (AU) which is an average of the top 3 values in response to ACh (red circles in Fig. 2.7A), (3) an XY graph denoting percentage change (%Δ) over time normalised to the first baseline scan (presented in Fig. 2.7B), or (4) a column graph denoting %Δ in response to ACh, calculated as maximum ACh-induced vasodilation compared to maximum PE-induced vasoconstriction. The latter is calculated by subtracting the bottom 3 PE-induced value (blue circles Fig 2.7A) from the average of the top 3 ACh-induced values (red circles Fig 2.7A), and then converting this difference into % change from the PE-induced value.

The baseline flux is not normalised and is therefore likely to be variable between mice. It will be sensitive to factors such as temperature, hormone levels, when the mouse last ate, blood pressure, and isoflurane administration. To account for this, the microcirculation is normalised across animals by preconstricting the vessels with PE[145,348]. The baseline measurement is still analysed herein, as it may contain interesting information about the animal models. However, the data must be interpreted carefully and with full awareness of possible confounding factors.

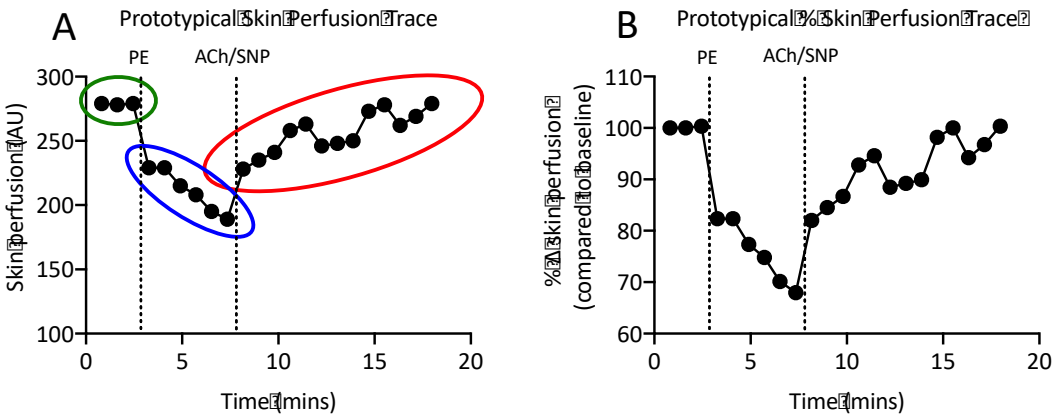

Figure 2.7 Prototypical traces of cutaneous skin perfusion in response to PE and ACh/SNP

(A) Skin perfusion values (AU) against time at baseline (green circle), after PE application (blue circle), and after ACh/SNP application (red circle). (B) Typical % skin perfusion trace (% of first baseline reading) at baseline, after PE application, and after application of a vasodilatory agent.

2.6 Tissue biochemistry

2.6.1 Vessel enriched fractionation

Vessel enriched fractions were obtained using a modified protocol from Yousif and colleagues[349]. Mice were culled via cervical dislocation and major artery laceration. The brain was dissected from the skull and, after removal of the hypothalamus, cerebellum and olfactory bulbs, was separated into two hemi-brains. Hemi-brains were homogenised in 1ml ice-cold PBS each using a loose-fit 1ml glass Dounce homogeniser. Once minced, the homogenate was placed in a 15ml falcon tube and spun at 250g for 10 minutes at 4°C. The supernatant was removed, and the pellet was resuspended in 3ml 17.5% Ficoll-400 (Sigma, F9378-25G). Ficoll preparations work on the principle that higher density cells will accumulate in a pellet at the bottom of the centrifuge tube, whereas lower density cells will not be able to migrate through the Ficoll mixture and will remain at the top of the solution. The suspension was then centrifuged at 3200g for 25 minutes at 4°c. This spin results in a pellet referred to as the vessel-enriched (VE) fraction, which is thought to contain ECs, pericytes, and potentially astrocytic end-feet, and two layers on top which contain the brain parenchyma, deemed the S_0 fraction. The S_0 fraction was removed and placed in a fresh 15ml Falcon tube. 3ml of ice-cold PBS was added and the resulting mixture was centrifuged at 3200g for 10 minutes at 4°C. The supernatant was poured off and the pellet was resuspended in 1ml ice-cold PBS and spun at 6000g for 10 minutes at 4°C. The two VE fraction pellets are pooled together in 1ml ice-cold PBS and centrifuged at 6000g for 10 minutes at 4°C. A schematic of this process is shown in Fig. 2.8. Both VE and S_0 fractions were stored at -80°C until required for further processing.

To validate that the VE fraction did indeed contain enriched vessels, ICAM (a protein that is highly expressed on endothelium[350,554]) expression was measured in both the VE fraction and the S_0 (or parenchymal) fraction (Fig. 2.9). Indeed, the VE fraction expressed high levels of ICAM whereas the S_0 fraction only possessed very low, residual levels (likely due to a small amount of contamination of endothelial cells).

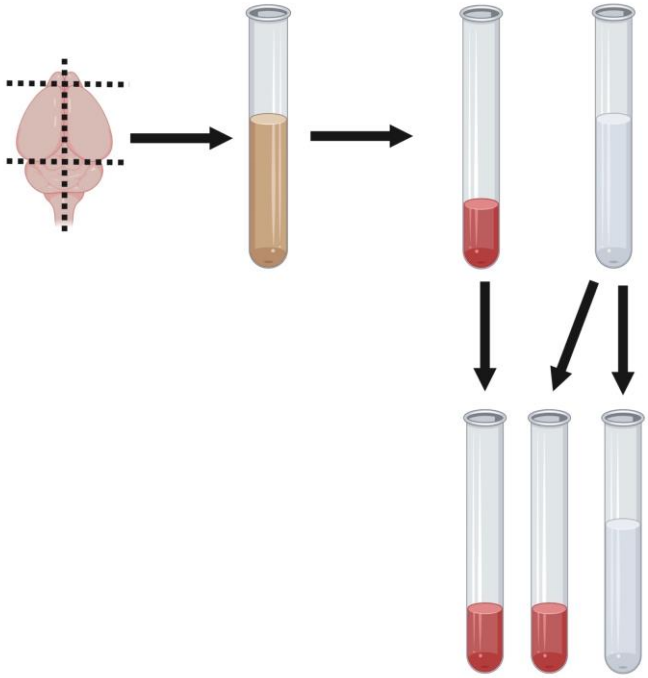

Figure 2.8 Schematic of vessel enrichment protocol

Homogenised hemi-brain is pelleted and then resuspended in Ficoll (brown). Centrifugation of this suspension results in the separation of the brain suspension and formation of a pellet which contains a vessel enriched fraction (red), termed the VE fraction. The supernatant containing the parenchyma is removed (termed S_0 frac, white) and is centrifuged a second time, resulting in a second VE fraction pellet. The two VE fraction pellets are pooled together. From each hemi-brain, the protocol produces one pellet containing the VE fraction and one pellet containing the S_0 fraction.

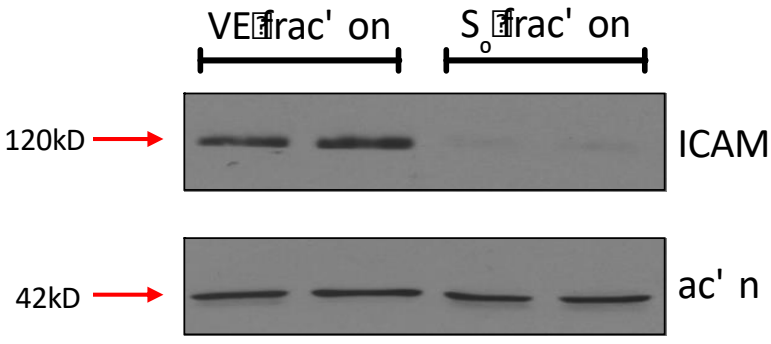

Figure 2.9 Validation of vessel enrichment protocol using ICAM protein expression

Protein was isolated (2.6.5) from VE fractions and S_0 fractions. 20µg of sample was loaded onto an acrylamide gel and separated using SDS-PAGE (2.6.7). ICAM protein expression was probed for using conventional western blotting (2.6.7). Actin was used as a loading control.

Step	Temperature (°C)	Duration
1. Polymerase activation	95	10 minutes
2. Denaturation	95	15 seconds
3. Annealing	60	1 minute
4. Extension	60	1 minute
Repeat steps 2-4 x 40 cycles		

Table 2.3 Real-time PCR cycle protocol for Taqman® analysis

Probe name	Specificity	Code
Actin	Mouse	Mm02619580_g1
APP	Mouse	Mm01344172_m1
BACE1	Mouse	Mm00478664_m1
ICAM	Mouse	Mm00516023_m1

Table 2.4 Summary of Taqman® probes used herein

Constituent	Volume
dH_20	4.15ml
Lower buffer	3.15ml
30% acrylamide	3.75ml
10% SDS	100µl
TEMED	11µl
20% APS	55.35µl

Table 2.5 Components of lower gel (makes 2 gels)

Constituent	Volume
dH_20	2.8ml
Upper buffer	1.25ml
30% acrylamide	0.85ml
10% SDS	50µl
TEMED	5.35µl
20% APS	50µl

Table 2.6 Components of upper gel (makes 2 gels)

2.6.2 RNA extraction

Cells were lysed in 500µl of TRIzol Reagent (Thermo-Fisher Scientific; 155906018). 100µl chloroform was added and the sample was shaken vigorously for 15 seconds. Samples were allowed to stand at room temperature for 15 minutes before being centrifuged at 12000 x g for 15 minutes. The clear aqueous phase containing RNA was removed and placed in a fresh Eppendorf™ and 250µl of isopropanol was added. The isopropanol, when centrifuged, gathers the RNA at the bottom of the tube. Samples were again allowed to stand at room temperature for 10 minutes before being spun at 12000 x g for 10 minutes to form a visible RNA pellet. The supernatant was removed, and the pellet was washed with 1ml 75% ethanol. The samples were spun again at 12000 x g for 5 minutes and the supernatant was removed. The RNA pellets were allowed to air dry for 7.5 minutes in a fume hood before being dissolved in 15-30µl PCR grade RNase free water by heating at 60°C for 15 minutes. RNA was stored at -80°C until required for cDNA synthesis.

2.6.3 cDNA synthesis

RNA concentration was measured using the Nanodrop ND-8000 Spectrophotometer. Purity was also assessed at this stage with a 260/280 ratio ≥ 1.8 used as a lower limit. cDNA was produced according to the Invitrogen protocol and reagents for Superscript II reverse transcriptase (Invitrogen, 18064022). Briefly, a mix containing 1µl random primers (Invitrogen, 48190011), 1µl 10mM dNTP mix (Invitrogen, 18427013), 1µg of RNA sample made up to a total volume of 13µl with PCR grade, RNase free water was made in a 1.5ml Eppendorf™ tube and heated to 65°C for 5 minutes and then chilled on ice. 4µl 5x first strand buffer (Invitrogen, 18064022) and 1µl 0.1M DTT (Invitrogen, 18064022) was added, gently mixed and left at room temperature for 1 minute before adding 1µl Superscript II RT and mixing gently again. The samples were then allowed to stand at room temperature for a further 10 minutes before being incubated at 42°C for 50 minutes, after which the reaction was inactivated by heating at 70°C for 15 minutes. cDNA was diluted 1:10 with 180µl PCR grade, RNase free water and stored at -20°C until required for TaqMan® qPCR.

2.6.4 Gene expression analysis using TaqMan® analysis

TaqMan® technology uses a primer/probe mix consisting of a normal PCR primer targeted toward the gene of interest in addition to a probe molecule, which has a FAM dye label on the 5' end and a quencher on the 3' end. When the target gene is amplified by the exogenously added DNA polymerase, the exonuclease activity of the enzyme separates the FAM dye from the quencher. With each cycle of PCR, more dye molecules are released, and this results in increased fluorescence which is proportional to the amount of amplified product. This information can then be used to quantify gene expression.

To perform TaqMan® analysis, 2.5µl of synthesised cDNA sample was loaded into a 96-well MicroAmp Fast 96-Well Reaction Plate (Applied Biosystems, 4346907). 17.5µl of a pre-made master mix consisting of 6.5µl of PCR grade water, 1µl of the appropriate TaqMan® probe (Applied Biosystem, Table 2.4) and 10µl TaqMan® 2X Mastermix (Applied Biosystems, 4324020) was then added to each sample. Once loaded, the plate was covered with a film lid and spun in a centrifuge to ensure the collection of the sample at the bottom of the wells. The plate was then run in a real-time PCR machine (Applied Biosystems, 7900HT) according to the protocol in Table 2.3. Steps 2-4 were repeated for a total of 40 cycles.

2.6.5 Protein extraction

Tissues, VE/S_0 pellets, and cells were lysed in an appropriate volume of lysis buffer (2.9 Commonly used lab solutions). Aorta and muscle tissues were dissociated using the Fisherbrand Bead Mill 24 Homogenizer (ThermoFisher, 15515799) with 0.9-2mm stainless steel beads (Next Advance, SSB14B) with the settings speed = 5, time = 20s, cycles = 5, dwell = 4s. This homogenate was then sonicated (130 Watt ultrasonic processor, Sonics, VCX 130) at 25% amplitude for 20s (5 pulses of 4 seconds on 1 second off). Sonication at this amplitude is known to rupture organelle membranes. The homogenate was then spun down at 13000 x g for 15 minutes to remove cell debris. The

supernatant was removed and placed in a fresh Eppendorf™ and stored at -80°C until required.

2.6.6 Bradford assay

Protein concentration was determined using the Bradford assay (Bradford, 1976). Briefly, standard wells of known protein concentration were loaded in triplicate into a 96-well plate using 2mg/ml BSA (Thermo Fisher Scientific; 23209) to create a standard curve. 1µl of sample was loaded in triplicate followed by 9µL of ddH_20 per well. 250µl Bradford reagent was added to each well and the plate was allowed to stand at room temperature for 5-10 minutes to ensure colour development. The absorbance of the wells was read at 595nm using an EnVision 2104 Multilabel Plate Reader. The standard curve was then created using the mean absorbance of wells against known protein concentration. The protein concentration of unknown samples can then be extrapolated from the standard curve using the mean absorbance values. Equal amounts of protein were mixed with 4X sample buffer (2.9 Commonly used lab solutions) and boiled at 95°C for 5 minutes. Samples were stored at -20°C until required.

2.5.7 SDS-PAGE and western blotting

Sodium dodecyl sulfate (SDS)-polyacrylamide gel electrophoresis (PAGE) is a widely used method allowing for the separation of proteins. SDS is a detergent that gives proteins a net negative charge. During SDS-PAGE, charges proteins migrate relative to their size, thus allowing accurate separation of proteins by size. Typical SDS-PAGE consists of loading protein samples from tissue and cell lysates onto a polyacrylamide gel. The gel contains pores of differing size (determined by the acrylamide percentage used to make the gel) that act to impede the paths of proteins that have been loaded on to the gel. Smaller proteins will move through the gel faster than larger proteins, resulting in a separation of proteins with low kD-proteins at the bottom of the gel and high kD proteins at the top of the gel. A protein ladder consisting of known proteins of known sizes is also loaded onto the gel to allow for identification of proteins of interest during western blotting.

Gels were hand casted using BioRad casting equipment (BioRad, 1658001FC). Separating (lower) gels and stacking (upper) gels were made as per Tables 2.5 and 2.6 respectively. Samples of known protein concentration were loaded on to gels against the protein ladder SeeBlue Pre-stained Protein Standard (ThermoFisher, LC5925). The gel was then run at 150V for around 1.5 hours to allow protein separation. The running tank applies a current in a vertical plane to attract proteins to the bottom of the gel from the top. Once the gel had ran sufficiently, proteins were transferred onto a nitrocellulose membrane (SIGMA, GE10600002) at 80V for 1.5 hours. The transfer tank applies a current in a horizontal plane to attract proteins onto the nitrocellulose membrane. Following transfer, membranes were incubated in Ponceau S solution to ensure efficient protein transfer. Ponceau was washed off with TBST (2.9 Commonly used lab solutions) and blocked (to reduce non-specific anti-body binding) for 1 hour in 5% w/v milk/TBST or 5% w/v BSA/TBST depending on the primary antibody used for protein detection (Table 2.7). Following blocking, membranes were washed in TBST to remove milk and then incubated at 4°c overnight in a primary antibody directed toward the protein of interest (see antibodies table for details). The following day, antibody was removed, and the membrane was washed 5 x 5 minutes in TBST. The membrane was then incubated for 1 hour at room temperature in a secondary antibody directed toward the species that the primary antibody was reared in. Secondary antibodies were conjugated to either horseradish peroxidase or a fluorophore. Following this, membranes were washed 5 x 5 minutes and imaged using the LI-COR Odyssey CLx Imaging System at 685nm or 785nm, dependent on the conjugated fluorophore (Table 2.7). Blots were analysed by densitometry using Image Studio Lite (LI-COR) and the numerical outputs were normalised as fold change compared to the control group.

Antibody	Blocking agent	Dilution	Species	Secondary antibody	Provider	Product code
Beta actin	5% milk/TBST	1:1000	Rabbit	Goat anti-rabbit 800CW	Abcam	ab14128
BACE1	5% milk/TBST	1:1000	Rabbit	Goat anti-rabbit 800CW	Sigma	SAB2100200
Phospho-Drp1 serine 616	5% BSA/TBST	1:1000	Rabbit	Goat anti-rabbit 800CW	CST	4494S
Phospho-Drp1 serine 657	5% BSA/TBST	1:1000	Rabbit	Goat anti-rabbit 800CW	CST	6319S
Total Drp1	5% milk/TBST	1:1000	Rabbit	Goat anti-rabbit 800CW	CST	8570
Phospho-eNOS	5% milk/TBST	1:1000	Mouse	Donkey anti-mouse 680RD	BD Transductions	612393
ICAM	5% milk/TBST	1:10000	Goat	Donkey anti-goat 680RD	R&D Systems	AF796
Mitofusin 1	5% milk/TBST	1:200	Mouse	Donkey anti-mouse 680RD	Abcam	ab126575
Mitofusin 2	5% milk/TBST	1:200	Mouse	Donkey anti-mouse 680RD	Abcam	ab56889
OPA1	5% milk/TBST	1:1000	Rabbit	Goat anti-rabbit 800CW	Rabbit	80471S
Phospho-PKB serine473	5% BSA/TBST	1:1000	Rabbit	Goat anti-rabbit 800CW	CST	9271S

Table 2.7 Summary of anti-bodies used herein

2.5.8 Nitrite concentration

Investigating NO levels can be difficult, due to it being a small, diffusible radical molecule with a short half-life. Therefore, alternative methods to indirectly measure NO have been developed. One such method is measuring nitrite (NO_2^-), which is a stable, non-volatile metabolite of NO. The assay was first developed by Peter Griess (1879) and utilises a diazotisation reaction that occurs when sulfanilamide is added to a biological sample containing NO_2^-. The diazonium salt that is formed in this reaction can then react with the azo dye agent (N-1-napthylethylenediamine dihydrochloride; NED) to form an azo compound, which is pink in colour. The samples can be measured using an absorbance reader, where absorbance and NO_2^- concentration are positively correlated.

NO_2- concentration was determined in both plasma and cellular media using the Griess Reagent System (Promega, G2930). Standard wells of known nitrite concentration were loaded in triplicate into 96-well plate using the 0.1M Nitrite Standard supplied in the assay kit to create a standard curve ranging from 0-100µM. 50µl of sample (plasma diluted 1:10 in dH_20) was loaded in duplicate. 50µl of the Sulfanilamide Solution was added on all experimental samples and the wells containing the Nitrite Standard. After 5-10 minutes incubating at room temperature, 50µl of the NED Solution was added. The plate was incubated again at room temperature for 5-10 minutes, whilst being protected from light, and the sample absorbance measured at 540nm using the EnVision 2104 Multilabel Plate Reader. The standard curve was then created using the mean absorbance of wells against known NO_2^- concentration, thus the NO_2^-concentration of unknown samples could be extrapolated from the standard curve using the mean absorbance values.

2.5.9 Endothelin-1 ELISA

Since the discovery of ET-1, several studies have suggested a link between high circulating levels of ET-1 and CVDs such as atherosclerosis and hypertension. Raised ET-1 has also been associated with metabolic disorders (obesity and T2D) and neurodegenerative disorders, including AD. Therefore, ET-1 is measured herein.

The ET-1 ELISA was completed by Dr Alison McNeilly in a shared plate in order to reduce waste. ET-1 was measured using an assay which employs the quantitative sandwich enzyme immunoassay technique (R&D Systems, DET100). The assay contains a microplate that has been pre-coated with a monoclonal antibody specific for ET-1. Standards and samples are loaded into the plate and ET-1 present in the samples will be bound by the antibody. After wash steps, a horseradish peroxidase-linked antibody, also specific for ET-1 (ET-1 conjugate) is added to the wells. Following wash steps, substrate solution is added, which reacts with horseradish peroxidase to induce a colour change. The colour development is directly proportional to the amount of ET-1 bound.

In brief, 150µl of Assay Diluent RD1-105 was added to each well. Standard wells of known ET-1 concentration (75µl) were loaded in duplicate, whilst 75µl of sample (plasma) was added to experimental wells before the plate was covered incubated for 1 hour at room temperature on an orbital shaker to allow antibody binding. Solutions were decanted and wells were washed four times with 400µl Wash Buffer. 200µl of ET-1 conjugate was added to each well using a multichannel and the plate was covered and incubated for 3 hours at room temperature on the shaker. Once again, solutions were decanted and wells were washed four times with 400µl Wash Buffer. 200µl substrate solution was added to each well and the plate was incubated for 30 minutes at room temperature, protected from light. Following this incubation, 50µl stop solution was added to each well and the plate was read at 450nm using the EnVision 2104 Multilabel Plate Reader. The standard curve was then created using the mean absorbance of wells against known ET-1 concentration. Therefore, ET-1 concentration of unknown samples can be calculated.

2.6 Cell culture

All cell culture was done under sterile conditions. All cell lines were maintained at 37°C in an incubator with an atmospheric O_2:CO_2 ratio of 95:5%.

2.6.1 Palmitate

100mM palmitate was dissolved in a 15ml Falcon tube in 5ml 0.2M NaOH at 70°c (water bath) for 15 minutes. Once dissolved, palmitate was conjugated to 2% BSA by adding 0.5ml of dissolved palmitate to 4.5ml of 2% fatty acid free BSA (Sigma, A8806-5G)/dH_20 and placing the Falcon tube at 55°c (water bath) for a further 15 minutes. The vehicle control was made by adding 0.5mL of 0.2M NaOH to 4.5ml of 2% BSA/dH_20 and placing the Falcon tube at 55°c (water bath) for a further 15 minutes. These solutions were filter sterilised before being aliquoted and stored at -20°C. Prior to a palmitate incubation, palmitate aliquots were defrosted then heated (heat block) at 55°c for 15 minutes. The solution was only used if it remained clear (cloudy solutions are indicative that the palmitate is not conjugated to the BSA).

2.6.2 RBE4 cell culture

The rat brain endothelial cell line RBE4 was a kind gift from Michael Aschner (Albert Einstein College of Medicine, New York, USA). To create the cell line, cells were isolated from rat brains, cultured and subsequently transfected after two passages with the plasmid pE1A/neo[351]. The plasmid pE1A/neo carries the E1A region of Adenovirus 2 and the neomycin-resistance gene for selection by resistance to G418.

Cells were maintained in T-75 cell culture flasks in 1:1 Alpha MEM (Gibco, 12571089) to Ham's F10 (Gibco, 11550043), supplemented with 10% foetal bovine serum (SeraLab, discontinued), 1% penicillin/streptomycin (p/s; Gibco, 15140122), 2 mM L-glutamine (Gibco, 25030081) and 300 µg/ml G418 (Gibco, 10131027). RBE4 cells were passaged 2-3 times per week.

2.6.3 bEnd.3 cell culture

The mouse brain endothelial cell line bend.3 was a generous gift from Brenda Kwak (University of Geneva, Switzerland). The cell line was originally transformed by infecting isolated cerebral endothelial cells (BALB/c mice) with a middle T antigen expressing N-TKmT retrovirus and the endothelial nature of these cells was confirmed by the expression of von Willebrand factor[352].

bEnd.3 cells were maintained in 1% gelatin (Sigma, G1393) coated flasks in Dulbecco's modified Eagle's medium (DMEM) diluted 1:5 with Hank's Buffered Saline Solution (HBSSl Invitrogen, 14060073), to reduce the concentration of amino acids (AA), especially L-glutamine (L-glut), to physiological levels. The reason for using this reduced-AA method is because L-glut levels are 8x higher in cellular media than they are in the blood (culture media = ~4mM, blood – ~0.5mM[353]). Other AAs are also present at higher concentrations in cellular media compared to blood, such as leucine, iso-leucine, valine, and methionine[353]. The reason for such high concentrations, particularly L-glut, is to give the cells extra fuel in times of glucose scarcity, meaning cultured cells are easy and flexible model systems for researchers. However, 25mM glucose and high AA concentration together could act as a nutrient overload, stressing cells and inducing dysfunction. This reduced-AA DMEM was then supplemented with either 5mM or 25mM sterile D-glucose (Sigma, G8270) 5% foetal bovine serum and 1% p/s. Therefore, bEnd.3 cells were cultured at either 5mM glucose (normal glucose) or 25mM glucose (high glucose). bEnd.3 cells were passaged 2-3 times per week.

2.6.4 Insulin stimulations

Cells (bEnd.3 or RBE4) were seeded at $2.5x10^5$ cells per well (6-well plate) in 2ml growth media and left to adhere overnight. Prior to insulin stimulations, cells were starved of serum for 2 hours (RBE4s) or 0, 2, 8, or 16 hours (bEnd.3). Insulin was applied to the cells at concentrations ranging from 0-100nM for 5, 10, or 30 minutes. Details of serum starve length and insulin concentrations can be found in the figure legends. After insulin incubations, media was removed and cells were washed with ice-cold PBS before being lysed in 100µl lysis buffer (2.9 Commonly used lab solutions). The cell suspension was then centrifuged at 13000g for 15 minutes to pellet cellular debris. Supernatant was retained for protein concentration determination.

2.6.5 Glucose and palmitate experiments

bEnd.3 cells were plated at a seeding density of $2.5x10^5$ cells per well (6-well plate) in 2ml media (5mM glucose or 25mM glucose) and allowed to adhere overnight. The next day media was removed and replaced with fresh media, before the cells were exposed to varying concentrations of palmitate (in 2% fatty acid free BSA/0.02M NaOh) or vehicle (2% BSA/0.02M NaOH) for varying incubation times. Details of incubation time and concentration are stated in figure legends. Post-incubation, media was removed and retained for further analysis. Cells were washed in PBS and then lysed in 100µl lysis buffer (2.9 Commonly used lab solutions) or 500µl TRIzol. The cell suspension was then sonicated at 25% amplitude for 20s (5 pulses of 4 seconds on 1 second off) to lyse mitochondrial membranes and centrifuged at 13000g for 15 minutes to pellet cellular debris. Supernatant was retained for protein concentration determination (section 2.6.5). Cells lysed in TRIzol were subjected to RNA extraction, cDNA synthesis, and gene expression analysis protocols (sections 2.6.2 – 2.6.4)

2.7 Measuring mitochondrial bioenergetics

2.7.1 Seahorse XF24 Analyser

The Seahorse XF24 Analyser allows continuous direct measurements of the bioenergetics of cultured cells. The analyser uses a sensor cartridge in a 24-well plate format. Each sensor has two fluorophore-embedded probes, one of which is sensitive to oxygen (O_2) and the other is sensitive to changes in pH. During a measurement, the sensor cartridge moves to approximately 200µm away from the cell monolayer, creating a microenvironment of around 7µl. The Seahorse instrument uses fibre optic light that, when emitted, excites the fluorophores embedded in the sensors. The fluorophores emit light of a different wavelength (Stoke's shift), which is then detected by the instrument. The extent by which the wavelength changes is sensitive to the presence of O_2 and varying pH levels. The instrument can therefore automatically calculate the oxygen consumption rate (OCR) and the extracellular acidification rate (ECAR). This is useful for measuring the capacity of cellular respiration. Actively respiring mitochondria consume O_2, allowing for the OCR to be taken as a direct measure of OXPHOS. ECAR

reflects the release of lactic acid into the media as a result of its conversion from pyruvate during glycolysis.

2.7.2 Mito Stress Test Kit

The Mito Stress Test Kit measures key parameters of mitochondrial function by directly measuring changes in OCR in real time. The assay makes use of pharmacological inhibitors toward key parts of the respiratory chain to underpin the mitochondrial function of cells of interest. The OCR read out can then be used to extrapolate information regarding respiratory status such as the rate of oxygen used by the cell for basal respiration, ATP-linked respiration, respiratory capacity, maximal respiration, proton leak and non-mitochondrial oxygen consumption (Fig. 2.10).

Oligomycin is a potent inhibitor of ATP synthase (complex V) and its addition via the injection ports acts to decrease electron flow through the ETC. It is used to investigate the extent of oxygen used for mitochondrial-dependent ATP production. The second injection is carbonyl cyanide-4 (trifluoromethoxy) phenylhydrazone (FCCP), an uncoupler that collapses the proton gradient and disrupts mitochondrial membrane potential. This allows for the maximum respiratory ability of the mitochondria to be measured, as the ETC works at maximum to maintain the dissipated proton gradient.

The third and final injection is a mixture of rotenone and antimycin A, a complex I inhibitor and complex III inhibitor respectively. These inhibitors cause the respiratory chain in the mitochondria to shut down completely and allows calculation of non-mitochondrial respiration.

2.7.3 Mito Stress Test Optimisation

To optimise cell density, cells were plated in a normal 96-well plated at various densities ranging from $1x10^4$ – $1x10^5$ cells and left to settle and grow for two days. Optimum density was identified by visualising cells; bEnd.3 cells should be utilised when they are

a confluent monolayer. $3x10^4$ cells/well was chosen as the optimum cell density. Two days before performing the Seahorse protocol, bEnd.3 cells were seeded at $3x10^4$ cells/well into a Seahorse XF24 Microplate (Agilent, 100777-004) in 200µl normal growth media (20/80 DMEM/HBSS, 5mM glucose). The day previous to performing Seahorse, a sensor cartridge was hydrated in 1ml of Seahorse XF calibrant (Agilent, 100840-000) per well and left to incubate overnight at 37°C in the absence of CO_2. The day of the Seahorse assay, cells were retrieved from the incubator and 150µl of media was removed, leaving 50µl behind so as not to let the cells 'dry out'. 950µl of assay media was added to the cells and then removed. Assay media is composed of Seahorse XF DMEM Medium (Agilent, 103575), 0.8mM L-glut (Agilent, 103579-100), and 5mM glucose (Agilent, 103577-100). 450µl of assay media was then added to the cells (500µl final volume assay media) and they were allowed to incubate in the absence of CO_2 for 45 minutes to an hour. Using the Mito Stress Test Kit (Agilent, 103015-100) optimisation of oligomycin was performed first. Oligomycin concentrations of 20µM, 15µM, 10µM and 5µM were made up in assay media. FCCP was made up at a concentration of 10µM, whilst rotenone and antimycin A were made up at a concentration of 5µM. The sensor cartridge was retrieved from the incubator and 56µl of the differing oligomycin concentrations (Fig. 2.11A), 62µl of 10µM FCCP and 69µl of 5µM rotenone/antimycin A was added to port A, B, and C respectively. When these compounds are injected during the assay, they are diluted 1:10 into the Seahorse media, resulting in working concentrations of 2µM, 1.5µM, 1µM, and 0.5µM oligomycin, 1µM FCCP and 0.5µM rotenone/antimycin A. Once loaded, the sensor cartridge was calibrated in the Seahorse machine before the cells were loaded into the machine and the Mito Stress Test protocol was started. The protocol is a modifiable algorithm embedded in the Seahorse software, that dictates to the machine when to inject compounds, mix the media, and take OCR/ECAR measurements. From the results seen in Fig. 2.11B, it was decided that for future experiments 1.5µM oligomycin would be used.

Following the oligomycin optimisation, FCCP concentration was optimised in the same manner from the following concentrations: 2µM, 1µM, 0.5µM, and 0.25µM (2.12A). From the results seen in fig 2.12B, a concentration of 1µM was taken forward for future experiments.

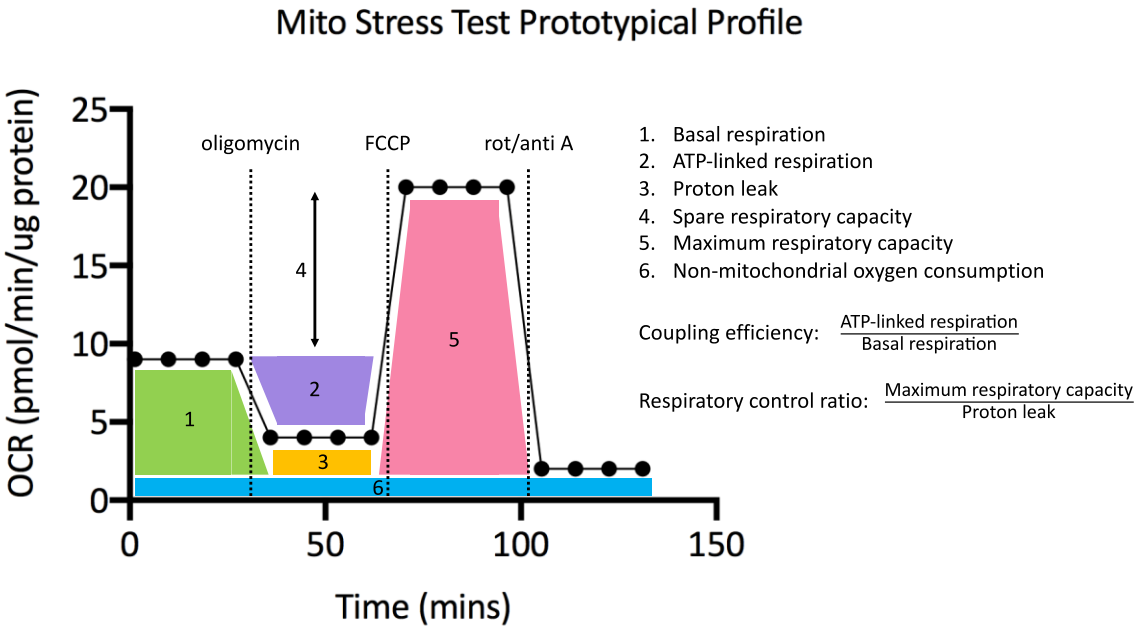

Figure 2.10 Prototypical representation of a Mito Stress Test profile

Schematic showing representative oxygen consumption rate (OCR) per µg of protein of cells in response to varying mitochondrial modulators (oligomycin, FCCP, and rotenone/antimycin A). The numerical key indicates the different parameters of mitochondrial respiration that can be extrapolated from these data.

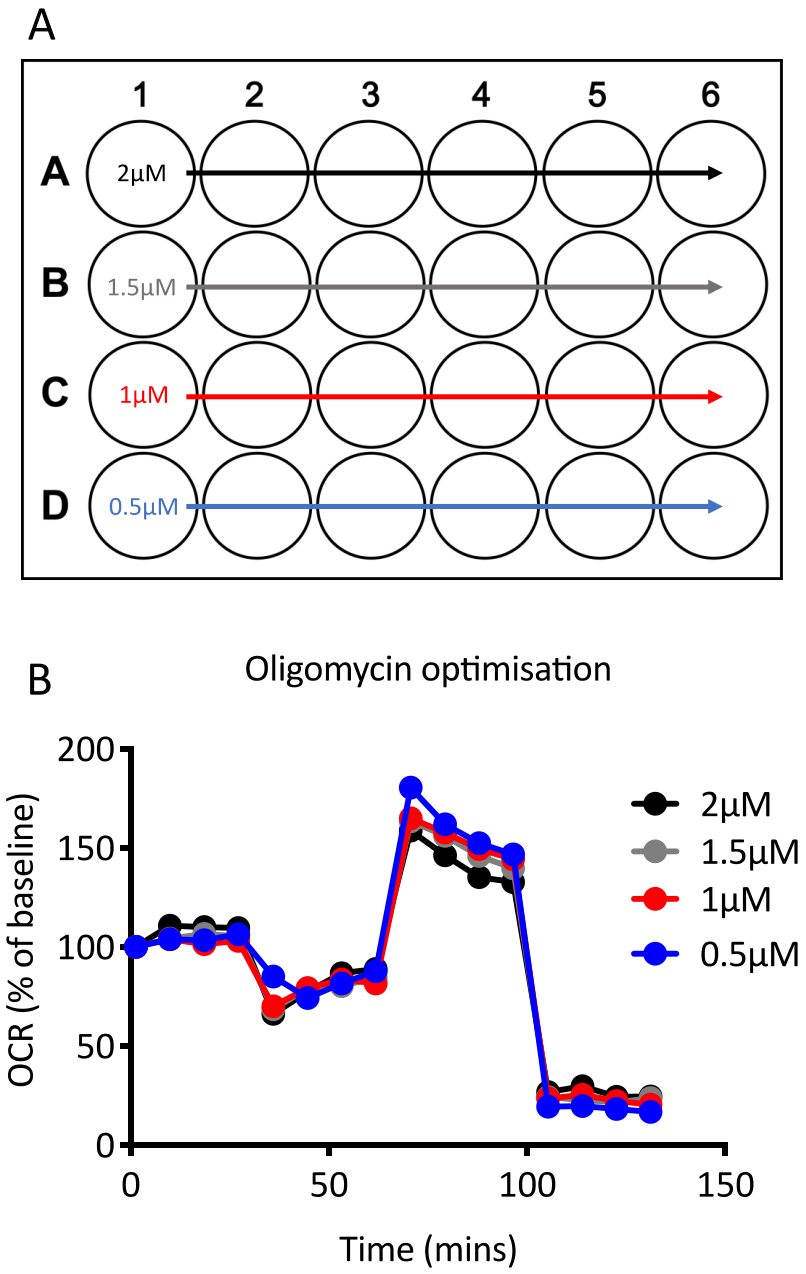

Figure 2.11 Oligomycin optimization

(A) Seahorse microculture plate layout depicting final oligomycin concentrations used for optimisation. (B) % OCR values (baseline = 100%) during a Mito Stress Test with differing concentrations of oligomycin ranging from 0.5-2µM. Wells A1, B5, C3, and D6 were used as background wells, in which no cells were plated.

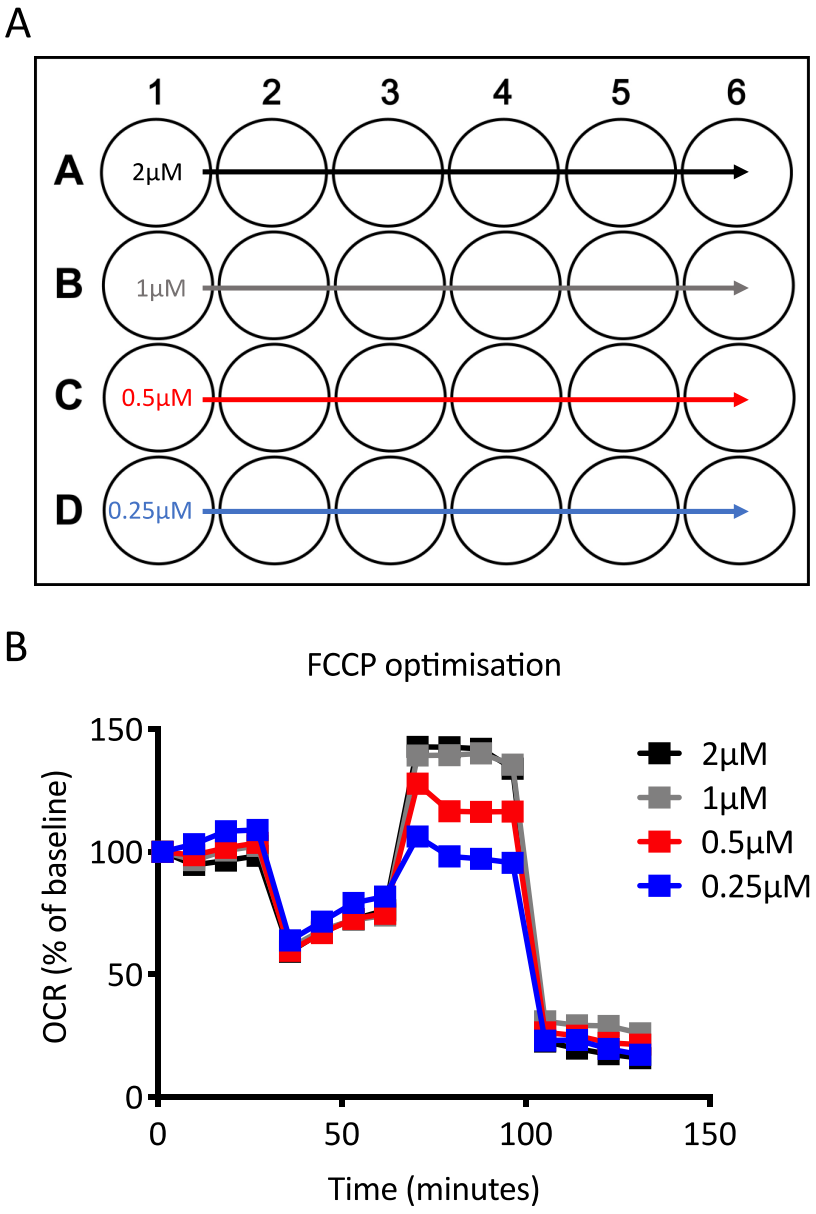

Fig. 2.12 FCCP optimisation

(A) Seahorse microculture plate layout depicting final FCCP concentrations used for optimisation. (B) % OCR values (baseline = 100%) during a Mito Stress Test with differing concentrations of FCCP ranging from 0.25-2µM. Wells A1, B5, C3, and D6 were used as background wells, in which no cells were plated.

2.7.4 Glucose and palmitate experiments

Two days before performing the Seahorse assay, bEnd.3 cells were seeded at $3x10^4$ cells/well into a Seahorse XF24 Microplate in 200µl normal growth media (20/80 DMEM/HBSS, 25mM glucose). The day previous to performing Seahorse, a sensor cartridge was hydrated in 1ml of Seahorse XF calibrant (Agilent, 100840-000) per well and left to incubate overnight at 37°C in the absence of CO_2. For 24-hour palmitate exposures, 25 hours prior to the assay 100µl media was removed and 100µl of fresh media containing 200µM palmitate or control was added. This produce a final concentration of 100µM palmitate. For 6-hour palmitate exposures, 7 hours prior to the assay 100µl media was removed and 100µl of fresh media containing 800µM palmitate or control was added. This produced a final concentration of 400µM. Following palmitate exposures, cells were retrieved from the incubator and 150µl of media was removed, leaving 50µl behind so as not to let the cells 'dry out'. 950µl of assay media was added to the cells and then removed. Assay media is composed of Seahorse XF DMEM Medium, 0.8mM L-glutamine, and 5mM glucose. 450µl of assay media was then added to the cells and they were allowed to incubate in the absence of CO_2 for 45 minutes to an hour. During this degassing period, the cartridge plate was loaded with 56µl of 15µM oligomycin in port A, 62µl of 10µM FCCP in port B, and 69µl of 5µM rotenone/antimycin in port C. Once loaded, the sensor cartridge was calibrated in the Seahorse machine before the cells were loaded into the machine and the Mito Stress Test protocol was started. Plates were retained for calculating protein content for further analysis.

2.7.5 $A\beta_{42}$ Mito Stress Test experiments

2nM $A\beta_{42}$ or ScrP was 'aged' in experimental media (20/80 DMEM/HBSS, 25mM glucose) in a 37°C cell culture incubator for 5 days prior to cell exposure to allow the peptide to aggregate slightly. A previous PhD project in the lab completed by Dr Jennie Gabriel optimised this 'ageing' time period and observed via Western blot that $A\beta_{42}$ is present mostly in dimers, with some oligomerisation, after 5 days[354]. Purified Aβ from human

CSF has revealed that dimers are indeed associated with neurodegeneration[355]. Two days before performing the Seahorse assay, bEnd.3 cells were seeded at $3x10^4$ cells/well into a Seahorse XF24 Microplate in 200µl media (20/80 DMEM/HBSS, 25mM glucose). The day previous to performing Seahorse experiment, a sensor cartridge was hydrated in 1ml of Seahorse XF calibrant per well and left to incubate overnight at 37°C in the absence of CO_2. 25 hours prior to the assay 100µl media was removed and 100µl of ScrP or $A\beta_{42}$ media containing 200µM palmitate or control was added. This produced a final concentration of 1nM ScrP or $A\beta_{42}$ and 100µM palmitate (or control). Following a 24-hour exposure, the same steps as in the glucose/palmitate experiments were performed.

2.7.4 Mito Stress Test analysis

Extrapolated data obtained from Mito Stress Tests is indicated in Fig. 2.10. Data are expressed as OCR (pmol/min), which is usually normalised to protein or DNA content. Four readings are taken prior to and after each injection. These values are then averaged and used to deduce the parameters exhibited in Fig. 2.10. A description of these parameters and what the measurements may be sensitive to are given in Table 2.8[356]. Data can also be expressed as %OCR over time in order to obtain internally normalised data. The reason for expressing OCR as an internally normalised % is to identify changes in individual mitochondrial parameters or whether mitochondrial function is changed due to substrate availability (changes to TCA cycle or glycolysis).

Parameter	Definition	What sets the rate
Basal respiration	Resting mitochondrial respiration performed by the cell to meet the endogenous ATP demand and drive proton leak.	Rate of basal respiration is set by ATP demand, substrate availability/oxidation, and proton leak.
ATP-linked respiration	The rate of mitochondrial respiration that is sensitive to oligomycin (ATP-synthase inhibitor), and therefore the rate that is used to drive ATP synthesis.	The rate of ATP-linked respiration is set by ATP demand. High ATP demand = high ATP-linked respiration values.
Proton leak	OXPHOS is not completely coupled to ATP synthesis, and protons will leak across the IMM. Proton leak is the rate of mitochondrial respiration that remains in the presence of oligomycin.	Oligomycin-insensitive respiration is set by proton leak. Rate of respiration can be set by basal proton leak (membrane leakiness, ADP translocase) or inducible proton leak (UCPs). High proton leak could be indicative of mitochondrial dysfunction, or a normal adaptation.
Spare respiratory capacity	The difference between maximum respiratory capacity and basal respiration. The ability of a cell to meet an increased energy demand. Also indicates how the cell is working basally	Spare respiratory capacity is dependent on factors affecting basal respiration, as well as factors affecting maximal respiration.
Maximum respiratory capacity	FCCP is a mitochondrial uncoupler that dissipates mitochondrial membrane potential. In response to uncoupling, mitochondria will maximise substrate oxidation and ETC activity to maintain mitochondrial membrane potential.	Maximal respiration is set by substrate availability and the capacity of mitochondria to oxidise them (substrate transport, metabolic enzymes, ETC complexes). A reduced maximum respiratory capacity may be indicative of impaired function or may be due to reduced substrate availability.
Non-mitochondrial oxygen consumption	Mitochondrial respiration can be inhibited upon inhibiting ETC complexes I and III using rotenone and antimycin A respectively. Therefore, respiration remaining after the injection of these compounds is dependent on oxygen utilised by the cell for other processes.	May be sensitive to cytoplasmic oxidases and cytoplasmic ROS production.
Coupling efficiency	The fraction of basal respiration used to drive ATP-synthesis. Calculated by dividing ATP-linked respiration by basal respiration.	Coupling efficiency is sensitive to ATP demand, substrate availability, and proton leak. A high coupling efficiency may be due to a high ATP demand. Reductions in coupling efficiency may be due to increased proton leak, or reduced substrate availability or transport.
Respiratory control ratio	The fraction of maximal respiration used for proton leak. A measure of mitochondrial metabolic flexibility and ability to respond to cellular demand.	The respiratory control ratio is sensitive to substrate oxidation and proton leak, but not to ATP turnover. Reduced respiratory control ratio may be due to increased proton leak or reduced maximum capacity and is therefore sensitive to factors affecting both of these parameters.

Table 2.8 Mito Stress Test analysis

2.7.6 Glycolysis Stress Test

The Glycolysis Stress Test, by measuring pH of the culture media, gives a direct measure of glycolytic function. During glycolysis, glucose is converted to pyruvate, which is then converted to lactate in the cytoplasm or CO_2 and water in the mitochondria. The conversion of glucose to pyruvate to lactate results in the production and extrusion of protons out of the cell, therefore acidifying the surrounding culture media. Thus, changes in ECAR, which is positively correlated with the rate of lactate production, is a good measure of glycolytic function. The Glycolysis Stress Test exploits the use of 3 compounds that are modulators of glycolytic function: glucose, oligomycin, and 2-deoxyglycose (2-DG). Cells are initially incubated in assay medium without substrate (glucose and pyruvate) and basal ECAR is measured. 10mM glucose is then injected in order to record glycolytic rate for a given concentration of glucose. The ATP-synthase inhibitor oligomycin is added next to measure the glycolytic capacity of the cells as they are forced to maintain their ATP production via glycolysis instead of OXPHOS. The final injection is 2-DG, a glucose analogue that inhibits glycolysis through competitive binding to hexokinase, the first enzyme in the glycolytic pathway. This final injection can be used as a confirmation that the changes in ECAR measured throughout were due to glycolytic rate and not OXPHOS, which does have acidification capacity. A prototypical Glycolysis Stress Test can be observed in Fig. 2.13.

2.7.7 Glycolysis Stress Test experiments

Two days before performing the Seahorse assay, bEnd.3 cells were seeded at $3x10^4$ cells/well into a Seahorse XF24 Microplate in 200µl media (20/80 DMEM/HBSS, 5mM glucose). Sensor cartridges were hydrated overnight in 1ml of Seahorse XF calibrant per well at 37°C in the absence of CO_2. On the day of the assay, cells were retrieved from the incubator and 150µl of media was removed, leaving 50µl behind so as not to let the cells ‘dry out’. 950µl of assay media was added to the cells and then removed. Assay media for Glycolysis Stress Tests is composed of Seahorse XF DMEM Medium, supplemented 0.8mM L-glutamine. No glucose or pyruvate can be present. 450µl of assay media was then added to the cells and they were incubated in a non-CO_2 incubator

for 45 minutes to an hour. During this degassing period, the cartridge plate was loaded with 56µl of 100mM glucose, 62µl of 15µM oligomycin in port B, and 500mM 2-DG in port C. Once loaded, the sensor cartridge was calibrated in the Seahorse machine before the cells were loaded into the machine and the Glycolysis Stress Test protocol was started. Plates were retained for calculating protein content for further analysis.

2.7.8 Glycolysis Stress Test analysis

Typical data obtained from Glycolysis Stress Tests can be observed in Fig. 2.13. Data are expressed as ECAR (mpH/min), which is usually normalised to protein or DNA content. Similar to Mito Stress Tests, four basal readings are taken as well as four measurements after each injection. Averages of these four readings are then made in order to work out different parameters of glycolysis (Fig. 2.10). Description of the varying parameters regarding glycolytic function that can be obtained from these tests are given in Table 2.9.

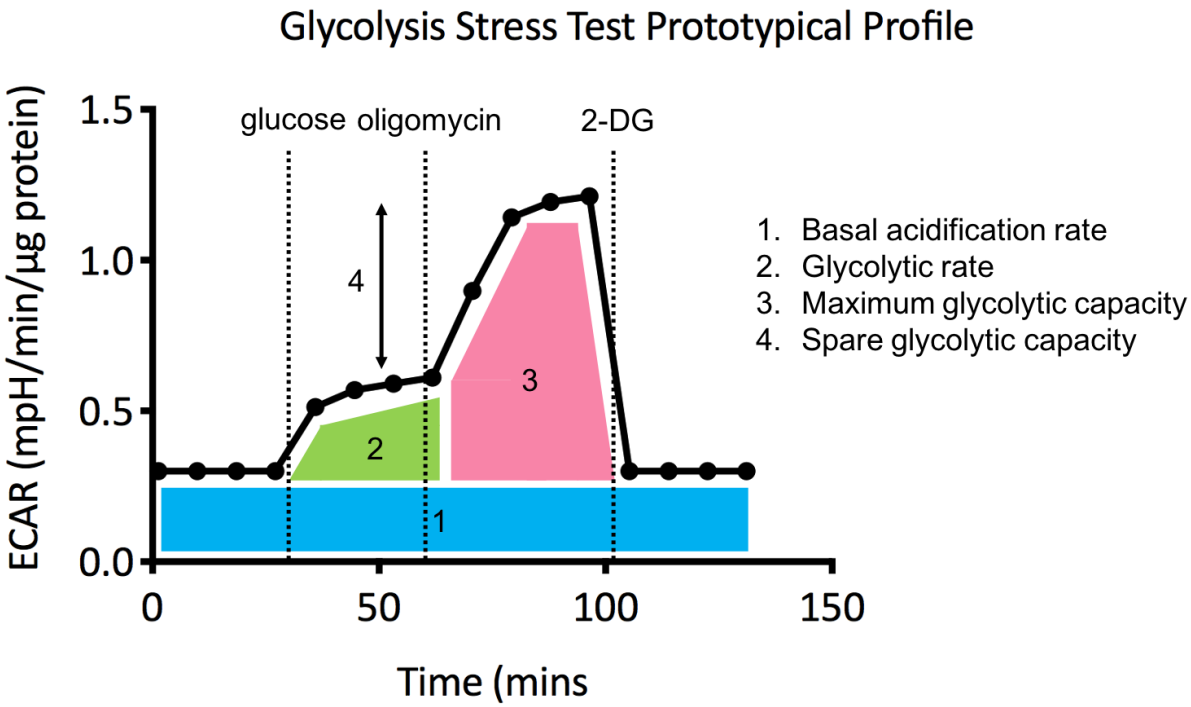

Figure 2.13 Prototypical representation of a Glycolysis Stress Test profile

Schematic showing representative extracellular acidification rate (OCR) per µg of protein of cells in response to varying glycolytic modulators (glucose, oligomycin, 2-DG). The numerical key indicates the different parameters of glycolytic function that can be extrapolated from these data.

Parameter	Definition	What sets the rate
Basal acidification rate	The cells contribution to acidification of the media at rest. Should be relatively low and constant without available substrate (glucose/pyruvate).	Any metabolic pathways that expel protons (H^+) as a by-product, or CO_2, which is hydrated to carbonic acid and released as bicarbonate with H^+. In assay medium, the only available substrate is L-glutamine. Glutaminolysis leads to production of alpha-ketoglutarate, thus basal acidification may come from CO_2 expulsion during TCA cycle.
Glycolysis	The rate of acidification due to the conversion of glucose to pyruvate to lactate (anaerobic glycolysis).	Glycolytic rate will be sensitive to ATP demand, glucose availability, and activity of glycolytic enzymes, as well as the metabolic preference cells have for ATP production via glycolysis over OXPHOS.
Maximum glycolytic capacity	The rate of acidification due to glycolysis in the presence of the ATP synthase inhibitor oligomycin. Under these conditions, ATP production is solely performed by glycolysis, therefore ECAR should increase.	Maximum glycolytic capacity depends strongly on ATP demand of the cell, as well as substrate availability and activity of glycolytic enzymes.
Spare glycolytic capacity	The difference between maximum glycolytic capacity and normal glycolytic rate gives the spare glycolytic capacity. It is a good measure of the cells ability to respond to stress, as well as giving an indication as to how much the cell relies on glycolysis under normal conditions.	Since it is a measure derived from both glycolytic rate as well as maximum glycolytic capacity, it is sensitive to both of these parameters and the factors affecting them. If normal glycolytic rate is high or maximum glycolytic capacity low, then spare glycolytic capacity will be low.

Table 2.9 Glycolysis Stress Test analysis.

2.9 Mitochondrial staining

bEnd.3 cells (cultured in either 5mM glucose or 25mM glucose) were plated at a density of 250,000/well (6-well plate) on #1.5 (0.16-0.19mm thickness) square gelatin (1%) coated-coverslips and allowed to adhere overnight in growth media. The following day, media was removed and replaced with media containing either 100µM palmitate or vehicle control and incubated overnight. Following this, palmitate/control media was removed, and cells were washed once with pre-warmed PBS. The cells were then incubated for an optimised incubation time of 30 minutes with an optimised concentration of 250nM Mitotracker Red CMXRos (ThermoFisher, M7512) diluted in growth media. The media was removed, and the cells were washed twice in pre-warmed PBS before being fixed in 1ml 3.7% formalin at 37°C for 15 minutes. Formalin was removed and cells were washed twice with pre-warmed PBS. Cells were then incubated in 1µM DAPI in PBS (ThermoFisher, D1306) for 5 minutes at room temperature before being washed twice in Tris-buffered saline (TBS). Cells were then mounted onto glass slides using Prolong™ GOLD Antifade Mountant (ThermoFisher, P36930). Slide preparations were kept protected from light at 4°C. The following day, cells were imaged using a DeltaVision widefield fluorescent microscope. All images were taken and deconvolved by Dr Iain Porter.

2.9 Commonly used lab solutions

Constituent	**Quantity**
1M Tris-HCl pH 7.4	40mL
4M NaCl	74mL
Tween 20	1mL
dH_2O	Up to 2L

Table 2.10 2 litres Tris-buffered saline tween (TBST)

Constituent	Quantity
Tris-HCl	150g
Glycine	720g
dH_2O	Up to 5L

Table 2.11 5 litres 10x stock running buffer

Constituent	Quantity
10 x stock running buffer	200mL
10% SDS	20mL
dH_2O	Up to 2L

Table 2.12 2 litres 1x running buffer

Constituent	Quantity
Methanol	400mL
Tris-HCl	11.62g
Glycine	5.86
dH_2O	Up to 2L

Table 2.13 2 litres transfer buffer

Constituent	Quantity
1M Tris-HCl pH 7.4	12.5ml
750mM NaF	33.5ml
4M NaCl	12.5ml
500mM EDTA	10ml
200mM EGTA	12.5ml
Triton x-100	5ml
500mM NaPPi	10ml
dH_2O	400ml

Table 2.14 1x stock lysis buffer

Constituent	Quantity (per 1mL lysis buffer)
Sucrose	92mg
β-mercaptoethanol	1µL
1mM Na_3VO_4*	1µL
1mM benzamidine	1µL
0.1nM PMSF	1µL

* heat activate at 95°c for 5 minutes immediately prior to use

Table 2.15 Lysis buffer (immediately prior to use)

Constituent	Quantity
0.5M Tris pH 6.8	4mL
Glycerol	3.2mL
20% SDS	3.2mL
β-mercaptoethanol	1.6mL
Bromophenol blue	Pipette pinch

Table 2.16 4x sample buffer.

Chapter 3

Investigating endothelial and hypothalamic mitochondrial dynamics in mouse models of nutrient excess

3.1 Introduction

Nutrient excess is associated with many non-communicable diseases, including obesity, T2D, CVDs, and dementias[3,4]. Nutrient excess-associated diseases share common pathologies such as hyperglycaemia, dyslipidaemia, ED, and mitochondrial dysfunction.

ED is characterised by an impaired responsiveness to vasodilatory agents, reduced NO bioavailability, and decreased eNOS activity/coupling[90,94,102,357]. Furthermore, ED is associated with proinflammatory responses in the EC, termed activation, where ECs exhibit increased cell surface expression of cell surface adhesion molecules such as ICAM and VCAM[102]. Proinflammatory signalling molecules such as TNFα and IL-6 will induce an increase in the expression of cell-surface adhesion molecules, which facilitate leukocyte binding and diapedesis[102]. ED present in peripheral ECs reduces blood flow and promotes atherosclerosis, and reduces insulin transport, contributing to CVD development or insulin resistant states respectively. ED present in brain ECs impairs cerebral haemodynamics, reduces cerebral blood flow, and damages BBB integrity. Investigation into the development of nutrient excess-associated ED is therefore warranted.

ED is associated with pathologies linked to nutrient excess, such as hyperglycaemia and dyslipidaemia. Indeed, multiple studies investigating both *ex vivo*[138–141,153–156] and *in vitro*[154,162–164,171,172] models have reported ED is a direct consequence of nutrient excess. However, studies investigating nutrient excess on brain EC function are limited.

Furthermore, it is not clear exactly how nutrient excess leads to ED, but it has been proposed that mitochondria may play a role. Indeed, proper mitochondrial function is important for EC health[127]. Nutrient excess has been shown on numerous occasions to induce mitochondrial stress, evidenced by increased mROS production[198,273,276], reduced respiratory capacity[268–271,276,280], and dysregulated mitochondrial biogenesis[274,278,281–284]. As previously mentioned, chronically upregulated ROS production may be detrimental to EC function, as it is known to induce uncoupling of eNOS, inactivate NO to form $ONOO^-$, upregulate arginase activity, promote inflammation, and inhibit growth

factor signalling[357]. Furthermore, reduced mitochondrial respiration is associated with loss of BBB integrity[127]. Nutrient excess is also known to impair mitochondrial dynamics, with HG and high saturated fats promoting fission over fusion[274,278,281–284], resulting in dysfunctional and fragmented mitochondria in several cell types. However, the effects of nutrient excess on EC mitochondrial dynamics, and how this relates to brain EC dysfunction is not well understood.

Therefore, to establish how nutrient excess may affect endothelial mitochondrial dynamics, two models of nutrient excess were investigated. The first was a 6-month old 'mature adult' 10-week HFD-fed mouse vs. an age-matched NC-fed control. The reason for choosing 10 weeks HFD is that we have observed HFD-dependent vascular dysfunction *in vivo* with only 5 weeks HFD. It should be noted that two other groups – a 12-week old 'young adult' 10-week HFD-fed mouse vs. age-matched NC-fed control – were investigated as part of this study in order to determine the two-way effect of both age and diet on vascular function. Unfortunately, the weight trajectory of the 12-week old young adult HFD-fed mice suggested diet-induced obesity resistance (DIOR) at the beginning of the study, or perhaps under eating. At the time the young adult HFD-fed mice were on the study, the Medical School Resources Unit (MSRU; the animal unit at which the animal work is carried out) was suffering from ongoing structural and technical problems. It is assumed that many mice that were undergoing studies during this period were experiencing increased levels of stress, which could in turn lead to DIOR. For this reason, the *in vivo* data sets from HFD-fed young mice are not used herein. Young adult HFD-fed data sets are shown in Appendix S1, where both the weight trajectory and the anxious phenotype of the mice can be seen. The young adult NC-fed group is still used herein as a control group for testing the effect of purely aging on vascular function.

The other model of nutrient excess used was an 8-week old db/db mouse vs. wt/db and wt/wt age-matched controls. The phenotype of the db/db mouse is detailed in Methods section 2.2.4 Briefly, db/db mice are obese, hyperinsulinaemic, hyperglycaemia, and hyperphagic by 4-5 weeks of age. They are therefore an excellent model of severe metabolic syndrome and nutrient excess.

Body weight and *in vivo* endothelial function was assessed in these models, as well as expression of proteins involved in mitochondrial dynamics in tissues of interest - aorta, VE fraction, and hypothalamus. The aorta and VE fraction were used to investigate vascular mitochondrial dynamics. As previously mentioned in section 1.10, capillaries comprising the BBB at the ARC are fenestrated and leaky, meaning the hypothalamus is vulnerable to the effects of nutrient excess. Therefore, the hypothalamus is an area of interest. The hypothesis was that mitochondrial dynamics in these two models of nutrient excess would be impaired in the stated tissues and said impairment would be associated with ED and body weight gain.

3.2 Results

6-month 'mature adult' male WT mice were placed on either HFD or NC diet for 10 weeks to investigate the effect of diet. Mice were randomly assigned to HFD or NC groups, but the groups were weight matched. Alongside these groups, a group of 12-week old 'young adult' NC mice were used as a control against 'mature adult' NC-fed mice to investigate the effect of ageing. MATURE NC mice are compared to YOUNG NC mice to investigate the effect of age. The 6-month old groups will be referred to as MATURE NC and MATURE HF and the 12-week old group will be referred to as YOUNG NC. Therefore, in the *in vivo* data sets, MATURE HF mice are compared to MATURE NC mice to investigate the effect of diet. A timeline of this study can be observed in Fig 3.1. 3-week old female db/db mice, along with their wt/db and wt/wt littermates were used in the second study. A summary of this study timeline is provided in Fig. 3.2.

3.2.1 HFD-feeding increases body weight in 6-month old mice compared to controls

Body weights of mice were measured weekly over 10 weeks. MATURE HF mice gained significantly more weight than MATURE NC mice (Fig. 3.3B – MATURE NC 1.05g ± 0.85g vs. MATURE HF 8.87g ± 1.59g, $p < 0.001$, n = 9-11). When expressed as a percentage, MATURE HF mice gained significantly more weight than MATURE NC mice (Fig 3.3D – MATURE NC 0.73% ± 2.18% vs. MATURE HF 18.45% ± 5.14%, n = 9-11, $p < 0.01$). MATURE

NC mice did not differ from YOUNG NC mice in terms of body weight. From the weight trajectories (Fig. 3.3A, C), it is apparent that MATURE NC mice can maintain their weight at a steady value.

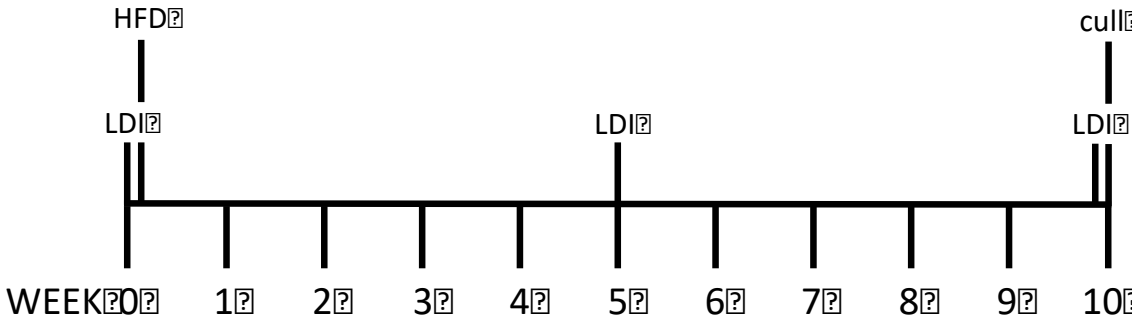

Figure 3.1 Study timeline for young/mature adult mice on NC or HFD

6-month old male mice were weight matched before undergoing an LDI scan on week 0 (basal scan). Following this basal scan, mice were placed on 45% HFD or maintained on NC diet. Microvascular EC function was measured again at weeks 5 and 10. At the end of the study mice were fasted overnight and culled the following morning. Tissue was harvested for post-mortem biochemical analysis.

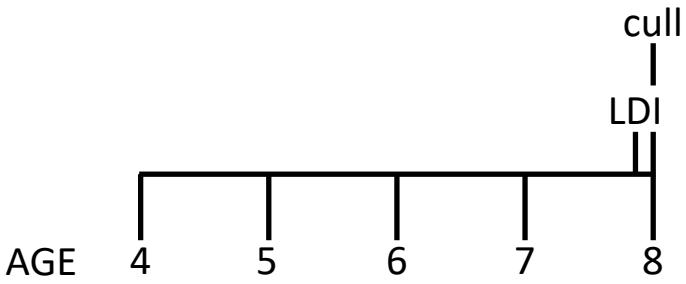

Figure 3.2 Study timeline for db/db mice

Wt/wt, wt/db, and db/db mice were weighed weekly from 4 until 8 weeks of age. Microvascular EC function was measured using LDI, before mice were fasted overnight and culled the following morning. Tissue was harvested for post-mortem biochemical analysis.

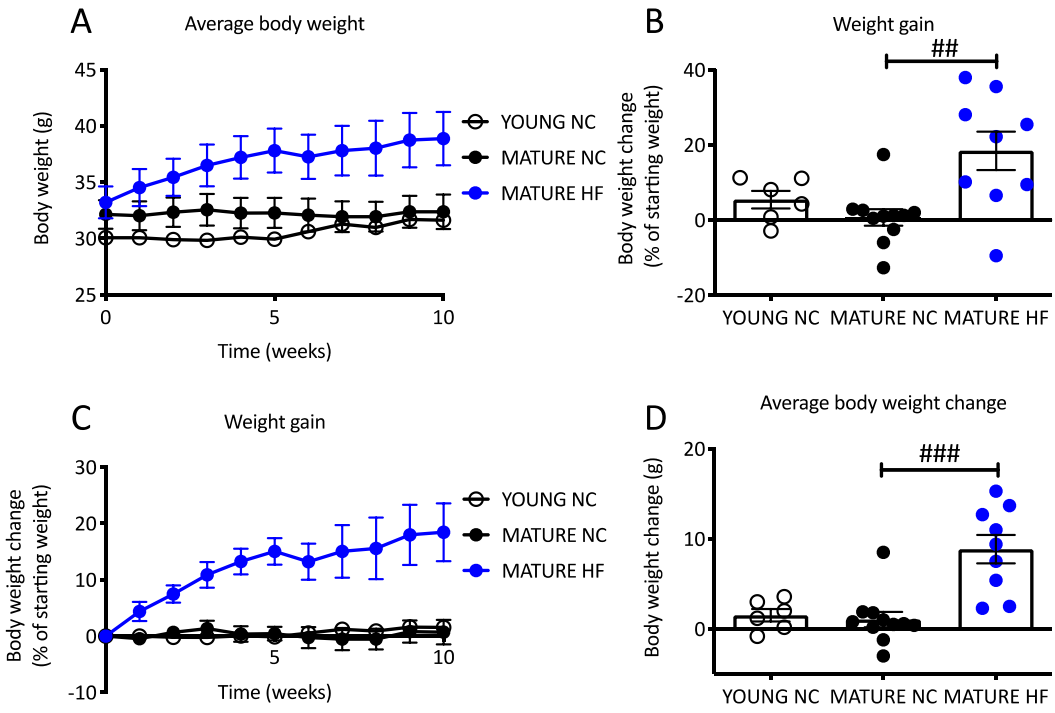

Figure 3.3 HFD-feeding in mature adult mice promotes weight gain

Young adult mice were fed NC diet for 10 weeks. Mature adult mice were fed either NC or HFD for 10 weeks. (A) Average weight of the mice over the 10 weeks of the study. (B) Net weight gain at the end of the study. (C) Percentage weight gain over the 10 weeks of the study. (D) Percentage weight gain at the end of the study.

Data are expressed as mean ± standard error of the mean.

n = 6-11. (B) and (D) ordinary one-way ANOVA with Bonferroni multiple comparison. ## = $p < 0.01$, ### = $p < 0.001$.

3.2.2 Ageing, but not HFD-feeding, is associated with impaired endothelial function *in vivo*

To measure endothelial function *in vivo*, mice undergo LDI and iontophoresis of vasoactive agents (phenylephrine [PE] to cause vasoconstriction and acetylcholine [ACh] to induce endothelium-dependent vasodilation). There are three main outputs that can provide information about EC health – 1) baseline flux skin perfusion (AU), 2) % Δ skin perfusion in response to ACh compared to PE-induced baseline, and 3) peak flux skin perfusion after ACh application (AU).

Pre-diet, the two cohorts of mice did not differ in terms of baseline skin perfusion as expected (Fig. 3.4A). Furthermore, mature NC did not differ from young NC mice in terms of baseline skin perfusion (Fig. 3.4A). After 5 weeks of dietary intervention, mature HF exhibited significantly lower baseline skin perfusion compared to mature NC (Fig. 3.4B – mature NC 289.2 ± 13.8 vs. mature HF 232.6 vs. 14.4, n = 9-11, $p < 0.05$), but mature NC mice did not differ from mature NC mice (Fig. 3.4B). At 10 weeks dietary intervention, mature HF exhibited a trend toward decreased baseline flux (AU) compared to mature NC, but this did not reach significance. Mature HF mice exhibited a decline in baseline flux compared to young NC mouse however, suggesting an additive effect of HFD-feeding and age on baseline skin perfusion (Fig. 3.4C – young NC 270.6 ± 16.0 vs. 198.2 ± 14.4, n = 6-9, $p < 0.05$). When internally normalised and expressed as a percentage change in baseline skin perfusion over time (compared to the basal pre-diet scan), mature HF mice exhibited a trend toward a decline in % baseline skin perfusion compared to the basal scan at 5 and 10 weeks dietary intervention, but this decline was not significant compared to mature NC (Fig. 3.4D).

To investigate EC function, the response in skin perfusion to PE application (constriction) followed by Ach application (dilation) was measured. This is expressed herein in two ways. Fig. 3.4A, C, E express % Δ in skin perfusion (first scan = 100%) against time. The time of PE and ACh application is represented by dotted lines. Fig. 3.4B, D, F exhibit % Δ skin perfusion in response to ACh where PE-constricted baseline is 100%. At baseline, there is no effect of age or diet on endothelial responsiveness to ACh (Fig. 3.5B). After 5 weeks of diet, ACh response is markedly reduced in both mature groups compared to

young NC, but this change is not sensitive to diet (Fig. 3.5D – YOUNG NC 39.18% ± 4.06% vs. MATURE NC 8.75% ± 5.05% vs. mature HF 10.39% ± 5.28%, n = 6-11, $p < 0.01$). Similarly, after 10 weeks of diet, ACh response in both mature groups is significantly reduced compared to the young NC group, but diet has no affect (Fig. 3.5F – young NC 40.61% ± 4.44% vs. mature NC 18.6% ± 3.39% vs. mature HF 13.43% ± 6.31%, n = 6-11, $p < 0.01$ mature NC vs. young NC, $p < 0.001$ mature HF vs. young NC). In terms of PE response, no strong effect of age or diet is observed. At the 5-week point, mature groups appear to exhibit a larger response to PE with increase vasoconstriction compared to young NC mice (Fig. 3.5C), but this effect disappears at the 10-week time point so may be a false result.

Peak skin perfusion (AU) was measured in response to ACh. Mature groups did not differ from one another or from the young NC group pre-diet (Fig. 3.6A). However, after 5 weeks of dietary intervention, both mature groups exhibited significantly reduced ACh-induced peak skin perfusion values (Fig. 3.6B – young NC 342 ± 6.4 vs. mature NC 266.50 ± 17.01, n = 6-11, $p < 0.01$; young NC 342 ± 6.4 vs. mature HF 216.60 ± 16.95, n = 9-11, $p < 0.001$), suggesting age is having an effect. At 10 weeks of dietary intervention, both mature groups exhibited reduced ACh-induced peak skin perfusion compared to young NC (Fig. 3.6C – young NC 357.3 ± 9.48 vs. mature NC 230.9 ± 13.34, n = 6-11, $p < 0.001$; young NC 357.3 ± 9.48 vs. mature HF 199.3 ± 8.63, n = 6-9, $p < 0.001$), suggesting an age-related effect. When internally normalised and expressed as a percentage of the basal scan, at 5 and 10 weeks both mature groups exhibit a significant reduction in peak skin perfusion compared to young NC but are not significantly different from one another (Fig. 3.6D – 5 weeks – young NC 115.37% ± 8.04% vs. mature NC 80.5% ± 6.89%, n = 6-11, $p < 0.01$; young NC 115.37% ± 8.04% vs. mature HF 65.81% ± 6.1% vs., n = 6-9, $p < 0.001$; 10 weeks – young NC 121.81% ± 11.95% vs. mature NC 68.85% ± 4.7%, n = 6-11, $p < 0.001$; young NC 121.81% ± 11.95% vs. mature HF 64.08% ± 6.91%, n = 6-9, $p < 0.001$).

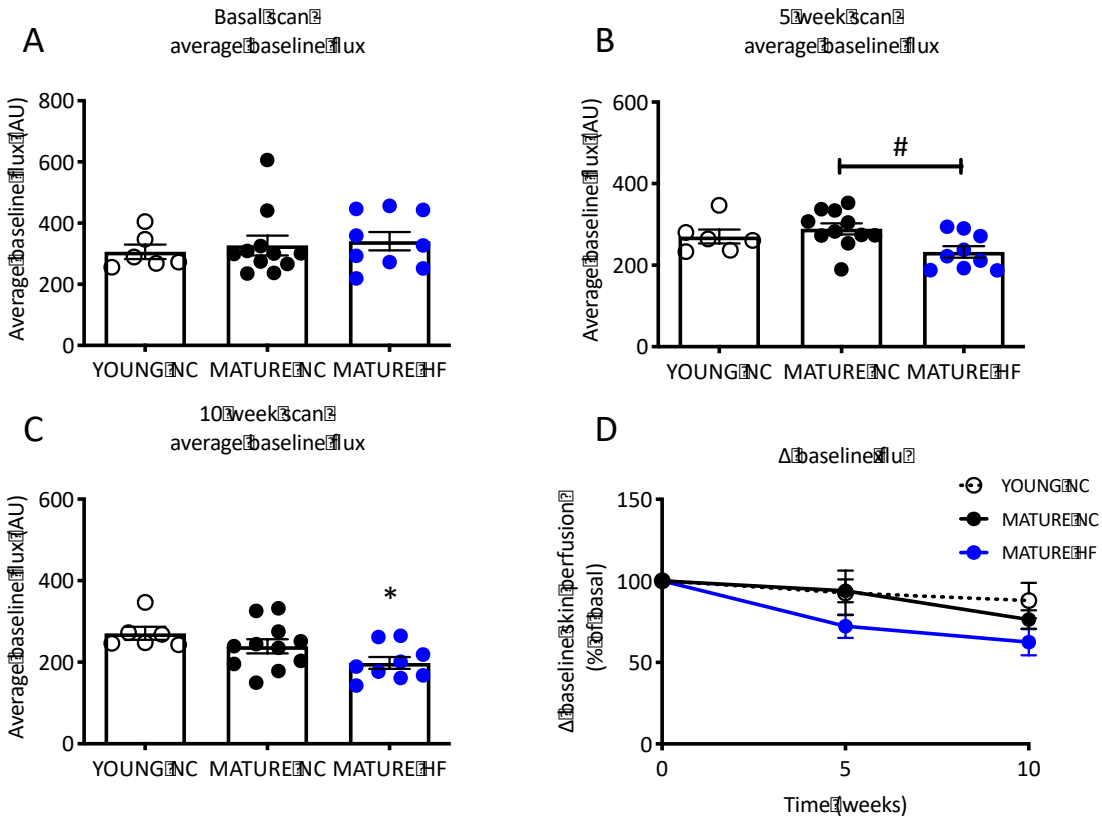

Figure 3.4 Effect of age and diet on baseline skin perfusion

Baseline skin perfusion (AU) was measured using LDI pre-diet (A), after 5 (B), and 10 weeks of dietary intervention (C). Data are also expressed as % Δ in baseline skin perfusion over time (weeks) in comparison to the basal pre-diet scan (D).

Data are expressed as mean ± standard error of the mean.

n = 6-11. (A), (B), and (C) – Welch's ANOVA with Dunnett's multiple comparison. * = $p < 0.05$ compared to YOUNG NC. # = $p < 0.05$. (D) – repeated measures with Bonferonni multiple comparison.

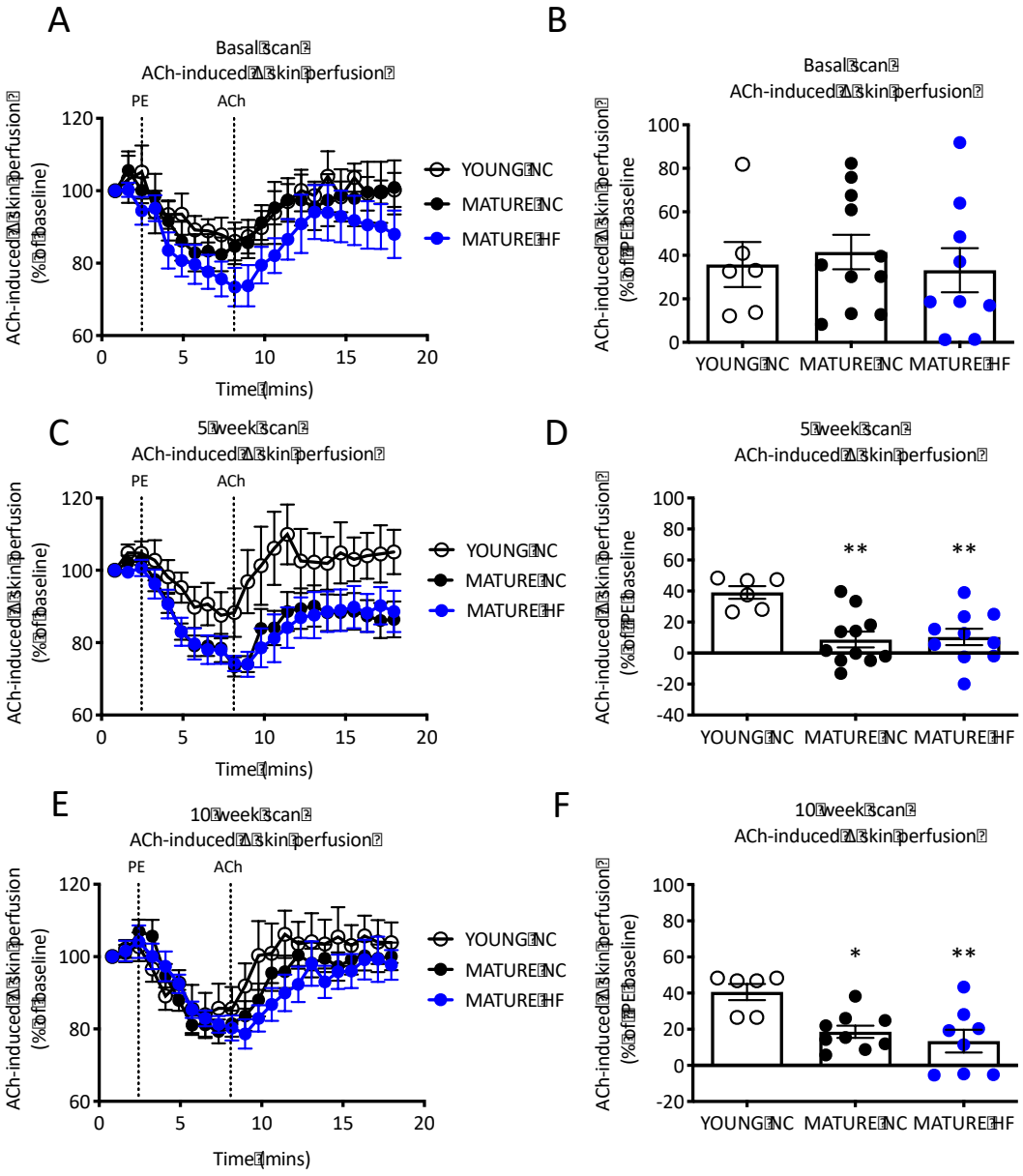

Figure 3.5 Ageing impairs endothelial response to ACh, but HFD-feeding has no effect

The effect of ageing and HFD on endothelial function was investigated by measuring endothelial response to the vasodilator ACh. PE- and ACh-induced Δ skin perfusion as a percentage of baseline (baseline is 100%) against time (minutes) pre diet (A), and after 5 (C) and 10 (E) weeks of dietary intervention. ACh-induced Δ skin perfusion as a percentage of the PE-induced normalised baseline pre diet (B), and after 5 (D) and 10 (F) weeks of dietary intervention

Data are expressed as mean ± standard error of the mean

n = 6-11. (B), (D), and (F) – Welch's ANOVA with Dunnett's multiple comparison. * = $p < 0.05$ in comparison to WT NC, ** = $p < 0.01$ in comparison to YOUNG NC.

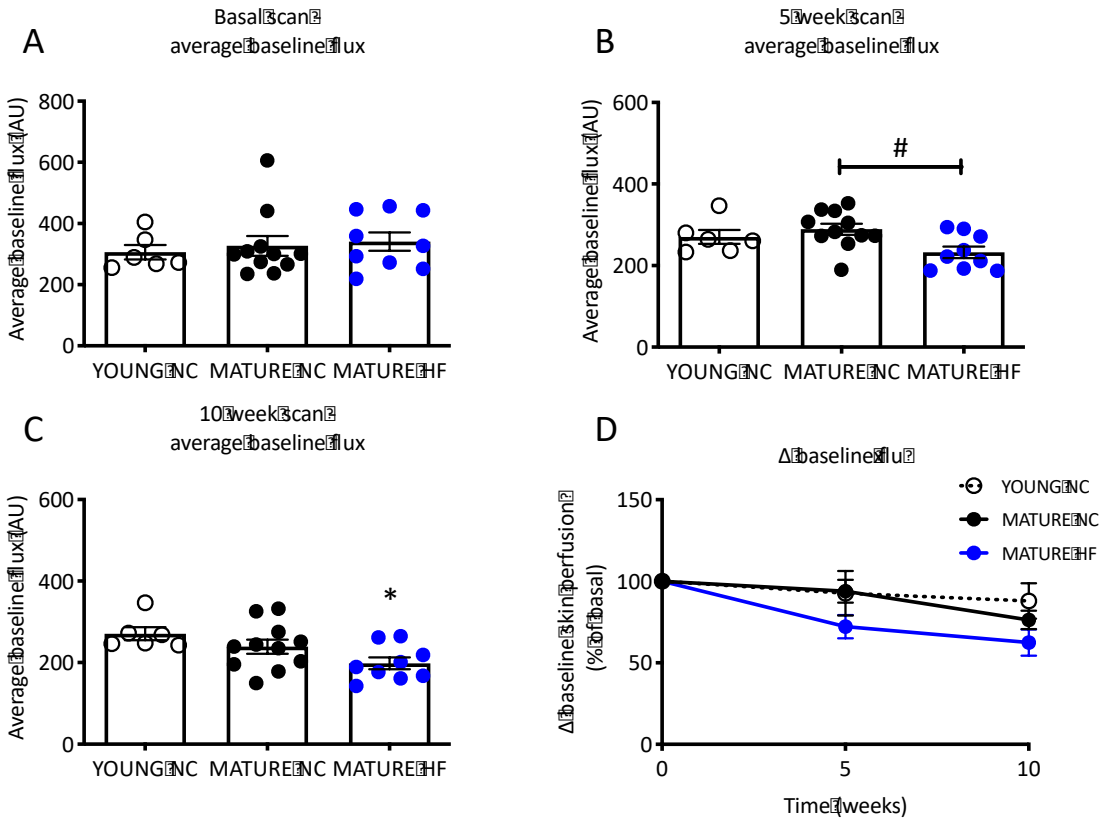

Figure 3.6 Ageing and diet induce defects in ACh-induced peak skin perfusion

Peak skin perfusion (AU) in response to the vasodilatory agent ACh was measured pre dietary intervention (A), and after 5 (B) and 10 (C) weeks dietary intervention. Data are also expressed as a % Δ in baseline skin perfusion in comparison to the basal pre-diet scan (D).

Data are expressed as mean ± standard error of the mean.

n = 6-11. (A), (B), and (C) – Welch's ANOVA with Dunnett's multiple comparison. (D) – repeated measures with Bonferonni multiple comparison. ** = $p < 0.01$, *** = $p < 0.001$ when compared to YOUNG NC.

3.2.3 Db/db mice gain significantly more weight than their wt/db and wt/wt littermates

Wt/wt, wt/db, and db/db mice were weaned at 3 weeks old and weighed weekly from 4-8 weeks old. By 8 weeks old, db/db mice gained significantly more weight than WT/WT (Fig. 3.7B – wt/wt 5.48g ± 0.86g vs. db/db 20.08g ± 1.64g, n = 5-7, $p < 0.001$) and wt/db littermates (Fig. 3.7B – wt/db 4.09g ± 0.64 vs. db/db 20.08g ± 1.64g, n = 6-7, $p < 0.001$). When expressed as percentage weight gain compared to starting weight, by 8 weeks old db/db mice exhibited a higher percentage weight gain compared to starting weight than wt/wt littermates (Fig. 3.7D – wt/wt 39.94% ± 7.99% vs. db/db 106.9% ± 19.47%, n = 5-7, $p < 0.05$) and wt/db littermates (Fig. 3.7D – wt/db 22.59% ± 3.65% vs. db/db 106.9% ± 19.47%, n = 6-7, $p < 0.05$).

3.2.4 Db/db mice exhibit severe fasting hyperglycaemia

Fasting blood glucose levels were measured after a 16-hour overnight fast. Db/db mice exhibited significantly increased fasting blood glucose levels compared to wt/wt littermates (Fig. 3.8 – wt/wt 6.06 mmol/l ± 0.66 mmol/l vs. db/db 22.1 mmol/l ± 1.63 mmol/l, n = 4-5, $p < 0.01$) and wt/db littermates (Fig. 3.8 – wt/db 6.93 mmol/l ± 1.86 mmol/l vs. db/db 22.1 mmol/l ± 1.63 mmol/l, n = 4, $p < 0.01$).

3.2.5 Db/db mice exhibit endothelial dysfunction *in vivo*

Endothelial function was measured in wt/wt, wt/db, and db/db mice using LDI and iontophoresis of the vasodilator ACh. Db/db mice showed severe blunted responsiveness to both the vasoconstrictor PE and the vasodilator ACh (Fig. 3.9A, C, D). Interestingly, wt/db mice display a reduced ACh response compared to wt/wt at certain time points (Fig 3.9B – 5^{th} scan post ACh – wt/wt 116.35% ± 5.7% vs. wt/db 81.87% ± 7.4%, n = 5-7, $p < 0.05$; 10^{th} scan post ACh – wt/wt 112.45% ± 10.24% vs. wt/db 81.89% ± 7.09%, n = 5-7, $p < 0.01$). At scans 5, 10, and 11 post ACh, db/db mice exhibited significantly reduced % skin perfusion compared to wt/wt (Fig 3.9C – 5^{th} scan post ACh – wt/wt 116.35% ± 5.7% vs. db/db 88.91% ± 5.47%, n = 5-8, $p < 0.05$; 10^{th} scan post ACh – wt/wt 112.45% ± 10.24% vs. db/db 86.7% ± 3.84%, n = 5-7, $p < 0.05$; 11^{th} scan post

ACh – wt/wt 113.5% ± 10.2% vs. db/db 88.24% ± 6.05, n = 5-7, $p < 0.05$), but not wt/db littermates (Fig. 3.9D). When expressed as % Δ skin perfusion in response to ACh compared to PE-induced normalised baseline, no differences between groups were observed. Db/db mice also exhibited significantly reduced baseline flux compared to wt/wt (3.10A – wt/wt 352.1 ± 36.63 vs. db/db 217.4 ± 17.91, n = 5-8, $p < 0.05$) and wt/db littermates (3.10A – wt/db 409.3 ± 39.16 vs. db/db 217.4 ± 17.91, p 7-8, $p < 0.01$). The reduced baseline in db/db mice suggests their microvasculature is already very constricted and may be a reason why they do not respond well to PE. Furthermore, db/db mice display an impaired ACh response, exhibited by a lower peak flux in response to ACh compared to wt/wt (3.10B – wt/wt 445.4 ± 49.97 vs. db/db 236.3 ± 15.79, n = 5-8, $p < 0.05$) and wt/db littermates (3.10B – wt/db 384.4 ± 37.97 vs. db/db 326.3 ± 15.79, n = 7-8, $p < 0.05$).

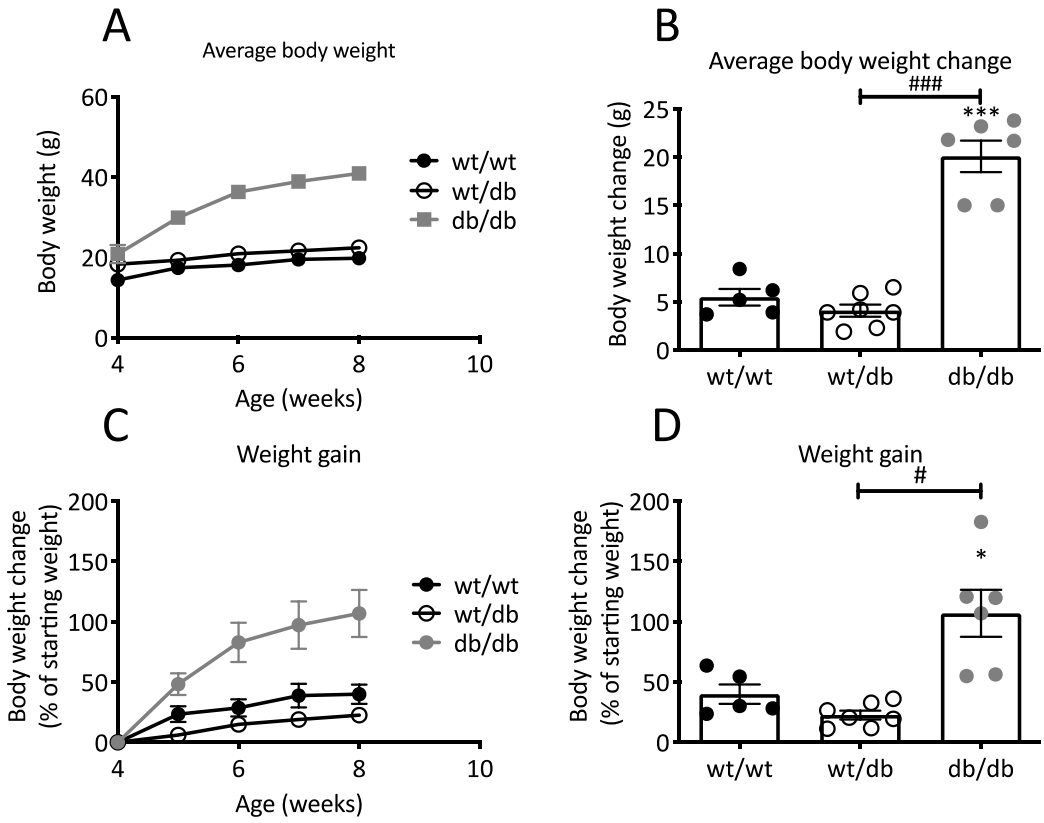

Figure 3.7 Db/db mice gain significantly more weight than their wt/wt and wt/db littermates

Wt/wt, wt/db, and db/db mice were weighed weekly from 4 weeks old to 8 weeks old. (A) Average weight of the mice from 4 to 8 weeks old. (B) Average body weight gained by 8 weeks old. (C) Weight gain as a % of starting weight from 4 to 8 weeks old. (D) Percentage weight gain at 8 weeks old.

Data are expressed as mean ± standard error of the mean.

n = 5-7. (B) and (D) – Welch's ANOVA with Dunnett's multiple comparison. * = $p < 0.05$, *** = $p < 0.001$ when compared to wt/wt, # = $p < 0.05$, ### = $p < 0.001$ when compared to wt/db.

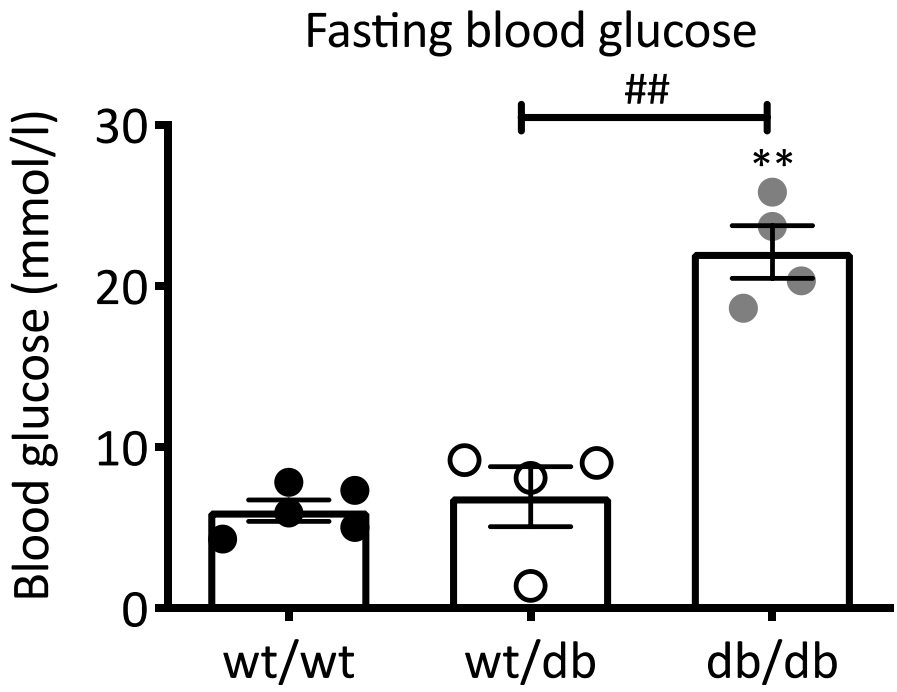

Figure 3.8 Db/db mice exhibit severe fasting hyperglycaemia

Blood glucose levels (mmol/l) were measured after a 16-hour fast in wt/wt, wt/db, and db/db mice.

Data are expressed as mean ± standard error of the mean.

n = 4-5. Welch's ANOVA with Dunnett's multiple comparison. ** = $p < 0.01$ when compared to wt/wt, ## = $p < 0.01$ when compared to wt/db.

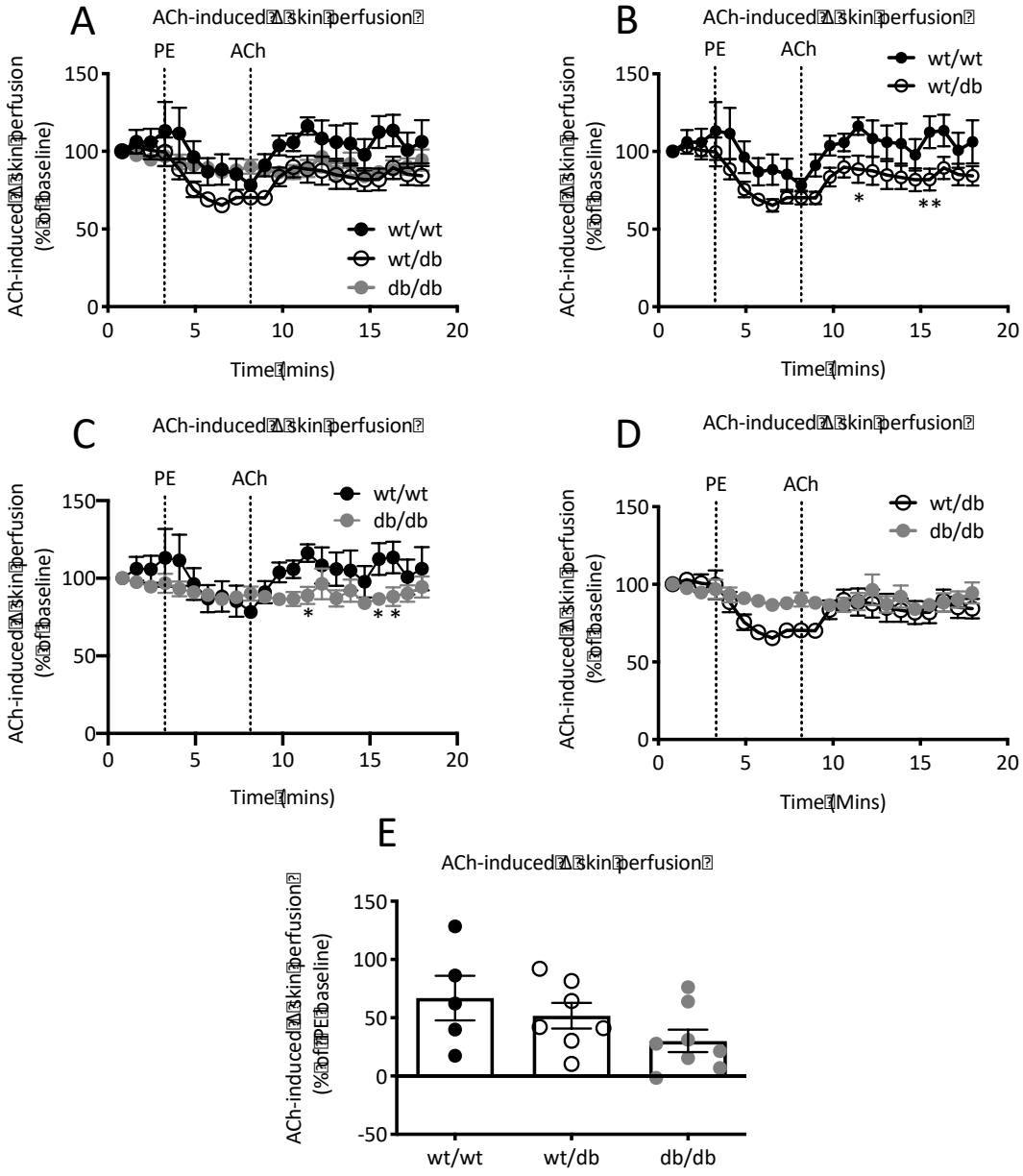

Figure 3.9 Db/db mice exhibit reduced responsiveness to vasoactive agents

To measure endothelial function *in vivo*, wt/wt, wt/db, and db/db underwent LDI with iontophoresis of PE and ACh. (A) ACh-induced skin perfusion as a percentage of baseline (baseline is 100%) over time in wt/wt, wt/db, and db/db mice. (B) ACh-induced skin perfusion as a percentage of baseline over time in wt/wt and wt/db mice. (C) ACh-induced skin perfusion as a percentage of baseline over time in wt/wt and db/db mice. (D) ACh-induced skin perfusion as a percentage of baseline over time in wt/db and db/db mice. (E) ACh-induced Δ skin perfusion compared to PE-induced normalised baseline in wt/wt, wt/db and db/db mice. The dotted lines represent the induction of the iontophoresis of PE and ACh.

Data are expressed as mean ± standard error of the mean.n = 5-8. (A), (B), (C), and (D) – repeated measures with Bonferroni multiple comparison. (E) – Welch's ANOVA with Bonferroni multiple comparison. * = $p < 0.05$ when compared to wt/wt, ** = $p < 0.01$ when compared to wt/wt.

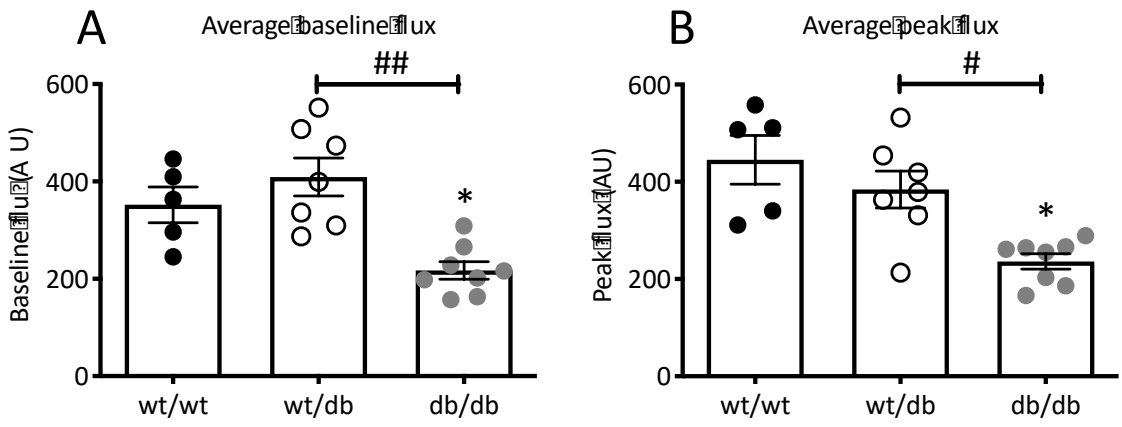

Figure 3.10 Db/db exhibit lower baseline and peak fluxes

Baseline skin perfusion (A) and peak skin perfusion (B) were measured in wt/wt, wt/db, and db/db mice.

Data are expressed as mean ± standard error of the mean.

n = 5-8, ordinary one-way ANOVA, * = $p < 0.05$ when compared to wt/wt. ## = $p < 0.01$ when compared to wt/db.

3.2.6 Differential effects of age and HFD on aortic expression of proteins controlling mitochondrial dynamics

To investigate the effects of age and HFD on aortic mitochondrial dynamics, aortae were harvested, and protein was extracted from the four groups of mice: YOUNG NC, YOUNG HF, MATURE NC, and MATURE HF. As previously mentioned, the YOUNG HF group exhibited resistance to HFD for the first 6 weeks of the study. However, they did eventually put on weight from weeks 7-10, and were heavier than their YOUNG NC littermates by the end of the study (Appendix S1). Therefore, we decided to use their tissues for post-mortem biochemical analysis. The final age of the mice when tissues were taken was YOUNG NC/YOUNG HF = 22 weeks old and MATURE NC/MATURE HF = 32 weeks old. Proteins were separated using SDS-PAGE and proteins of interest were probed for using standard Western blotting.

Representative blots for Mfn1, Mfn2, and OPA1 and phospo-Drp1 s637 and total Drp1 are shown in Fig. 3.11 (A) and (B) respectively. Actin was used as a loading control. YOUNG HF mice exhibited a trend toward decreased Mfn1 expression in aorta compared to YOUNG NC mice. Power calculations reveal a sample size of 15 is required in order to test the null hypothesis adequately. Furthermore, there was a trend toward MATURE-associated decline in aortic Mfn1 expression ($p = 0.08$). Mfn2 expression was reduced in both MATURE groups when compared to YOUNG HF mice (Fig. 3.11D – YOUNG HF 1.4 ± 0.26 vs. MATURE HF 0.64 ± 0.11, n = 5-6, $p < 0.01$; YOUNG HF 1.4 ± 0.26 vs. MATURE NC 0.56 ± 0.08, n = 5-6, $p < 0.01$). Indeed, the two-way ANOVA identified a main effect of age ($p = 0.0049$). There was also a trend toward increased Mfn2 expression in YOUNG HF mice compared to YOUNG NC mice, with power calculations revealing a sample size of 11 is required to test for significance. There was no change in OPA1 expression (Fig. 3.11E). We observed HFD-associated increased phosphorylation of Drp1 at s637 (Fig. 3.11F, $p = 0.02$), as well as age-associated decline in total Drp1 (Fig. 3.11G, $p = 0.02$). The latter may be exacerbated by HFD. Interestingly, when expressed as a ratio of phospho/total, there was a significant interactive effect ($p = 0.002$) in that the additive effect of age and diet significantly increased the ratio. Indeed, post-hoc tests reveal the MATURE HF group exhibited significantly higher levels compared to MATURE NC (Fig. 3.11H – MATURE NC 0.61 ± 0.2 vs. MATURE HF 2.74 ± 0.39, n = 5-6, $p < 0.001$) and

YOUNG HF (Fig. 3.11H –YOUNG HF 1.05 ± 0.21 vs. MATURE HF 2.74 ± 0.39, n = 5-6, $p < 0.01$), as well as YOUNG NC (Fig. 3.11H – YOUNG NC 1 ± 0.26 vs. MATURE HF 2.74 ± 0.39, n = 5-6, $p < 0.01$), indicating an age- and HFD-associated increase in the phospho s637/total Drp1 ratio.

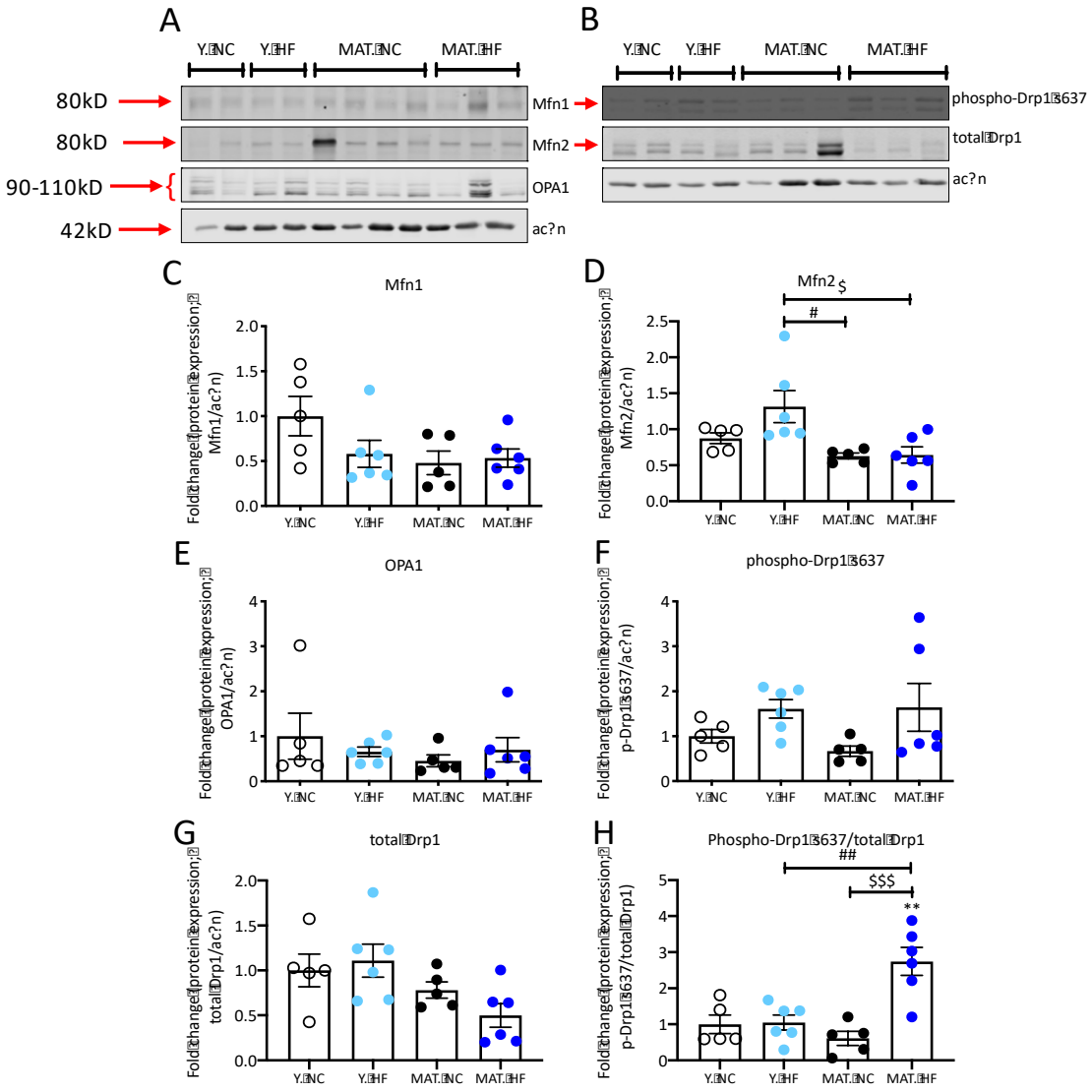

Figure 3.11 Aortic expression of mitochondrial dynamics proteins in YOUNG NC, YOUNG HF, MATURE NC, and MATURE HF mice

YOUNG mice were culled at 22 weeks of age and MATURE mice were culled at 34 weeks. Aortae were harvested and protein extracted. 20µg of protein was loaded onto acrylamide gels and separated by SDS PAGE. (A) and (B) Representative western blots showing expression of proteins regulating mitochondrial dynamics in the murine aorta with actin as a loading control. Quantification of western blots normalised to actin of (C) Mfn1, (D) Mfn2, (E) OPA1, (F) p-Drp1 s637, (G) total Drp1, and (H) p-Drp1/total Drp1 ratio. The molecular weight of (phospho)Drp1 is 81kD.

Data are expressed as mean ± standard error of the mean.

n = 5-6. (C) – (H) – ordinary two-way ANOVA with Bonferroni multiple comparison. ** = $p < 0.01$ when compared to YOUNG NC, # = $p < 0.05$ and ## = $p < 0.01$ when compared to YOUNG HF, $ = $p < 0.05$ and $$$ = $p < 0.001$ when compared to MATURE NC.

3.2.7 Ageing and HFD do not influence VE fraction expression of proteins controlling mitochondrial dynamics

Hemi-brains were harvested and VE fractions (NVU) were isolated. Proteins isolated from VE fractions were separated using SDS-PAGE and proteins of interest were probed for using standard Western blotting. Representative blots for Mfn2 and OPA1 are shown in Fig. 3.12 (A). Actin was used as a loading control. In the case of OPA1, the double band was quantified to calculate total OPA1 expression, the higher band was quantified to calculate long-form OPA1 expression, and the lower band was quantified to calculate short-form OPA1 expression.

Interestingly, we observed a trend toward a dietary effect in reducing total OPA1 expression ($p = 0.08$). There was also a trend toward reduced total OPA1 (~30%, 3.12C), short-form OPA1 (~30%, 3.12D), and long-form OPA1 (~30%, 3.12E), in YOUNG HF vs. YOUNG NC. Power calculations suggest sample sizes of 12 to test for significance adequately. There was no effect of age or diet on VE fraction Mfn2 expression (Fig. 3.12B).

3.2.8 Age-related decline in hypothalamic expression of mitochondrial fusion proteins

Hypothalami were harvested from mice. Protein was isolated and separated using SDS-PAGE and proteins of interest were probed for using standard Western blotting. Representative blots for Mfn2 and OPA1 are shown in Fig. 3.13 (A). Actin was used as a loading control. In the case of OPA1, the double band was quantified to calculate total OPA1 expression, the higher band was quantified to calculate long-form OPA1 expression, and the lower band was quantified to calculate short-form OPA1 expression.

When performing two-way ANOVA, there was an age-related effect of reduced Mfn2 ($p < 0.0001$), total OPA1 ($p < 0.0001$), long-form OPA1 ($p < 0.0001$), and short-form OPA1 ($p < 0.0001$).

Indeed, MATURE NC and MATURE HF mice exhibited reduced hypothalamic Mfn2 levels when compared to YOUNG NC mice (Fig. 3.13B – YOUNG NC 1 ± 0.06 vs. MATURE NC 0.55 ± 0.06, n = 6-11, $p < 0.01$; YOUNG NC 1 ± 0.03 vs. MATURE HF 0.44 ± 0.06, n = 6-9, $p < 0.01$) as well as to YOUNG HF mice (Fig. 3.13B – YOUNG HF 1.1 ± 0.04 vs. MATURE NC 0.55 ± 0.06, n = 6-11, $p < 0.01$; YOUNG HF 1.1 ± 0.04 vs. MATURE HF 0.44 ± 0.06, n = 6-9, $p < 0.01$).

Both MATURE groups exhibited significant reductions in OPA1 total protein compared to YOUNG NC (Fig. 3.31C – YOUNG NC 1 ± 0.03 vs. MATURE NC 0.5 ± 0.03, n = 6-11, $p < 0.001$; YOUNG NC 1 ± 0.03 vs. MATURE HF 0.44 ± 0.06, n = 6-11, $p < 0.001$) and YOUNG HF (Fig. 3.31C – YOUNG HF 0.93 ± 0.09 vs. MATURE NC 0.5 ± 0.03, n = 6-11, $p < 0.001$; YOUNG HF 0.93 ± 0.09 vs. MATURE HF 0.44 ± 0.06, n = 6-11, $p < 0.001$). MATURE groups also exhibited reductions in in OPA1 short-form compared to YOUNG NC (Fig. 3.13D – YOUNG NC 1 ± 0.13 vs. MATURE NC 0.57 ± 0.05, n = 6-11, $p < 0.01$; YOUNG NC 1 ± 0.13 vs. MATURE HF 0.42 ± 0.59, n = 6-11, $p < 0.001$) and YOUNG HF (Fig. 3.13D – YOUNG HF 0.92 ± 0.08 vs. MATURE NC 0.57 ± 0.05, n = 6-11, $p < 0.05$; YOUNG HF 0.92 ± 0.08 vs. MATURE HF 0.42 ± 0.59, n = 6-11, $p < 0.001$).

MATURE groups further showed decreased OPA1 long-form compared to YOUNG NC (Fig. 3.13E – YOUNG NC 1 ± 0.12 vs. MATURE NC 0.49 ± 0.08, n = 6-11, $p < 0.001$; YOUNG NC 1 ± 0.12 vs. MATURE HF 0.3 ± 0.03, n = 6-11, $p < 0.001$) and YOUNG HF (Fig. 3.13E – YOUNG HF 0.91 ± 0.07 vs. MATURE NC 0.49 ± 0.08, n = 6-11, $p < 0.001$; YOUNG HF 0.91 ± 0.07 vs. MATURE HF 0.3 ± 0.03, n = 6-11, $p < 0.001$). No effect of diet was observed.

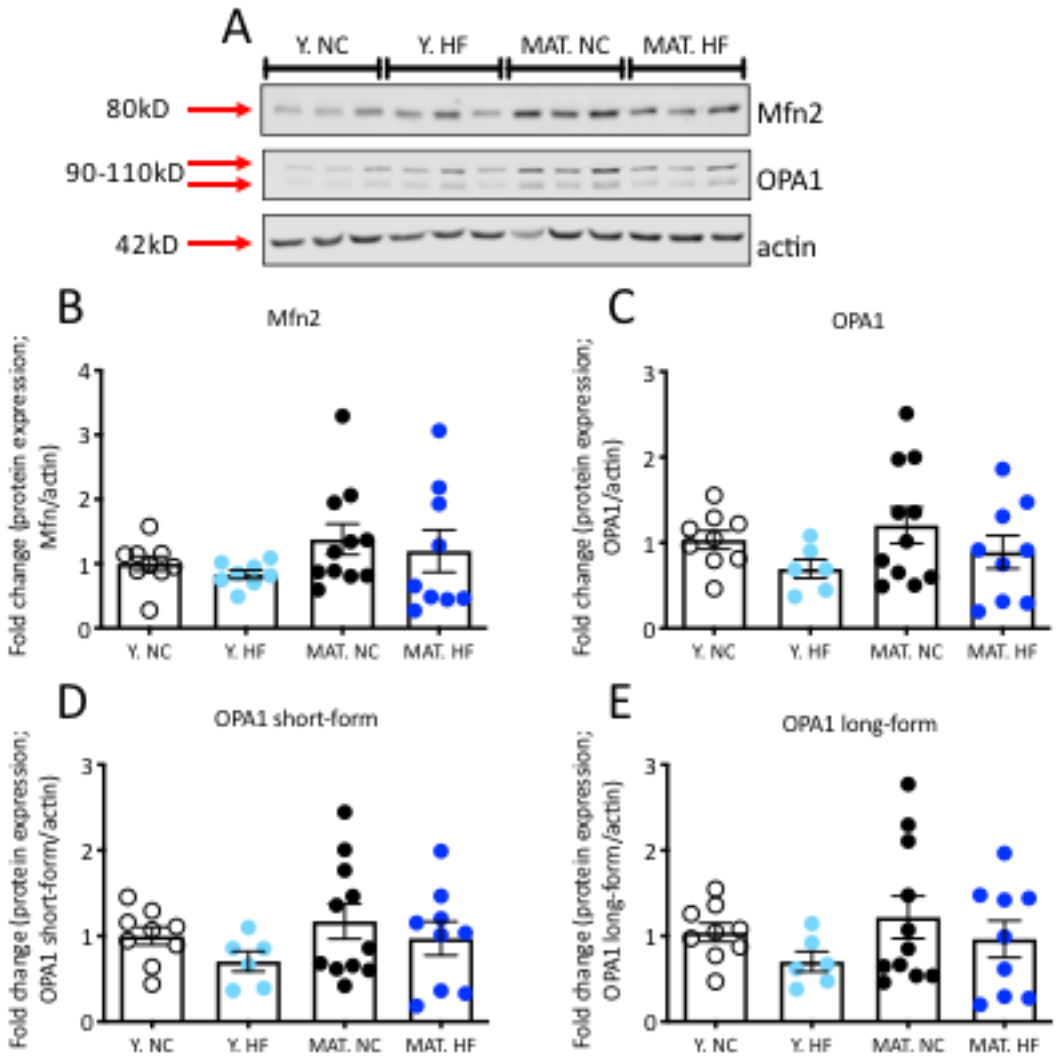

Figure 3.12 VE fraction expression of mitochondrial fusion proteins in YOUNG NC, YOUNG HF, MATURE NC, and MATURE HF mice

YOUNG mice were culled at 22 weeks of age and MATURE mice were culled at 34 weeks. VE fractions were harvested from hemi-brains and protein extracted. 20µg of protein was loaded onto acrylamide gels and separated by SDS PAGE. (A) Representative western blots showing expression of proteins regulating mitochondrial fusion in the murine NVU with actin as a loading control. Quantification of western blots normalised to actin of (B) Mfn2, (C) total OPA1, (D) OPA1 short-form, (E) OPA1 long-form.

Data are expressed as mean ± standard error of the mean.

n = 6-11. (B) – (E) – ordinary two-way ANOVA with Bonferroni multiple comparison.

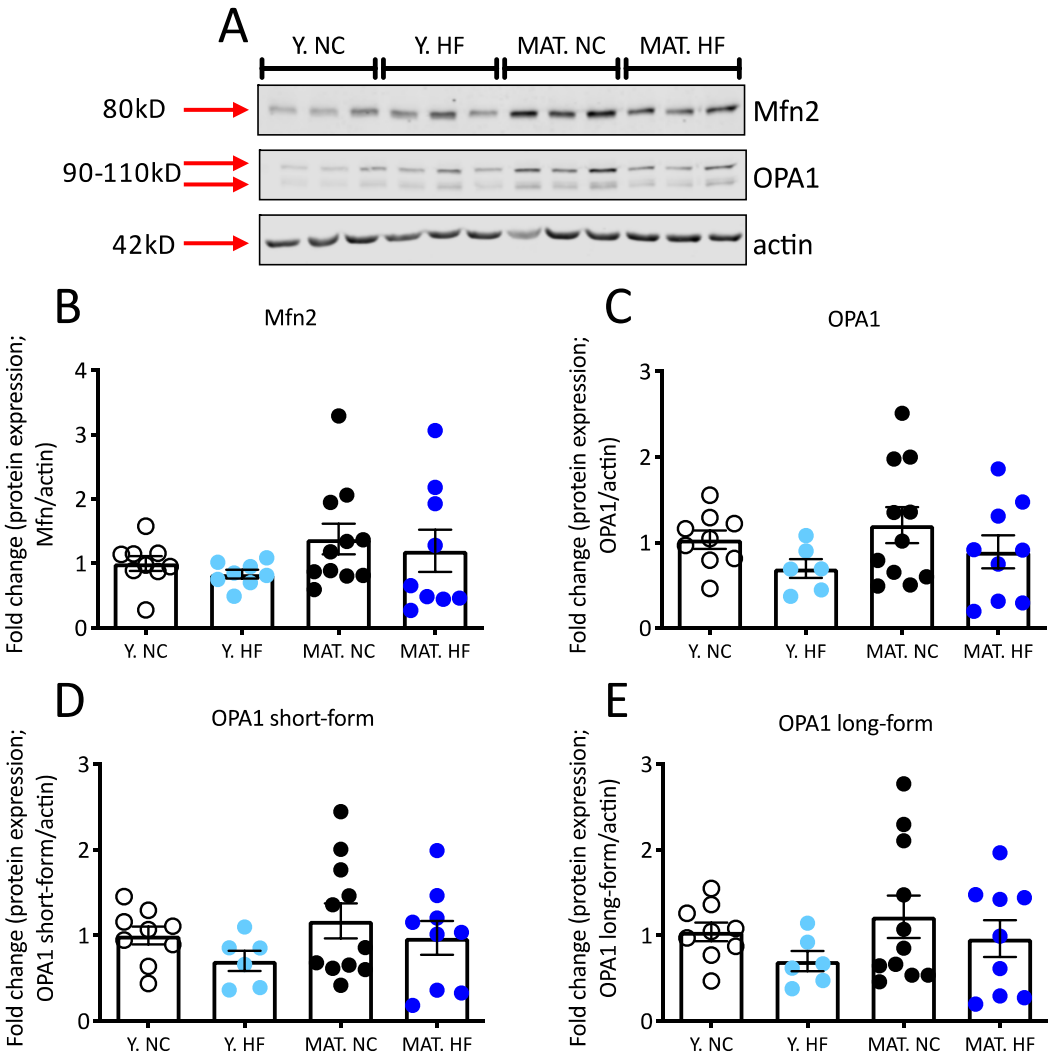

Figure 3.13 Hypothalamic expression of mitochondrial fusion proteins in YOUNG NC, YOUNG HF, MATURE NC, and MATURE HF mice

YOUNG mice were culled at 22 weeks of age and MATURE mice were culled at 34 weeks of age. Hypothalami were harvested and protein extracted. 20µg of protein was loaded onto acrylamide gels and separated by SDS PAGE. (A) Representative western blots showing expression of proteins regulating mitochondrial fusion in the murine hypothalamus with actin as a loading control. Quantification of western blots normalised to actin of (B) Mfn2, (C) total OPA1, (D) OPA1 short-form, (E) OPA1 long-form.

Data are expressed as mean ± standard error of the mean.

n = 6-11. (B) – (E) – ordinary two-way ANOVA with Bonferroni multiple comparison. ** = $p < 0.01$ and *** = $p < 0.001$ when compared to YOUNG NC. # = $p < 0.05$, ## = $p < 0.01$, and ### = $p < 0.001$ when compared to YOUNG HF.

3.2.9 Aortic expression of mitochondrial fusion and fission proteins is not altered in db/db mice

Db/db mice and their wt/wt and wt/db littermates were culled at 8 weeks of age. Aortae were excised from mice and protein was extracted. Proteins were separated using SDS-PAGE, and proteins involved in the control of mitochondrial fusion and fission were probed for by Western blot. Representative Western blots are shown in Fig. 3.14A. Actin was used as a loading control. Db/db mice exhibited no alterations in Mfn1 (3.14B), Mfn 2 (3.14C), OPA1 (3.14D), or total Drp1 (3.14F). However, there is a trend toward decreased phospho-Drp1 s616 expression in db/db mice compared to both wt/wt and wt/db (3.14E), with power calculations suggesting a sample size of 12 to accurately detect significance. When measuring phospho/total ratio, both wt/db and db/db groups exhibit trends toward reduced levels (3.14G) compared to wt/wt. Power calculations reveal that sample sizes of only 9 for both wt/db an db/db are required to detect significance for the current effect size (compared to wt/wt).

3.2.10 VE fraction expression of mitochondrial fusion and fission proteins is not altered in db/db mice

VE fraction was isolated from hemi-brains using a protocol described in Methods 2.6.1. Protein was extracted from VE fractions and separated using SDS-PAGE. Proteins involved in the control of mitochondrial dynamics were probed for using Western blotting. Representative Western blots are shown in Fig 3.15A. Actin was used as a loading control. Db/db mice exhibited no alterations in VE fraction expression of Mfn1 (3.15B), Mfn2 (3.15C), total OPA1 (3.15D), OPA1 short-form (3.15E), OPA1 long-form (3.15F), or phospho-Drp1 s616 (3.15G). However, wt/db mice exhibited a trend toward increased (~70%) tDrp1 expression compared to wt/wt, an effect that was not present in db/db mice (Fig 3.15H). Power calculations reveal a sample size of 8 is required to detect significance at this effect size. When expressed as phospho/total, there was no change between groups.

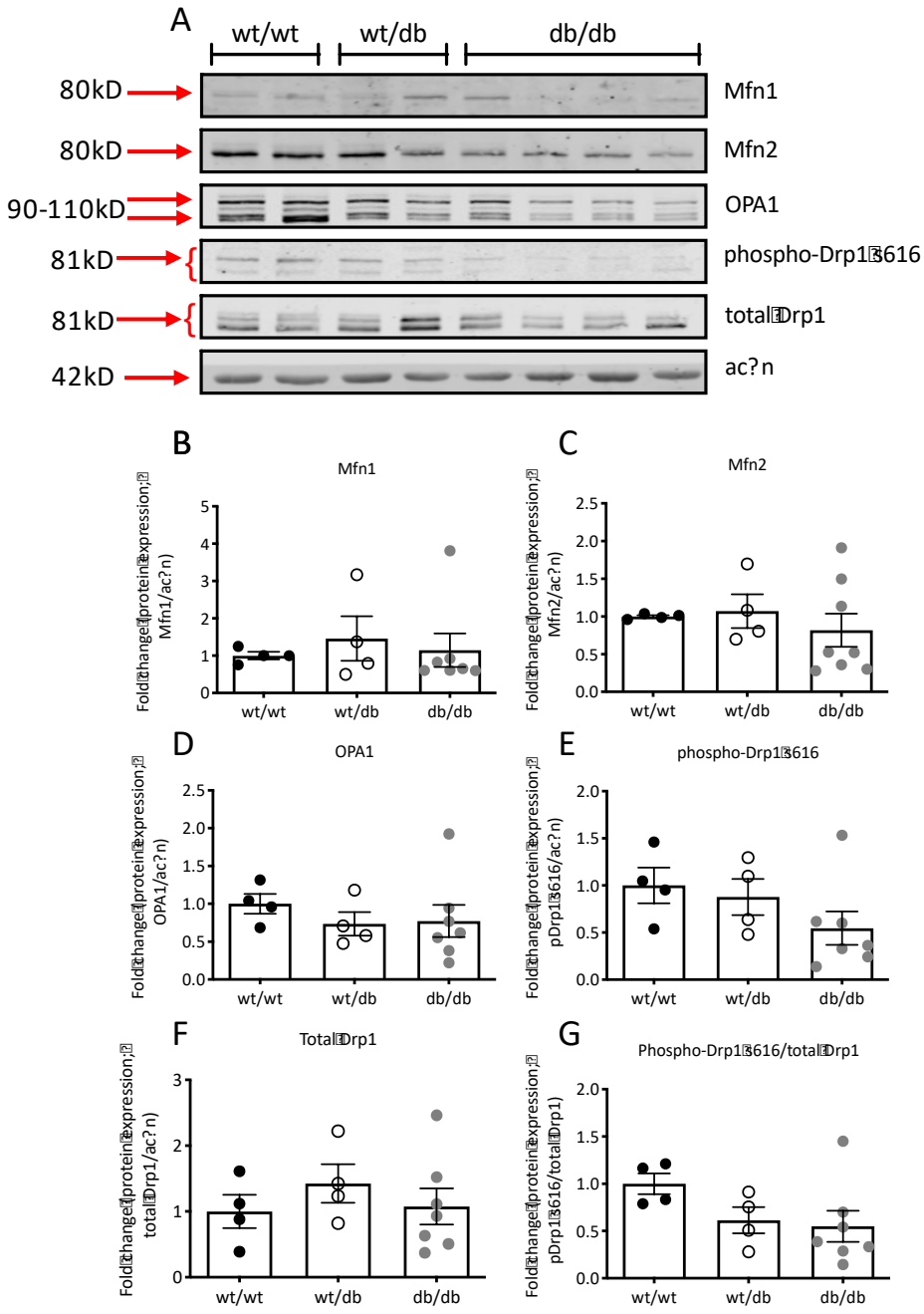

Figure 3.14 Aortic expression of proteins involved in mitochondrial dynamics in wt/wt, wt/db, and db/db mice

Aortae were harvested and protein extracted. 20µg of protein was loaded onto acrylamide gels and separated by SDS PAGE. (A) Representative western blots showing expression of proteins regulating mitochondrial dynamics in the murine aorta with actin as a loading control. Quantification of western blots normalised to actin of (B) Mfn1, (C) Mfn2, (D) OPA1, (E) p-Drp1 s616, (F) total Drp1, and (G) p-Drp1/total Drp1 ratio.

Data are expressed as mean ± standard error of the mean.

n = 4-8. (B)-(G) Welch's ANOVA with Dunnett's multiple comparison.

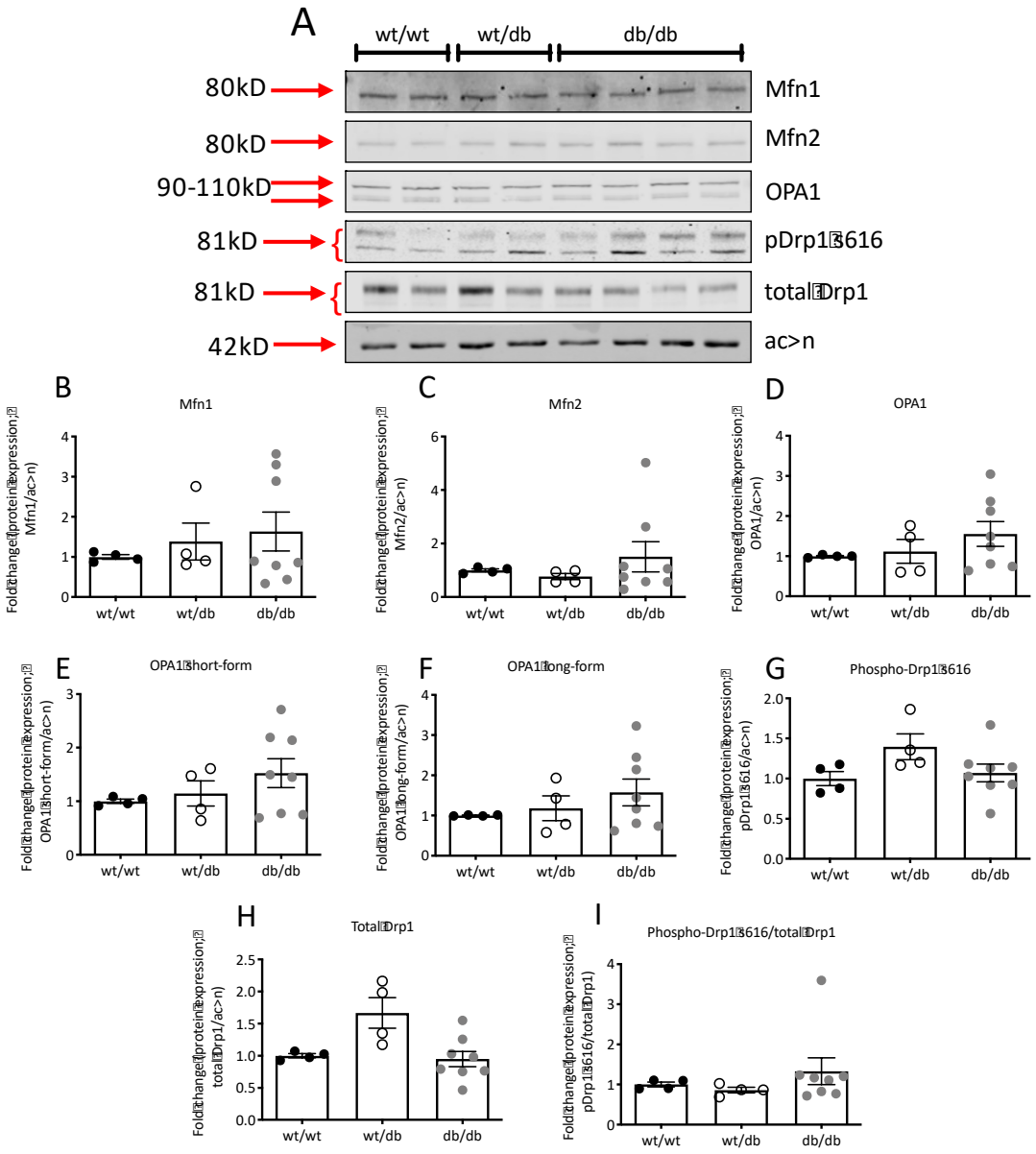

Figure 3.15 VE fraction expression of proteins controlling mitochondrial dynamics in wt/wt, wt/db, and db/db mice

VE fractions (NVU) and protein extracted. 20µg of protein was loaded onto acrylamide gels and separated by SDS PAGE. (A) Representative western blots showing expression of proteins regulating mitochondrial dynamics in the murine NVU with actin as a loading control. Quantification of western blots normalised to actin of (B) Mfn1, (C) Mfn2, (D) OPA1, (E) OPA1 short-form, (F) OPA1 long-form, (G) p-Drp1 s616, (H) total Drp1, and (I) p-Drp1/total Drp1 ratio.

n = 4-8. (B)-(I) – Welch's ANOVA with Dunnett's multiple comparison.

3.2.11 Db/db mice exhibit increased hypothalamic phosphorylation of Drp1 at serine 616

Hypothalami were harvested and protein was extracted. Proteins were separated using SDS-PAGE, and proteins involved in the control of mitochondrial fusion and fission were probed for by conventional Western blot. Representative blots are shown in 3.16A. Actin was used as a loading control.

Db/db mice did not significantly differ from control groups in terms of hypothalamic Mfn1 (Fig. 3.16B) and OPA1 (total Fig. 3.16C, short-form Fig. 3.16D, long-form Fig. 3.16E). Db/db mice exhibited increased phospho-Drp1 s616 expression compared to wt/wt (Fig. 3.16F – wt/wt 1 ± 0.05 vs. db/db 1.63 ± 0.17, n = 4-8, $p < 0.05$) and a trend toward reduced total Drp1 expression (Fig. 3.16G). Power calculations reveal a sample size of 9 would be required to test for significance. When expressed as a ratio, db/db mice exhibited elevated phospho/total ratio compared to wt/wt (3.16H – WT/WT 1 ± 0.09 vs db/db 2.16 ± 0.18, n = 4-8, $p < 0.001$).

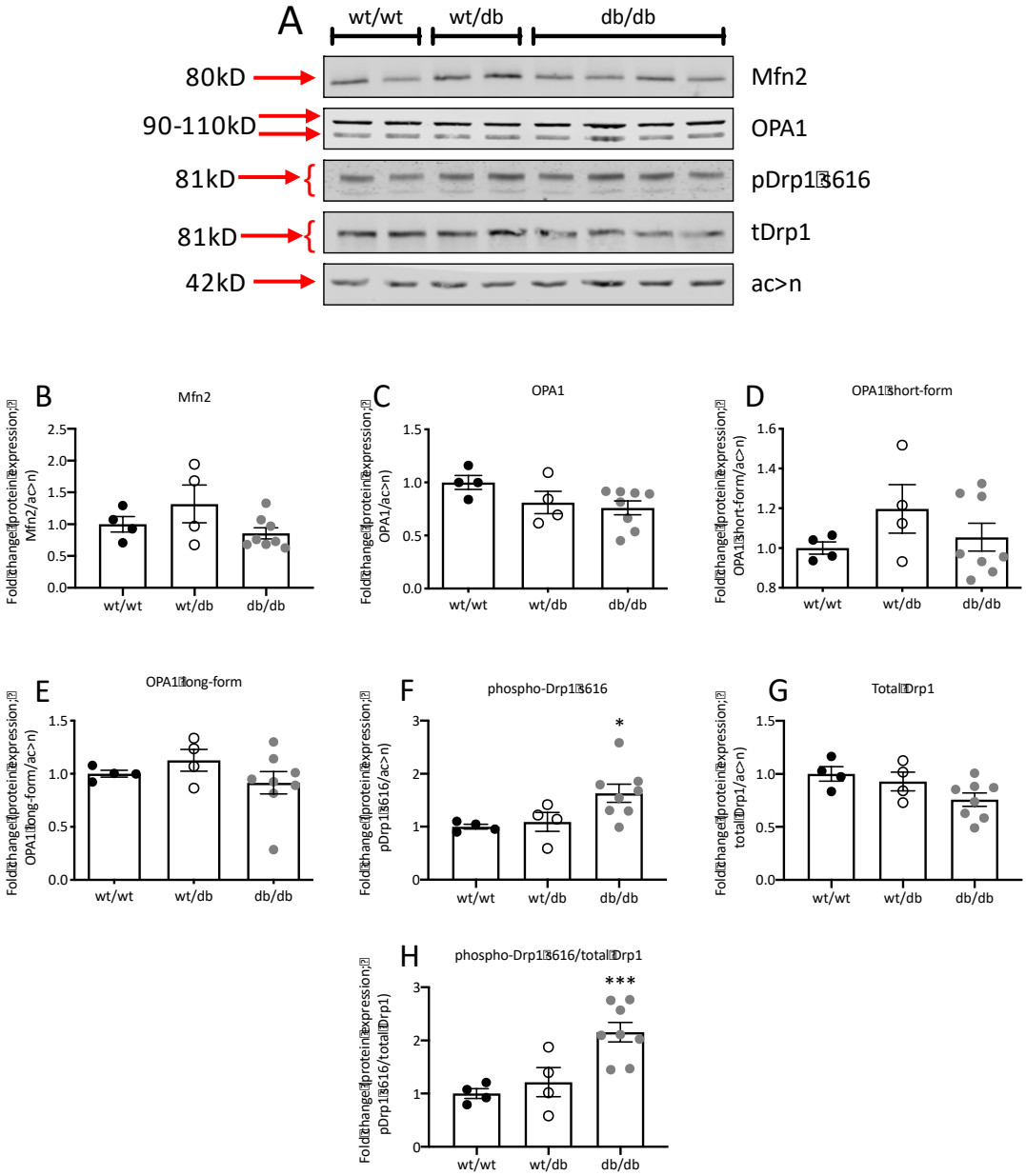

Figure 3.16 Hypothalamic expression of proteins controlling mitochondria dynamics in WT/WT, WT/db, and db/db mice

Hypothalami were harvested and protein extracted. 20µg of protein was loaded onto acrylamide gels and separated by SDS PAGE. (A) Representative western blots showing expression of proteins regulating mitochondrial dynamics in the murine hypothalamus with actin as a loading control. Quantification of western blots normalised to actin of (B) Mfn1, (C) total OPA1, (D) OPA1 short-form, (E) OPA1 long-form, (F) p-Drp1 s616, (G) total Drp1, and (H) p-Drp1/total Drp1 ratio.

Data are expressed as mean ± standard error of the mean.

n = 4-8. (B)-(H) – Welch's ANOVA with Dunnett's multiple comparisons. * = $p < 0.05$, *** = $p < 0.001$ when compared to wt/wt.

3.2.12 Db/db mice do not exhibit aortic or VE fraction endothelial activation

Aortae and VE fractions were isolated and protein extracted. Proteins were separated using SDS-page and proteins known to be involved in controlling mitochondrial dynamics were probed for using conventional Western blotting. Representative blots of aortic and VE fraction ICAM expression are shown in Fig. 3.17A and B respectively. Actin was used as a loading control. Db/dbs exhibited no significant difference in ICAM expression in aorta (Fig 3.17C) or VE fraction (Fig. 3.17D) compared to control groups.

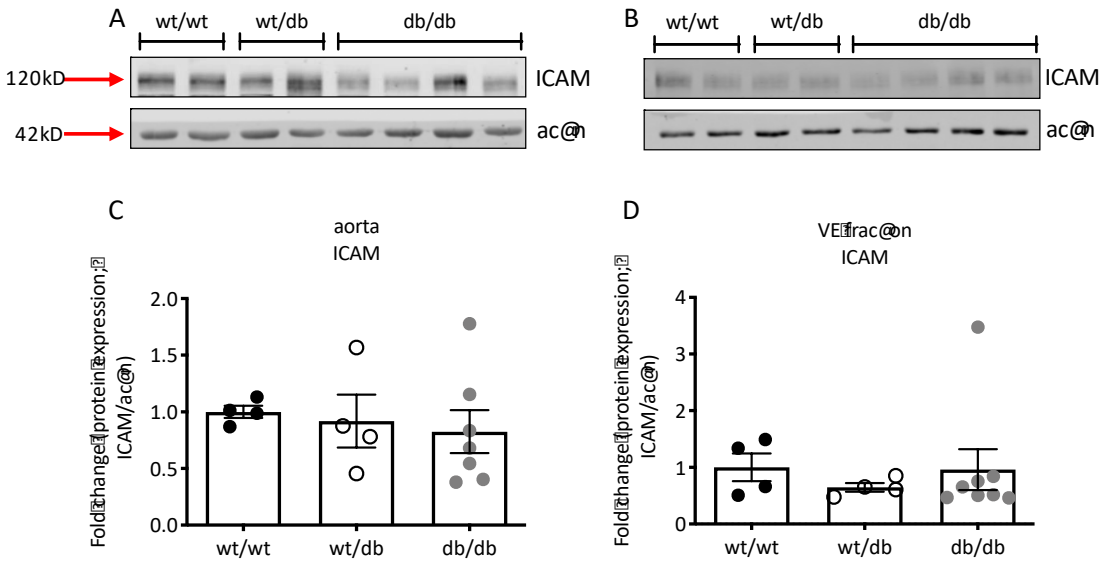

Figure 3.17 Aortic and VE fraction ICAM expression in wt/wt, wt/db, and db/db mice

Aortae and VE fractions were harvested and protein extracted. 20µg of protein was loaded onto acrylamide gels and separated by SDS PAGE. Representative western blots showing expression of ICAM in aorta (A) and VE fraction (B) with actin as a loading control. Quantification of western blots normalised to actin of aortic ICAM (C) and VE fraction ICAM (D).

Data are expressed as mean ± standard error of the mean.

n = 4-8. (B)-(H) – Welch's ANOVA with Dunnett's multiple comparisons.

3.3 Discussion

3.3.1 Modeling nutrient excess using a mature adult, HFD-fed mouse

The first aim of this study was to establish a mature adult, HFD-fed model of nutrient excess. To clarify the effects of HFD-feeding, mice were weighed weekly. As expected, mature adult HFD-fed mice gained significantly more weight than their NC-fed counterparts. Mature adult mice on NC diets maintained their weights steadily across the 10 weeks of the study, not differing in terms of weight gain from the young adult NC group. This is likely due to the fact that the mice have reached their stable adult body weight by this age. Indeed, human studies suggest fat mass peaks at middle age (40-70 years)[358], and declines thereafter[359]. It would be of interest to investigate the effect of age on susceptibility to HFD; that is compare mature adult HFD-fed mice to young adult HFD-fed mice. As previously mentioned in 3.1, this was attempted herein but the weight trajectory of the young adult HFD-fed mice was unusual (Appendix S1). HFD-fed mice should exhibit rapid increases in weight upon HFD feeding, but in this case young adult HFD-fed mice showed remarkably similar weight trajectories to young adult NC-fed mice, suggesting DIOR or perhaps under eating. To reiterate, MSRU was experiencing a high level of technical and structural issues which was likely to have some kind of impact on the mice. We proposed that mice were not putting on weight due to heightened anxiety brought on by these issues and tested for such using an open-field test. Young adult HFD-fed stayed close to the edges of the open-field box, rarely venturing into the middle. These data suggest that mice have an anxious phenotype as opposed to a curious or exploratory phenotype. It would have been useful to investigate the anxious phenotype of a separate cohort of young adult HFD-fed mice at a time that the MSRU was not experiencing these issues for comparison. However, these issues are ongoing, and resolution of the problems are unfortunately out with the scope of this PhD project.

3.3.2 Ageing, but not HFD-feeding, is associated with impaired endothelial function *in vivo*

Within this chapter, it was demonstrated that mature adult mice exhibited reduced endothelial responsiveness *in vivo* when compared to young adult mice, but there was

no effect of diet. Mature adult mice, both on NC and HF diet, showed impairment in % change in vasodilation in response to the potent vasodilator ACh compared to their younger counterparts, as well as a lower peak skin perfusion in response to ACh. However, mature adult mice did not show any reductions in baseline skin perfusion compared to young adult, thus suggesting a clear endothelial-specific dysfunction in this case. We did observe a reduction in baseline skin perfusion after 5 weeks of dietary intervention in HFD-fed mature adult mice compared to their NC-fed age-matched counterparts. Baseline skin perfusion is analogous to resting vessel tone. These data suggest that HFD-fed animals may exhibit constricted microvasculature at rest, which may indicate ED or VSMC dysfunction. This may be due to a number of factors including increased ROS and increased cellular inflammation.

There is a lot of evidence to suggest age-related decline in vascular health. Increasing age has been associated with reduced eNOS activity[114,360], eNOS uncoupling[361], reduced NO bioavailability[114,360,361], increased endothelial ROS production[114,360,361], increased endothelial inflammation[114,361] and increased ET-1[360,361]. Human studies investigating the effect of age on endothelial function also utilise laser imaging and iontophoresis of ACh. Indeed, many studies have reported that peak response to ACh of forearm skin perfusion progressively declines with age[362–365], and this is a good predictor of CVD risk[366]. In mice, 6 months old is considered a mature adult model, bordering on middle-aged, rather than an elderly model. There are limited studies looking at the specific effect of middle-age on ED, but Celermajer and colleagues found that endothelium-dependent vasodilation (response to reactive hyperaemia) begins declining as early as 40 years old in men and 50 years old in women[367]. Therefore, these data from our mouse model corroborate previous studies, in that middle-age is associated with reduced endothelial function.

Interestingly, feeding mature adult mice HFD did not exacerbate age-related ED *in vivo*. Previous literature suggests HFD rodent models (6-24 weeks on HFD) exhibit a blunted vasodilatory response in *ex vivo* aortae, indicating ED[139–141], findings that our study could not corroborate *in vivo*. Similarly to the study herein, Noronha and colleagues reported no effects of HFD (8 week duration) on ACh response in *ex vivo* aortae[138]. They attributed

this lack of ED to a compensatory mechanism; the hyperpolarising capacity of increased H_2O_2 levels. Indeed, early ED is associated with increased oxidative stress. We did not test for the presence of oxidative stress in our model due to time constraints, but it would be interesting to investigate whether H_2O_2 is increased in our HFD model and whether this acts as a potential hyperpolarising agent, allowing for vasodilation. Furthermore, it is possible that our HFD-fed model exhibits increased NO bioavailability due to an increase in iNOS as a result of inflammation in the endothelium.

Although we did not measure oxidative stress in our models, we did attempt to investigate endothelial function in a mouse model of oxidative stress – Nrf2 KO mice. Nrf2 (NFE2-related factor 2) is a transcription factor known for its role in regulating oxidative balance. Nrf2 acts to upregulate the levels of anti-oxidant molecules, leading to catabolism of superoxides and other ROS[368]. Indeed, Nrf2 KO mice exhibit increased oxidative stress[369] and susceptibility to a range of diseases associated with oxidative pathologies, whereas enhancing Nrf2 activity protects animals against oxidative damage[370].

Male Nrf2KO mice and WT controls were fed HFD for 10 weeks and we measured metabolic parameters including body weight and body composition, as well as vascular parameters using LDI. These data can be observed in Appendix S2. Due to the afore-mentioned issues within the MSRU, HFD-fed Nrf2KO mice, which are known to stay lean, were significantly heavier than HFD-fed WT counterparts. Increased weight was attributed to a higher fat mass than WTs. As previously mentioned, we presumed that the DIOR in the WT mice may be due to increased anxiety and under eating due to the ongoing problems in the MSRU. When performing open-field tests, the Nrf2KO mice did not exhibit an overt anxious phenotype like the WT mice, suggesting they have a more placid nature (Appendix S2). This may indicate why they continued eating in this stress-inducing environment and thus why they rapidly gain weight and the WT mice did not. Due to these reasons we did not continue with the Nrf2KO study so as to properly prioritise experiments that were not affected by the MSRU issues.

Other pathologies associated with HFD, such as hyperglycaemia and dyslipidaemia, have been shown to lead to ED. Interestingly, Da Silva Rocha and colleagues' model of obesity

(HFD-induced, 20% of calories from fat, 27 weeks), whilst significantly heavier than regular chow controls, did not exhibit associated pathologies of obesity including dyslipidaemia or hyperglycaemia[144]. They also observed no impairments in aortic dilatory response to ACh, implying HFD-induced ED may be dependent on obesity-related pathologies, such as those suggested above. We did not measure fasting blood glucose levels, nor did we investigate the lipid profile of our HFD-fed mice herein, but this is a potential explanation as to why we did not observe HFD-induced ED *in vivo*. Moving forward, fed and fasted blood glucose levels could be measured using a blood sample from the tail and a Glucometer and blood lipids can be investigated using a simple colorimetric/fluorimetric triglyceride or cholesterol assays. If indeed this duration of HFD is not sufficiently long enough to induce hyperglycaemia/dyslipidaemia, then a longer exposure to HFD or a higher fat content (65%) may be required. Additionally, Western diet, which contains cholesterol and is typically used as an atherogenic diet, could be used. The addition of fructose/sucrose to the drinking water could also be used to increase calorie intake and encourage a diabetic phenotype, which could aid the development of ED. In order to adequately model human metabolic syndrome, Della Vedova and colleagues used an DIO model fed with a diet consisting of 45% HFD (22% chicken-derived fat), and 10% fructose in the drinking water[371]. Control groups, instead of chow, were fed a diet of similar content but with only 6% fat and normal drinking water. Moving forward, we would consider this dietary paradigm in order to model human metabolic disease sufficiently.

3.3.3 Db/db mice gain significantly more weight than WT/WT and WT/db mice, and are severely hyperglycaemic

The db/db mouse is a well-known and extensively utilised model of obesity and diabetes. We report here that female db/db mice gain significantly more weight than their wt/wt and wt/db littermates from 4-8 weeks old. Db/db mice were already heavier than both their wt/wt and wt/db littermates by 5 weeks old. Kobayashi and colleagues were among the first to phenotype the db/db mouse and report that by 6 weeks of age, db/db mice develop obesity[372], a finding corroborated herein. Other studies have also reported the severe obese phenotype of db/db mice[373,374]. In terms of glucose

tolerance, we report here that female db/db mice develop severe fasting (after 16 hours) hyperglycaemia, suggesting glucose intolerance and a diabetic phenotype. This corroborates previous findings that obesity and hyperglycemia are observed at 8 weeks old[372–374].

3.3.4 Db/db mice exhibit blunted responses to endothelium-dependent vasoactive agents *in vivo*

We report here that db/db mice exhibit an impaired response to endothelium-dependent vasoactive agents PE and ACh. The reduced responsiveness to PE indicates that the microvasculature of db/db mice is already maximally constricted whereas the blunted response to ACh suggests reduced endothelial responsiveness. Together, these findings suggest the presence of severe ED. However, it cannot be ignored that the contractile responses to PE from 'true' baseline are not standardised across groups, making it difficult to quantify the PE response. Concentration-response curves could be performed, or different vasoconstrictors could be tested in order to understand whether the skin microvasculature is already maximally constricted and cannot respond to any vasoconstrictor molecule appropriately, or whether it is due to a direct irresponsiveness specifically to PE. The latter may involve downregulation of receptors for PE, such as adrenergic receptors on the VSMCs. In wt/wt and wt/db mice, we observed a reduction in % skin perfusion in response to the vasoconstrictor PE, followed by an increase in % skin perfusion in response to the vasodilator ACh. These data suggest that wt/wt and wt/db mice have healthy, responsive endothelium in their skin microvasculature. As previously mentioned, % skin perfusion response to ACh was blunted in db/db mice. This is likely due to impaired NO bioavailability, due to the fact that ACh-induced vasodilation depends on NO production[375]. Reduced NO bioavailability occurs due to reduced eNOS activity, increased eNOS uncoupling, increased NO degradation secondary to increased ROS presence[376], or increased ET-1 expression[377]. Due to time constraints, this has not been measured in our db/db model, but could be measured by Western blotting for phosphorylation of eNOS at serine 1177 in the vasculature, measuring nitrite (derivative of NO) concentration in the blood using Griess assay, and measuring ET-1 expression (mRNA or protein) in the vasculature. Others have

reported decreased eNOS expression, increased eNOS uncoupling[378,379], reduced intracellular NO production[380], increased superoxide production[379], increased eNOS mRNA (due to H_2O_2 extending mRNA half-life)[379], and increased ET-1 expression[381] in db/db mice. When looking at physiological changes, Solini and colleagues measured ACh response in *ex vivo* mesenteric arteries and reported that arteries from 16-week old db/db mice displayed a blunted response to ACh[379]. To our knowledge, PE and ACh-induced changes in skin perfusion *in vivo* have not previously been measured in db/db mice. Therefore, this is the first report of reduced endothelial responsiveness *in vivo* in db/db mice.

The severe fasting hyperglycaemia present in db/db mice may be in part responsible for the observed ED. Hyperglycaemia has consistently been reported as a potential cause of ED. Mice with STZ-induced diabetes exhibit very high fasting blood glucose levels (>25mmol/l) and a marked reduction in *in vivo* ACh-dependent vasodilation[183]. Others have reported STZ mice exhibit reduced ACh-induced vasodilation in *ex vivo* aortic myograph studies[153,154], increased eNOS mRNA[155], and increased aortic superoxide production[154]. High glucose levels have been proposed to induce ED through increased ROS production, which subsequently activates PARP, inhibiting GAPDH and resulting in accumulation of glycolysis intermediates. Several glycolysis intermediates have been indicated to be involved in the onset of ED, details of which can be found in 1.8.2.

Due to time constraints, we did not investigate oxidative stress in our db/db model, but it is well known that they do display increased O_2^-[379] and this may be a mechanism of action in the hyperglycaemia-induced ED seen in db/db mice. If time permitted, we could measure O_2^- and other ROS using one of the many chemiluminescent and fluorescent detection methods that exist as simple plate-based assay. However, the majority of these assays are not mitochondrial-specific[382] and are subject to artifacts. However, a commonly used and relatively robust detection method for production of mitochondrial O_2^- is mitoSOX, which is a fluorescent-based probe that can be used as stain for microscopy or flow cytometry, or as a plate-based assay[383]. O_2^- has an extremely short half-life, reported to be between 5-15s[384]. For this reason, it is not advised to investigate O_2^- levels in stored tissue[385]. MitoSOX can be used *in vitro*[386] or in fresh

tissue[385]. Other methods that could be utilised to detect increased oxidative stress in our model include using Taqman qPCR to investigate NOX mRNA expression, WB to measure NOX protein expression, or assays to measure NOX activity[387]. However, these methods are not specific to mitochondrial ROS. Furthermore, assays to detect O_2^- derivatives such as H_2O_2 are also available[388].

Db/db mice are known to exhibit increased plasma TGs and LDL, suggesting dyslipidaemia at about 14 weeks of age, which is older than our current model. It is unlikely that at 8 weeks the mice are dyslipidaemic, but this was not tested in our model. Dyslipidaemia is associated with ED. FFA, which can be produced from TGs, are increased in subjects with obesity and T2D[186–188], and are a known risk factor in the development of CVD[188]. The FFA palmitate is associated with ED, in that it has been shown to induce oxidative stress[191–196], activate proinflammatory signalling pathways[195] (including TLR2/NF-κB[191,197], IL-6[191,197], IL-8[197]), increase ICAM expression[191,192,194,197,198], increase monocyte adhesion[194,197], increase RAGE expression[196], and dysregulate mitochondrial bioenergetics[194,198]; pathologies known to be linked with reduced EC responsiveness. The association between high LDL and reduced vascular function is well established. Treatment with statins (resulting in lower plasma LDL) shows marked improvements in EC function in humans[389]. LDLR KO have delayed clearance of VLDL and LDL[390], therefore have elevated plasma levels of these lipids, whilst ApoE mice that have impaired lipid uptake, resulting in hypercholesterolaemia[390]. Both models show severe EC dysfunction and atherosclerosis development on NC diets. LDL has been shown to enhance monocyte adhesion[202] and promote oxidative stress[204]. It is therefore possible that plasma lipids can promote endothelial dysfunction, but the lipid profile of our mice would need to be further investigated to elucidate whether dyslipidaemia plays a role in the ED seen in our model.

Aside from the observed reduced endothelial responsiveness to the vasodilator ACh in db/db mice, they also exhibit a reduced baseline skin perfusion compared to control suggesting db/db mice have very constricted microvasculature at rest. It is difficult to interpret this outcome, as the extent of basal skin perfusion is likely a result of many circulating vasoactive factors, as well as pressure-induced vasoactivation, temperature-

induced vasoactivation, and the effects of isoflurane anaesthetic[391] amongst other contributing factors. Therefore, basal skin perfusion is very sensitive to change in every individual animal depending on but not limited to the temperature of the animal, the last time it ate, how the animal responds to isoflurane, and differing isoflurane % inhalation. To combat this, the temperature of the room is maintained at the same value and mice are placed on a heat mat which is set to the same temperature. Furthermore, isoflurane is kept to 1-1.5% to attempt to control for this. It may be of use to use a rectal thermometer to control for body temperature more efficiently. In any case, these factors may result in a variation in baseline skin perfusion, especially in treated animals. However, we see a large significant reduction in baseline skin perfusion in the db/db mice, suggesting further that their endothelium is already, even prior to PE application, very constricted. This may be due to a number of issues including reduced NO bioavailability or increased ROS. Interestingly, at the age of 8 weeks (the same age of the mice used for vascular measurements herein), db/db mice show no difference in mean arterial pressure values compared to littermates[392], meaning it is not a confounding factor in these measurements. Db/db mice begin to exhibit increased mean arterial pressure at 11 weeks of age.

3.3.5 Ageing and nutrient excess produce differing effects on aortic mitochondrial dynamics

The ED observed in our mature adult mice may be due to impaired mitochondrial function, perhaps resulting from dysregulation of mitochondrial dynamics. As previously discussed, mitochondria that are ‘stuck’ in either a fused or fragmented state may exhibit reduced ATP production, impaired mitochondrial respiration, as well as increased ROS production. Impaired mitochondrial dynamics may further lead to dysfunctional mitophagic processes. Therefore, we investigated the effects of two metabolic stressors, ageing and nutrient excess, on aortic mitochondrial dynamics. We did this through conventional Western blot, probing for proteins known to regulate mitochondrial dynamics.

There was a trend toward an age-related decline in aortic expression of the fusion protein Mfn1. Furthermore, in comparison to young adult HFD-fed mice, both groups of mature adult mice exhibited a reduction in aortic Mfn2 protein expression, with no effect of diet. We did not observe any changes in aortic OPA1 expression. Overall, these data suggest an age-associated decline in mitochondrial fusion proteins, perhaps indicative of increased mitochondrial fragmentation.

The existing literature on age-associated changes in mitochondrial dynamics is contradictory. Some report age-related decline in expression of fusion proteins in various tissues, whereas others observe counterintuitive increases in mitochondrial fusion. Son and colleagues investigated Mfn1 protein and mRNA expression in normal human fibroblasts (NHFs) from donors of varying ages[393]. They reported that Mfn1 expression (both protein and mRNA) was significantly increased in donor NHFs from a 61-year old compared to a 3-day old donor, perhaps suggesting Mfn1 expression increases with age. This data was further strengthened when the authors reported that Mfn1 mRNA expression increased significantly with age in NHFs from the same donor (29 compared to 36 compared to 46 years old). It is possible that we did not see similar findings because our mouse model is a mature adult, bordering on middle-aged, at 6 months, rather than older adult/elderly at 12-24 months of age. The fact that fusion proteins appear increased with age in donor NHFs is counterintuitive as one would expect that ageing would lead to dysfunctional mitochondria and increased fragmentation[241]. However, mitochondrial hyperfusion may occur for the mitochondria to deal with the increasing age-related mtDNA mutations. By undergoing hyperfusion, mitochondrial content will be mixed and mtDNA mutations will become diluted and less harmful. This is supported by Chen and colleagues who reported that Mfn1 deletion can result in mitochondrial dysfunction in mtDNA-mutator genetically altered mice[253]. Highly interconnected, giant mitochondria are also frequently observed in aged muscle[394] and hyperfused mitochondria can often become dysfunctional, due to the inability to target impaired areas for degradation (as this requires mitochondrial fragmentation)[241].

In contrast, another study observed significant reductions in Mfn1 and Mfn2 mRNA expression in muscle biopsies from older adult humans (mean age = 69.8) vs. young adult humans (mean age = 27.3)[395]. However, in this study the older group was described as 'sedentary' meaning there could also be a metabolic factor contributing to reduction in mitochondrial fusion proteins. Indeed, when the authors compared Mfn1/2 mRNA expression in young muscle biopsies with biopsies from senior 'sportsmen', they observed no differences between groups. Another study investigating muscle biopsies from healthy young (mean age = 22.5) and healthy older (mean age = 70.5) adult humans corroborates this[396]. In terms of animal models, Sebastián and colleagues reported a reduction in Mfn1 protein expression in gastrocnemius muscle in older mice (22-months) versus adult younger mice (6-months), suggesting an age-related decline in skeletal muscle mitochondrial fusion proteins[397], coupled with reductions in Mfn2 protein expression in soleus muscle, tibialis muscle, gastrocnemius muscle, liver tissue, and heart tissue. However, they did not measure protein expression in young adult mice, so it is hard to determine whether their 6-month old mouse is comparable to the mouse model used herein. Primary myocytes from young vs. older rabbits showed no age-related decline in Mfn2 protein expression unless further challenged with HFD[398].

Although we observed no alterations in OPA1 expression, others have reported age-associated decline in OPA1 protein expression in murine gastrocnemius muscle[399], murine tibialis muscle[395], and muscle biopsies from sedentary older humans (mean age = 69.8 vs young mean age =27.3)[395]. However, in NHFs, OPA1 mRNA expression followed an age-associated increase in cells from the same donor (29 compared to 36 compared to 46 years old). Furthermore, this study also reported a significant increase in OPA1 protein expression in cells from a 61-year old donor compared to cells from a 3-day old donor, suggesting an age-associated increase in OPA1. The reported human and animal data are somewhat contradictory, and it appears likely that age-associated changes in mitochondrial fusion proteins are tissue-dependent and sensitive to lifestyle factors such as diet and exercise.

When investigating dietary effects in aortic tissue, we observed trends toward reduced aortic Mfn1 expression and increased aortic Mfn2 expression in HFD-fed young adult

mice compared to their NC counterparts, suggesting differential effects of HFD on mitochondrial fusion proteins. HFD-feeding in mature adult mice did not produce an additive nor protective effect on aortic Mfn1/2 expression. Furthermore, diet had no effect on aortic OPA1 expression.

The existing literature on HFD-feeding and Mfn1/2 expression in various tissues is contradictory. Short-term HFD feeding (2-weeks duration) produced increased mRNA expression of Mfn2 in the soleus of rats, whereas protein expression was unaffected[400]. Longer-term HFD exposure in rats (28-weeks duration) led to decreased Mfn2 protein and gene expression in myocardium[401], whereas HFD-feeding (16-weeks) in mice led to reduced Mfn1 protein expression in heart tissue[402]. It is possible that shorter duration of nutrient excess acts as an acute stressor, resulting in an increase in mitochondrial fusion processes in order for the mitochondria to deal with the high ATP-demand the cell exhibits in times of acute stress[403]. A longer, more chronic exposure to nutrient excess upwards of 16 weeks HFD may result in reduced aortic expression of mitochondrial fusion proteins. Indeed, chronic nutrient excess is often associated with increased fragmentation. Mitochondrial fission is associated with mitochondrial uncoupling from ATP synthesis (due to proton leak), essentially making ATP production less efficient, meaning energy from excess nutrients will be lost. This may be a protective mechanism by mitochondria in order to keep ROS production to a minimum in times of nutrient oversupply[403].

We observed an age-associated decline in aortic expression of total Drp1 protein. One study that investigated effects of age in murine muscle tissue observed no changes in Drp1 expression with age in gastrocnemius[397], whereas Tezze and colleagues report a reduction in Drp1 protein in muscle biopsies from aged humans (68.9 years old vs. 27.3 years old). Reduced total Drp1 expression suggests reduced mitochondrial fission, depending on the levels of the opposing fusion proteins. However, activity of Drp1 is largely controlled by post-translational modification (PTM). PTM of Drp1 largely consists of phosphorylation, acetylation, *S*-nitrosylation, ubiquitination, SUMOylation, and *O*-GlcNAcylaton[404], and has varying effects on activity. A diet-associated trend was observed herein, where HFD-feeding in both young and mature adult mice produced a

slight increase in aortic phosphorylation of serine site 637 of Drp1. Due to an age-associated trend toward reduced aortic expression of total Drp1, this resulted in a significant increase in phospho-Drp1 s637/total Drp1 ratio in mature adult HFD-fed mice compared to both young adult HFD-fed mice as well as mature adult NC-fed mice. In general, phosphorylation of Drp1 at serine 637 has been reported to reduce Drp1 activity, by promoting detachment of Drp1 from mitochondria and therefore inhibiting mitochondrial fission[405,406]. However, the effect of phosphorylation on Drp1 activity is largely kinase and tissue-dependent. For example, Ca^{2+}/calmodulin-dependent protein kinase Iα induces phosphorylation of Drp1 at s637 and acts to promote Drp1 translocation to mitochondria, allowing for fission to occur[407]. In contrast, cAMP-dependent protein kinase phosphorylates Drp1 at s637 to inhibit Drp1 activity[408]. In a cardiomyocyte model of anoxia-reoxygenation injury, an increase in mitochondrial fission was observed, but accompanied by a reduction in phosphorylation of s637[409]. Wang and colleagues observed a significant increase in phosphorylation at site s637 on Drp1 induced by high glucose (25mM for 36 hours) exposure in immortalised endothelial cells, which resulted in increased recruitment of Drp1 to the mitochondria[406]. These data suggest that there are differential effects of phosphorylation of Drp1 in varying disease models. In terms of nutrient excess *in vivo*, HFD-feeding mice for 18 weeks has been shown to decrease phosphorylation of Drp1 at s637 and increase phosphorylation at s616 in heart tissue[410]. The authors further observed increased mitochondrial fragmentation via electron microcopy in heart tissue, suggesting that reduced phosphorylation at s637 in this case contributed toward increased mitochondrial fission. This is contradictory to our observations in that the additive metabolic stressors ageing and HFD-feeding induced a significant increase in phosphorylation of s637 on Drp1, in comparison to young HF-fed mice, as well as in comparison to mature NC-fed mice. Drp1 phosphorylated at s616 was undetectable in aortic tissue of these mice. It is unclear at this time whether the increased phosphorylation at s637 in our model results in mitochondrial fragmentation due to contradictory reports in the literature. To investigate whether mitochondria are fused or fragmented in response to increased Drp1 s637 phosphorylation, electron microscopy could be used to image the morphology of mitochondria, or cellular localisation of Drp1 could be investigated to observe whether there is increased or decreased Drp1 recruitment to mitochondria. An

alternative approach may be to perform a GTPase activity assay, but this would not be specific to Drp1 activity.

3.3.6 VE fraction expression of mitochondrial dynamics proteins is unchanged in response to ageing and/or HFD

It has been reported that mitochondrial crisis in brain ECs can greatly exacerbate inflammation-induced BBB disruption and therefore contribute to cerebrovascular pathologies[127]. Therefore, we chose to investigate alterations in VE fraction expression of mitochondrial dynamics proteins in response to the metabolic stressors ageing and HFD.

HFD-feeding in young mice produced a trend toward reduced expression of OPA1 (total, short, and long forms), but there was no effect of diet on Mfn2. This change in OPA1 needs to be further investigated by increasing the sample size. Where possible, it is important to measure density of OPA1 protein bands in isolation. OPA1 can undergo cleavage by the proteases OMA1 and YME1L to form short-form and long-forms of OPA1, the functions of which are somewhat distinct. As the OPA1 bands in VE fraction Western blots herein were distinguishable from each other, they were densitometrically analysed separately to produce short-form, long-form, and total OPA1 protein levels. The general consensus in the literature is that long-form OPA1 is fusion competent, in that it can perform mitochondrial fusion in the absence of the short-form, whereas this is not true of the short-form. On the other hand, the short-form alone has been shown to be more capable of maintaining mitochondrial bioenergetics[411]. However, Del Dotto and colleagues report that an intricate balance between long and short-forms is required for fully functioning mitochondria[247]. In any case, we did not observe any measured differences between long- and short-forms of OPA1 across our groups, and any trends toward changes in OPA1 expression were the same across short-form, long-form, and total protein.

These data, showing no change in Mfn2 expression upon HFD feeding but trends toward reduced OPA1 expression, are not consistent with existing studies. Reductions in Mfn2

protein and gene expression were observed in rat myocardium after exposure to HFD for 28 weeks[401]. 16 weeks of HFD in mice led to reduced Mfn1 (which was not detected herein) protein expression in heart tissue[402], whilst a 40-week HFD intervention in mice produced a significant reduction in skeletal muscle protein expression of Mfn1/2, but not OPA1[412]. The potential reduction in mitochondrial fusion with HFD feeding may be a protective measure that the mitochondrial undergo to uncouple mitochondrial respiration from ATP, meaning energy from excess nutrients (HFD) will be lost as heat (proton leak). This would also keep ROS production by the ETC to a minimum and therefore prevent oxidative stress[413].

Blotting for expression of total Drp1, and phosphorylation of Drp1 at s616 and s637 was attempted, but neither were detectable. Due to the low protein content of the VE fraction, the number of Western blots that can be attempted are limited. To further investigate VE fraction expression and PTM of Drp1, a greater number of animals would need to be used and their VE fractions would need to be pooled to produce a higher protein concentration.

The role of Drp1 in cerebrovascular integrity and BBB disruption has been investigated to an extent *in vitro* in murine primary brain microvascular ECs. LPS-induced BBB disruption was associated with increases in Drp1 phosphorylation at s616, which the authors report suggests a shift toward mitochondrial fission[414]. The authors report an increase in endothelial activation (ICAM expression), reduction in mitochondrial respiration, increased BBB permeability, and increased cellular ROS production upon stimulation with LPS, which were all associated with phosphorylation of Drp1 at s616. Interestingly, when cells were treated with LPS in combination with P110 (an inhibitor of Drp1 activity), these effects were abrogated. This suggests a role for Drp1-mediated mitochondrial fission in cerebrovascular dysfunction, and it would be interesting to measure VE fraction Drp1 activity (by phosphorylation status) or Drp1 cellular location in our model of HFD and ageing. In a rat model of subarachnoid haemorrhage (SAH), BBB disruption is a devastating consequence presenting with reduced whole-brain long-form OPA1 expression post-SAH. However, when rats are treated with mitoquinone (MitoQ; a mitochondrial-targeting drug that has been shown to activate Nrf2 in kidney

tissue), BBB disruption was rescued with significant increases in short- and long-form OPA1 (Nrf2-dependent) and improved neurological outcome[415]. These data suggest reductions in OPA1 due to insult may mediate BBB disruption and contribute to neurological deficits. A similar study from Zhang and colleagues corroborates this. They report that intravenous administration of the omega-3 fatty acid docosahexaenoic acid (DHA) protected against SAH-induced BBB disruption and cognitive deficits, associated with upregulation of OPA1 and downregulation of pDrp1 s616 and improved mitochondrial health[416].

3.3.7 Hypothalamic expression of Mfn2 and OPA1 is reduced by ageing, but not HFD-feeding

As previously mentioned, in the ARC of the hypothalamus, AgRP and NPY neurons promote orexigenic behaviour and inhibit thermogenesis of brown adipose tissue[230], whilst POMC neurons exert anorexigenic effects. These well-known control centres govern metabolic homeostasis. Impaired hormonal signalling (leptin/insulin/ghrelin) and insufficient neuronal firing in the hypothalamus contributes to obesity, dysregulation of systemic metabolism, infertility, and obesity-driven hypertension. These pathologies are also age-related, and thus the hypothalamus is of interest when studying health and unhealthy ageing processes. Neuronal activity of POMC neurons is impaired in aged mice, resulting in increased food intake and weight gain[417], which is reversed when rapamycin is administered due to its activation of POMC signalling pathways. Furthermore, adenovirus overexpression of POMC can ameliorate age-associated metabolic dysfunction[418]. Paradoxically, NPY expression is reduced in the ARC of aged rats[419], and its induction in response to fasting is impaired with ageing[420]. These data suggest an age-related dysfunction in hypothalamic metabolic signalling; however, it is presently unclear how and when these neurons become dysfunctional.

Hypothalamic mitochondrial function is an attractive target in age-related metabolic dysfunction. Ma and colleagues reported an increase in mitochondrial ROS production and reduction in mitochondrial function in the hypothalamus of obese mice[421], and furthermore the association of T2D with mitochondrial dysfunction is beyond doubt. It

remains unclear whether alterations to mitochondria are causative or consequential in ageing and metabolic disease. ROS production has been shown to be a direct modulator of the aforementioned hypothalamic neuronal populations[422–425]. Therefore, hypothalamic mitochondrial function may play a role in regulation of metabolism, and furthermore alterations in mitochondrial function during ageing may further exacerbate age-related metabolic dysfunction.

We observed age-related reductions in hypothalamic Mfn2 expression and OPA1 expression (total, long-form and short-form), with no effect of diet. These suggest that there is an age-associated reduction in proteins controlling mitochondrial fusion; suggesting hypothalamic mitochondria may appear fragmented and dysfunctional. Employment of electron or fluorescent microscopy is necessary hereafter to investigate ultrastructure of mitochondria. Reductions in these fusion proteins is consistent with previously discussed literature; reduced OPA1 protein expression in aged murine gastrocnemius muscle[399], aged murine tibialis muscle[395], and muscle biopsies from sedentary (mean age = 68.9 years old) humans[395]. Mfn2 protein expression was reduced in muscle biopsies from aged humans (mean age = 69.8) vs. young humans (mean age = 27.3)[395], as well as muscle biopsies from healthy older (mean age = 70.5) and healthy young (mean age = 22.5) adults, with aged human muscle tissue also exhibiting reduced Mfn2 mRNA expression[396]. These studies have focused on the effects of ageing in skeletal muscle; there is not a lot of existing literature on how ageing affects mitochondrial dynamics in brain tissue. Hypothalamic mitochondrial dynamics has however been investigated in relation to metabolic disorders. Studies have investigated genetic deletion of Mfn2 in specific hypothalamic neuronal populations, including both an AgRP-specific Mfn2 KO, as well as a POMC-specific Mfn2 KO. The POMC-Mfn2-KO mouse exhibits obesity, due to increased food intake, reduced energy expenditure, and decreased thermogenesis[426]. These mice exhibit hypothalamic leptin resistance, as well as expected mitochondrial dysfunction such as defective mitochondrial respiration and increased ROS production. This study closely links Mfn2 with endoplasmic reticulum (ER) stress, which is a known causative factor in the development of obesity and hypothalamic leptin resistance. Mfn2 ablation resulted in loss of mitochondria-ER contacts, resulting in ER stress and promotion of the unfolded protein response (UPR).

Genetic deletion of Mfn2 in AgRP neurons resulted in electrical silencing of these neurons due to reduced ATP production, and protected mice against DIO with reduced fat mass and significantly lower circulating leptin[427]. It is possible that in these two models lack of Mfn2 and subsequent reduction in mitochondrial fusion results in reduced ATP production. Reduced intracellular ATP content would reduce neuronal firing[428], thus reducing the downstream effects of these neurons on feeding behaviour and energy expenditure. These complimentary studies suggest that Mfn2 reduction induces differing effects on systemic metabolic physiology depending on the type of neuron involved. Since the data herein only investigates whole hypothalamic lysate, to move forward with our current data, we would have to investigate how ageing effects Mfn2 expression in different neuronal populations of the hypothalamus and whether this then exerts any effect of whole-body metabolic homeostasis. If our mature adult model exhibited reduction in Mfn2 in POMC neurons alone, this may be a possible mechanism in age-associated metabolic dysfunction, due to the potential promotion of ER stress and hypothalamic leptin resistance, as well as reduced ATP production and neuronal firing. However, the reduction in hypothalamic Mfn2 expression observed in our 6-month old mice is not associated with increased body weight.

We did not observe any changes in hypothalamic Mfn2 protein expression with HFD-feeding for 10 weeks. Schneeburger and colleagues report reductions in Mfn2 mRNA expression in hypothalamic lysates in response to as little as 4 days of HFD feeding[426], before the onset of increased body weight. However, upon longer HFD-feeding durations they do not report any further decline in Mfn2 mRNA expression, suggesting a plateau. Since they did not measure hypothalamic Mfn2 protein expression in response to HFD, and we did not measure Mfn2 mRNA, it is difficult to directly compare these data. However, when measuring mitochondrial ultrastructure Schneeburger and colleagues observe mitochondrial fission in POMC neurons of DIO mice. Paradoxically, Dietrich and colleagues observed increased mitochondrial fusion in AgRP neurons of mice fed HFD when employing electron microscopy to investigate mitochondrial ultrastructure[427]. These data further highlight the importance of investigating individual hypothalamic neuronal populations in isolation when researching the effects of nutrition. Mitochondrial dynamic processes are clearly sensitive to dietary changes, and

it is possible that we do not observe any changes in whole hypothalamic lysate in response to HFD due to expression of Mfn2 in individual neuronal populations being diluted by the presence of other neurons and cell types (astrocytes, microglia etc.). The best way to investigate mitochondrial morphology in isolated neuronal populations is through electron or fluorescent microscopy with immunohistochemistry.

It should be noted that the differential effects on mitochondrial morphology in these neuronal populations may be due to DIO mediated changes in circulating hormones that contribute to hypothalamic signalling, or indeed hypothalamic resistance toward these hormones. Diseases associated with nutrient excess (obesity in particular) are characterised by increased circulating insulin[429] and leptin[430] and decreased circulating ghrelin concentrations[431].

These hormones exert differential effects upon POMC and AgRP neuron. For example, leptin activates POMC but inhibits AgRP neurons[432]. In mice with ablated insulin receptors, re-expression of the receptor has been reported to suppress hepatic glucose production in AgRP neurons but enhance it in POMC neurons[433]. Finally, ghrelin can enhance the activity of AgRP neurons, but inhibit POMC neurons[434]. Furthermore, in certain pathological situations neurons can become resistance to these circulating hormones themselves; hypothalamic leptin resistance is associated with nutrient excess and obesity. Hypothalamic leptin resistance would result in reduced POMC neuron activity and increased AgRP neuron activity, resulting in hyperphagic behaviour and reduced energy expenditure[432]. Neuronal mitochondrial dysfunction may be a direct consequence of this, or indeed may be causal, but this is presently unclear. These data suggest these two neuronal populations act differentially in response to DIO mediated changes in circulating metabolic hormones and this is a very interesting avenue to consider.

The role of OPA1 in hypothalamic function is less well studied. A study that aimed to investigate the role of OPA1 in pancreatic beta cell function made use of the RIP2-Cre mouse to induce a tissue-specific knockout of OPA1 in pancreatic beta cells. However, RIP2-Cre is also expressed in hypothalamic tissue. Consequently, the authors

investigated metabolic status as well as feeding and locomotor behaviour in these mice to determine whether there was any effect of hypothalamic deletion of OPA1 that may affect their pancreatic-induced phenotype. They observed no change in body weight, food intake, lean mass, or fat mass[435]. Of note was that these mice were studied when they were 2-12 weeks old, when young mice are likely to compensate for genetic deletions and fed a NC diet. Therefore, it is presently unknown whether hypothalamic OPA1 is important for metabolic homeostasis in older mice, or in nutrient-associated diseased models. It is difficult to speculate how the reduction of OPA1 in the hypothalamus of our mature adult mice may affect whole-body homeostasis, considering we have investigated whole hypothalamic lysate and not individual neuronal populations. If fusion was disturbed in either neuronal population it may result in reduced intracellular ATP production and reduced neuronal firing, resulting in dysregulated hypothalamic control of feeding behaviour and energy expenditure. Global OPA1 heterozygous KO mice exhibit increased mitochondrial ROS production in the cortex, measured by reduced aconitase activity and reduced SOD expression[436]. The observed reduction in OPA1 in mature adult hypothalamus may be associated with increased mitochondrial ROS production, which as previously described is known to regulate hypothalamic metabolic signalling[422–425]. Furthermore, OPA1 governs mitochondrial cristae structure, as knockdown of OPA1 results in disorganised cristae, which would likely affect the ETC and thus hypothalamic mitochondrial respiration. Clearly, this warrants further investigation.

3.3.8 Aortic expression of proteins involved in mitochondrial dynamics remain unchanged in db/db mice

To investigate the effects of nutrient excess on mitochondrial dynamics, we also utilised a more severe model of obesity – the db/db mouse. As previously discussed, db/db mice exhibited extreme vasoconstriction basally, as well as a blunted response to both PE and ACh, suggesting severe endothelial dysfunction. They also exhibit increased weight gain and severe fasting hyperglycaemia compared to wt/wt and wt/db littermates. To elucidate the cause of this ED in db/db mice, and to study the effects of hyperglycaemia on vascular mitochondrial function, we looked to further investigate the cause of the

observed endothelial dysfunction, by probing for known regulators of mitochondrial dynamics in aortic tissue.

Surprisingly, we observed no changes in aortic expression of proteins governing mitochondrial dynamics; Mfn1, Mfn2, OPA1, phospho-Drp1 616, and total Drp1. This suggests that the ED in this model is not a consequence of dysregulated mitochondrial dynamics. There is a slight trend toward reduced phosphorylation of Drp1 at s616 in db/db mice; sample size needs to be increased in order to test whether this is a genuine result. A reduction in phosphorylation of this site would, as discussed earlier, result in reduced Drp1 activity and translocation to mitochondria, resulting in a potential shift toward mitochondrial fusion. As mentioned previously, nutrient excess has been reported to induce fragmentation of mitochondria, likely resulting in dysfunction, which is contradictory to the result we observe herein. However, increased mitochondrial fusion has been observed in models of nutrient excess in some cell types[400,427], suggesting that the effects of nutrient excess on mitochondrial dynamics is both cell-dependent and situational. Due to the db/db mice being only 8 weeks old, it is possible that their hyperglycaemic phenotype acts as an acute stressor, resulting in an increase in endothelial mitochondrial fusion processes, in order for the mitochondria to respond to high-ATP demand that cells experience during times of acute stress[403]. Indeed, it would be useful to investigate expression of mitochondrial dynamics proteins in db/dbs in a time-dependent manner to investigate the effects of a more chronic hyperglycaemic stimulus. Indeed, chronic high glucose conditions have been previously reported to promote mitochondrial fission in primary cultured β-cells[282] and in an immortalised rat cardiomycoyte cell line[437,438].

3.3.9 VE fraction expression of proteins involved in mitochondrial dynamics are unchanged in db/db mice

We thought it important to also investigate VE fraction expression of mitochondrial dynamics proteins. Diseases of nutrient excess are associated with impaired BBB integrity and dysregulated cerebral haemodynamics[111]. Furthermore, proper BBB integrity is dependent on fully functioning mitochondria[127]. Therefore, we sought to

investigate whether db/db mice exhibited any changes in VE fraction expression of proteins governing mitochondrial dynamics.

No changes in VE fraction expression of Mfn1, Mfn2, or OPA1 (total, short-, and long-form) were observed in db/db mice. Wt/db, but not db/db mice seemed to exhibit a trend toward increased Drp1 expression compared to wt/wt. This peculiarality may be due to the small size, but also highlights the importance of using not only wt/db as controls, but wt/wt littermates as well in studies involving the db/db models. The majority of studies usually employ the use of solely the db/db and the wt/db models, but it is uncertain at this time whether the wt/db itself may exhibit a phenotype, therefore introducing false positives. No change in phosphorylation of Drp1 at s616 was observed, nor the phospho/total ratio. Phosphorylation of Drp1 at s637 was attempted but could not be detected.

3.3.9 Hypothalamic expression of proteins regulating mitochondrial dynamics remains largely unchanged in db/db mice

Due to the known hypothalamic dysfunction associated with models of obesity and nutrient excess, we sought to investigate whether db/db mice exhibited any alterations in hypothalamic mitochondrial dynamics. No changes in Mfn1, Mfn2, or OPA1 (total, short-, or long-form) were observed in the hypothalamus of db/db mice compared to controls. Furthermore, no changes in total Drp1 were observed, but phosphorylation at site s616 was increased in db/db mice compared to wt/wt mice. When expressing phospho/total as a ratio, db/db mice also displayed a significant increase compared to wt/wt. An increase in hypothalamic phospho s616/total ratio may suggest a shift toward mitochondrial fission, especially since opposing fusion proteins remain unchanged, which is in line with existing literature. Although mitochondrial dynamics has not been previously studied in the hypothalamus of db/db mice, Huang and colleagues report a significant increase in phosphorylation of Drp1 at site s616 in an isolated mitochondrial fraction from whole cortex[439]. As previously mentioned, nutrient excess is proposed to induce mitochondrial fission in many cell types. It is possible that the observed severe hyperglycaemia in db/db mice induces hypothalamic mitochondrial fission, further

exacerbating the metabolic dysfunction exhibited in these mice. It is presently unclear whether this is a cause or consequence of mROS production. Hyperglycaemia is a main contributor of mROS production, but since we have not measured ROS in our model, the mechanism cannot be elucidated at present. Db/db mice are reported by others to exhibit increased ROS production[379], but this has not been measured in hypothalamic tissue.

As mentioned previously, when investigating hypothalamic tissue, it is important that neuronal populations are studied in isolation, due to mitochondrial dynamics behaving differently under nutrient stress. Furthermore, other brain cells such as astrocytes and microglia may also be affected. Indeed, astrocytes can provide fuel for neurons in times of low glucose (in the form of lactate) or in times where neuronal activity is high and more ATP is required (lactate or glutamine). Astrocytes may also experience adverse effects due to nutrient excess[440], impairing intracellular metabolic processes and resulting in indirect effects on neurons. Hypothalamic mitochondrial morphology would have to be looked at more closely in our db/db model in order to investigate further.

3.3.10 Endothelial dysfunction observed in db/db mice is not associated with endothelial activation

Another contributor to impaired endothelial responsiveness is inflammation, termed endothelial activation (EA) in ECs. To determine whether the ED observed in db/db mice was associated with inflammation, we probed for ICAM protein expression in aortic tissue as well as in the NVU, which we hypothesised would be increased in db/db mice. We did not observe any changes in ICAM expression in aorta nor NVU. This is particularly interesting, as it suggests that ED can develop in the db/db mouse in the absence of an inflammatory environment. ICAM is reported to be increased in db/db mice in existing studies[441–443]. However, these studies utilise db/db male mice that are around the ages of 12-18 weeks old whereas we employed the use of 8-week old females, so there may be some sex- and age-specific differences. We observed severely blunted endothelial responsiveness to vasoactive agents in the absence of ICAM overexpression, but we did not investigate other inflammatory markers in our models such as VCAM, IL-1β, IL-6, or

TNFα, all of which are associated with ED. It would be necessary to investigate other markers of inflammation (via Taqman or a cytokine array assay) before coming to a more definitive conclusion.

3.3.11 Summary

This chapter aimed to investigate the effects of nutrient excess on *in vivo* endothelial function, as well as elucidate whether any ED observed in the models was associated with alterations in mitochondrial dynamics.

We observed an age-associated blunted response in endothelium to the vasodilator ACh, suggesting aging is associated with endothelial dysfunction. HFD-feeding did not induce ED in young adult mice, nor did it exacerbate ED observed in mature adult mice. No stark alterations in proteins governing mitochondrial dynamics were measured in vascular tissue (aorta, NVU). These data suggest age-related development of ED is independent of changes in mitochondrial dynamics. To further elucidate a mechanism, ROS production and blood glucose levels need to be measured in these models. Furthermore, it would be interesting to investigate older mice, perhaps at 12 months (middle-old aged) or 24 months (old aged) to track ED over time.

Interestingly, reductions in mitochondrial fusion proteins Mfn2 and OPA1 were observed in whole hypothalamic tissue of mature adult mice, suggesting age-associated reductions in mitochondrial fusion. This may result in reduced ATP production and reduced neuronal firing, promoting metabolic dysfunction, or may indeed be due to changes in other cell types present in the brain; astrocytes or microglia. Going forward, hypothalamic neuronal populations and individual cell types would need to be studied in isolation when investigating mitochondrial dynamics due to the opposing responses to nutrient excess. This is obviously rather difficult but could be achieved by using electron microscopy (EM) to investigating ultrastructure of mitochondria in individual cell types, or by isolating primary cells. It would also be interesting to perform single-cell RNA seq with technology from 10x Genomics to investigate the effects of nutrient excess on the transcript of differing cell populations.

Db/db mice gain significantly more weight and are severely hyperglycaemia compared to their control littermates. They exhibit a severely blunted response to vasoactive agents *in vivo* but this is independent of changes in vascular mitochondrial dynamics (aorta, NVU). ROS levels were not measured herein, but need to be further investigated, as the production of which is a potential middleman between the observed hyperglycaemia and ED in this model.

Hypothalamic mitochondrial dynamics remain largely unchanged in db/db mice, aside from a slight increase in phospho Drp1 s616/total Drp1 ratio in db/db mice compared to wt/wt mice, suggesting a potential shift toward mitochondrial fission. This shift toward fission is likely a consequence of nutrient excess and may be the result of the adaptive nature of mitochondria to uncouple their respiration from ATP synthesis in times of nutrient overload (hyperglycaemia seen in db/db mice) to minimise ROS production. It may also be a response to altered levels of circulating hormones that act hypothalamically, such as leptin, insulin, or ghrelin, or indeed an altered hypothalamic response to these signalling hormones. The circulating concentration of these hormones could be further investigated, but it has been reported that circulating leptin and insulin is increased in db/db mice[444] and ghrelin mRNA in the gastric fundus (stomach) is reduced[445].

In summary, age-associated decline in endothelial response is not associated with alterations in proteins governing mitochondria dynamics. Furthermore, 8-week old severely hyperglycaemic db/db mice exhibit stark impairments in endothelial response, independently of changes in proteins regulating mitochondrial dynamics.

Chapter 4

Investigating the effects of HFD, BACE1 activity, and amyloid beta on vascular mitochondrial dynamics

4.1 Introduction

BACE1 is an aspartic protease, best known for its role in APP processing (Fig. 1.15). Metabolic diseases are associated with increased levels and/or activity of BACE1, and thus increased levels of its final cleavage product Aβ. Indeed, BACE1 protein expression is increased by exposure to palmitate, and its derivative ceramide in differentiated C_2C_{12} myotubes[306]. Additionally, DIO mice (22 weeks 45% HFD) mice express significantly increased hypothalamic BACE1 mRNA and protein levels[308], and adipose tissue BACE1 protein levels[315]. Botteri and colleagues observed a HFD-dependent increase in BACE1 protein and mRNA in murine muscle tissue[307]. BACE1 levels are also increased in the livers of the diabetic mouse model db/db[300]. Further to these increases in expression, BACE1 activity is also increased with HFD-feeding; DIO mice exhibit increased hypothalamic sAPPβ and $Aβ_{42}$ levels, indicating increased BACE1 activity[305] and our most recent observations indicate HFD-dependent increases in aorta and plasma $Aβ_{42}$ in mice and plasma $Aβ_{42}$ in T2D humans[316]. Botteri and colleagues further report increased BACE1 levels in adipose tissue and increased sAPPβ in plasma from people with T2D[307]. Multiple publications indicate a role for BACE1 and Aβ in the development of metabolic disorders such as obesity and T2D[300,305,307,309,310,317], details of which are reported herein (Introduction 1.12.2).

Obesity and T2D are often associated with vascular diseases such as atherosclerosis[35–37]. One of the first key events in the development of atherosclerosis is ED, characterised by a reduced responsiveness of ECs to vasoactive signals, a low-grade chronic inflammatory state, and reduced NO bioavailability. Our recent findings implicate HFD-driven increases in BACE1 activity and therefore $Aβ_{42}$ production in the development of ED[446]. Indeed, HFD-driven reduction in endothelial function is rescued by BACE1 inhibition, whilst increasing circulating $Aβ_{42}$ levels (using subcutaneous minipump infusion) induces ED[316]. However, it is at present unclear how BACE1 and $Aβ_{42}$ regulate this progression.

BBB disruption is closely linked with obesity and T2D[112–122], with the presence of T2D systemically contributing to endothelial activation[123] and basement membrane

thickening[124–126]. Furthermore, impairments in peripheral EC function is a strong predictor of cerebrovascular dysfunction[346]. Interestingly, BACE1 is expressed in brain endothelium[319] and others have reported that APP overexpression[320] in mice, as well as direct $A\beta_{40}$ (but not $A\beta_{42}$) application to the brain reduces CBF[320], indicating brain EC dysfunction. These data suggest a role for increased Aβ species in the development of brain EC dysfunction and therefore perhaps BBB disruption. However, it is very important to note that these studies utilise knock-in mouse models with extremely high circulating levels of Aβ, or indeed simply apply supraphysiological μM concentrations of Aβ peptides directly to the cortex, which is not physiological.

Mitochondrial dysfunction is often observed in diseases of nutrient excess. Indeed, animal and cell models of nutrient excess exhibit impaired TCA cycle physiology[268–271], increased mROS production[198,273,276], decreased ATP production[272], reduced mitochondrial respiratory capacity[276,280], impaired mitochondrial biogenesis[275], and dysregulated mitochondrial dynamics[278,281–284]. Multiple studies also indicate a role for BACE1 and Aβ in initiating mitochondrial dysfunction[306,317,331–335], reported in detail in section 1.12.3. Mitochondrial crisis in brain ECs has also been shown to exacerbate BBB dysfunction in a model of systemic inflammation[127]. However, it is presently unclear whether nutrient access-associated increases in BACE1 activity and $A\beta_{42}$ production contribute to mitochondrial dysfunction in ECs, both peripheral and cerebral, therefore contributing to disease pathology.

The aim of this chapter is to confirm a role for BACE1 and $A\beta_{42}$ in endothelial function *in vivo,* and furthermore elucidate whether any impairments in EC function are associated with dysregulated EC mitochondrial dynamics. To do this, we employed the use of 4 animal models of varied BACE1 activity.

The first model was a HFD-fed BACE1KO mouse, with HFD-fed WT and HET littermates, as well as NC-fed WT controls. These models were used to investigate the effects of a 10-week HFD on endothelial function *in vivo*, and the contribution of BACE1 to HFD induced endothelial dysfunction

The second and third models were HFD-fed WT mouse centrally or peripherally infused with $A\beta_{42}$ vs. ScrP control, to investigate how raising $A\beta_{42}$ (as per HFD-induced BACE1 activity) either centrally or peripherally might affect endothelial function *in vivo.*

The final model was a NC-fed APP23 mouse infused with a BACE1 inhibitor vs. vehicle control. This model is genetically engineered to harbor pathological levels of $A\beta_{42}$, so we used this mouse to investigate the effects of increased $A\beta_{42}$ on endothelial function *in vivo*, and whether reducing $A\beta_{42}$, through BACE1 inhibition, would modulate any observed effects. Study timelines can be found in Fig. 4.1-4.3. We investigated EC function *in vivo* and, where possible (BACE1 KO, $A\beta_{42}$ centrally infused), investigated mitochondrial dynamics proteins in tissues of interest (aorta, NVU). We hypothesised that, whilst genetic or pharmacological reduction of BACE1 activity would protect mice against HFD-induced ED, mice with increased $A\beta_{42}$ levels (APP23, peripherally/centrally infused $A\beta_{42}$) would exhibit exacerbated ED. Furthermore, this ED may be further associated with mitochondrial dysfunction, as measured by dysregulation of proteins involved in mitochondrial dynamics.

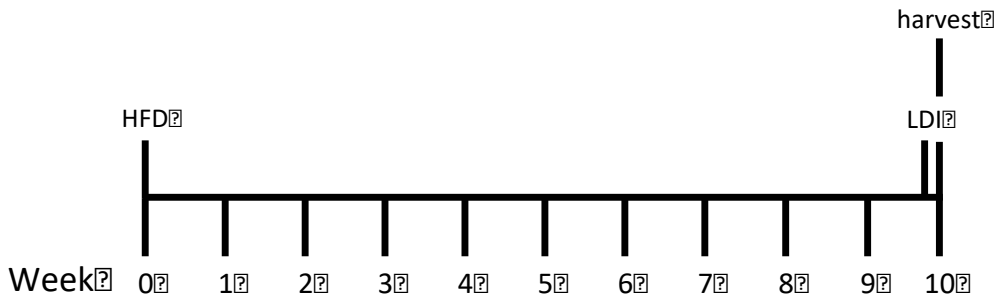

10-12 week old male BACE1 KO mice and their WT and HET littermates were placed on HFD for 10 weeks. A group of age-matched WT mice were maintained on NC diet as a control. During the 10th week, mice underwent LDI accompanied with PE and ACh iontophoresis. Mice were fasted overnight before being culled the next morning. Plasma, aortae, and hemi-brains were harvested for post-mortem biochemical analysis.

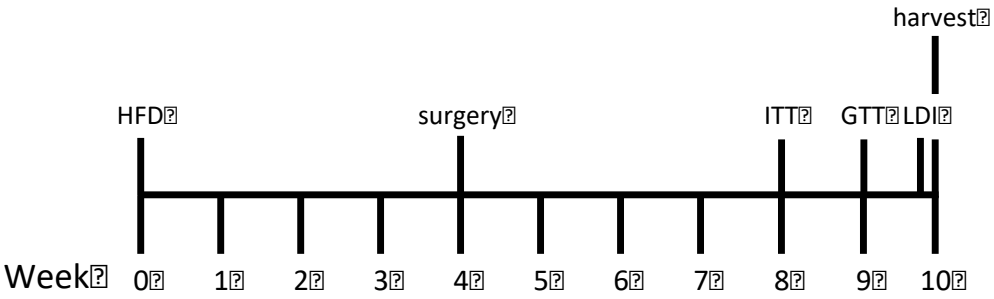

Figure 4.2 Study timeline of chronic $A\beta_{42}$ infused mice

10-12 week old male WT mice were placed on HFD for 4 weeks before undergoing surgery to fit either a subcutaneous minipump (peripheral infusion) or a subcutaneous minipump attached to an icv cannula (central infusion), in order to be infused with either $A\beta_{42}$ or ScrP peptide control. Mice were maintained on HFD during the infusion period. ITT and GTT were performed on central $A\beta_{42}$ mice during weeks 8 and 9 respectively, but not on peripheral $A\beta_{42}$ mice. During the 10th week, LDI plus PE and ACh iontophoresis was performed on the mice to measure endothelial function. Mice were fasted overnight before being culled the next morning. Tissue from centrally infused mice (plasma, aortae, and hemi-brains) was harvested for post-mortem biochemical analysis. Peripherally infused mice were perfuse-fixed in order to provide tissues for IHC experiments required by a study, separate from the current PhD project.

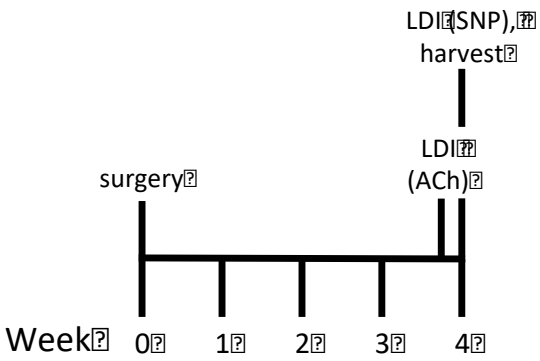

Figure 4.3 Study timeline of BACE1 inhibitor treated APP23 mice

8-10 week old NC-fed male and female APP23 mice underwent surgery to fit a subcutaneous minipump in order to infuse the BACE1 inhibitor or saline control for 4 weeks. During week 4, mice underwent LDI and ACh iontophoresis to measure endothelium-dependent skin perfusion. Two days later, mice underwent LDI again, but with SNP iontophoresis to measure endothelium-independent skin perfusion. Whilst still under anaesthetic, mice were culled, and tissue was harvested in order to provide tissues for experiments required by a study, separate from the current PhD project.

4.2 Results

4.2.1 Genetically reducing BACE1 protects mice against HFD-induced weight gain

Male BACE1 KO mice, alongside WT and HET littermates, were placed on HFD for 10 weeks. Age-matched NC-fed WT mice were used as a control. This gave rise to four experimental groups: WT NC, WT HF, HET HF, and KO HF. Mice were weighed weekly.

WT HF and HET HF mice gained weight over the course of the 10-week study, whereas the weights of KO HF and WT NC mice remained steady (Fig. 4.4A, C). WT HF mice gained more weight than WT NC mice (Fig. 4.4B – WT NC 1.53g ± 0.68g vs. WT HF 9.00g ± 1.40g, n = 6-10, $p < 0.01$), whereas HET HF mice exhibited only a trend toward more weight gain compared to WT NC. KO HF mice gained a similar amount of weight to WT NC mice (Fig. 4.5B – WT NC 1.53g ± 0.68g vs. KO HF 2.23g ± 0.57g) and gained significantly less weight than their WT HF counterparts (Fig. 4.5B – WT HF 9g ± 1.4g vs. KO HF 2.23g ± 0.57g, n = 6-10, $p < 0.01$). When expressed as percentage weight gain, WT HF mice gained significantly more weight than WT NC mice (Fig. 4.5D – WT NC 4.46% ± 2.34% vs. WT HF 29.08% ± 4.47%), whereas KO HF exhibited similar weight gain to WT NC mice (Fig. 4.5D – WT NC 4.46% ± 2.34% vs. KO HF 6.58% ± 0.86%) and gained significantly less weight than WT HF counterparts (Fig. 4.5D WT HF 29.08% ± 4.47% vs. KO HF 6.58% ± 0.86%).

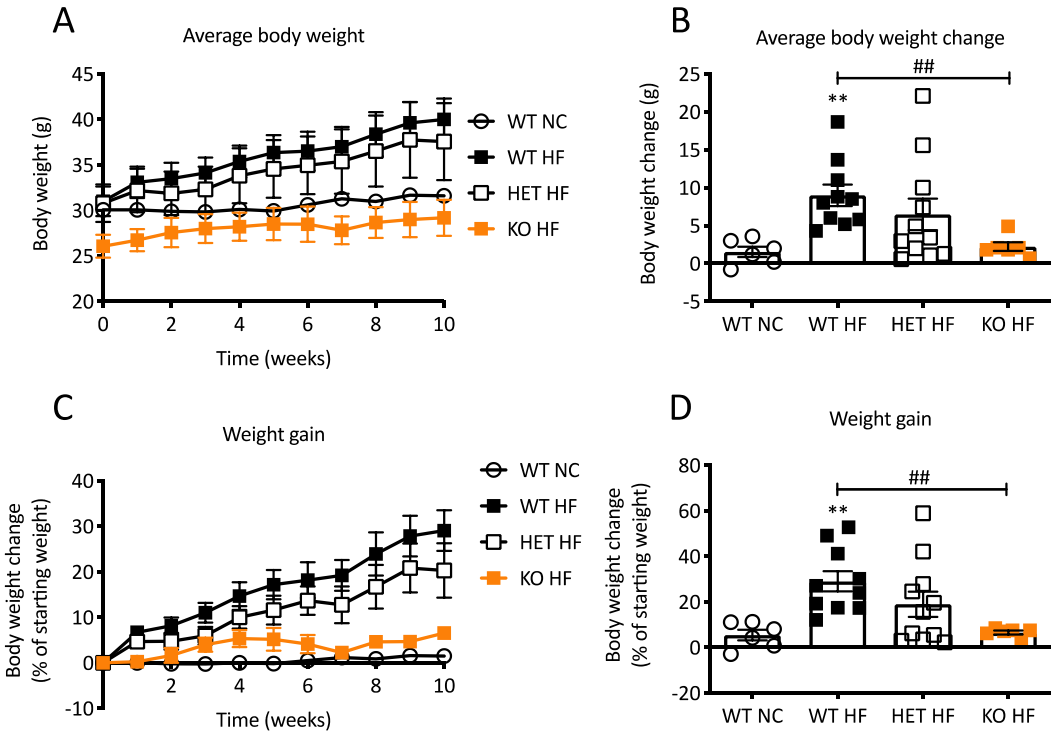

Figure 4.4 Global genetic reduction of BACE1 protects mice against HFD-induced weight gain

10-12 week old WT (WT HF), BACE1 heterozygous (referred to as HET HF), and BACE1 KO (referred to as KO HF) were placed on 45% HFD for 10 weeks. Body weight was measured weekly. WT NC mice were used as a control. (A) Average weight of the mice over the 10 weeks of the study. (B) Net weight gain at the end of the study. (C) Percentage weight gain over the 10 weeks of the study. (D) Percentage weight gain at the end of the study.

Data are expressed as mean ± standard error of the mean.

n = 6-10. (A) and (C) – Repeated measures ANOVA with Bonferroni's multiple comparison. (B) and (D) – Welch's ANOVA with Dunnett's T3 multiple comparison. ** = $p < 0.01$ when compared to WT NC. ## = $p < 0.01$ between WT HF and KO HF.

4.2.2 Genetically reducing BACE1 protects mice against HFD-induced endothelial dysfunction

To measure endothelial function *in vivo*, mice underwent LDI and iontophoresis of vasoactive agents (PE to induce vasoconstriction and ACh to induce endothelium-dependent vasodilation). To gather information about endothelial health, three main outputs of the above technique were analysed; baseline skin perfusion (AU), % Δ skin perfusion in response to ACh compared to PE-induced baseline, and peak skin perfusion in response to ACh (AU). A detailed description of this technique can be found in Methods.

Fig. 4.5A-E shows percentage change in skin perfusion against time in response to PE and ACh (baseline is 100%) in all four groups. These data are split in to two groups per graph for clarity. All groups of mice responded to PE with reduced skin perfusion, and then exhibited increased skin perfusion in response to ACh application (Fig. 4.5A-E), suggesting their cutaneous microvascular ECs are responsive to these vasoactive agents. WT HF and HET HF exhibited a slightly blunted response to ACh compared to WT NC mice (Fig. 4.5A, C) and compared to KO HF mice (Fig. 4.5B, D), whereas as KO HF exhibited a trajectory more comparable to WT NC mice (Fig. 4.5E). Baseline skin perfusion did not differ between groups (Fig. 4.5F). WT HF and HET HF displayed significantly reduced ACh-induced vasodilation (as a % of PE normalised baseline) compared to WT NC (Fig. 4.5G – WT NC 40.61% ± 4.44% vs. WT HF 10.28% ± 3.88%, n = 6-10, $p < 0.01$; WT NC 40.61% ± 4.44% vs. HET HF 9.22% ± 3.5%, n = 6-10, $p < 0.001$). KO HF mice exhibited a trend towards improved ACh response compared to WT HF and HET HF (Fig. 4.5G). However, KO HF mice also exhibited a trend toward reduced ACh response compared to WT NC and power calculations reveal a sample size of at least 10 is required to test the null hypothesis properly. However, it seems KO HF mice still possess healthier vasculature than WT or HET HF mice. WT HF and HET HF mice exhibit reduced ACh-induced peak flux compared to WT NC (Fig. 4.5H – WT NC 357.3 ± 9.48 vs. WT HF 257.8 ± 17.04, n = 6-10, $p < 0.01$; WT NC 357.3 ± 9.48 vs. HET HF 212.9 ± 8.6, n = 6-10, $p < 0.001$). KO HF displayed a trend toward an increased ACh-induced peak flux compared to WT HF and HET HF and similar ACh-induced peak flux to WT NC mice (Fig.

4.5H – WT NC 357.3 ± 9.48 vs. KO HF 333.5 ± 33.62). Power calculations reveal that a sample size of 13 would be required to detect whether KO HF are significantly different from WT HF or HET HF mice in terms of peak flux.

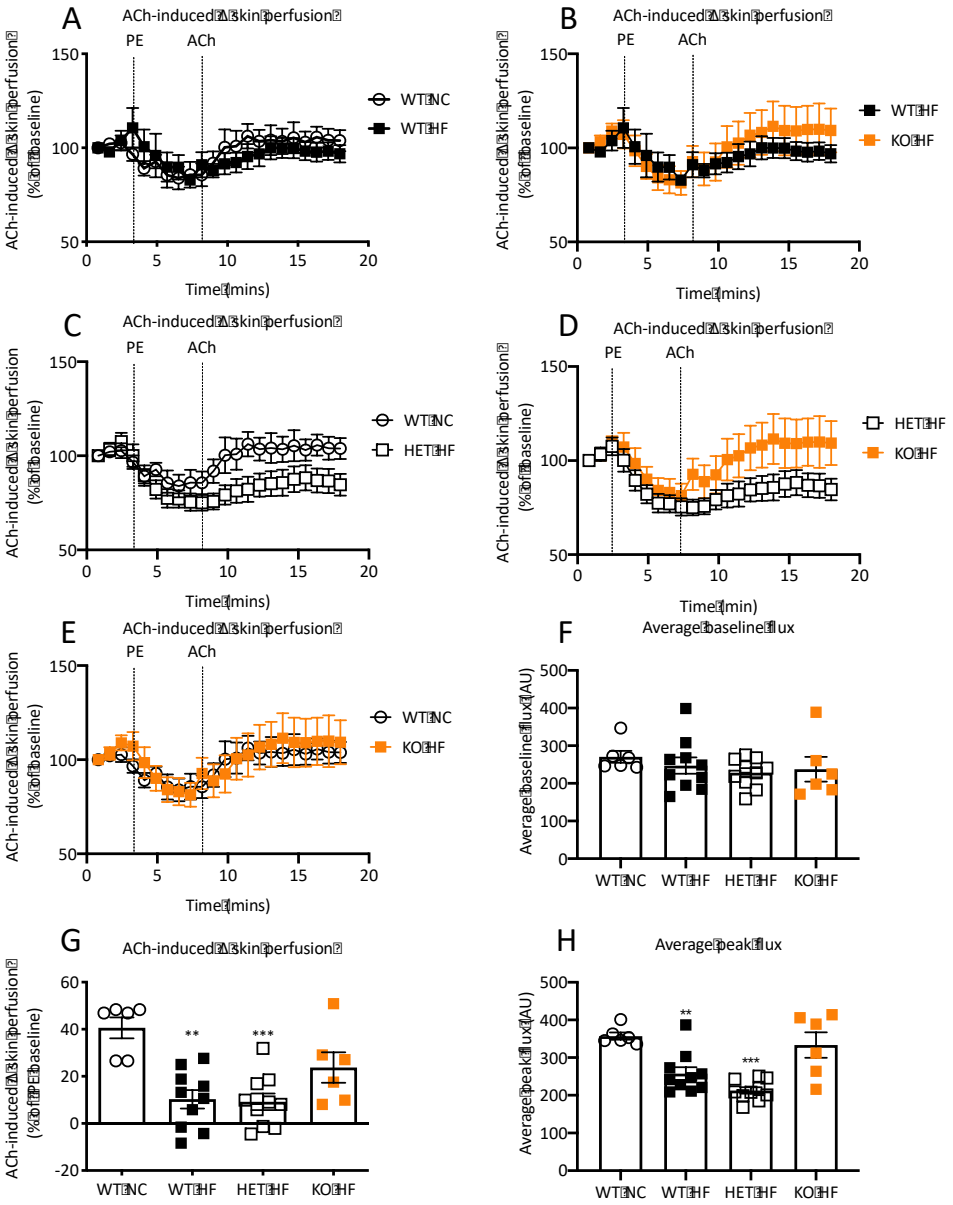

Figure 4.5 Global genetic reduction of BACE1 protects mice against HFD-induced endothelial dysfunction *in vivo*

To measure endothelial function *in vivo*, NC-fed WT and HFD-fed WT, HET and KO mice underwent LDI after 10 weeks of dietary intervention, with iontophoresis of PE and ACh, the application time of which are represented by a dotted line. ACh-induced skin perfusion as a percentage of baseline (baseline is 100%) over time in (A) WT NC and WT HF, (B) WT HF and KO HF, (C) WT NC and HET HF, (D) HET HF and KO HF, and (E) WT NC and KO HF. (F) ACh-induced skin perfusion as a percentage of PE baseline in HFD-fed WT, HET, and KO mice, and NC-fed controls. (G) Baseline skin perfusion in HFD-fed WT, HET, and KO mice, and NC-fed controls. (H) ACh-induced peak skin perfusion in HFD-fed WT, HET, and KO mice, and NC-fed controls.

Data are expressed as mean ± standard error of the mean.

n = 6-10. (F), (G) and (H) - Welch's ANOVA with Dunnett's T3 multiple comparison. ** = $p < 0.01$ and ***

4.2.3 Central chronic infusion of $A\beta_{42}$ does not affect HFD-induced weight gain

Mice were fed HFD for 4 weeks before undergoing subcutaneous icv minipump surgery in order to infuse $A\beta_{42}$ centrally. ScrP was used as a control. Mice were weighed daily for 5 weeks following surgery. Percentage weight gain (Fig. 4.6C-D) starts at 7 days post-surgery, once mice had fully recovered. Although mice are extremely resilient when it comes to surgery, they are known to drink and eat less, lose weight, and have difficulty regulating their body temperature for up to 9 days after surgery, depending on the complexity of the operation and how long they are under anaesthetic[447]. Therefore, we allow our mice one week to recover, after which they have regained their appetite and their body weight has stabilised.

Centrally $A\beta_{42}$ infused mice did not differ from ScrP infused control in terms of average body weight across the study (Fig. 4.6A), net weight gain (4.6B), or percentage weight gain (Fig. 4.6C-D).

4.2.4 Central chronic infusion of $A\beta_{42}$ promotes endothelial dysfunction

To investigate effects of centrally infused $A\beta_{42}$ on endothelial function *in vivo*, mice underwent LDI and iontophoresis of vasoactive agents (PE to induce vasoconstriction and ACh to induce endothelium-dependent vasodilation). As previously stated, ACh-induced percentage change in skin perfusion, baseline skin perfusion, and ACh-induced peak skin perfusion were extrapolated for analysis.

When plotted as change in skin perfusion over time, the responsiveness to PE in $A\beta_{42}$ appears to be delayed compared to ScrP mice (Fig 4.7A). $A\beta_{42}$ mice also appear to exhibit a slightly blunted response to ACh (Fig. 4.7A). When expressed as % Δ skin perfusion in response to ACh compared to PE-induced normalised baseline, $A\beta_{42}$ infused mice displayed a significantly blunted response to ACh (Fig. 4.7B – ScrP 13.88% ± 1.46% vs. 2.64% ± 2.66%, $n = 7$, $p < 0.001$). Baseline and ACh-induced peak skin perfusion were unaffected by $A\beta_{42}$ infusion.

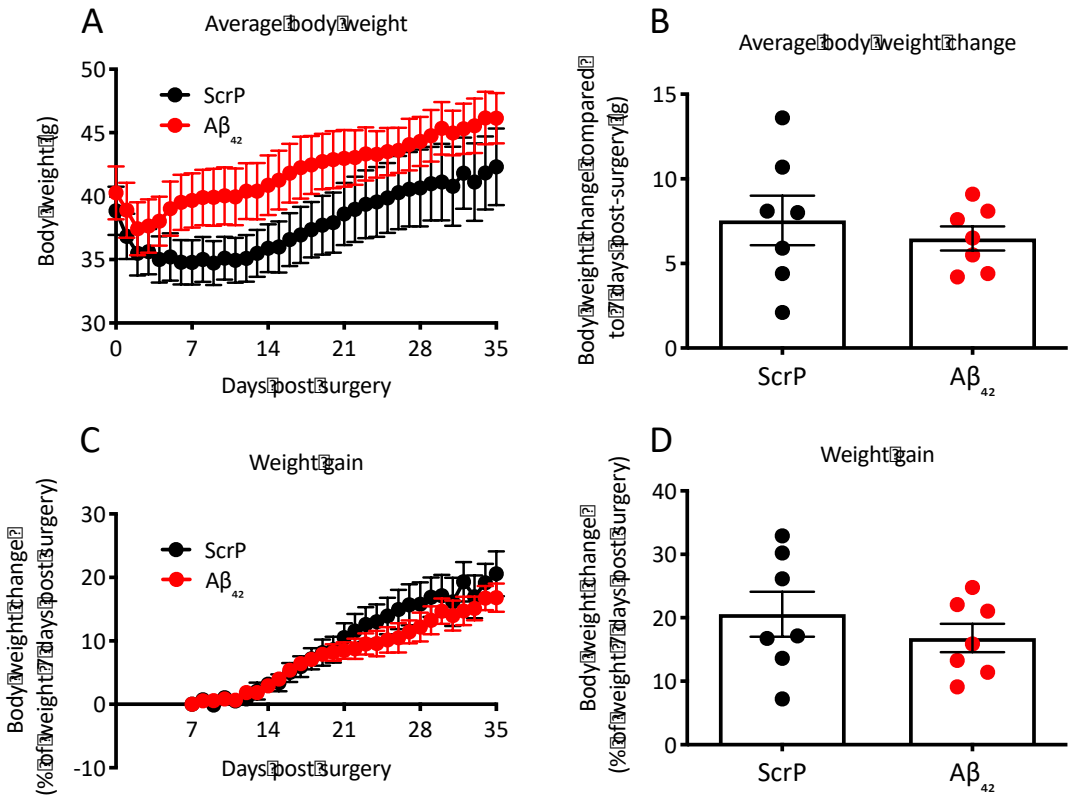

Figure 4.6 Central chronic infusion of Aβ42 has no effect on body weight

10-12 week old WT mice were placed on HFD for 4 weeks before undergoing surgery to fit a subcutaneous minipump with an icv catheter in order to infuse Aβ42 or ScrP control centrally for 4 weeks. Mice were maintained on HFD during the infusion period. Body weight was measured daily post-surgery. (A) Average daily body weight. (B) Net weight gain at the end of the study. (C) Daily body weight gain as a percentage of body weight at 7 days post-surgery. (D) Percentage weight gain at the end of the study.

Data are expressed as mean ± standard error of the mean.

n = 7. (B) and (D) – Unpaired t-test with Welch's correction.

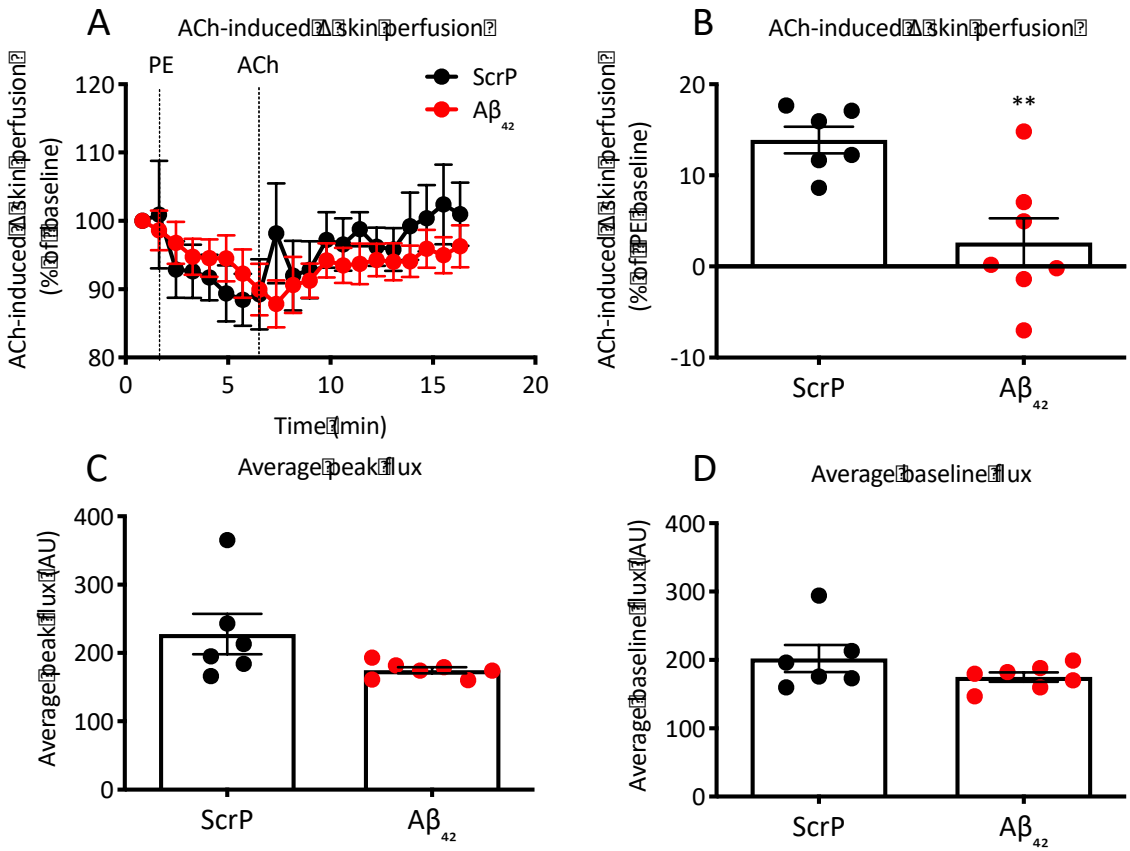

Figure 4.7 Central chronic infusion of Aβ42 promotes peripheral endothelial dysfunction

10-12 week old WT mice were placed on HFD for 4 weeks before undergoing surgery to fit a subcutaneous minipump with an icv catheter in order to infuse Aβ42 or ScrP control centrally for 4 weeks. Mice were maintained on HFD during the infusion period. To measure endothelial function *in vivo*, ScrP and Aβ42 infused mice underwent LDI with iontophoresis of PE and ACh. Time of application of PE and ACh are represented by dotted lines. (A) ACh-induced skin perfusion as a percentage of baseline (baseline is 100%) over time in Aβ42 and ScrP mice. (B) ACh-induced skin perfusion as a percentage of PE baseline in Aβ42 and ScrP mice. (C) ACh-induced peak skin perfusion in Aβ42 and ScrP mice. (D) Baseline skin perfusion in Aβ42 and ScrP mice.

Data are expressed as mean ± standard error of the mean.

n = 7. (B), (C), and (D) – Unpaired t-test with Welch's correction. ** = $p < 0.01$ when compared to ScrP.

4.2.5 Central chronic infusion of $A\beta_{42}$ increases fasting blood glucose levels

To investigate whether the $A\beta_{42}$-induced ED observed was due to impaired glucose homeostasis, we measured systemic glucose tolerance (GTT) and insulin sensitivity (ITT) in $A\beta_{42}$ infused mice. ITT and GTT were completed and fasting blood glucose levels were measured after a 4-hour fast and a 16-hour fast.

ITTs and GTT measurements did not differ between $A\beta_{42}$- and ScrP infused mice (Fig. 4.8A-C). Blood glucose levels after a 4-hour fast remained unchanged between groups (Fig. 4.8D), however after 16 hours of fasting, $A\beta_{42}$ infused mice exhibited hyperglycaemia (Fig. 4.8E – ScrP 6.94mmol/l ± 0.77mmol/l vs. $A\beta_{42}$ 9.97mmol/l ± 1.09mmol/l, $n = 7$, $p < 0.05$). However, this is a small sample size and more experiments would have to be performed in order to know whether this is a genuine result. Hyperglycaemia at 16 hours fast, but not at shorter timepoints, suggests $A\beta_{42}$ mice may exhibit increased hepatic gluconeogenesis. This is discussed further herein in section 4.3.3.

3.2.6 Peripheral chronic infusion of $A\beta_{42}$ does not affect HFD-induced weight gain

Mice were fed HFD for 4 weeks before undergoing subcutaneous minipump surgery in order to infuse $A\beta_{42}$ peripherally. ScrP was used as a control. Mice were weighed daily for 5 weeks following surgery. Percentage weight gain given herein (Fig. 4.9C-D) starts 7 days post-surgery, once mice had fully recovered. $A\beta_{42}$ infused mice did not differ from ScrP infused control in terms of average body weight across the study (Fig. 4.9A), net weight gain (4.9B), or percentage weight gain (Fig. 4.9C-D).

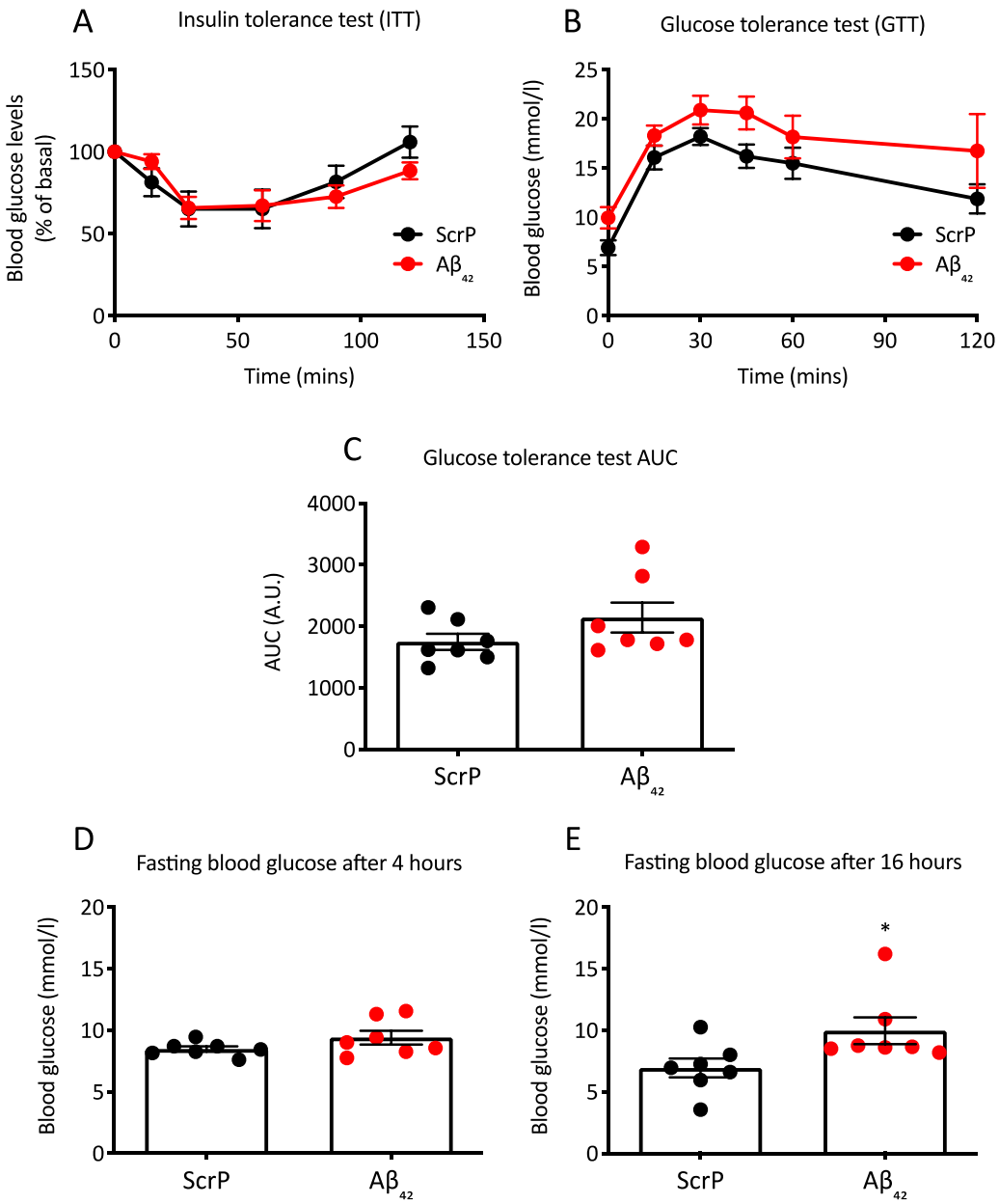

Figure 4.8 Glucose homeostasis in chronic centrally Aβ42 infused mice

10-12 week old WT mice were placed on HFD for 4 weeks before undergoing surgery to fit a subcutaneous minipump with an icv catheter, in order to infuse Aβ42 or ScrP control centrally for 4 weeks. Mice were maintained on HFD during the infusion period. Mice underwent various metabolic measurements in order to determine the effects of chronic Aβ42 or ScrP infusion of systemic metabolism. (A) Insulin tolerance test. (B) Glucose tolerance test. (C) AUC of (B) glucose tolerance test. (D) Blood glucose levels after a 4 hour fast and (E) after 16 hour fast.

Data are expressed as mean ± standard error of the mean.

n = 7. (A) and (B) – Repeated measures ANOVA with Bonferroni's multiple comparison. (C), (D), and (E) – Unpaired t-test with Welch's correction. * = $p < 0.05$ when compared to ScrP control.

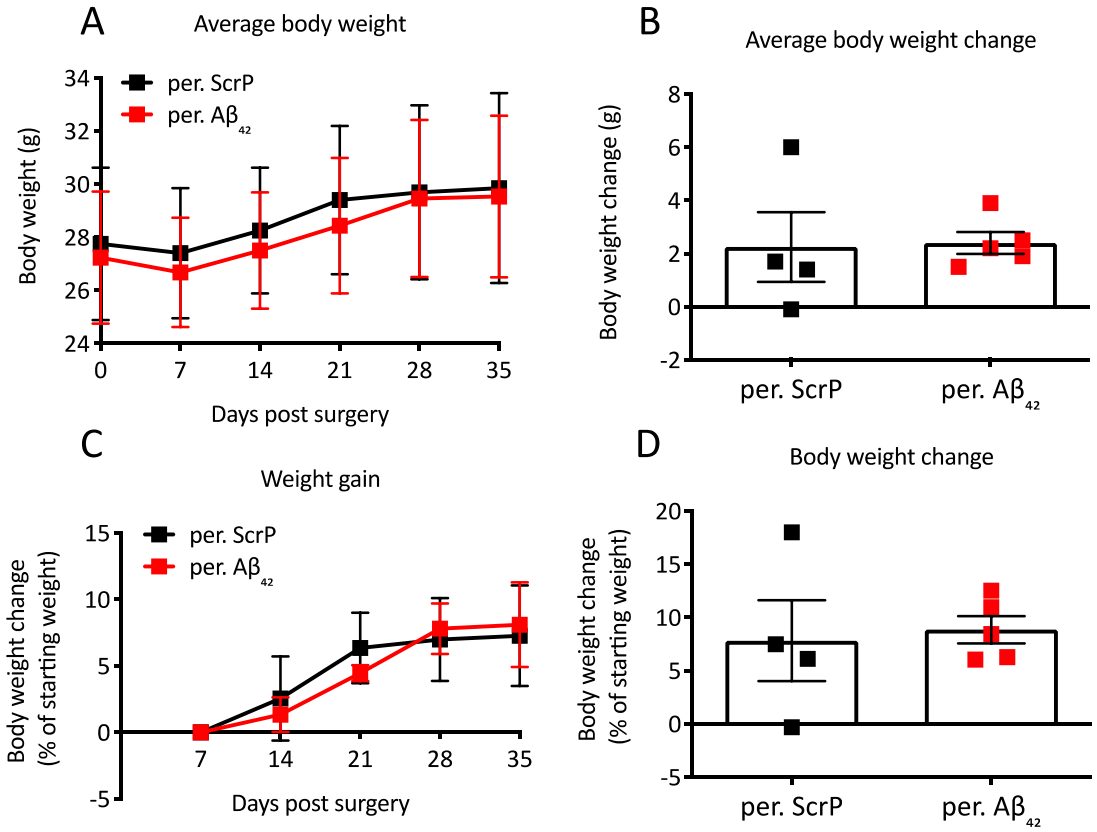

Figure 4.9 Peripheral chronic infusion of Aβ42 has no effect on body weight

10-12 week old WT mice were placed on HFD for 4 weeks before undergoing surgery to fit a subcutaneous peripheral minipump in order to infuse Aβ42 or ScrP control peripherally for 4 weeks. Mice were maintained on HFD during the infusion period. Body weight was measured weekly post-surgery. (A) Average daily body weight. (B) Net weight gain at the end of the study. (C) Daily body weight gain as a percentage of weight 7 days post-surgery. (D) Percentage weight gain at the end of the study.

Data are expressed as mean ± standard error of the mean.

n = 4-5 from the datasets shown (B) and (D) – Unpaired t-test with Welch's correction.

3.2.7 Peripheral chronic infusion of $A\beta_{42}$ produces a trend toward reduced endothelial responsiveness to ACh *in vivo*

To investigate effects of peripherally infused $A\beta_{42}$ on endothelial function *in vivo*, mice underwent LDI and iontophoresis of vasoactive agents (PE to induce vasoconstriction and ACh to induce endothelium-dependent vasodilation). Peripherally infused $A\beta_{42}$ mice, similarly to ScrP controls, exhibited reduced % skin perfusion in response to PE. However, whilst ScrP exhibited increased % skin perfusion in response to ACh, $A\beta_{42}$ mice displayed a blunted response (Fig. 4.10A). When expressed as ACh-induced change in skin perfusion (compared to PE baseline), there was no observed difference between $A\beta_{42}$ and ScrP controls (Fig 4.10B). Furthermore, no change was observed in baseline skin perfusion (Fig. 4.10C), or ACh-induced peak skin perfusion (Fig. 4.10D). The sample size in this study is very small (n = 4-5). We have observed reduced ACh response in peripherally infused $A\beta_{42}$ previously[316] in studies with higher sample sizes and thus less variability. It is likely that if we increased experimental numbers, we would observe similar findings.

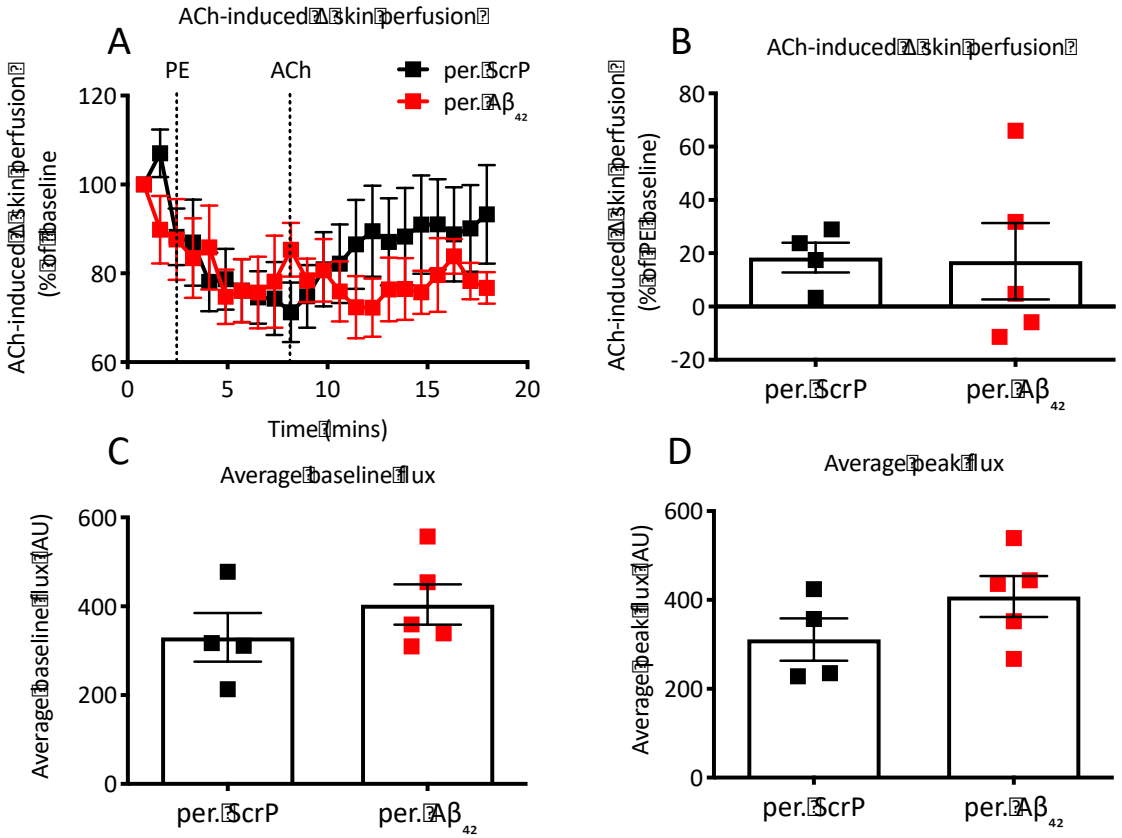

Figure 4.10 Peripherally chronically infused Aβ42 mice exhibit a trend toward reduced endothelial responsiveness

10-12 week old WT mice were placed on HFD for 4 weeks before undergoing surgery to fit a subcutaneous peripheral minipump in order to infuse Aβ42 or ScrP control peripherally for 4 weeks. Mice were maintained on HFD during the infusion period. To measure endothelial function *in vivo*, ScrP and Aβ42 infused mice underwent LDI with iontophoresis of PE and ACh. Application times of PE and ACh are represented by the dotted line. (A) ACh-induced skin perfusion as a percentage of baseline (baseline is 100%) over time, (B) ACh-induced skin perfusion as a percentage of PE baseline, (C) ACh-induced peak skin perfusion, and (D) baseline skin perfusion in Aβ42 or ScrP peripherally infused mice.

Data are expressed as mean ± standard error of the mean.

n = 4-5. (A) - Repeated measures ANOVA with Bonferroni multiple comparison. (B), (C), and (D) – Unpaired t-test with Welch's correction.

3.2.8 Pharmacological inhibition of BACE1 activity improves endothelial and smooth muscle cell response in APP23 mice in vivo

To further consolidate the observed outcome of $A\beta_{42}$ on endothelial function *in vivo*, we investigated how inhibition of BACE1 activity in a model of genetically raised $A\beta_{42}$ levels would influence endothelial and smooth muscle cell responsiveness. NC-fed APP23 mice underwent surgery to fit a peripheral subcutaneous minipump to infuse the BACE1 inhibitor M-3 or a vehicle control. M-3 is a compound produced by Merck that inhibits BACE1 enzymatic activity. We have shown previously that infusing the inhibitor leads to vast reductions in $A\beta_{42}$ circulating and tissue concentrations[308,316,317]. However, it should be noted that the there is no peer-reviewed published data on the selectivity or the off-target effects of this compound. Mice underwent LDI and iontophoresis of vasoactive agents (PE to induce vasoconstriction, ACh to induce endothelium-dependent vasodilation, and SNP to induce endothelium-independent vasodilation). Baseline skin perfusion, ACh-induced and SNP-induced percentage change in skin perfusion, and ACh-induced or SNP-induced peak skin perfusion were extrapolated for analysis.

As mentioned in Methods 2.2.6, 16 APP23 mice were purchased in order to obtain a sample size of 8 per group. However, several mice were found dead within the first couple of weeks of arriving and further mice were found dead/had to be euthanised following minipump surgery. It should be noted that peripheral minipump surgery is very non-invasive. Mice are under anaesthetic for no longer than 10-15 minutes and there is a very high success rate. In our experience, there is roughly <5% death rate after minipump surgery. However, with APP23 mice, there was ~50% death rate. This was concerning and Jax Labs were informed regarding these issues. For these reasons, sample size for this study is very small.

To confirm BACE1 activity inhibition, we measured plasma $A\beta_{42}$ and observed a trend toward reduced levels of $A\beta_{42}$ in M-3 infused APP23 mice compared to vehicle controls (Fig. 4.11), but sample size is very low (n = 2).

There was no observed change in baseline skin perfusion (Fig. 4.12A) or peak skin perfusion in response to ACh (4.12D) or SNP (4.12E). APP23 mice did not respond to ACh application in terms of skin perfusion (Fig. 4.12B). There were slight trends toward increased ACh- and SNP-induced change in skin perfusion in M-3 infused APP23 mice compared to vehicle infused (Fig. 4.12F and G). Our power calculations prior to the experiment suggested a sample size of 6-8 for this study, but as previously mentioned, many of the mice that were purchased died or had to be euthanized.

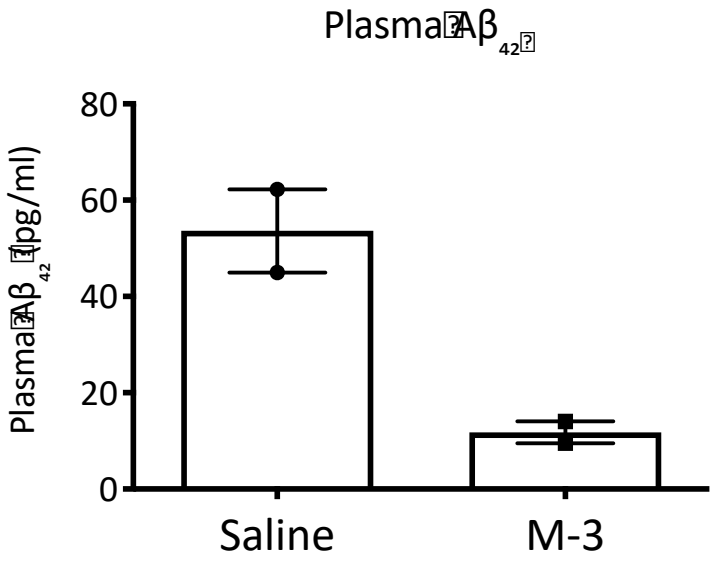

Figure 4.11 Plasma $A\beta_{42}$ is reduced in M3 infused APP23 mice

8-10 week old APP23 mice underwent surgery to peripherally infuse the BACE1 inhibitor M-3 vs. saline vehicle for 4 weeks. At the end of the study, blood was harvested and plasma extracted. $A\beta_{42}$ concentration was measured using an ELISA.

Data are expressed as mean ± standard error of the mean.

n = 2. Sample size too small to perform statistical analysis.

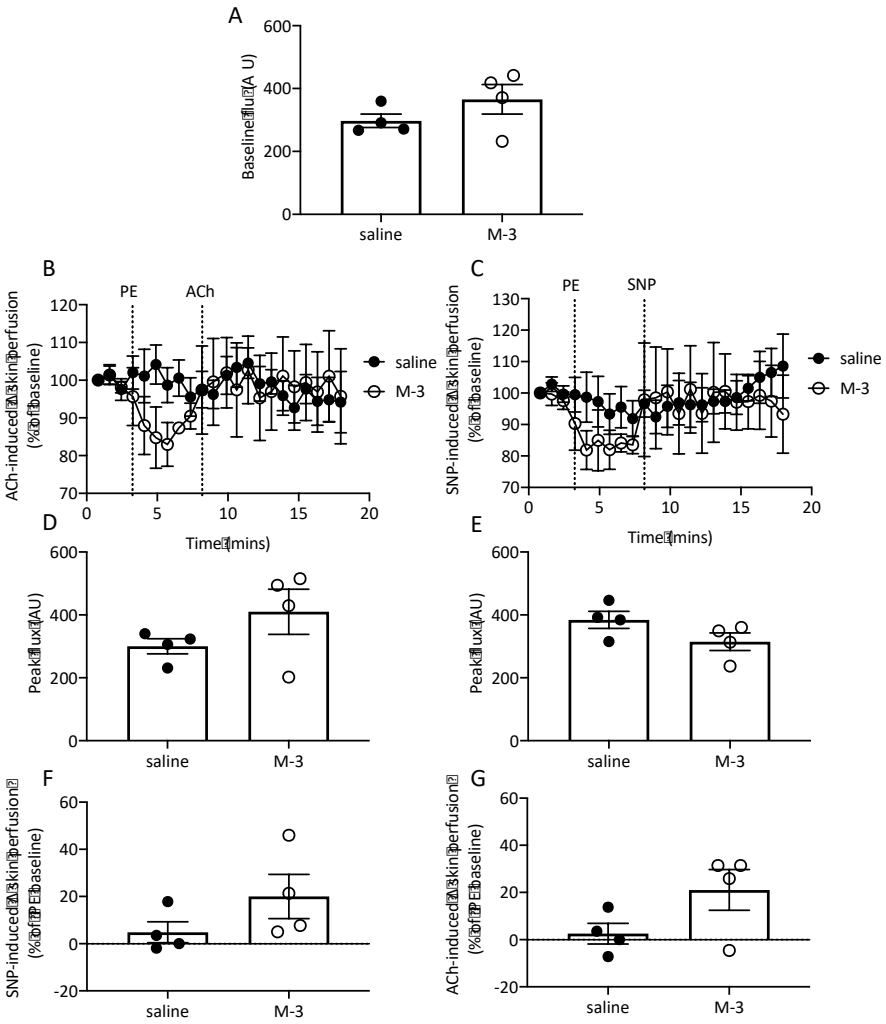

Figure 4.12 Inhibition of BACE1 activity in APP23 mice improves endothelial and smooth muscle responsiveness *in vivo*

8-10 weeks old APP23 mice underwent surgery to infuse the BACE1 inhibitor M-3 vs. saline vehicle for 4 weeks. To measure endothelial function *in vivo*, mice underwent LDI with iontophoresis of PE and ACh. In order to measure endothelium-independent vasodilation, mice underwent LDI and iontophoresis of PE and SNP. Times point of ACh and SNP application are labeled. (A) Baseline skin perfusion. (B) ACh-induced skin perfusion as a percentage of baseline (baseline is 100%) over time in minutes. (C) SNP-induced skin perfusion as a percentage of baseline (baseline is 100%) over time in minutes. (D) ACh-induce peak skin perfusion. (E) SNP-induced peak skin perfusion. (F) ACh-induced skin perfusion as a percentage of PE baseline. (G) SNP-induced skin perfusion as a percentage of PE baseline.

Data are expressed as mean ± standard error of the mean.

n = 4. (B) and (C) – repeated measures ANOVA with Bonferroni's multiple comparison. (A), (D), (E), (F), (G) – Unpaired t-test with Welch's correction.

3.2.9 Effects of varying $A\beta_{42}$ levels on nitric oxide bioavailability

We measured plasma nitrite concentration (direct metabolite of NO) as well as plasma ET-1 concentration to investigate whether $A\beta_{42}$ was promoting the observed ED *in vivo* through reduced NO bioavailability. Plasma nitrite remained unchanged in centrally infused $A\beta_{42}$ mice compared to ScrP controls (Fig. 4.13A) or in M-3 infused APP23 mice compared to vehicle controls (Fig. 4.13B). We observed a strong trend in reduced ET-1 levels upon M-3 infusion in APP23 mice compared to controls (4.13C – vehicle 4.63pg/ml ± 0.14pg/ml vs. M-3 2.9pg/ml ± 0.67pg/ml, n = 4, p = 0.07). ET-1 levels were not measured in $A\beta_{42}$ mice in the current study due to financial constraints.

3.2.9 Genetically reducing BACE1 does not affect aortic or VE fraction expression of proteins governing mitochondrial dynamics

Aortae and hemi brains were harvested from NC-fed WT mice, as well as HFD-fed BACE1 KO mice and their WT and HET littermates. VE fractions were isolated from hemi-brains. Protein was extracted from tissues and separated using SDS-PAGE. Proteins of interest were probed for using conventional Western blotting methods.

Representative blots showing aortic Mfn2 and OPA1 expression are shown in Fig. 4.14A. Actin was used as a loading control. HFD-feeding and genetic reduction of BACE1 did not induce any changes in aortic OPA1 expression (Fig. 4.14C). However, BACE1 KO mice did exhibit a trend toward increased Mfn2 expression compared to all three groups (Fig. 4.14B). Power calculations reveal a sample size of around 12 is needed to test the null hypothesis accurately. Blotting for total Drp1 and phosphorylation status of Drp1 (s616 and s637) was attempted in the aortae of these mice, but proteins were undetectable. Due to lack of sample, blots could only be attempted once. We were also not able to probe for Mfn1 in these tissues due to lack of sample. More mice would need to be harvested in order to further investigate aortic expression of Drp1 and Mfn1 protein.

Representative blots showing VE fraction expression of Mfn1, Mfn2, OPA1, and Drp1 protein is shown in Fig. 4.15A. Actin was used as a loading control. VE fraction expression

of Mfn1 (Fig. 4.15B), Mfn2 (Fig. 4.15C), and total Drp1 (Fig. 4.15G) was unchanged by HFD feeding or BACE1 reduction. BACE1 HET and BACE1 KO mice exhibit a trend toward reduced VE fraction protein expression of the short form of OPA1 (Fig. 4.15E). Power calculations reveal a sample size of at least 7 is required to test significance sufficiently. Again, phosphorylation status of Drp1 (s616 and s637) was attempted but could not be detected herein.

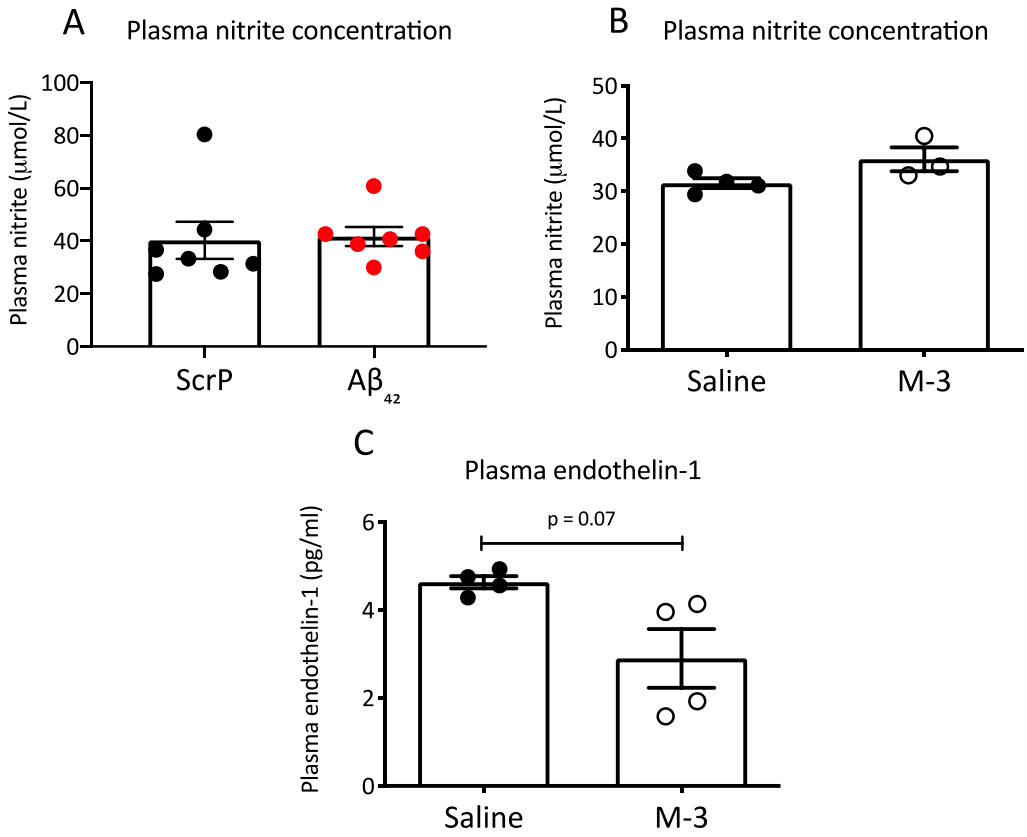

Figure 4.13 Effects of differing Aβ$_{42}$ levels on nitric oxide bioavailability

10-12 week old WT mice were placed on HFD for 4 weeks before undergoing surgery to fit a subcutaneous peripheral minipump, in order to infuse Aβ$_{42}$ or ScrP control peripherally for 4 weeks. Mice were maintained on HFD during the infusion period. 8-10 weeks old APP23 mice underwent surgery to infuse the BACE1 inhibitor M-3 vs. saline vehicle for 4 weeks. (A) Plasma nitrite concentration in Aβ$_{42}$ and ScrP mice. (B) Plasma nitrite concentration in APP23 ± M-3. (C) Plasma endothelin-1 concentration in APP23 ± M-3. (D) Plasma Aβ$_{42}$ concentration in APP23 ± M-3.

Data are expressed as mean ± standard error of the mean.

Aβ$_{42}$ vs. ScrP, n = 7. APP23 ± M-3, n = 3-4. Unpaired t-test with Welch's correction.

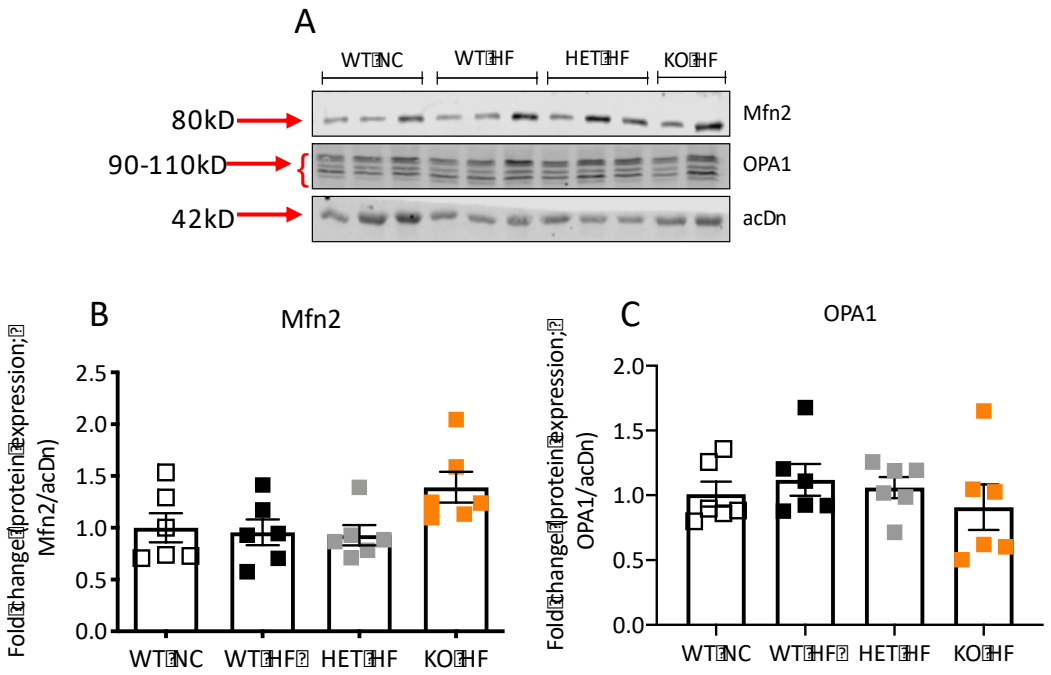

Figure 4.14 Aortic expression of proteins governing mitochondrial fusion are unchanged by genetically reducing BACE1

10-12 week old WT, BACE1 heterozygous (referred to as HET), and BACE1 KO (referred to as KO) were placed on 45% HFD for 10 weeks. At the end of the study, aortae were harvested and protein extracted. 20µg of protein was loaded onto acrylamide gels and separated by SDS PAGE. (A) Representative western blots showing expression of proteins regulating mitochondrial fusion in the murine aorta with actin as a loading control. Quantification of western blots normalised to actin of (B) Mfn2 and (C) OPA1.

Data are expressed as mean ± standard error of the mean.

n = 6. (B) and (C) – Welch's ANOVA with Dunnett's multiple comparison.

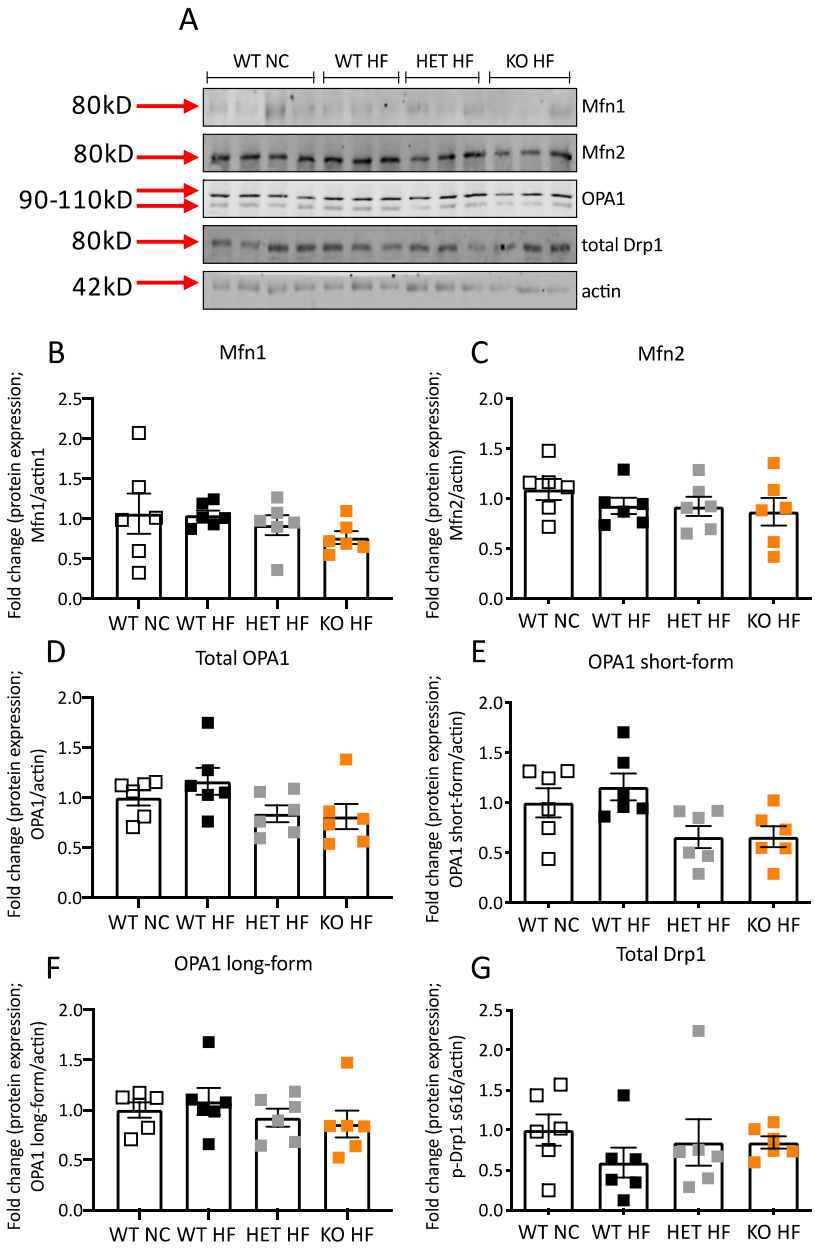

Figure 4.15 VE fraction expression of proteins governing mitochondrial dynamics remain unchanged by genetically reducing BACE1

10-12 week old WT, BACE1 heterozygous (referred to as HET), and BACE1 KO (referred to as KO) were placed on 45% HFD for 10 weeks. At the end of the study, hemi-brains were harvested, VE enriched fractions were isolated, and protein extracted. 20µg of protein was loaded onto acrylamide gels and separated by SDS PAGE. (A) Representative western blots showing expression of proteins regulating mitochondrial fusion in the murine NVU with actin as a loading control. Quantification of western blots normalised to actin of (B) Mfn1, (C) Mfn2, (D) total OPA1, (E) short-form OPA1, (F) long-form OPA1, and (G) total Drp1.

Data are expressed as mean ± standard error of the mean.

n = 6. (B) - (G) – Welch's ANOVA with Dunnett's multiple comparison.

3.2.10 Central $A\beta_{42}$ infusion increases VE fraction expression and phosphorylation of Drp1, but other proteins remain unchanged

Hemi-brains were harvested from $A\beta_{42}$ infused mice and their controls, and VE fractions were isolated. Protein was extracted from VE fractions and separated using SDS-PAGE. Proteins of interest were probed for using conventional Western blotting. Representative western blots are shown in Fig. 4.16A. Actin was used as a loading control. In the case of OPA1, the double band was quantified together to give total OPA1, the lower band was quantified separately to give short-form OPA1, and the higher band was quantified separately to give long-form OPA1.

VE fraction expression of Mfn2, total OPA1, short-form OPA1, and long-form OPA1 remained unchanged by central $A\beta_{42}$ infusion (Fig. 4.16B and C) Interestingly, phosphorylation of Drp1 at site s616 was increased in $A\beta_{42}$ infused mice compared to vehicle control (Fig. 4.16D – vehicle 1 ± 0.1 vs. $A\beta_{42}$ 1.44 ± 0.15, $n = 7$, $p < 0.05$) and total Drp1 protein was also increased by ~2-fold upon $A\beta_{42}$ infusion (Fig. 4.16E – vehicle 1 ± 0.25 vs. $A\beta_{42}$ 2.11 ± 0.41, $n = 7$, $p < 0.05$). When expressed as phospho/total ratio, $A\beta_{42}$ did not promote any changes in the NVU compared to vehicle controls. Due to lack of sample, Mfn1 was not probed for herein, but would be interesting to investigate in relation to $A\beta_{42}$ infusion.

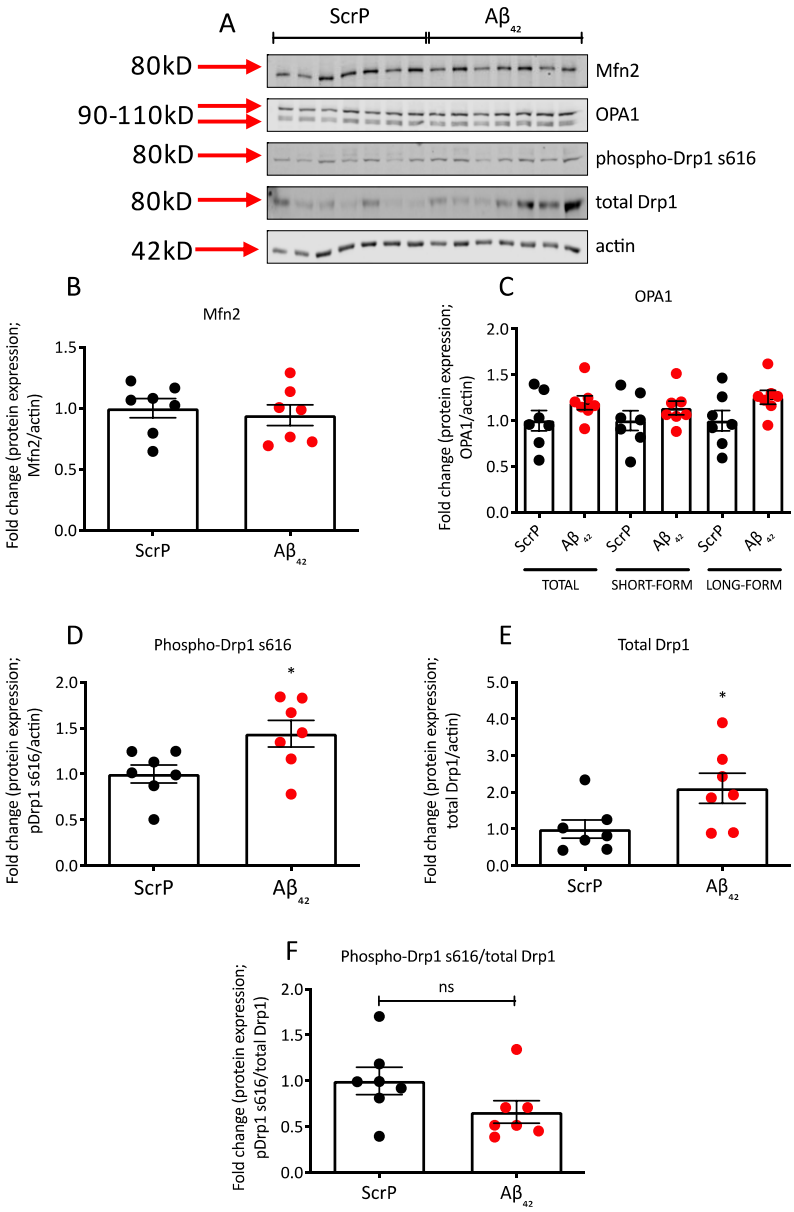

Figure 4.16 VE fraction expression of Drp1 is increased upon Aβ42 central infusion

10-12 week old WT mice were placed on HFD for 4 weeks before undergoing surgery to fit a subcutaneous peripheral minipump with a central catheter, in order to infuse $A\beta_{42}$ or ScrP control icvly for 4 weeks. Mice were maintained on HFD during the infusion period. At the end of the study, hemi-brains were harvested, VE enriched fractions were isolated, and protein extracted. 20µg of protein was loaded onto acrylamide gels and separated by SDS PAGE. (A) Representative western blots showing expression of proteins regulating mitochondrial fusion in the murine NVU with actin as a loading control. Quantification of western blots normalised to actin of (B) Mfn2 (D) total, short, and long-form OPA1, (D) phospho-Drp1 s616, (E) total Drp1, and (F) phospho/total.

Data are expressed as mean ± standard error of the mean.

n=7. (B) – (F) Unpaired t-test with Welch's correction.

3.2.11 Genetically reducing BACE1 does not affect VE fraction of aortic ICAM expression

Aortae and hemi-brains were harvested and VE fractions were isolated from hemi-brains. Protein was extracted from aortae and VE fractions and separated using SDS-PAGE. ICAM was probed for using conventional Western blotting as a marker for endothelial activation – an inflammatory pathology associated with ED. Actin was used as a loading control. Representative blots can be found in Fig. 4.17A (VE fraction expression) and B (aortic expression).

A trend towards reduced VE fraction ICAM expression was observed in all three HFD-fed groups (WT HF, HET HF, KO HF) compared to WT NC controls. Indeed, the reduction in VE fraction ICAM was close to significance in WT HF mice compared to WT NC mice (Fig. 4.17C – WT NC 1 ± 0.16 vs. WT HF 0.54 ± 0.11, n = 6, p = 0.07). No effect of diet was observed on aortic ICAM expression (Fig. 4.17D). Furthermore, genetic reduction of BACE1 (as in HET HF and KO HF) groups did not produce any observable difference in neither VE fraction nor aortic ICAM expression (Fig. 4.17C and D). Due to lack of tissue, ICAM was not probed for in $A\beta_{42}$ mice, but it would be of value to investigate this.

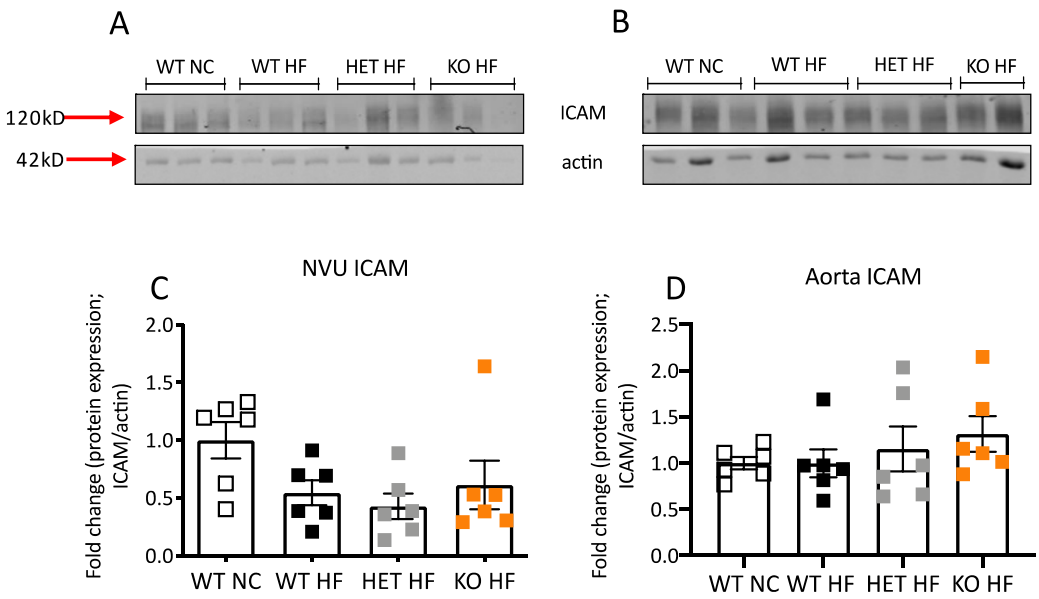

Figure 4.17 HFD feeding and genetically reducing BACE1 has no effect on ICAM expression

10-12 week old WT, BACE1 heterozygous (referred to as HET), and BACE1 KO (referred to as KO) were placed on 45% HFD for 10 weeks. At the end of the study aortae and hemi-brains were harvested. VE enriched fractions were isolated, and protein extracted. 20µg of protein from aortic and VE fraction lysate was loaded onto acrylamide gels and separated by SDS PAGE. (A) Representative western blots showing expression of ICAM in the murine NVU and (B) aorta with actin as a loading control. (C) Quantification of NVU ICAM normalised to actin. (D) Quantification of aortic ICAM normalised to actin.

Data are expressed as mean ± standard error of the mean.

n = 6. (B) and (C) – Welch's ANOVA with Dunnett's multiple comparison.

Discussion

4.3.1 Genetically reducing BACE1 protects against diet-induced weight gain

In order to confirm the previously observed protective metabolic phenotype of BACE1 KO mice, we fed 45% HFD to BACE1 KO mice (KO HF), as well as their heterozygous and WT littermates (HET HF and WT HF), for 10 weeks and measured body weight weekly. In line with our existing publications, we observed that globally reducing BACE1 levels protects against diet-induced weight gain[317]. Although body composition was not measured in the present study, the reduced weight gain is likely due to reduced fat mass as previously observed[317]. Body composition was not measured herein as *in vivo* measurements in mice can be stress inducing and can result in weight loss. We expected that this potential weight loss might interfere with our *in vivo* vascular measurements, which we deemed more important as the main *in* vivo experimental output of this study. The reduced weight gain in these mice could also be due to increased energy expenditure and metabolic inefficiency, as we have previously observed increased in expression of uncoupling proteins (UCPs) in BACE1 KO mice[317]. UCP1 protein was upregulated in brown adipose tissue (BAT) in BACE1KO mice (both NC-fed and HFD-fed) compared to WT mice, as well as increased *Ucp2* and *Ucp3* mRNA in skeletal muscle. HET HF mice do not exhibit the same protective phenotype, suggesting the remaining copy of the BACE1 gene is sufficient to contribute to HFD-induced weight gain. Indeed, we have shown that chronic HFD feeding induces upregulation of BACE1 protein levels in BACE1 HET mice in skeletal muscle[317].

4.3.2 Genetically reducing BACE1 protects against diet-induced endothelial dysfunction *in vivo*

Due to the known association between nutrient excess and vascular disease, we investigated the effects of HFD and BACE1 genetic reduction on endothelial function *in vivo*.

ACh-induced percentage change in vasodilation as well as ACh-induced peak skin perfusion was reduced in WT HF and HET HF mice compared to WT NC, suggesting HFD-induced ED. However, BACE1 KO mice did not differ from WT NC mice, and exhibited a trend toward improved endothelial response compared to WT HF and HET HF, indicating protection against diet-induced ED. The data herein suggest a role for BACE1 in the development of ED and subsequent vascular complications.

It must be considered that the reduced response to ACh may in fact was not due to endothelial unresponsiveness, but due to VSMC dysfunction. When NO diffuses into neighbouring VSMCs, it activates a cGMP-PKG-dependent mechanism to induce muscle relaxation. This signalling pathway has been implicated in the development of vascular dysfunction, and we have reported that animals challenged with HFD for 20 weeks exhibit reduced cGMP and PKG expression in aortic tissue[316]. We did not measure VSMC function *in vivo*, but this can be done by applying the NO donor SNP to the skin and measuring the skin perfusion response.

As previously discussed, ED may result from reduced NO bioavailability, increased EA, increased ROS production, and/or mitochondrial dysfunction. Although not measured herein due to lack of tissue and time constraints, we have previously observed increased NO bioavailability in HFD-fed (10 weeks) BACE1 KO mice compared to WT littermates, reporting increased plasma nitrite and reduced ET-1[316]. Furthermore, HFD-fed BACE1 KO mice exhibit increased aortic phosphorylation of eNOS at s1177 compared to WT littermates, indicating increased eNOS activity. They also display increased aortic phosphorylation of PKB at s473, a potent activator of eNOS. These data suggest that BACE1 KO mice are protected against HFD-induced ED due to their retention of eNOS activity and thus NO bioavailability.

HFD-fed (20-weeks) BACE1 KO mice exhibit reduced fasting blood glucose levels compared to WT littermates, improved glucose tolerance, and a preference for carbohydrate oxidation rather than fatty acid oxidation[317]. These results indicate that BACE1 KO mice harbor an enhanced ability to dispose of glucose. As previously

mentioned, hyperglycaemia has on numerous occasions been closely linked with ED. To briefly recap, mice with very high fasting blood glucose levels (>25mmol/l) exhibit a marked reduction in *in vivo* ACh-dependent vasodilation[183]. Others have reported diabetic mice exhibit reduced ACh-induced vasodilation in *ex vivo* aortic myograph studies[153,154], increased eNOS mRNA[155], and increased aortic superoxide expression[154]. Hyperglycaemia is linked with increased ROS production[287,290], leading to inhibition of GAPDH, an important glycolysis enzyme. The inhibition of GAPDH results in the accumulation of glycolysis intermediates (G6P, F6P), which, through several diverging pathways, can result in ED. For example, G6P can lead to DAG accumulation[174] and increased methylglyoxal levels, which is known to forms AGEs[176]. F6P can enter the hexosamine pathway, forming UDP-GlcNAc and upregulating O-linked GlcNAcylation. Glucose can be converted to sorbitol, increasing uric acid accumulation. This model is described in more detail in section 1.8.2. Due to the increased capacity for glucose disposal in BACE1 KO mice, it may be that the resulting reduction in blood glucose *per se* contributes to the improved endothelial function in these mice. Due to time constraints, ROS production was not measured in these mice, but this would be an important future step in this study. Section 3.3.4 indicates several assays that we would consider performing in order to measure ROS in this model.

It is possible that BACE1 KO mice also possess greater mitochondrial flexibility, as indicated by the fact they express increased uncoupling protein expression (UCP1 protein in brown adipose tissue, *Ucp2* and *Ucp3* mRNA in skeletal muscle)[317]. These data suggest that energy from excess nutrients can be lost due to enhanced proton leak (by UCPs) in BACE1 KO mice, protecting mitochondria from nutrient-excess induced dysfunction. Due to the known deleterious effects of nutrient excess on endothelial function, enhanced endothelial proton leak may protect against ED. This is because excessive nutrient supply can lead to enhanced ETC activity and increased MMP, which overwhelms mitochondria leading to RET and superoxide production. This is discussed in greater detail in section 1.12.4. Uncoupling mitochondria from ATP production (through increased UCP expression) and dissipating MMP may protect against mROS production by nutrient excess-induced RET and superoxide production.[286–288]. UCP

expression has not been investigated in the vasculature from BACE1 KO mice, but it would be interesting to perform qPCR or conventional WB for UCP mRNA/protein expression in aortic or VE fraction tissue.

4.3.3 Chronic infusion of $A\beta_{42}$ promotes endothelial dysfunction independently of metabolic impairments

Due to the observed role of BACE1 in protecting against HFD-induced ED, we decided to investigate the products of increased BACE1 enzymatic activity. Indeed, infusion of a BACE1 inhibitor protects against ED in DIO mice (20 weeks HFD; manuscript in review). To study the effects of increased BACE1 activity in relation to its most well-known substrate APP, we investigated the vascular consequences of chronically infusing of $A\beta_{42}$ vs. ScrP both centrally and peripherally using surgical minipumps.

Chronic central infusion of $A\beta_{42}$ produced a blunted response to ACh-induced vasodilation compared to ScrP infused controls, indicating central infusion of $A\beta_{42}$ causes ED. Due to the strong link between metabolic dysfunction and vascular impairments, we also investigated whether metabolic parameters were changed by central $A\beta_{42}$ infusion. Interestingly, $A\beta_{42}$ did not induce any changes in body weight, insulin sensitivity, or glucose tolerance. This indicates the vascular impairments observed in $A\beta_{42}$ infused mice are not due to metabolic dysfunction. However, central $A\beta_{42}$ mice did exhibit higher fasting blood glucose levels, but only after 16 hours of fasting, potentially suggesting dysregulation of gluconeogenesis. Sample size is small however, and more experiments would need to be performed in order to be sure. It is possible that the observed fasting hyperglycaemia may contribute to the reduced response to ACh. As previously mentioned, hyperglycaemia can result in decreased NO bioavailability and consequently ED[153–155,183,287,290].

It is interesting that central infusion of $A\beta_{42}$ can induce systemic effects. There is an emerging role for the hypothalamus in controlling peripheral metabolic homeostasis

outside of appetite regulation. It is possible that central $A\beta_{42}$ infusion can regulate glucose homeostasis through a hypothalamic mechanism. Indeed, we have shown central infusion of $A\beta_{42}$ can promote hypothalamic leptin resistance[305] and perhaps contribute to the development of obesity. The hypothalamus is home to glucose-sensing neurons, which are known to respond to varying levels of blood glucose and result in altered autonomic output. The autonomic nervous system (ANS) transmits efferent signals through nerves to the pancreas, skeletal muscle, and liver in order to control blood glucose levels. It is possible that $A\beta_{42}$ can regulate the action of the neurons that govern the autonomic output to increase fasting blood glucose levels. This would need to be further investigated. Firstly, we would have to measure $A\beta_{42}$ concentration in the plasma and brain tissue of $A\beta_{42}$ and ScrP mice to elucidate whether the centrally infused $A\beta_{42}$ is entering the systemic circulation, which would shed some light on whether $A\beta_{42}$ is exerting its effects centrally or systemically. We did attempt to measure $A\beta_{42}$ levels in these mice, but they were undetectable. The low pM concentrations of $A\beta_{42}$ that we infuse may be difficult to detect using simple MSD ELISAs. A better ELISA-like method for measuring $A\beta_{42}$ would be the Simoa, which employs an ultra-sensitive bead technology and is reportedly 1000 times more sensitive than traditional methods. An in-house assay for $A\beta_{42}$ is set up and is currently being used for other studies within the School of Medicine. It is possible that we could use this technique to measure $A\beta_{42}$ levels in the plasma and brain tissue of our mice. If the $A\beta_{42}$ is indeed acting centrally (likely in the hypothalamus) we could employ several techniques to further investigate the effects of raised hypothalamic BACE1 activity on peripheral glucose homeostasis. Indeed, we could specifically raise BACE1 levels in the hypothalamus by stereotaxically injecting a BACE1-overexpressing adenovirus into this part of the brain and investigate the effects on glucose homeostasis. Coupling this model with infusion of a BACE1 inhibitor would give insight into role of hypothalamic BACE1 enzymatic activity in this process. A model of increased $A\beta_{42}$ could be used. One such model is the called BRI-Aβ42, which overexpresses $A\beta_{42}$ without overexpressing APP. BRI-Aβ42 mice exhibit amyloid pathology in brain tissue as well as cerebral vessels as early as 3 months of age[448]. This model could be investigated alongside the BRI-Aβ40 mouse which interestingly does not exhibit overt amyloid pathology[448]. An existing model of raised

pyroglutamate Aβ ($A\beta_{3(pE)}$) exists, whereby $A\beta_{3(pE)}$ is produced under the Thy-1 promoter (which is thought to be mainly neuronal specific)[449]. It would be possible to employ a similar technique using $A\beta_{42}$ and a specific promoter of interest present in cells known to be involved in regulating systemic metabolism, such as POMC/CART or AgRP/NPY neurons, or astrocytes, which are now recognised for their role in sensing nutrients[450].

The ANS has been also been reported to control vascular tone. The ANS, the control of which is governed by the hypothalamus and brain stem, can be further split into parasympathetic and sympathetic nervous systems. Both the parasympathetic and sympathetic nervous systems can regulate vascular tone and have been reported to induce vasodilation and vasoconstriction through β- and α-adrenoreceptors (ARs) present on the vasculature respectively[451]. For example, β_1-, β_2-, and β_3-ARs expressed on endothelium mediate vasodilation through an NO-dependent mechanism[452–454], and are likely activated by circulating adrenaline produced by the adrenal gland. α_1-ARs present on VSMCs respond to noradrenaline released from postganglionic neurons by inducing VSMC contraction and thus vasoconstriction[455]. Central infusion of $A\beta_{42}$ may modulate central pathways that control ANS output to contribute to regulation of vascular tone. It is possible that this could result in a blunted response to ACh, but not much is known about the cross talk between ANS- and ACh-dependent regulations of vascular tone. It has been reported that NO itself can be released from sympathetic nerve fibres to act on the vasculature, so this could also be a mechanism by which $A\beta_{42}$ modulates peripheral vasculature through central mechanisms. Furthermore, we have only measured endothelium-dependent vasodilation in our $A\beta_{42}$ centrally infused model. It would also be useful to measure endothelium-independent vasodilation to elucidate whether central $A\beta_{42}$ infusion is affecting only the sympathetic regulation of AR signalling on ECs, or also contributes to impairment in VSMC function. To investigate this, iontophoresis of SNP can be used in conjunction with LDI technology. SNP can surpass the endothelium, acting directly on VSMCs to induce vasodilation[456]. Using this agent would elucidate whether the effects $A\beta_{42}$ are due specifically to ED, or due to an impairment in the response VSMC response to NO. SNP iontophoresis was not completed in these mice. A derivative of SNP is cyanide, meaning that when applied to mice they must be culled immediately after. This prevents tissue from being harvested

after a fasting period, which is required when investigating protein changes in tissues of HFD-fed mice. We prioritised overnight fasting and tissue harvested over LDI and SNP iontophoresis, with the intention of using a separate batch of central $A\beta_{42}$ vs. ScrP mice for SNP at a later date. Due to financial and time constraints this was not completed.

It should be noted that the infused $A\beta_{42}$ may be sequestered out of the brain into the circulation through $A\beta_{42}$ transporters at the BBB such as LRP1[457]. As previously mentioned, to shed light on this an MSD ELISA was performed to measure $A\beta_{42}$ concentration in the hypothalamus vs. plasma of these mice. Unfortunately, $A\beta_{42}$ was completely undetectable in both tissues. This left us hesitant about the validity of our centrally infused $A\beta_{42}$ mouse and is the reason why tissue processing from this $A\beta_{42}$ study was not prioritized. Therefore, it can be observed in this chapter that only the VE fraction tissue was processed for subsequent Western blot. Due to the nature of the minipumps the maximum infusion time is 4 weeks, meaning there is a week at the end of the study during which $A\beta_{42}$ is no longer being infused, but we still observe the reduced endothelial response. Of course, there is the possibility of $A\beta_{42}$ being degraded by one of its catabolic enzymes, such as insulin degrading enzyme (IDE), gelatinase A/B, or cathepsin D[458], and the reduced endothelial response may be due to lasting regulatory effects of $A\beta_{42}$ on endothelial function. Indeed, we cannot be certain that the ED observed in this model is due to central effects, or whether $A\beta_{42}$ is leaking into the plasma and exerting direct effects on the endothelium, similarly to a chronic systemic infusion.

Chronic peripheral infusion of $A\beta_{42}$ produced a trend toward reduced vasodilatory response to ACh, indicating ED. The sample size would have to be increased in order to reach significance. Using datasets from centrally infused $A\beta_{42}$ mice, power calculations indicate that if a similar effect size were observed, a minimum sample size of 7 would be required to reach significance. The observed trend in reduced response to ACh in peripherally infused $A\beta_{42}$ mice was independent of any changes in weight gain compared to ScrP. Further descriptive metabolic parameters were not investigated, such as body composition (echoMRI) or a glucose stimulated insulin secretion test (GSIS). This minimised the amount of stress the animals had to endure in order to obtain the best

experimental results from the *in vivo* vascular imaging. Furthermore, tissue from these peripherally infused $A\beta_{42}$ was required for postmortem pathological staining procedures and therefore we thought it best to minimise procedures involving large boluses of glucose/insulin that can produce lasting transcriptional effects.

These results agree with our existing data currently in review. Here, we reported that chronic peripheral infusion of $A\beta_{42}$ on NC background causes blunted vasodilatory to ACh *in vivo*. When animals are on HFD, this effect is exacerbated. $A\beta_{42}$ resulted in a blunted response to ACh due to reduced NO bioavailability, suggesting ED. The existing data indicate that $A\beta_{42}$ infusion in HFD-fed mice could reduce plasma nitrite and increase plasma ET-1 concentration, as well as reduce aortic phosphorylation of PKB (s473), and eNOS (s1177). This corroborates previous work, where others have reported that $A\beta_{42}$ application results in reduced phosphorylation of eNOS at s1177[459,460]. The finding that raised $A\beta_{42}$ was associated with reduced PKB (as detected through phosphorylation of PKB at s473), indicates $A\beta_{42}$ may interfere with PKB signalling to reduce PTM of eNOS. This is supported by a previous *in vitro* study on cultured ECs, which showed that μM application of soluble Aβ peptides of varying lengths inhibited PKB phosphorylation and p-eNOS[461]. This may occur through the interference of Aβ peptides with the formation of the activation complex of PKB with PDK1[460]. As previously mentioned, we reported previously that raising circulating $A\beta_{42}$ levels increased plasma ET-1 concentration on HFD background. However, it should be noted that raising circulating $A\beta_{42}$ levels on a NC background failed to increase ET-1 levels, suggesting that upregulating of ET-1 in this case requires a metabolic stressor as well as increased $A\beta_{42}$.

In the study herein, our centrally infused $A\beta_{42}$ mouse did not exhibit reduced plasma nitrite concentrations. This could be a genuine finding, in that the measured ED caused by central $A\beta_{42}$ infusion is independent of reduced NO bioavailability. However, this could equally be due to issues with reproducibility due to nature of nitrite measurements. To measure nitrite, the Griess assay is used. The Griess assay is simple absorbance assay, meaning it is sensitive to changes in the existing absorbance of plasma itself. If plasma samples are slightly haemolysed, this can introduce false positives. There is also the possibility of nitrite degradation in frozen plasma samples, as

well as degradation of the nitrite standard, and other reagents involved in the assay. We did not measure nitrite in the plasma of the peripherally infused mice herein as they underwent perfuse-fixation, meaning blood could not be harvested.

Overall, the data collected herein on $A\beta_{42}$ infused mice (both central and peripheral) point toward a role for HFD-induced raised $A\beta_{42}$ levels in the development of nutrient excess-associated ED. The peripheral microvascular ED measured *in vivo* is a good predictor of potential dysfunction in brain ECs, suggesting that $A\beta_{42}$ may impair cerebral haemodynamics, further contributing to nutrient excess-associated disease. It would be useful to measure CBF *in vivo*, in order to confirm this. CBF *in vivo* can be measured using laser technology, but the laser needs to be powerful enough to penetrate bone. This was attempted using the laser speckle moorFLPI-1. Unfortunately, the signal produced from this laser was not strong enough to measure CBF through the skull. It is possible that this laser is outdated. Other groups have employed the use of the newer model, the moorFLPI-2, and it seems a useful method to measure changes in CBF in real time[462,463].

4.3.4 APP23 mice exhibit vascular dysfunction, which is rescued by BACE1 inhibition

To further consolidate the role of raised $A\beta_{42}$ in the development of ED, we investigated the vascular profile of APP23 *in vivo*, and whether inhibiting BACE1 activity had a protective effect.

Firstly, to confirm BACE1 inhibition, we measured plasma $A\beta_{42}$ levels in APP23 that had undergone 4 weeks of infusion of the BACE1 inhibitor M-3 or saline control. Although sample size is small (n=2), M-3 treated mice exhibited reduced plasma $A\beta_{42}$ levels, suggesting the treatment had successfully lowered BACE1 activity. Power calculations on this data set reveal that in order for statistical significance to be reached, a sample size of only 3 is needed for this effect size. This is because the effect size is very large. If possible, the $A\beta_{42}$ levels of every mouse receiving M-3 or control would have been

measured, and any outliers (any APP23 M3 mice that did not exhibit reduced $A\beta_{42}$) would be removed from each dataset.

Although we observed no differences between groups in resting vascular tone (baseline skin perfusion), NC-fed APP23 mice of around 12 weeks of age did exhibit a trend toward a blunted response to vasodilator compounds which was rescued upon M-3 infusion. However, sample size is very small and further experiments would have to be done. In agreement with the aforementioned studies, these data suggest raised Aβ levels contribute to ED. However, we cannot be certain from this particular study that it is $A\beta_{42}$ that is taking effect. APP23 mice have a 7-fold overexpression of the human APP gene harboring the Swedish mutation[464], and thus possess higher than normal levels of soluble $A\beta_{40}$ as well as $A\beta_{42}$[465]. As they age, soluble levels decrease and Aβ begins to deposit as plaques[465]. It is likely that M-3 infusion will reduce the levels of both $A\beta_{40}$ and $A\beta_{42}$ in the APP23 mouse. Therefore we cannot be certain at present which peptide is affecting EC function in the APP23 mouse, or whether it is a combined effort. Again, the use of amyloid overexpressing mice, BRI-Aβ42 and BRI-Aβ40, could be employed to better understand this. A number of studies indicate a role for $A\beta_{40}$, $A\beta_{42}$, or both, in mediating vasoactivity in the brain[320,466,467], and the periphery[468]. However, it should be noted that previous experiments on mice conducted in our lab indicate that only $A\beta_{42}$ levels are sensitive to HFD-feeding and that $A\beta_{40}$ levels do not change, thus HFD-associated ED in mice may be due to $A\beta_{42}$ alone. Furthermore, we found that plasma of T2D humans exhibited increased $A\beta_{42}$ levels compared to controls, but $A\beta_{40}$ was unchanged. Contradictory to this, recent analysis of human datasets from Professor Faisel Khan's group suggests that it is plasma $A\beta_{40}$ in humans that possesses a stronger link with vascular dysfunction. Indeed, circulating $A\beta_{40}$, and to a lesser extent $A\beta_{42}$ levels, were found to be strongly correlated with reduced cutaneous microvascular responsiveness to ACh and SNP, and arterial stiffness (unpublished data). These data suggest there may be species variation when it comes to Aβ and the development of ED.

Aside from ACh-induced vasodilation, we also investigated SNP-mediated vasodilation in the APP23 mouse with and without BACE1 inhibition. SNP application will induce

endothelium-independent vasodilation, as SNP is a NO donor that can act directly on VSMCs. APP23 mice exhibited a delayed and somewhat blunted vasodilatory response to SNP, which was rescued by M-3. The change in percentage vasodilation due to SNP was almost significantly different between groups ($n = 4$, $p = 0.05$) and power calculations reveal that a larger sample size of 5 is required to properly test for significance. A blunted SNP response suggests that APP23 mice have dysfunctional VSMCs, potentially due to downregulation of proteins involved in NO-induced vasodilation, such as PKG and cGMP. Although these proteins were not measured herein, previous studies from our lab indicate that $A\beta_{42}$ infusion can reduce PKG expression and cGMP activity in aortic tissue (manuscript in review).

Postmortem biochemical analysis in plasma from these mice was performed in an attempt to investigate a potential mechanism. Plasma nitrite was found to be unaffected by BACE1 inhibition in APP23 mice. However, when compared to WT NC levels[316], APP23 mice seem to exhibit overall lower levels of nitrite (WT NC ~70µmol/l vs. APP23 ~ 30µmol/l), suggesting reduced NO bioavailability. A trend toward reduced plasma ET-1 levels was observed upon BACE1 inhibition in APP23 mice ($n = 4$, $p = 0.07$). Power calculations suggest a sample size of 9 to accurately test statistical significance for the proposed effect size. The trend toward decreased ET-1 upon BACE1 inhibition, independently of any change in plasma nitrite, suggests a more direct effect of raised BACE1 activity on ET-1 expression. Indeed, it has been reported that ET-1 mRNA is increased in the temporal cortex[469] and leptomeningeal vessels[470] of AD patients and that $A\beta_{42}$ incubation can increase ET-1 protein expression in the neuroblastoma cell line SH-SY5Ys[469] and primary human brain ECs[470].

It is unclear at this time whether the raised Aβ found in the APP23 mouse is promoting vascular dysfunction due to upstream impairments in the EC (decreased NO bioavailability through reduced PKB or eNOS activity, or increased ET-1), or downstream damage in NO-mediated VSMC signalling (through reduced PKG or cGMP activity), or perhaps a combination of both. Further postmortem biochemical analysis is required in order to understand this mechanism.

4.3.5 Genetically reducing BACE1 may increase aortic Mfn2 expression, but has no effect on OPA1

Mitochondrial dysfunction is a direct consequence of nutrient excess burden. HFD-feeding can contribute to the development of ED and genetically reducing BACE1 levels is protective. For these reasons, we decided to investigate whether proteins governing mitochondrial dynamics (Mfn2 and OPA1) were affected in aortae from HFD-fed BACE1 KO mice (alongside WT and HET littermates, and WT NC controls).

We report here that HFD-feeding and genetically reducing BACE1 levels does not affect aortic OPA1 expression. However, HFD-fed BACE1 KO mice seemed to exhibit a trend toward ~45% increase in Mfn2 levels compared to WT littermates. Power calculations reveal that a sample size of 12 is to test for significance, but the current sample size is only 6. Therefore, more mice would need to be investigated to clarify whether this was a genuine result.

If it did transpire that BACE1 KO mice do indeed express higher aortic Mfn2 levels, this could be due to increased EC Mfn2, or VSMC Mfn2, or both. This is because harvested aortic tissue will contain both of these cell types. Primary isolation of these cells could be performed to clarify which cell type is affected.

BACE1 KO exhibit improved endothelial responsiveness to ACh. It is possible that this is due to improved mitochondrial function. Indeed, as discussed in section 1.12.3, APP processing, and thus BACE1, has been implicated in regulating mitochondrial function. Aβ has been shown to accumulate in mitochondria prior to plaque deposition[245,330,331], several APP mutant mouse models have exhibited mitochondrial dysfunction[331–333], and immortalised neuronal cells overexpressing APPswe possess reduced OPA1 and Mfn1/2 protein expression, a higher percentage of fragmented mitochondria, and reduced ATP production[334]. This is in line with our BACE1 KO model, which possesses very low or non-detectable Aβ, potentially expressing increased Mfn2 levels in aortic tissue.

If Mfn2 levels were increased, this could potentially mean a shift toward mitochondrial fusion, however expression of opposing mitochondrial fission proteins would have to be investigated (Drp1). Furthermore, mitochondrial morphology would need to be studied to clarify whether any observed changes in expression of proteins governing mitochondrial dynamics actually resulted in changes in ultrastructure. Morphological studies can performed using electron microscopy[471], or immunofluorescence coupled with fluorescent microscopy. Common antibodies for investigating mitochondrial morphology in fixed tissue include TOM20, cytochrome *c* oxidase IV (COX IV), or manganese superoxide dismutase (MnSOD). A more recently developed method for staining mitochondria in fixed tissue is using an iridium coordination complex called IraSolve-Mito, an inorganic fluorophore that is highly specific for mitochondria[472]. Iridium and other transition metal complexes are particularly attractive as imaging agents as their mechanism of action does not depend on membrane potential, they can be used for mitochondrial detection in fixed tissue, they have superior photostability, and large Stokes' shifts[473]. Fluorescent imaging relies on the principles of Stokes' shift, which is described as the change in wavelength light undergoes when it is absorbed by a fluorophore vs. when it is omitted. A small Stokes' shift can result in reabsorption of the emitted light, resulting in high background and inaccurate signal. Large Stokes' shifts are thus preferred as they minimise this issue.

Altered mitochondrial dynamics in the endothelium has been linked with cellular dysfunction. Mitochondrial fragmentation is observed in the endothelium following exposure to stressors such as H_20_2[474], HG[475,476], and ischaemia[477]. Furthermore, diabetic patients exhibit increased expression of the fission protein Fis1 in isolated venous ECs[476]. Human aortic ECs exposed to HG exhibit increased Fis1 and Drp1 expression, as well as increased mitochondrial fragmentation, increased ROS production, and inactivation of eNOS. Silencing of Fis1 or Drp1 expression prevents these glucose-induced changes[476]. Of particular interest, silencing Mfn1 or Mfn2 in cultured ECs reduces PKB-dependent activation of eNOS4. Thus it is possible that the trend toward increased Mfn2 in BACE1 KO mice is enhancing activation of eNOS. Although not measured herein, data that are

currently in review from our lab indicate that BACE1 KO mice do exhibit increased phosphorylation of eNOS at serine s1177[316], suggesting enhanced activation.

4.3.6 Genetically reducing BACE1 does not affect VE fraction expression of proteins governing mitochondrial dynamics

In this chapter we have shown that HFD-associated increases in BACE1 may promote EC dysfunction and genetic reduction of BACE1 may be protective, as measured by LDI of peripheral microvascular skin perfusion. It has been suggested that peripheral microvascular dysfunction is a good predictor of and may precede cerebrovascular dysfunction[346]. This suggests that BACE1 KO mice may also be protected against brain EC dysfunction.

We do not presently have the ability to measure CBF *in vivo.* This is unfortunate as it would give us a direct read of brain EC responsiveness to several stimuli including, but not limited to, reactive hyperaemia, or topical application of vasoactive agents (ACh, SNP, bradykinin)[320–324,466]. We decided to investigate brain EC function instead by measuring mitochondrial function. To do this we set out to detect any changes in VE fraction protein expression of mitochondrial dynamics proteins, due to the known importance of maintaining mitochondrial health at the BBB[127]. We measured VE fraction expression of these proteins in WT NC, WT HF, HET HF, and KO HF groups to investigate whether HFD-feeding or genetically reducing BACE1 could induce any changes. We did not observe any changes in VE fraction expression of proteins governing mitochondrial dynamics with HFD feeding, or with genetic BACE1 reduction.

It should be noted that the sample size is small (n=6) and the variability for some proteins is high in certain groups. The VE fraction (NVU) that is obtained from the hemi-brain is reported to contain different cell types. The majority of the fraction is made up of microvessels, but any cell that is present at the NVU may have been pulled down with the vessel. This means that the VE fraction likely contains ECs, pericytes, astrocytic end-feet, microglia, and neurons. This may account for some of the variability that is observed in some proteins, as no two isolated fractions will be identical in terms of cell

type. It would be more useful to isolate primary brain ECs in order to detect purely endothelial changes. Indeed, this was attempted extensively using the Miltenyi Biotec gentleMACS™ Tissue Dissociator followed by CD31+ selection of endothelial cells using magnetic microbead technology. Although the yield of ECs was pure, the number of cells obtained (and therefore protein and mRNA content) was not sufficient for the nature of the experiments we wished to perform (Western blots, qPCR). In order to obtain confluent monolayers in 2-3 wells of a 6-well plate, 12 4-6 week old mice had to be sacrificed and then cells were passaged 2-3 times. We thought this an inefficient method and decided to use immortalised cell lines instead (more information in Chapter 5).

BACE1 HET and BACE1 KO mice exhibit a trend toward reduced VE fraction protein expression of the short-form of OPA1. Power calculations on this data suggest a sample size of 7 is required in order to detect significance (current n = 6). This is not in line with the literature, where Wang and colleague report that neuronal cells overexpressing APPswe exhibit reduced OPA1 expression[334]. It should be noted however, when observing the OPA1 Western blots in this publication, it seems they did not separate the proteins sufficiently during the electrophoresis step, leaving them with two indistinguishable bands. Therefore it is difficult to know whether APPswe overexpression leads to a reduction in long-, or short-form OPA1, or both, as they have measured both bands as one. There is a resulting increase in mitochondrial fragmentation observed in APPswe overexpressing cells, which is blocked when BACE1 is inhibited, suggesting that these changes in mitochondrial dynamics are mediated through an APP cleavage product such as Aβ. From this information, one would expect BACE1 KO mice, that have reduced Aβ levels, would exhibit increased OPA1 levels. There is a noticeable lack of information regarding mitochondrial dynamics in brain ECs. The reason we are not seeing similar results to the literature regarding OPA1 could be because brain ECs may act differently in response to stressors than other cell types. Indeed, brain ECs are structurally dissimilar to peripheral ECs in that they express high levels of tight junction proteins, making them less permeable than the latter. Brain ECs are ultimately the main line of protection that the brain has from systemic insults and, for this reason, are perhaps more robust. Indeed, some reports suggest cerebral ECs

harbor more mitochondria than peripheral ECs, indicating the potential for a higher capacity to deal with metabolic stress[225–227].

4.3.7 Chronic central infusion upregulates VE fraction expression phosphorylation and expression of Drp1

Within this chapter, we reported that chronic central infusion of $A\beta_{42}$ resulted in a reduced response of ECs to ACh, as measured in the skin microvasculature. As previously mentioned, we do not have the technology to measure cerebral microvasculature *in vivo*, but we can isolate cerebral vessels and extract protein to study expression of mitochondrial dynamics proteins. We did not observe any changes in Mfn2 or OPA1 (short-form, long-form, or total) in the NVU of $A\beta_{42}$ compared to ScrP controls. However, we did see an increase in phosphorylation of Drp1 at s616 and an increase in total Drp1 expression in the NVU of $A\beta_{42}$ mice compared to ScrP controls. When expressed as a ratio of phospho/total, this change is lost, suggesting the true change is in total Drp1 expression.

Drp1 governs the fission component of mitochondrial dynamics. An increase in its expression, without any accompanying increase in fusion proteins (Mfn1/2 or OPA1), may indicate a shift toward mitochondria fission and fragmentation. Under normal conditions mitochondrial fission is likely an adaptive response to cellular stressors and may occur to remove damaged areas of mitochondria from the network and target them for mitophagy[239]. Chronically unopposed fragmentation may lead to reduced capacity to produce ATP, increased heterogeneity of mitochondria, increased mitophagy, alteration in Ca^{2+} signalling, and/or increased ROS production[239]. Therefore, the $A\beta_{42}$ dependent increase in VE fraction Drp1 expression observed herein may result in mitochondrial crisis and contribute to damage at the NVU[127]. Interestingly, this is not in line with previous literature. Wang and colleagues, who overexpressed APPswe in a neuronal cell line, observed reductions in Drp1 expression[334]. However, when investigating overall mitochondrial morphology, they did observe that APPswe overexpression led to mitochondrial fragmentation. This is likely because they observed

reductions in Mfn1/2 and OPA1 and an accompanying increase in the fission protein Fis1. The actual morphology in fixed tissue in our $A\beta_{42}$ mice would have to be investigated to ensure that the observed increase Drp1 truly resulted in upregulated fragmentation. This can be done using mitochondrial stains following by microscopy, details of which are given in section 4.3.5.

It has been reported that nutrient rich environments, such as that in HFD-feeding, tend to lead to more fragmented mitochondria[281,282]. High saturated fat (HSD) feeding in rats promoted fission over fusion by increasing Drp1 hepatic protein expression[276], whilst skeletal muscle myotubes exhibit a higher percentage of fragmented mitochondria following exposure to nutrient excess *in vitro* (glucose and palmitate)[278]. This was accompanied by a modest increase in Drp1, a finding that has been corroborated by others[283,284]. Due to the fact that nutrient excess promotes BACE1 activity[305–309,317,335], it may be that nutrient excess-associated $A\beta_{42}$ is partly responsible for the observed increase in mitochondria fragmentation in these environments. This warrants further investigation.

If unregulated mitochondrial fragmentation is indeed occurring in the NVU in our $A\beta_{42}$ mice, this may contribute to BBB disruption[127] and impaired cerebral haemodynamics[478], contributing to known cerebrovascular diseases.

4.3.8 VE fraction and aortic ICAM expression is unchanged by genetically reducing BACE1

ED is associated with increased inflammatory markers (endothelial activation), including ICAM expression. Therefore, we investigated whether ICAM expression was changed with HFD-feeding or genetically reducing BACE1 in the aortae and NVUs of mice. Aortic expression of ICAM remained unchanged in all groups, which is not in line with our previous data currently in review, that exhibited decreases in aortic ICAM expression in HFD-fed BACE1 mice compared to WT controls. VE fraction ICAM expression trended toward a reduction in all three HFD groups (WT HF, HET HF, KO HF) compared to WT NC. Indeed, the reduction in VE fraction ICAM was close to significance in WT HF mice

compared to WT NC mice (~45% decrease, n = 6, p = 0.07). There was no effect of varying BACE1 levels on VE fraction ICAM expression.

This is an interesting finding as nutrient excess is often associated with increased ICAM expression both in peripheral and central vasculature. Indeed, exposure to HG[162], palmitate[191,192,194,197,198], and oxLDL[206,209] results in increased ICAM expression in peripheral cultured ECs. Furthermore, brain ECs incubated in oxLDL also exhibit increased ICAM expression[213], and T2Ds exhibit increased CSF ICAM levels[123]. There is no existing literature to explain why HFD-feeding in this case is resulting in a trend toward reduce ICAM expression. There may be a compensatory mechanism involved and perhaps 10 weeks of HFD feeding is not a lengthy enough duration to observe endothelial inflammation. It should be noted that WT NC mice are from our WT-only line, whereas WT HF, HET HF, and KO HF mice are littermates from the BACE1 KO line. Although these mice are both on a C57Bl6/J background, and the BACE1 KO line is backcrossed regularly with "true WT mice" from Charles River, there may be some discrepancies in genetics. WT littermates fed NC-diet would to be investigated to provide more clarity.

4.3.9 Summary

This chapter aimed to further confirm our previous findings that raised $A\beta_{42}$ levels are associated with the development of ED, as observed *in vivo* in cutaneous microvasculature. We also aimed to investigate whether any ED observed in the models of reduced $A\beta_{42}$ (BACE1 KO) and increased $A\beta_{42}$ ($A\beta_{42}$ central infusion) was associated with alterations in mitochondrial dynamics.

We observed a trend toward improved EC vasodilatory response to ACh in cutaneous microvasculature of HFD-fed BACE1 KO mice compared to WT and HET littermates, as well as a blunted EC vasodilatory response to ACh in $A\beta_{42}$ centrally infused mice. Furthermore, a trend toward reduced ACh dependent vasodilation was observed in peripherally infused $A\beta_{42}$ mice. We also observed blunted vasodilation to both ACh and

SNP in APP23 mice, which was rescued by BACE1 inhibition. These data suggest a role for BACE1 and $A\beta_{42}$ in the development of ED and is in line with our previous data that is currently in review. Neither $A\beta_{42}$ central infusion to WT HFD-fed mice, nor M-3 infusion to APP23 mice induced any changes in plasma nitrite concentration. M-3 infusion to APP23 mice did however produce a trend toward reduced circulating ET-1 levels. These data suggest a direct role for Aβ peptides in modulating ET-1 levels, which could contribute to ED onset.

Expression of proteins involved in mitochondrial dynamics in aortae and NVUs remained largely unchanged by HFD-feeding or BACE1 genetic reduction. Of note was an increase in aortic expression of Mfn2 in BACE1 KO mice, which may be involved in the observed protection these mice exhibit against ED. Further studies would need to be performed to investigate mitochondrial ultrastructure in vascular tissues.

$A\beta_{42}$ central infusion produced an increase in VE fraction expression of Drp1 levels, without accompanying increases in OPA1 or Mfn2, indicating a shift toward mitochondrial fission. This may contribute to the cerebrovascular dysfunction that is observed in APP overexpressing mice[320,324,466]. Furthermore, due to the similarities between cutaneous and cerebral mirovasculature[346], changes observed in the NVU may reflect the status of microvascular mitochondrial dynamics in the periphery, and therefore may contribute to the cutaneous ED observed *in vivo.*

In summary, there is a role for HFD-associated BACE1 and $A\beta_{42}$ in the development of microvascular ED, which may be linked to slight alterations in mitochondrial dynamics proteins. Sample sizes would need to be increased in order to clarify this. Future experiments could involve investigating brain EC function *in vivo* using laser speckle and studying mitochondrial ultrastructure to link observed changes in proteins with changes in morphology.

Chapter 5

Investigating the effects of nutrient excess on mitochondrial function in a cerebral endothelial cell line

5.1 Introduction

The BBB is an "interface" barrier between the blood and the interstitial fluid of the brain. It plays an important role in restricting the movement of potentially damaging particles from the blood, delivering essential nutrients to the brain, removing waste products, and is involved in haemodynamics and regulation of CBF. The integrity of the BBB is crucial to proper brain function and dysfunction in brain ECs is linked to impaired cerebral blood flow and BBB opening[110]. If the BBB becomes leaky, this will allow entry of potentially toxic blood-derived molecules into the brain and has been largely linked to neuroinflammation[111] and neurodegenerative disease[479].

BBB dysfunction is observed in many disease such as obesity and T2D, as well as CVD, and cerebrovascular integrity is altered during aging and age-related disorders[112–114]. HFD-fed rats exhibit increased BBB leakiness[115] and T2D induces downregulation of TJ proteins including claudin-5 and occludin, as well as the TJ-associated protein ZO-1[116–120], which could lead to BBB opening[121,122]. Inflammation is also observed in brain endothelium in T2D, with upregulated protein expression of ICAM and VCAM[123] and increased basement membrane (BM) thickening[124–126], which can result in cell detachment from the BM as well as BBB opening. Systemic inflammation, which is observed in multiple metabolic disorders, has also been shown to induce BBB opening[127].

Mitochondrial function is important for EC health. A study by Doll and colleagues suggests BBB breakdown may in fact be secondary to mitochondrial dysfunction[127]. Peripheral ECs exposed to nutrient excess (HG, palmitate, cholesterol) exhibit impaired mitochondrial bioenergetics[165,166,194,198,208], but there is limited research into how disorders of nutrient excess may lead to mitochondrial dysfunction in brain ECs. We attempted to answer this question in chapters 3 and 4, by investigating mitochondrial dynamic protein expression at the BBB in mice that were subjected to nutrient excess by HFD-feeding. However, few convincing results were obtained due to low sample size, and also potentially because the several cell types present in the VE fraction may dilute signals from individual cells. Jin and colleagues investigated the brain endothelial cell

line bEnd.3 and reported that HG exposure induced EC injury by promoting mPTP opening, reducing MMP, inducing mitochondrial Ca^{2+} overload, increasing Drp1 levels, and decreasing PGC1-α mRNA expression[173]. However, this study failed to investigate mitochondrial respiration in real-time, did not extensively investigate mitochondrial dynamics, and only studied the effects of HG, and not the effects of other potentially damaging nutrient such as fatty acids. Nevertheless, these data do imply that nutrient excess may result in mitochondrial dysfunction in brain ECs. Considering the absolute importance of healthy brain EC function to multiple processes (including cerebral haemodynamics, BBB integrity, nutrient transport), the contribution mitochondria make to maintain brain EC health[127], and furthermore that neurological complications are secondary to many metabolic diseases, it is imperative that further research into nutrient excess and brain ECs is undertaken. As previously discussed, brain ECs have more mitochondria than peripheral ECs; mitochondrial volume in brain ECs accounts for 2-4 times the mitochondrial volume of peripheral ECs. The higher mitochondrial volume may act as an advantage in brain ECs, increasing their capacity to deal with nutrient excess. However, this needs further investigation. Nutrient excess is also associated with increased BACE1 activity[300,305–307,309–311,317,335] and our previous findings suggest a role for increased $A\beta_{42}$ (due to nutrient excess) in the development of ED in peripheral vasculature[142] Furthermore, Aβ has been reported to induce mitochondrial dysfunction[306,317,331–335].

The aim of this chapter was to find a suitable cell culture model of brain ECs and use this model to investigate how nutrient excess (glucose and palmitate) affects endothelial mitochondrial function. In order to investigate mitochondrial physiology and respiration in real time, we employed the use of the Seahorse extracellular flux analyser. Furthermore, due to the known connection between metabolic syndrome, ED, and BACE1 and Aβ, we also investigated the effects of palmitate exposure on brain EC BACE1 levels and studied the effects of exogenous aged $A\beta_{42}$ dimer application on mitochondrial respiration. Due to the existing data that suggest a role for nutrient excess in mitochondrial dysfunction in brain ECs[173] and peripheral ECs[198,280,475], we hypothesised that HG and palmitate exposures would reduce the oxidative capacity of

bEnd.3 cells, suggesting mitochondrial dysfunction. We further hypothesised that $A\beta_{42}$ would exacerbate the effects of HG/palmitate exposure on mitochondrial respiration.

5.2 Results

5.2.1 Optimising a brain endothelial cell model

The first aim of this chapter was to optimise a suitable cell culture model for investigating brain EC function. We aimed to find an immortalised cell line that could be used to study 1) NO bioavailability (phosphorylation of PKB and eNOS, media nitrite concentration), 2) endothelial activation (exhibits an inflammatory response), and 3) mitochondrial function (possessed sufficient mitochondrial respiration that could be altered using known mitochondrial modulators). We obtained two potential immortalised cell lines, a rat brain endothelial cell line called RBE4 and a mouse brain endothelial cell line called bEnd.3.

In order to investigate NO bioavailability, the cells had to express eNOS and PKB, and the phosphorylation of which had to be sensitive to stimulation by known inducers of eNOS activity (insulin). Therefore, we investigated eNOS and PKB phosphorylation in response to insulin post-serum starve in RBE4 cells (Fig. 5.1). PKB exhibited a concentration-dependent increase in phosphorylation at s473 in response to insulin, which was also increased with duration of exposure to insulin. However, phosphorylation of eNOS at s1177 (~133 kDa) was undetectable in these cells in response to insulin. We then investigated insulin dependent phosphorylation of eNOS and PKB in bEnd.3 cells (Fig. 5.2). Interestingly, even after several durations of serum starvation (stated in figure legend), bEnd.3 cells exhibited high levels of phosphorylation of both eNOS (s1177) and PKB (s473), which was totally insensitive to insulin concentrations. bEnd.3 cells seemed to possess consistently activated PKB, and thus eNOS. Following this, we confirmed the absence of phosphorylation of eNOS in RBE4 cells (Fig. 5.3) by using bEnd.3 cells as a positive control, whilst simultaneously

confirming the unresponsiveness of bEnd.3 cells to both serum starvation and supraphysiological concentrations of insulin (Fig. 5.3). Following this finding, an extensive search through the literature revealed that RBE4 cells do not express eNOS mRNA[480]. Considering this, we decided that RBE4 cells should not be used in any further studies. bEnd.3 cells do express eNOS, meaning they are capable of producing NO, and thus are a better model of brain ECs. We moved forward with the bEnd.3 cell line and decided to investigate another parameter; mitochondrial function.

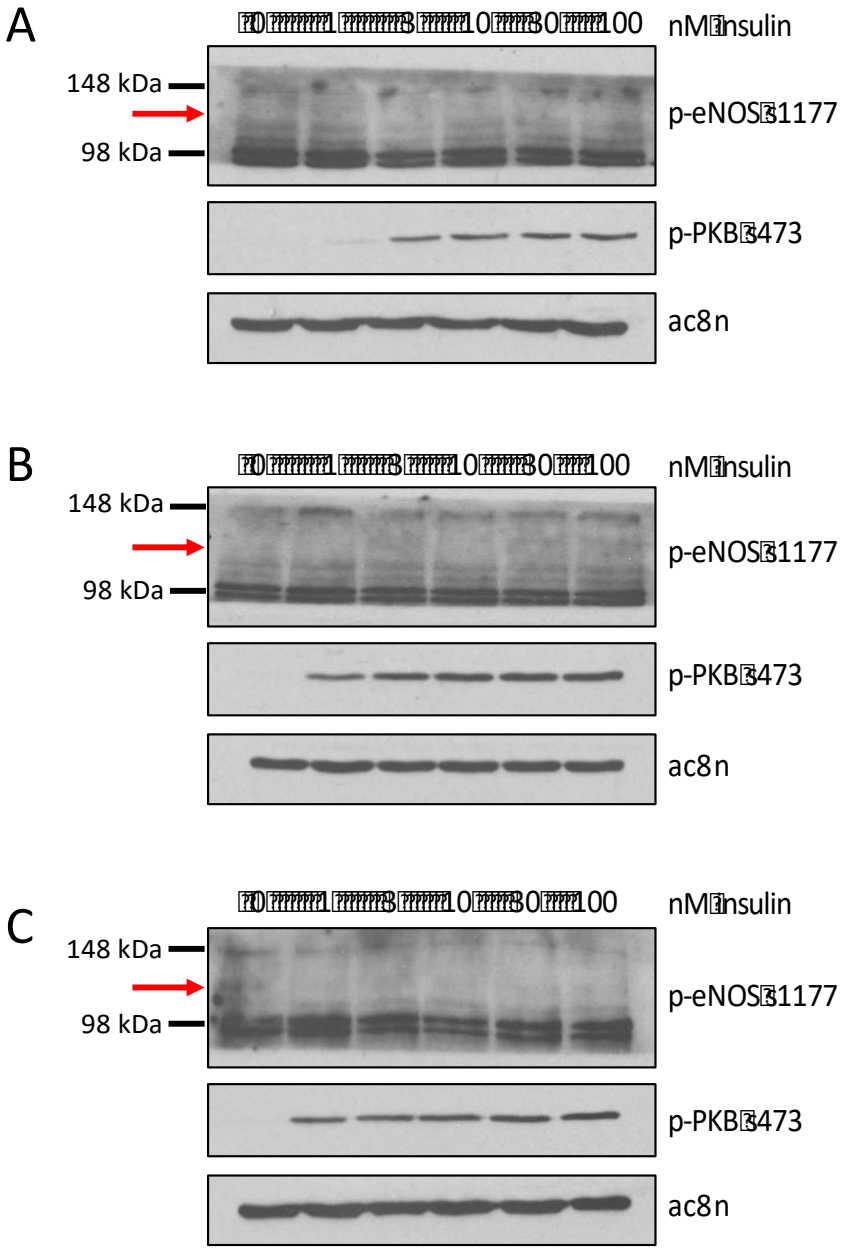

Figure 5.1 Insulin dependent phosphorylation of eNOS in RBE4 cells

RBE4 cells were serum-starved before being stimulated with insulin at the concentrations stated. Protein was extracted from cell lysates. 20µg of protein was loaded on to an acrylamide gel and separated using SDS-PAGE. Representative western blots showing phosphorylation of eNOS (s1177) and PKB (s473) in RBE4 cells in response to insulin stimulation for a duration of (A) 5 minutes, (B) 15 minutes, and (C) 30 minutes. Red arrows depict where eNOS (~133kDa) would be expected.

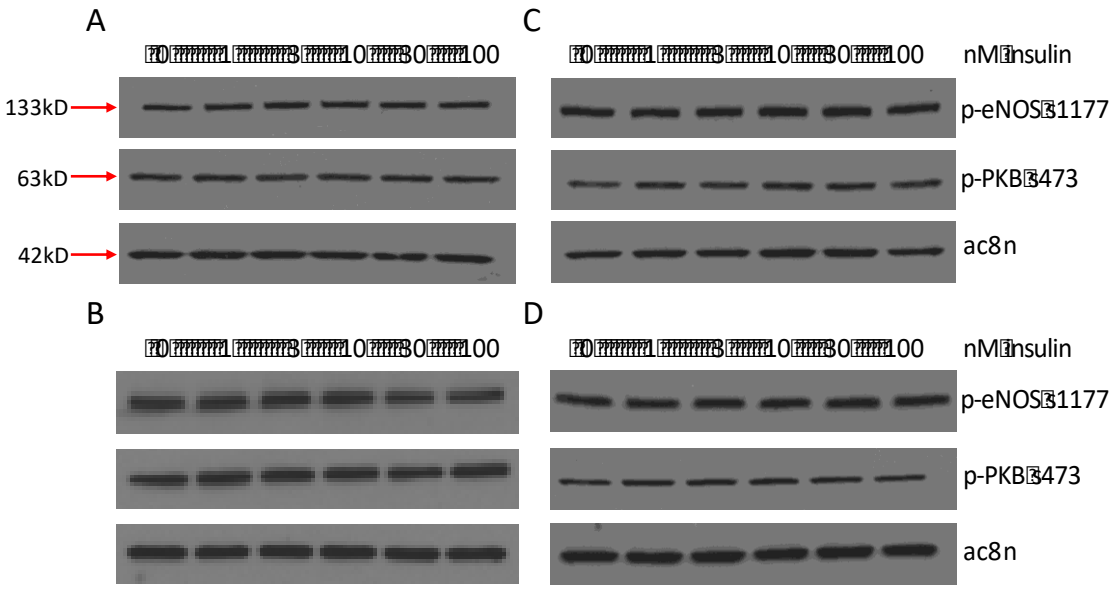

Figure 5.2 Insulin dependent phosphorylation of eNOS in bEnd.3 cells

bEnd.3 cells were stimulated with insulin at the stated concentrations for 30 minutes after being serum starved for (A) 0 hours, (B) 2 hours, (C) 8 hours, (D) 16 hours. Protein was extracted from cell lysates. 20µg of protein was loaded on to acrylamide gels and separated using SDS-PAGE. Representative western blots showing phosphorylation of eNOS (s1177) and PKB (s473) in bEnd.3 cells in response to insulin stimulation.

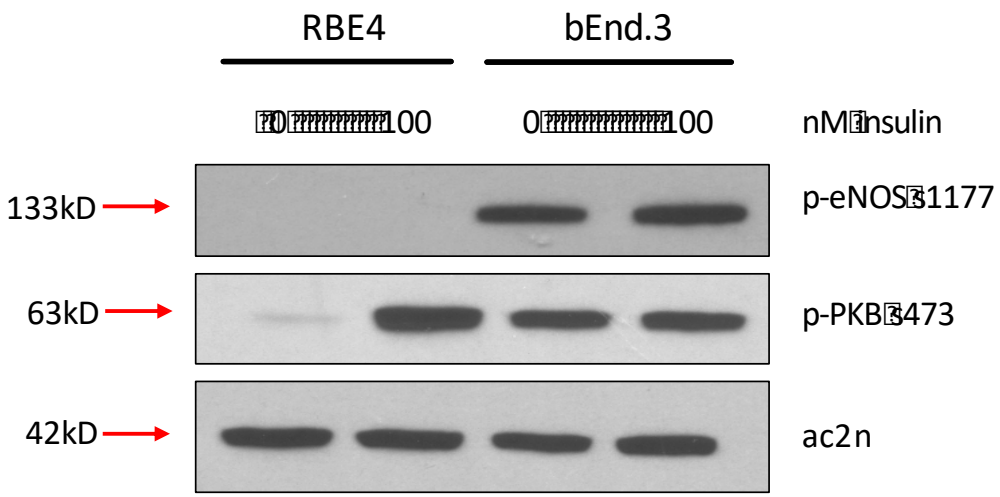

Figure 5.3 Insulin dependent phosphorylation of eNOS in RBE4 and bEnd.3 cells

RBE4 and bEnd.3 cells were stimulated with 0 or 100nM insulin for 30 minutes after being serum starved for 2 hours. Protein was extracted from cell lysates. 20µg of protein was loaded on to acrylamide gels and separated using SDS-PAGE. Representative western blots are shown depicting phosphorylation of eNOS (s1177) and PKB (s473) in RBE4 and bEnd3 cells in response to insulin stimulation.

5.2.3 Acute and chronic palmitate exposures increase ICAM mRNA expression

To confirm that the acute and chronic treatments were able to mimic previously published effects of palmitate[198,277,278], we measured ICAM mRNA expression in response to acute (400µM, 6 hours) and chronic (100µM, 24 hours) palmitate exposure with appropriate controls (Fig. 5.4). Acute palmitate treatment significantly increased ICAM mRNA expression (Fig. 5.4 – control 1 ± 0.04 vs. 400µM 1.68 ± 0.1, n = 4, $p < 0.05$) as did chronic palmitate exposure (Fig. 5.4 – control 1 ± 0.05 vs. 100µM 1.98 ± 0.1, n = 4-6, $p < 0.001$). These data confirm the validity of the concentrations and durations of the palmitate treatments. Further validation can be observed by MitoTracker staining in Appendix S3, where large cell vesicles can be depicted in cells that have been exposed to palmitate. Although this would need to be confirmed by BODIPY or oil red O lipid staining, it is possible that these are lipid droplets. Together, these data indicate that the palmitate/BSA conjugate used for the studies herein is capable of entering the cell and exerting effects.

5.2.6 Bioenergetic profile of untreated bEnd.3 cells

We investigated the oxidative and glycolytic profiles of bEnd.3 cells by performing Mito Stress Tests and Glycolysis Stress Tests respectively. OCR values for the oxidative profile and ECAR values for the glycolytic profile were internally normalised as a fold change of the first baseline. Presenting the data in this way allows observation of how hard the cells are working oxidatively/glycolytically at basal compared to their maximum and allows comparison of the data to previously published data on other cell types.

Figure 5.5A depicts the fold change in OCR compared to the first basal reading against time during a Mito Stress Test. Figure 5.5B shows the average of each of the four readings per treatment (basal, oligomycin, FCCP, and rotenone/antimycin). Fig. 5.5C depicts fold change in ECAR compared to the first basal reading against time during a Glycolysis Stress Test, and 5.5D shows the average of the four readings per treatment (basal, glucose, oligomycin, 2-DG).

Upon oligomycin application in the Mito Stress Test, OCR values were reduced by half and the subsequent FCCP injection caused OCR values to increase to about 1.7-fold higher than basal (Fig. 5.5A, B). The final injection, a combination of rotenone and antimycin A, caused OCR values to reduce by approximately 70% (Fig. 5.5A, B).

During the Glycolysis Stress Test, application of glucose caused ECAR to increase by 70%, but inhibition of ATP synthase by oligomycin in the second injection induced an increase in ECAR to approximately 3.7-fold higher than basal (Fig. 5.5C, D). 2-DG application, which inhibits glycolysis, reverted ECAR values to the same levels as basal (Fig. 5.5C, D).

The implications of the observed metabolic profiles are discussed in detail in the discussion of this chapter. Briefly, the Mito Stress Test profile indicates that, compared to other cell types[356], bEnd.3 cells have a low capacity for OXPHOS at 70% higher than basal. For example, differentiated cells such as neurons and adipocytes are reported to have high spare capacities for undertaking OXPHOS. bEnd.3 cells exhibit a much lower capacity for OXPHOS and were similar in nature to other undifferentiated cell lines such as L6 myoblasts. Furthermore bEnd.3 cells were using approximately 35% of their maximum oxidative capacity to drive ATP-synthesis, suggesting a high ATP turnover, similar to other proliferating cell types[356]. The Glycolysis Stress Test suggests bEnd.3 cells are capable of increasing glycolytic flux to produce ATP upon the addition of glucose, and further increase their glycolytic flux by almost 4-fold upon the addition of oligomycin. Together these data indicate that bEnd.3 cells have a high ATP drive, but are metabolically flexible with a large glycolytic capacity.

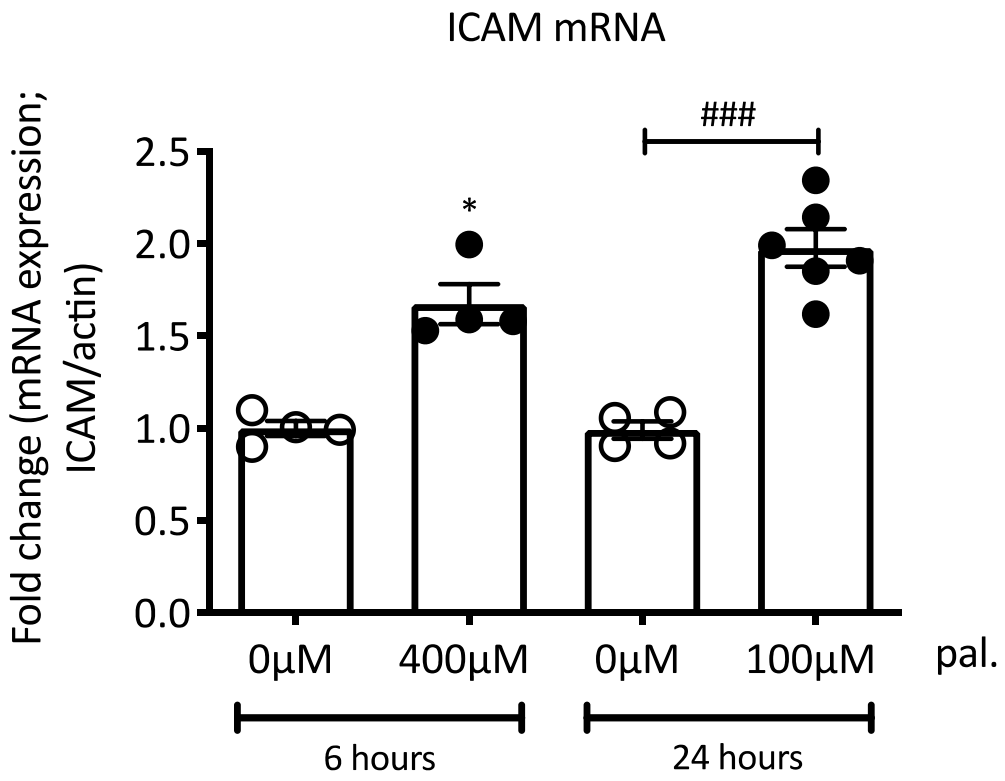

Figure 5.4 Palmitate exposure increases ICAM mRNA expression

bEnd.3 cells cultured at 25mM glucose were exposed to either 400µM palmitate (6 hours) or 100µM palmitate (24 hours), or the appropriate controls. mRNA was extracted and cDNA synthesised. ICAM expression was measured using Taqman qPCR. ICAM was normalised to actin and is expressed as a fold change of the control treatments (0µM for 6 or 24 hours).

Data are expressed as mean ± standard error of the mean.

n = 4-6. Welch's ANOVA with Dunnett's multiple comparison. * = $p < 0.05$ when compared to 0µM 6 hours. ### = $p < 0.001$ when compared to 0µM 24 hours.

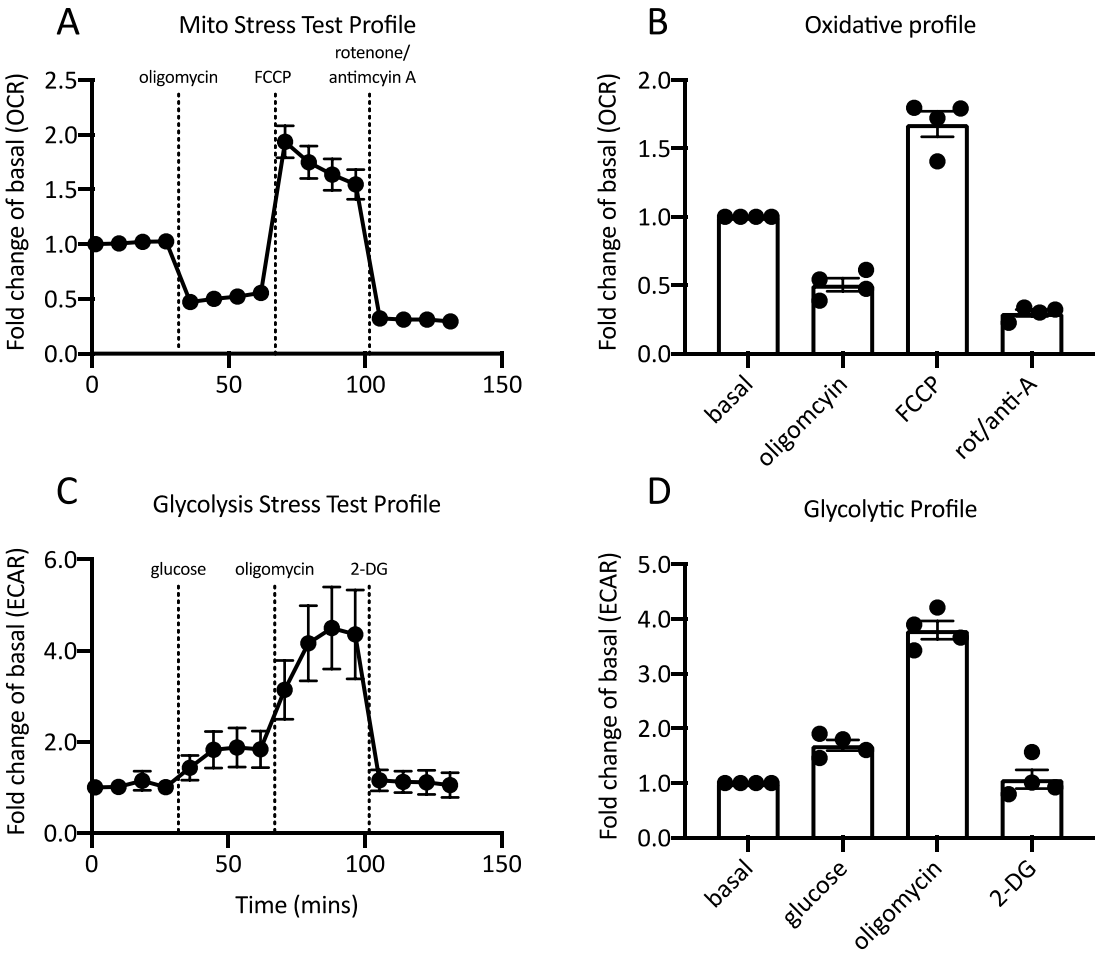

Figure 5.5 Bioenergetic profile of bEnd.3 cells

bEnd.3 cells cultured at 5mM glucose were subjected to a Mito Stress Test (A, B) to investigate functionality of different mitochondrial parameters or a Glycolysis Stress Test (C, D) to measure glycolytic parameters. Changes in OCR (Mito Stress Test) and ECAR (Glycolysis Stress Test) are given as fold change of the first baseline reading.

Data are expressed as mean ± standard error of the mean.

Technical replicates = 20, n = 4.

5.2.5 Effects of high glucose and acute palmitate exposure on mitochondrial function in bEnd.3 cells

bEnd.3 cells were exposed to four treatments (5mM glu. 0µM pal., 5mM glu. 400µM pal., 25mM glu. 0µM pal., and 25mM glu. 400µM pal.). For ease, these groups will be referred to as 1) low glucose control (LG control), low glucose palmitate (LG pal.), high glucose control (HG control), and high glucose palmitate (HG pal.). Cells were then subjected to a Mito Stress Test comprising injections of 1) ATP synthase inhibitor oligomycin, 2) mitochondrial uncoupler FCCP, and 3) mitochondrial respiration inhibitors rotenone and antimycin A. A detailed description of Mito Stress Tests, and the information they can provide regarding mitochondrial parameters, is given in sections 2.7.2-2.7.4.

Fig. 5.6 shows OCR normalised to protein content against time. The data are not internally normalised here as it is important to observe any changes in basal oxygen consumption, which would not be detected if the data were internally normalised. The four treatment groups are split into separate graphs for clarity. LG pal. did not induce any changes in OCR/µg protein over time compared to LG control in response to the Mito Stress Test (Fig. 5.6A). The same was true for HG pal. compared to HG control (Fig. 5.6C). There was an observed trend toward increased baseline OCR/µg protein in bEnd.3 cells cultured in HG control compared to LG control (Fig. 5.6B), and as were the OCR/µg protein readings in response to FCCP (Fig. 5.6B). Fig. 5.6D shows the effects of glucose levels on the acute palmitate exposure. bEnd.3 cells cultured in HG pal. had increased basal OCR/µg protein readings compared to LG equivalent (Fig. 5.6D – row 1 LG pal. 9.09 ± 0.85 pmol/min/µg protein vs. HG pal. 11.65 ± 0.65pmol/min/µg protein; row 2 LG pal. 9.15 ± 0.85 pmol/min/µg protein vs. HG pal. 11.95 ± 0.0.78 pmol/min/µg protein; row 3 LG pal. 0.16 ± 0.82 pmol/min/µg protein vs. HG pal. 12.13 ± 0.85 pmol/min/µg protein; row 4 LG pal. 9.09 ± 0.71 pmol/min/µg protein vs. HG pal. 12.15 ± 0.94 pmol/min/µg protein, $n = 4$, $p < 0.05$). HG pal. also showed a trend toward increased FCCP readings compared to LG pal. (Fig. 5.6D).

Fig. 5.7 shows OCR as a percentage of the first baseline reading, which is 100%. No changes were observed herein in any of the treatment groups.

Interesting information regarding different parameters of mitochondrial function can be extrapolated from the XY OCR/µg protein against time graphs. These data are shown in Fig. 5.8. bEnd.3 cells cultured at HG control/HG pal. exhibited increased basal respiration compared to the LG pal. group (Fig. 5.8A – LG pal. 6.07 ± 0.53 pmol/min/µg protein vs. HG control 7.84 ± 0.29 pmol/min/µg protein, $n = 4$, $p < 0.05$; LG pal. 6.07 ± 0.53 control group as well, but this did not reach significance presumably due to variation in the latter. According to power calculations, larger sample sizes of at least 7 are likely to be required to detect significance with the current effect sizes. Aside from basal respiration, no other parameters of mitochondrial function were significantly changed with the experimental conditions, but a couple of trends of interest were observed. HG control exhibited a trend towards increased ATP-linked respiration (Fig. 5.8C) and palmitate exposure was associated with trends toward increased proton leak (Fig. 5.8D) that is potentially further exacerbated by HG. Power calculations reveal sample sizes of 9 and 7 may be required to detect statistical significance in ATP-linked and proton leak respectively.

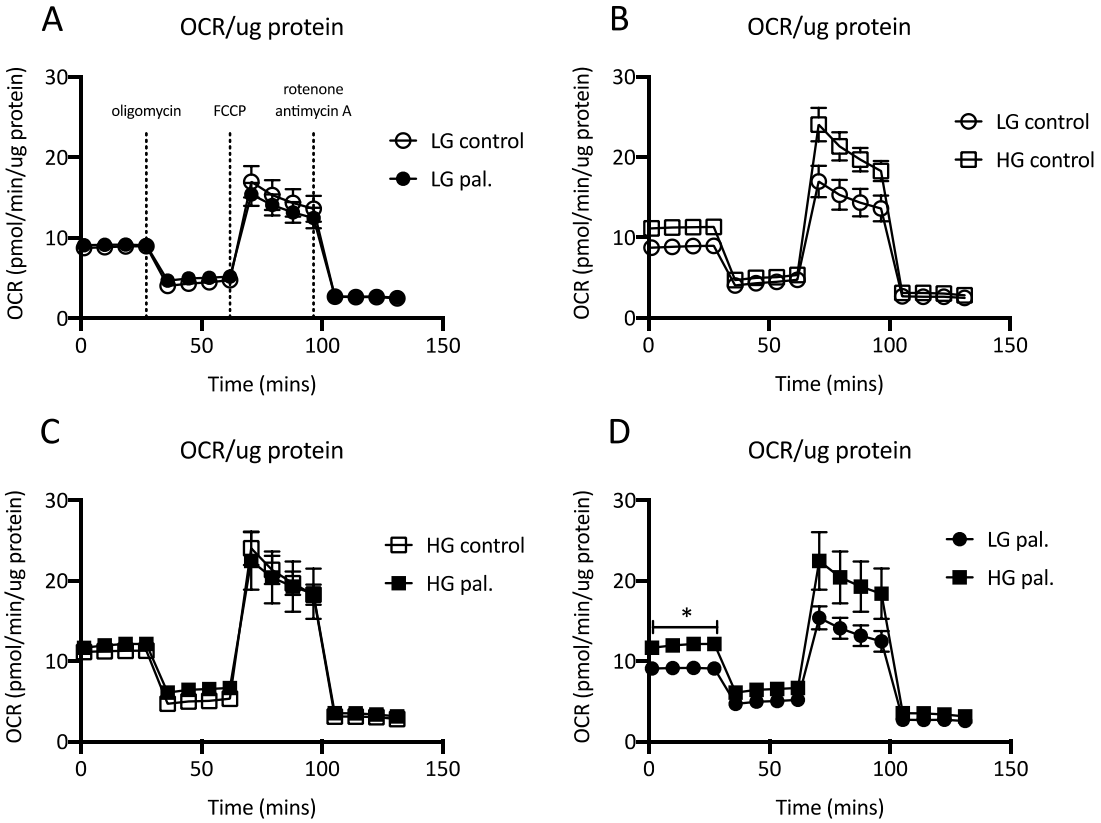

Figure 5.6 Effect of high glucose and acute palmitate exposure on mitochondrial respiration in bEnd.3 cells

bEnd.3 cells cultured at either 5 or 25mM glucose were exposed to 400µM palmitate (or control) for 6 hours before being subjected to a Mito Stress Test to investigate functionality of different mitochondrial parameters. Changes in OCR are normalised to protein concentration. (A) Effect of palmitate exposure at 5mM glucose. (B) Effect of high glucose. (C) Effect of palmitate at 25mM glucose. (D) Effects of glucose concentration on palmitate exposure.

Data are expressed as mean ± standard error of the mean.

Technical replicates = 20, n = 4. Repeated measures ANOVA with Bonferroni multiple comparison. * = $p < 0.05$.

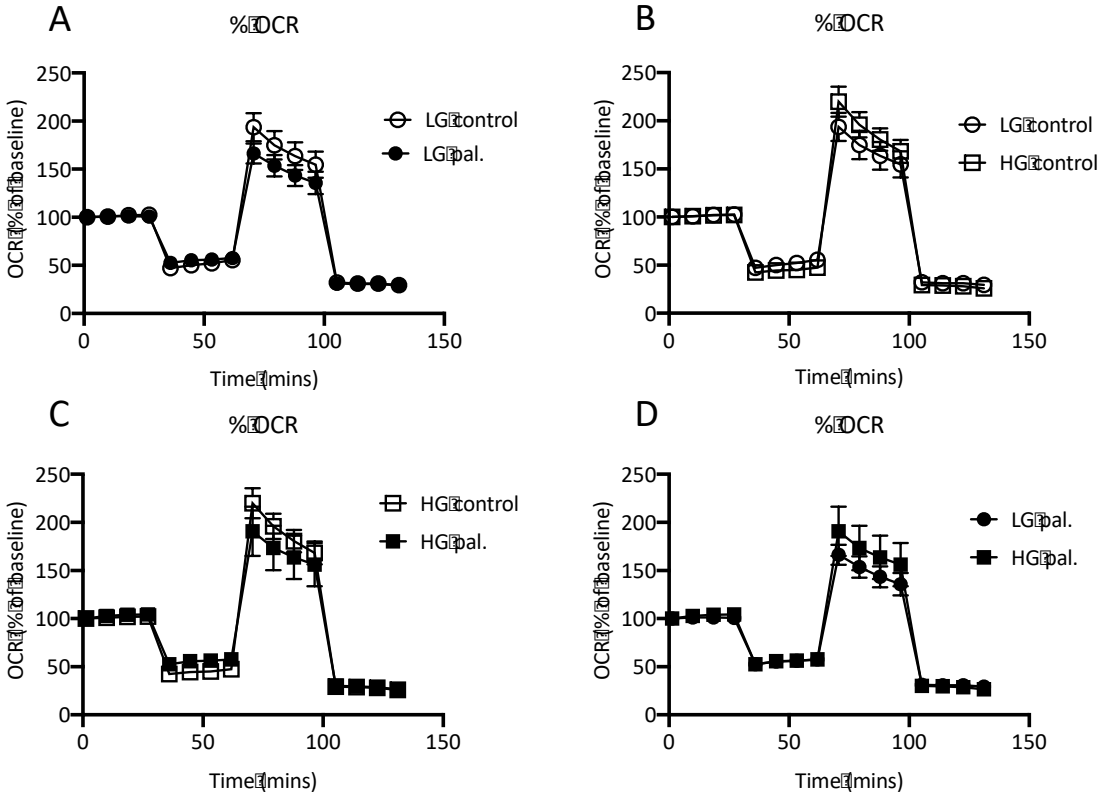

Figure 5.7 Effects of high glucose and acute palmitate exposure on mitochondrial respiration in bEnd.3 cells

bEnd.3 cells cultured at either 5 or 25mM glucose were exposed to 400µM palmitate (or control) for 6 hours before being subjected to a Mito Stress Test. Changes in OCR were internally normalised as a % of the baseline reading (baseline = 100%). (A) Effect of palmitate exposure at 5mM glucose. (B) Effect of high glucose. (C) Effect of palmitate at 25mM glucose. (D) Effects of palmitate at 5mM vs. 25mM glucose.

Data are expressed as mean ± standard error of the mean.

Technical replicates = 20, n = 4. Repeated measures ANOVA with Bonferroni multiple comparison.

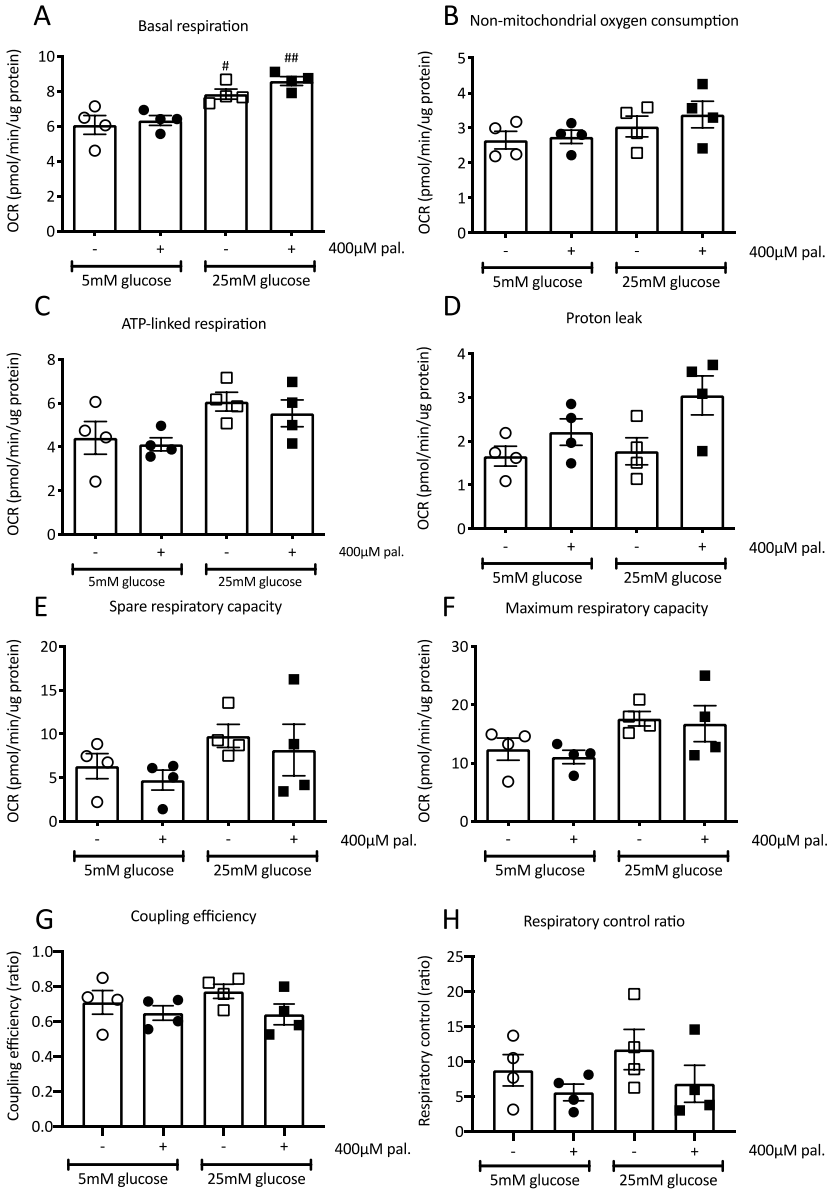

Figure 5.8 Effect of high glucose and acute palmitate exposure on mitochondrial respiration in bEnd.3 cells

bEnd.3 cells cultured at either 5 or 25mM glucose were exposed to 400μM palmitate (or control) for 6 hours before being subjected to a Mito Stress Test to investigate functionality of different mitochondrial parameters. The OCR corresponding to each parameter was calculated as described in Methods. (A) Basal respiration, (B) non-mitochondrial oxygen consumption, (C) ATP-linked respiration, (D) proton leak, (E) spare respiratory capacity, (F) maximum respiratory capacity, (G) coupling efficiency, and (H) respiratory control ratio.

Data are expressed as mean ± standard error of the mean.

Technical replicates = 20, n = 4. Welch's ANOVA with Dunnett's multiple comparison. # = $p < 0.05$ and ## = $p < 0.01$ when compared to 5mM glucose + 400μM palmitate group.

5.2.5 Effects of high glucose and chronic low-level palmitate exposure on mitochondrial function in bEnd.3 cells

To investigate the effects of high glucose and chronic low-level palmitate on bEnd.3 cells, cultures were exposed to four treatments (5mM glu. 0µM pal., 5mM glu. 100µM pal., 25mM glu. 0µM pal., and 25mM glu. 100µM pal.). bEnd.3 cells were exposed to the aforementioned experimental treatments before being subjected to Mito Stress Tests. Groups are referred to as 1) LG chronic control, 2) LG chronic pal., (3) HG chronic control, and (4) HG chronic pal.

Fig. 5.9 shows OCR over time during Mito Stress Tests of bEnd.3 cells normalised to protein content, whilst Fig. 5.10 depicts OCR as a percentage of the first baseline reading (baseline = 100%). We observed no changes in OCR/µg protein or %OCR in any of the four treatment groups.

Extrapolated data from Mito Stress Tests are shown in Fig. 5.11. No statistically significant changes were observed in any of the mitochondrial parameters. Proton leak exhibited an increased trend in palmitate treated groups (Fig. 5.11D). Sample size is low (n = 4) and variability is very high in these treatments. More experiments would have to be conducted to increase sample size and reduce standard deviation to investigate whether this was a genuine result. If this trend holds, it may be that palmitate exposure is inducing proton leak through increased activity of UCPs. This is discussed in more detail in section 5.3.4.

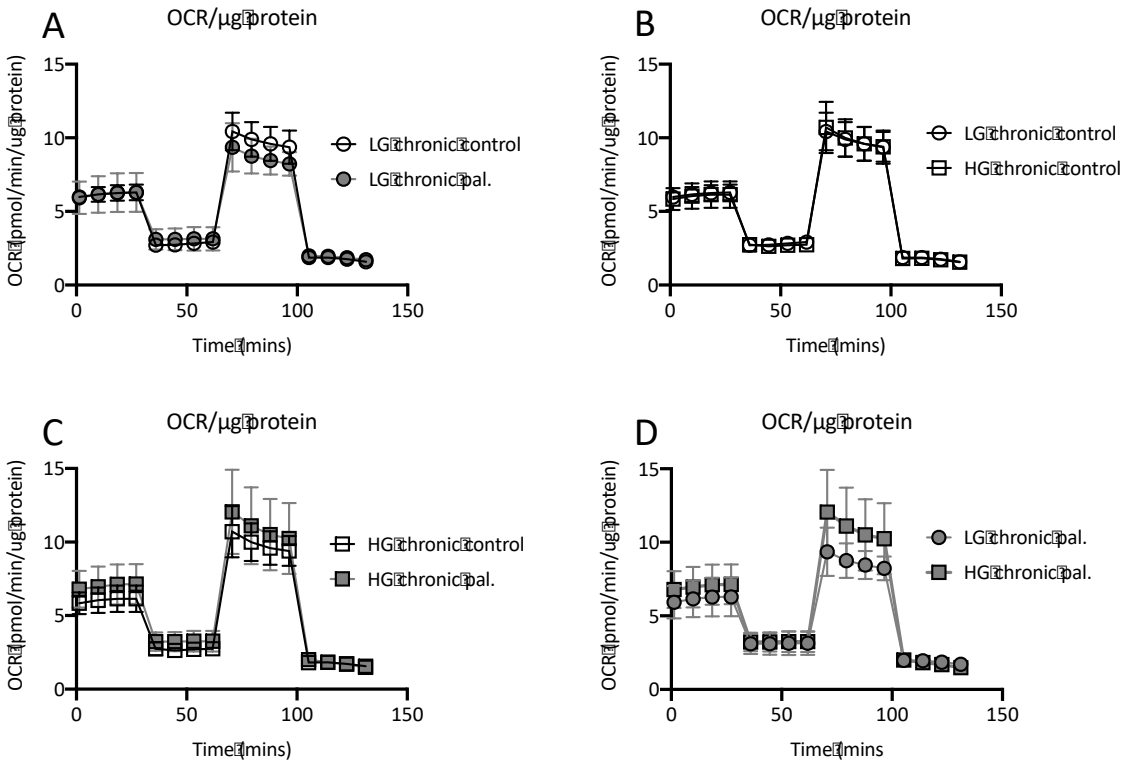

Figure 5.9 Effect of high glucose and chronic palmitate exposure on mitochondrial respiration in bEnd3 cells

bEnd.3 cells cultured at either 5 or 25mM glucose were exposed to 100µM palmitate (or control) for 24 hours before being subjected to a Mito Stress. OCR is normalised to protein concentration. (A) Effect of palmitate exposure at 5mM glucose. (B) Effect of high glucose. (C) Effect of palmitate at 25mM glucose. (D) Effects of glucose concentration on palmitate exposure.

Data are expressed as mean ± standard error of the mean.

Technical replicates = 20, n = 4. Repeated measures ANOVA with Bonferroni multiple comparison.

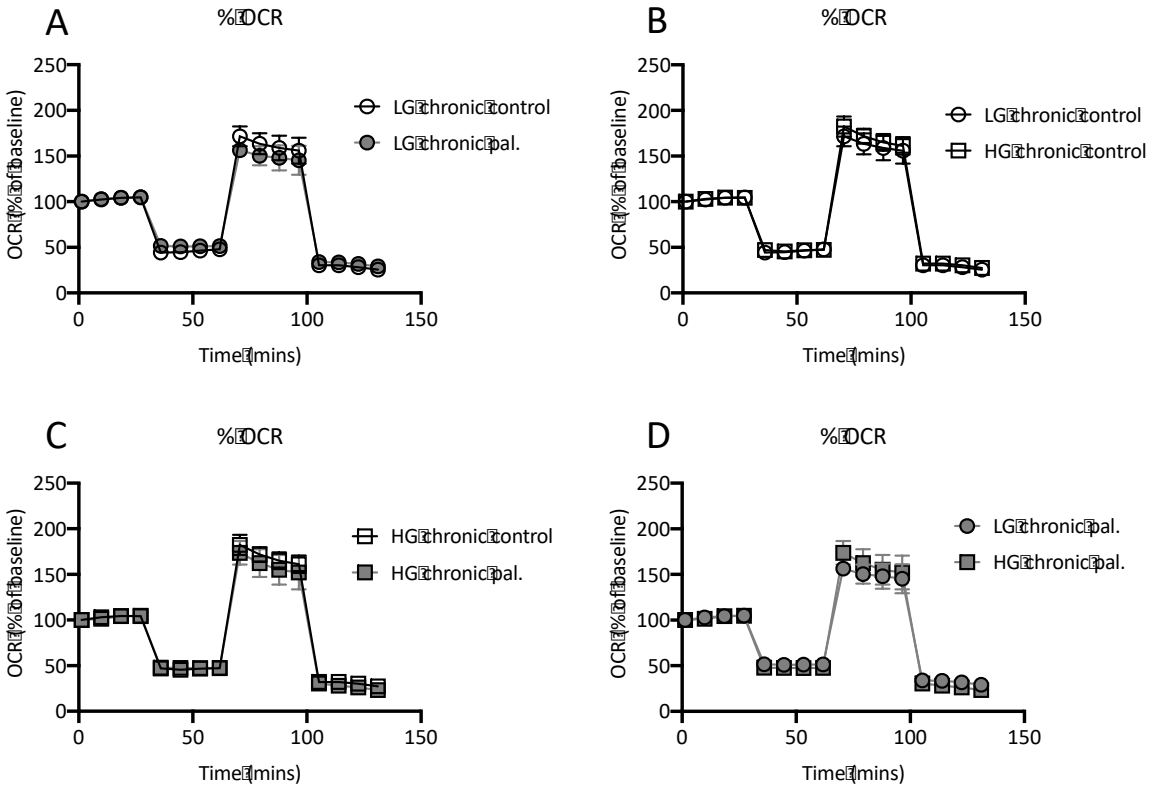

Figure 5.10 Effects of high glucose and chronic palmitate exposure on mitochondrial respiration in bEnd.3 cells

bEnd.3 cells cultured at either 5 or 25mM glucose were exposed to 100µM palmitate (or control) for 24 hours before being subjected to a Mito Stress Test to investigate functionality of different mitochondrial parameters. Changes in OCR were internally normalised as a % of the baseline reading. (A) Effect of palmitate exposure at 5mM glucose. (B) Effect of high glucose. (C) Effect of palmitate at 25mM glucose. (D) Effects of palmitate at 5mM vs. 25mM glucose.

Data are expressed as mean ± standard error of the mean.

Technical replicates = 20, n = 4. Repeated measures ANOVA with Bonferroni multiple comparison.

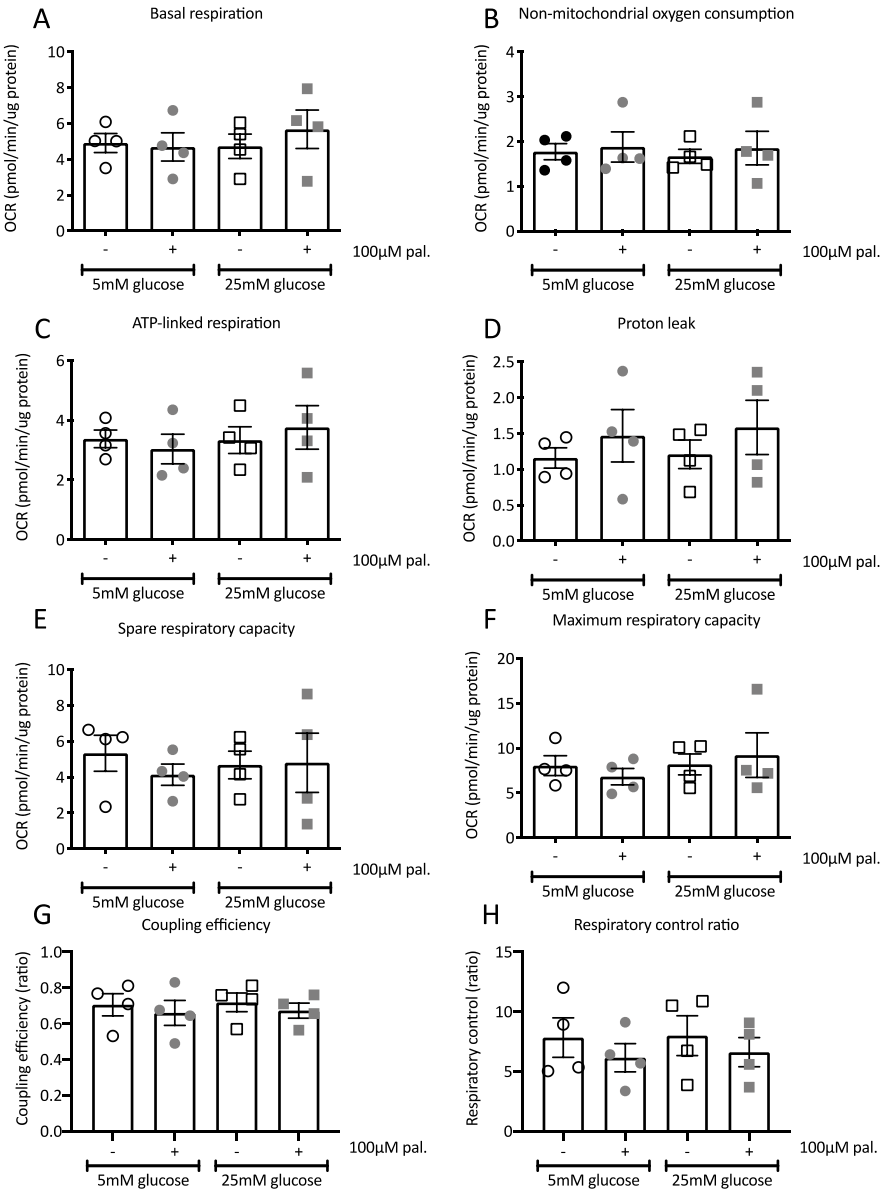

Figure 5.11 Effect of high glucose and chronic palmitate exposure on mitochondrial respiration in bEnd.3 cells

bEnd.3 cells cultured at either 5 or 25mM glucose were exposed to 100µM palmitate (or control) for 24 hours before being subjected to a Mito Stress Test to investigate functionality of different mitochondrial parameters. The OCR corresponding to each parameter was calculated as described in Methods. (A) Basal respiration, (B) non-mitochondrial oxygen consumption, (C) ATP-linked respiration, (D) proton leak, (E) spare respiratory capacity, (F) maximum respiratory capacity, (G) coupling efficiency, and (H) respiratory control ratio.

Data are expressed as mean ± standard error of the mean.

Technical replicates = 20, n = 4. Welch's ANOVA with Dunnett's multiple comparison.

5.2.7 Chronic, but not acute, palmitate exposure increases BACE1 mRNA and protein expression in bEnd.3 cells

Palmitate exposure has been shown to increase BACE1 expression and activity in cells[306,307], so we investigated whether acute (400µM 6 hours) and chronic (100µM 24 hours) palmitate exposure could influence BACE1 expression (protein and mRNA) in bEnd.3 cells cultured at 25mM glucose. We also investigated the effect of palmitate exposure on *App* mRNA levels.

Whilst there were no changes in *App* levels, *Bace1* expression was significantly increased with chronic exposure to 100µM palmitate compared to control (Fig. 5.12B - 0µM pal. 24 hours 1 ± 0.14 vs. 100µM pal. 24 hours 2.46 ± 0.44, n = 8, $p < 0.05$). Acute exposure to 400µM did not influence *Bace1* expression. bEnd.3 cells exposed to 100µM for 24 hours expressed significantly higher *Bace1* levels compared to cells exposed to 400µM palmitate for 6 hours (Fig. 5.12B - 400µM pal. 6 hours 0.76 ± 0.22 vs. 100µM pal. 24 hours 2.46 ± 0.44, n = 8-10, $p < 0.001$). Changes in mRNA expression were complimented by similar findings in BACE1 protein expression. BACE1 protein expression was increased by approximately 80% with chronic exposure to 100µM palmitate (Fig. 5.12C, E – 0µM pal. 24 hours 1 ± 0.16 vs. 100µM pal. 24 hours 1.8 ± 0.18, n = 5-6, $p < 0.01$). However, acute palmitate exposure of 400µM did not influence BACE1 protein expression (Fig. 5.12D, F).

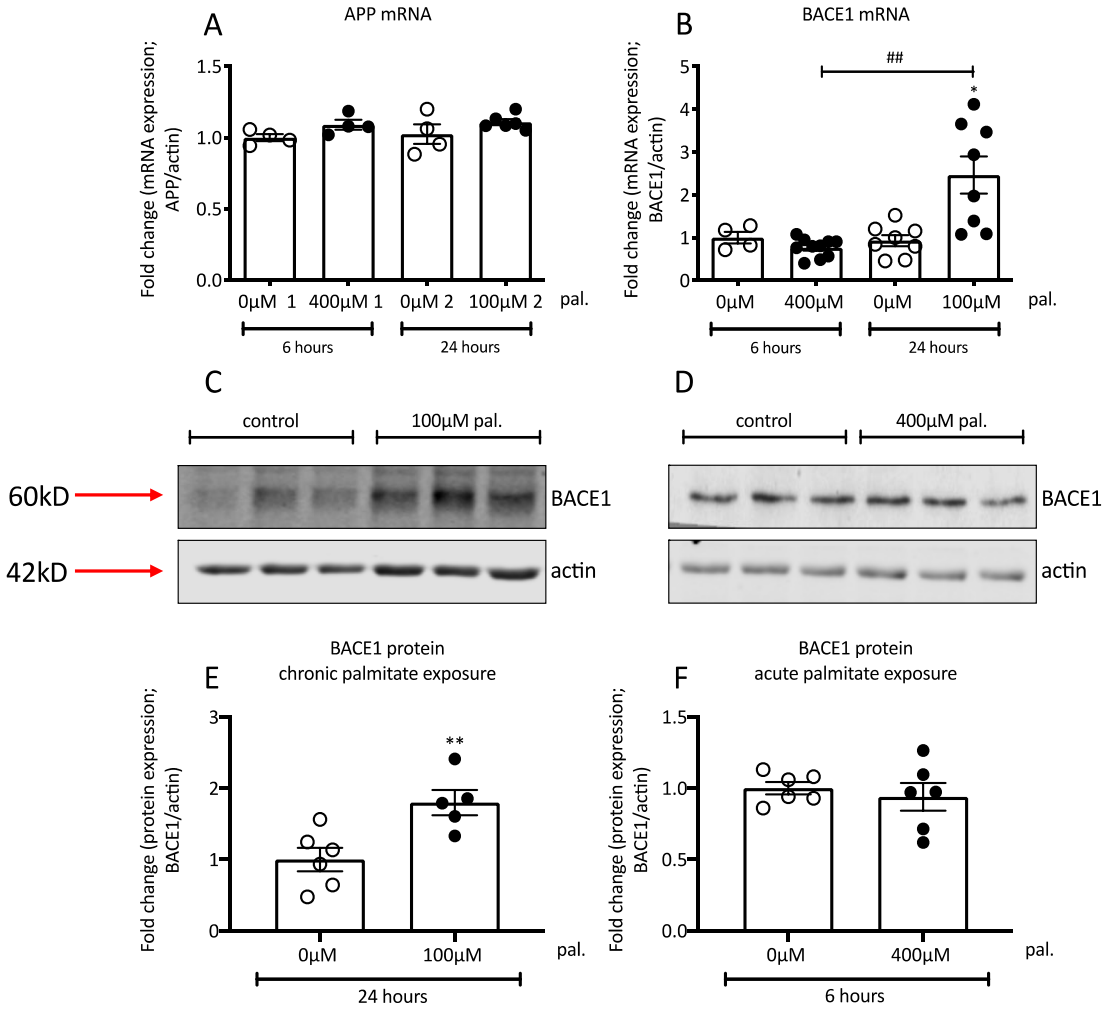

Figure 5.12 Chronic low-level palmitate exposure increases BACE1 mRNA and protein expression, whereas acute treatment does not

bEnd3 cells cultured at 25mM glucose were exposed to either 400μM or 100μM palmitate for 6 and 24 hours respectively, or appropriate controls. mRNA was extracted and cDNA synthesised. *App* (A) and *Bace1* (B) expression was measured using Taqman qPCR. Genes were normalised to *actin* and are expressed as a fold change of the control treatments (0μM for 6 or 24 hours). Protein was extracted from cell lysates. 20μg was loaded on to an acrylamide gel and separated using SDS-PAGE. Representative western blots for BACE1 expression in response to acute 400μM palmitate exposure (C) and chronic 100μM palmitate exposure (D). Actin was used as a loading control. Quantification of BACE1 blots normalised to actin for acute 400μM palmitate exposure (E) and chronic 100μM palmitate exposure (F). Data are expressed as mean ± standard error of the mean.

n = 4-10. (A) and (B) - Welch's ANOVA with Dunnett's multiple comparison. * = $p < 0.05$ when compared to 0μM 6 hours. ## = $p < 0.01$ when compared to 0μM 24 hours. (C) and (D) – Unpaired t-test with Welch's correction. ** = $p < 0.01$ when compared to control.

5.2.7 Effects of exogenous $A\beta_{42}$ and chronic palmitate exposure on mitochondrial function in bEnd.3 cells

There is a known link between nutrient excess, Aβ, and ED[321,324,466,481], and Aβ peptides have been reported to influence mitochondrial function[306,317,331–335]. These reports, together with the finding herein that chronic palmitate exposure can increase BACE1 expression, led us to investigate the effects of exogenous $A\beta_{42}$ accompanied by chronic palmitate exposure on mitochondrial function in bEnd.3 cells. bEnd.3 cells cultured in 25mM glucose were exposed to 1nM aged (5 days) $A\beta_{42}$ peptides (shown previously to be in dimeric form[354]) or aged ScrP peptide control for 24 hours in addition to 100µM palmitate or control. This gave rise to four experimental groups: ScrP 0µM pal., ScrP 100µM pal, $A\beta_{42}$ 0µM pal., and $A\beta_{42}$ 100µM pal, which will be referred to as ScrP control, ScrP pal., $A\beta_{42}$ control, and $A\beta_{42}$ pal. for ease.

Fig. 5.13 depicts OCR over time during Mito Stress Tests of bEnd.3 cells normalised to protein content. Data from the four experimental groups are split into separate graphs for clarity. Application of exogenous $A\beta_{42}$ for 24 hours with and without palmitate did not result in any statistical changes or trends. Fig. 5.14 exhibits OCR against time as a % of the first baseline reading, which is 100%. Again, %OCR was unchanged in the presence of $A\beta_{42}$ and/or palmitate.

Fig. 5.15 comprises the extrapolated data from the Mito Stress Tests. Overall, the variability in these data sets is very high, making it difficult to obtain conclusive results. However, proton leak was again observed to be increased upon palmitate treatment (~30% increase in $A\beta_{42}$ pal. group), which is potentially exacerbated by the presence of $A\beta_{42}$ (Fig. 5.15D). However, sample size is low and data are extremely variable, meaning that when power calculations are performed on these pilot data, the suggested sample size is 15.

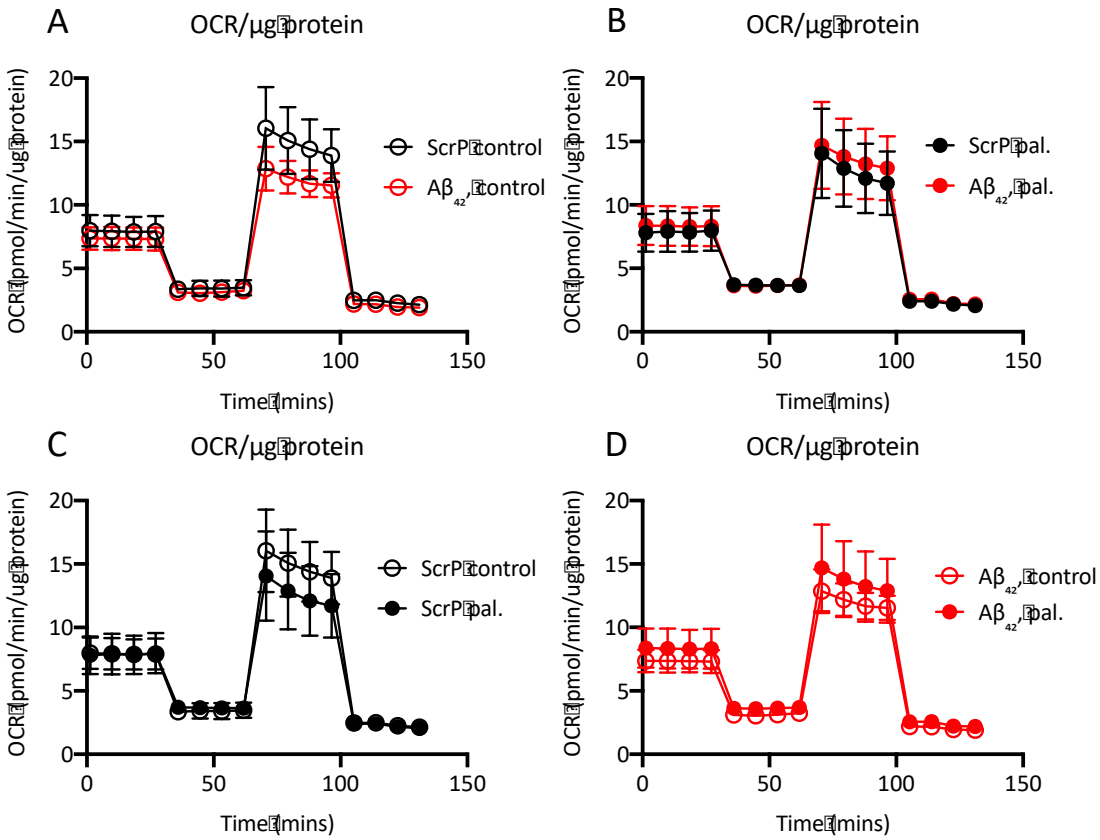

Figure 5.13 Effect of Aβ42 and chronic palmitate exposure on mitochondrial respiration in bEnd.3 cells

bEnd.3 cells cultured in 25mM glucose were exposed to either 1nM ScrP or Aβ42 as well as 100µM palmitate (or control) for 24 hours before being subjected to a Mito Stress Test to investigate functionality of different mitochondrial parameters. Changes in OCR are normalised to protein concentration. (A) Effect of Aβ42. (B) Effect of Aβ42 on palmitate exposure. (C) Effect of palmitate with ScrP exposure. (D) Effect of palmitate with Aβ42 exposure.

Data are expressed as mean ± standard error of the mean.

Technical replicates = 20, n = 4. Repeated measures ANOVA with Bonferroni multiple comparison.

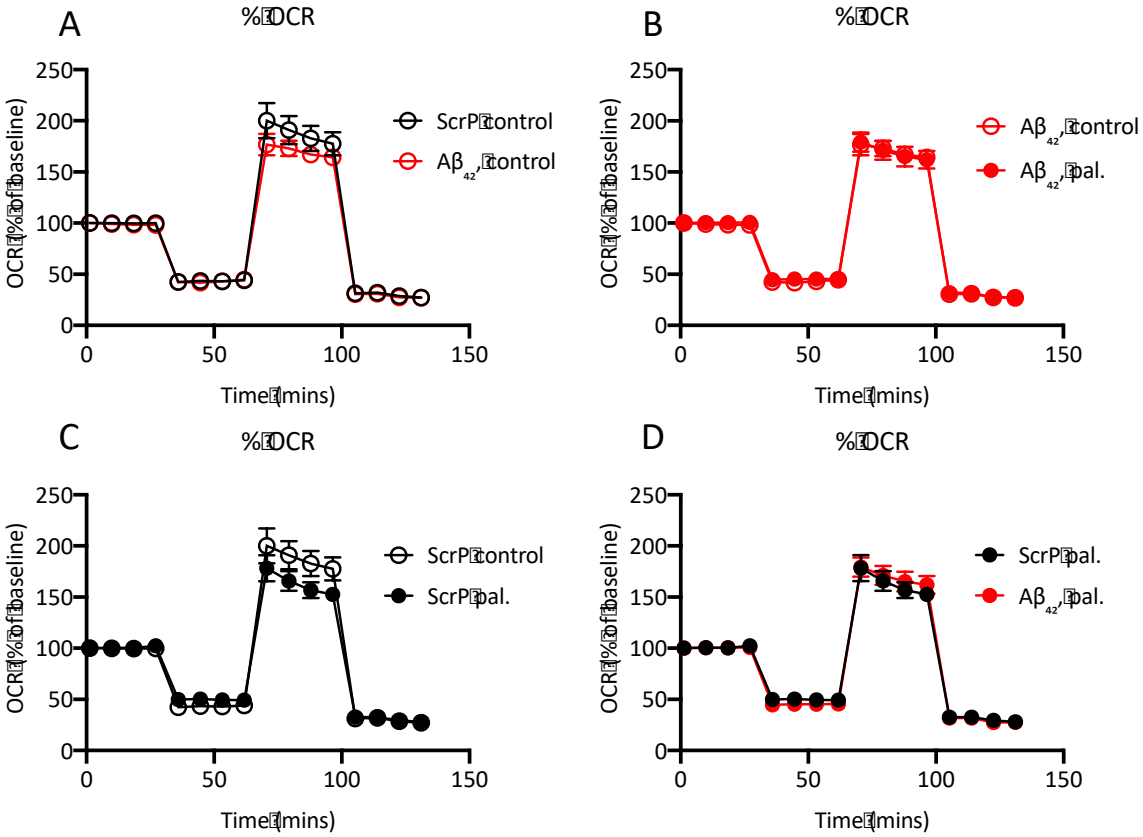

Figure 5.14 Effect of Aβ42 and chronic palmitate exposure on mitochondrial respiration in bEnd3 cells

bEnd.3 cells bEnd.3 cells cultured in 25mM glucose were exposed to either 1nM ScrP or Aβ42 as well as 100µM palmitate (or control) for 24 hours before being subjected to a Mito Stress Test to investigate functionality of different mitochondrial parameters. Changes in OCR internally normalised to the first baseline reading. (A) Effect of Aβ42. (B) Effect of Aβ42 on palmitate exposure. (C) Effect of palmitate with ScrP exposure. (D) Effect of palmitate with Aβ42 exposure.

Data are expressed as mean ± standard error of the mean.

Technical replicates = 20, n = 4. Repeated measures ANOVA with Bonferroni multiple comparison.

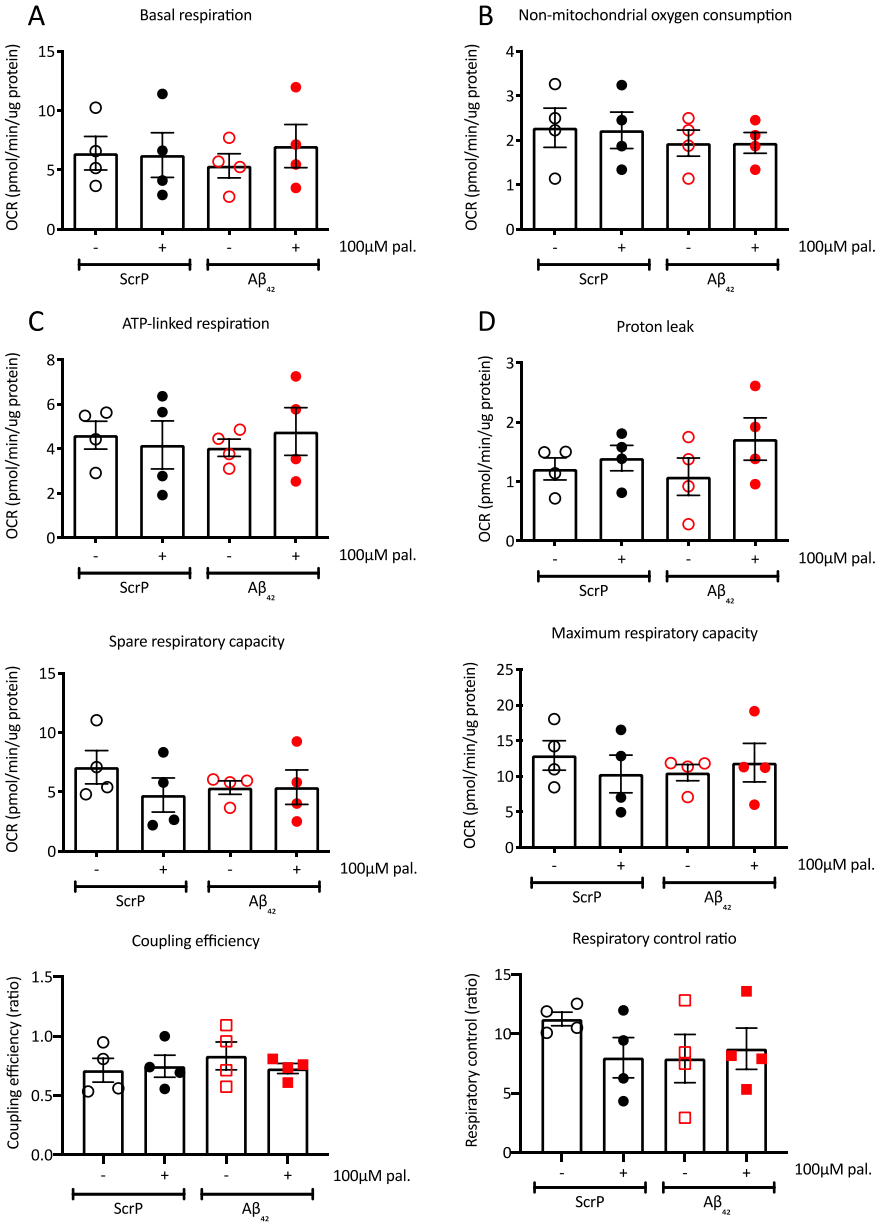

Figure 5.15 Effects of Aβ42 and chronic palmitate exposure on mitochondrial respiration in bEnd3 cells

bEnd.3 cells cultured in 25mM glucose were exposed to either 1nM ScrP or Aβ42 as well as 100µM palmitate (or control) for 24 hours before being subjected to a Mito Stress Test to investigate functionality of different mitochondrial parameters. The OCR corresponding to each parameter was calculated as described in Methods. (A) Basal respiration, (B) non-mitochondrial oxygen consumption, (C) ATP-linked respiration, (D) proton leak, (E) spare respiratory capacity, (F) maximum respiratory capacity, (G) coupling efficiency, and (H) respiratory control ratio.

Data are expressed as mean ± standard error of the mean.

Technical replicates = 20, n = 4. Welch's ANOVA with Dunnett's multiple comparison.

5.3 Discussion

5.3.1 Optimising a cell culture model of brain endothelial cells

We investigated the possibility of using either RBE4 cells or bEnd.3 cells. It was determined that it was important for the cell line to express eNOS, as well as have the ability to phosphorylate and activate it and thus produce NO, as this is a crucial function that all healthy ECs possess. Furthermore, we have observed that modulation of BACE1 activity and thus $A\beta_{42}$ levels *in* vivo resulted in reduced eNOS activity and thus aimed to able to test this parameter *in vitro*. To test this in RBE4 cells, cultures were serum-starved and stimulated with insulin; a known vasodilatory agent that can induce phosphorylation of eNOS at s1177 through a phospho-PKB (s473) dependent mechanism. Cells were stimulated with 0-100nM insulin for 3 different durations; 5 minutes, 15 minutes and 30 minutes. RBE4 cells exhibited a concentration- and time-dependent increase in phosphorylation of PKB at s473. However, they did not exhibit phosphorylation of eNOS under any of these conditions. In the representative western blot of phospho-eNOS there are detectable bands. However, these bands are not the correct size and are likely to be non-specific binding of the primary or secondary antibody. To confirm this, bEnd.3 cells were used as a positive control as they express sustained high levels of eNOS[482]. Indeed, we determined that RBE4 cells did not exhibit any phosphorylation of eNOS at s1177, which is in line with data from another group who could not detect eNOS mRNA in these cells[480]. However, contradictory to this, another group did detect eNOS in this cell line[483]. After several attempt in trying to detect eNOS with no success, it was decided that these cells would not be utilised for further studies modelling brain ECs. bEnd.3 cells were subsequently investigated to determine their suitability as a brain EC model. Cultures were serum-starved and stimulated with varying insulin concentrations for 30 minutes. In response to serum-starving, cells will exhibit reduced activation of the PI3K signalling pathway due to the fact that there are no growth factors present in their culture medium during starves. This means that when cells are stimulated with insulin, for example, it should produce an increase in PI3K signalling (measured here by phosphorylation of PKB at s473). Interestingly, bEnd.3 cells do not exhibit reduced PI3K signalling in response to the 4

different serum starve durations, indicated by their constitutive phosphorylation of PKB (s473) and eNOS (s1177). bEnd.3 cells were created by isolating primary brain ECs from BALB/c mice and infecting these cultures with a middle T antigen-expressing retrovirus, thereby transforming these cells[352]. Middle T antigen is an oncogenic protein that has been shown to activate PKB in a PI3K-dependent manner. This constant activation of PI3K and PKB may result in the constitutively high phosphorylation of PKB exhibited in bEnd.3 cells. This meant we were unable to investigate modulation of eNOS phosphorylation in our model. Despite this fact, we continued with the bEnd.3 cell line for mitochondrial studies due to the fact they 1) express endothelial-specific markers such as eNOS, von Willebrand factor[484], and TJ proteins[484,485]; 2) are commonly used as a model of the BBB as they exhibit low permeability relative to other immortalised cell lines[485]; and 3) have previously been used to measure mitochondrial function using Seahorse technology[486].

5.3.2 Validating the palmitate exposures using the inflammatory marker ICAM

We opted to model nutrient excess in bEnd.3 culture by altering glucose levels in the media and exposing cells to both acute (6 hours) and chronic (24 hours) palmitate incubations. Indeed, palmitate is commonly used *in vitro* as a model of elevated FFA[190]. From the literature it is apparent that researchers utilise varying concentrations of palmitate ranging from 100-750µM[195,198,277,278,306,335]. We opted for an acute palmitate incubation of 400µM as this has been shown to induce mitochondrial dysfunction in a skeletal muscle cell line[278]. It should be noted that we attempted longer exposure durations (16 and 24 hours) using 200 and 400µM palmitate, but these concentrations induced cell death. Therefore, chronic exposures were completed using 100µM palmitate. It should be noted that 'cell death' was measured herein simply by visualising live cultures before and after palmitate treatments using a cell culture microscope, during which extensive cell death was observed in 200/400µM 24-hour exposures. The experimenter can assume bEnd.3 cells are dead if they are small, floating, and circular in shape. Furthermore, when protein and mRNA was extracted from the remaining live cells in these treated cultures, the protein content and mRNA yield were too low to be

used for Western blot or Taqman respectively, suggesting extensive cell death. In order to quantify cell viability, an MTT assay could be performed, or cleaved caspase-3 or caspases-8/9 could be measured.

To validate the palmitate treatments, we investigated a common cellular response to palmitate; inflammation. Inflammation in ECs is termed endothelial activation (EA), and is characterised by, amongst other markers, an increased expression of the adhesion molecule ICAM. Changes in expression of ICAM mRNA in response to 400µM palmitate (6 hours) and 100µM (24 hours) was measured. ICAM mRNA expression was significantly increased by both palmitate exposures in bEnd.3 cells, which is line with the literature on peripheral ECs. Indeed, ICAM has been reported to be upregulated in peripheral ECs in response to 400-500µM palmitate 24 hours[192,198], 100µM for 24 hours[487], 200µM for 18 hours[197], 150µM for 24 hours[488], and 150µM for a much longer chronic incubation period of 6 days[198]. To the best of our knowledge this is the first report of the effects of palmitate treatment on ICAM expression on cultured brain ECs. An inflammatory environment induced by fatty acids in brain endothelium may result in ED by reducing *eNOS* mRNA half-life, as well as by reducing NO bioavailablity through induction of ROS[102]. It would have been interesting to investigate the effects of palmitate treatment on *eNOS* mRNA expression as well as ROS production in bEnd.3 cells if time permitted. ED in brain ECs can lead to impairments in barrier function or reduced control of cerebral haemodynamics. Inflammation can also increase the permeability of the BBB[127489], reduce mitochondrial function of brain ECs, and decrease expression of TJ proteins[490]. Prolonged expression of adhesion molecules such as ICAM can result in infiltration of peripheral inflammatory cells into the brain, promoting neuroinflammation which can be detrimental to brain function[491]. These data suggest a role for palmitate and nutrient excess in impairing brain EC function. This is in line with existing literature reporting that HFD-fed rats exhibit BBB dysfunction as early as 24-days post diet induction[115] and downregulation of TJ proteins including claudin-5, ZO-1, occludin, and caveolin[116–120] is observed in rodent models of T2D, leading to BBB opening[121,122]. T2D rodent models also exhibit upregulated protein expression of ICAM and VCAM[123] at the brain endothelium as well as increased basement membrane (BM) thickening[124–126].

ICAM gene transcription is mainly under the control of nuclear factor-kappa B (NFκB). Palmitate is capable of inducing NFκB signalling[278] and can do so through a number of mechanisms such as activation of toll-like receptors[492], induction of MAP kinase pathways[493], ROS generation[494], or promotion of inflammatory cytokines[495]. Indeed, if time permitted, the mechanism by which palmitate promotes ICAM mRNA expression in bEnd.3s could be further investigated by measuring whether IκB kinase (IKK) or NFκB expression is increased or whether IκBα is reduced by palmitate, or whether palmitate induced ICAM expression is prevented by an NFκB inhibitor. Interestingly, palmitate has been reported to increase NADPH oxidase activity, and thus ROS generation, through a toll-like receptor 4 (TLR4) dependent mechanism[191], which is also associated with increased ICAM expression. Furthermore, ROS generation could be measured in bEnd.3s in response to palmitate using one of the many existing chemiluminescent and fluorescent detection methods[382,383,388], or by measuring NADPH oxidase expression (mRNA or protein) or activity[387]. MAP kinase signalling could be investigated using conventional western blotting for phosphorylation of proteins involved in these pathways (p38 MAPK, JNK, ERK) or by using inhibitors toward the afore-mentioned pathways. Inflammatory cytokine expression could be measured by using Taqman to probe for markers such as TNFα and IL-6.

5.3.3 Bioenergetic profile of bEnd.3s cells

Metabolism of cerebral ECs has been largely overlooked for many years. Historically, ECs were thought of as only an inert lining of blood vessels, but it is becoming more apparent that ECs are a complex, metabolically active cell with important functions in health and disease.

Most research into EC fuel utilisation has been in the field of angiogenesis and tumor vascularization, so very little is known about brain EC metabolism. It is largely accepted that peripheral ECs prefer not to utilise OXPHOS for energy, but rely instead on glycolysis

for the vast majority of their ATP[216,218,220]. Mitochondrial content is significantly lower in ECs compared to other cell types; 5% in liver-derived ECs vs. 28% in hepatocytes[219].

Studies reporting on fuel utilisation in cerebral ECs is lacking. There is some information to suggest that cerebral ECs may harbor more mitochondria than peripheral ECs. Mitochondrial volume in brain ECs accounted for 8-11% of total cytoplasmic volume in rat brain capillary ECs, which is 2-4 times the mitochondrial volume of peripheral ECs[227], indicating a higher capacity for OXPHOS[225,226]. However, mitochondria possess many functions other than OXPHOS. They are important for ROS production and redox signalling, as well as modulating cell proliferation and growth[496]. Therefore, just because a cell possesses a larger volume of mitochondria, it does not necessarily mean it will perform OXPHOS to a higher capacity. Two studies by Xuefeng Ren's group investigated the role of mitochondria in brain EC function, particularly BBB permeability and effects on stroke[127,486]. Both the cultured cell model (bEnd.3) and their primary cell model of ECs indeed seemed to exhibit a relatively low spare respiratory capacity. As previously mentioned, FCCP application to cells will uncouple mitochondria and dissipate the proton gradient. In order to maintain MMP, mitochondria must compete with the uncoupling agent and increase ETC activity (respiration) to pump protons across the membrane. If the mitochondria of the cell in question have a high capacity for OXPHOS, spare capacity will be high. bEnd.3 cells exhibited a 1.75-fold increase in FCCP induced OCR compared to resting OCR, whereas primary cerebral ECs exhibited only a 1.6-fold increase. For comparison, terminally differentiated neurons, myotubes, and white adipocytes exhibit 3.5-, 3-, and 3.3-fold changes respectively in response to FCCP[356]. These data suggest that brain ECs may be metabolically similar to peripheral ECs, which have been reported to possess around a 1.75-fold increase in response to FCCP[497]. However it has also been reported that inhibiting various parts of the ETC rapidly increased cell permeability in bEnd3 cells, but did not induce cell death, indicating that mitochondrial respiration is key to healthy brain EC function[127].

We observed a similar oxidative phenotype in bEnd.3 cells when performing a Mito Stress Test. At rest, untreated bEnd.3 cells were working at approximately 59% of their

maximum oxidative capacity, as when stimulated with FCCP, a 1.7-fold increase in OCR was observed. In comparison to other cell types, such as the afore-mentioned neurons, this indicates a low capacity for OXPHOS. bEnd.3 cells were using approximately 35% of their maximum oxidative capacity to drive ATP-synthesis. This is unsurprisingly higher when comparing bEnd.3s to terminally differentiated primary cultured cells such as neurons (18%) and adipocytes (16%)[356], as immortalised cells are constantly proliferating and have a high ATP turnover. This high ATP drive is similar to other proliferating cell types including C_2C_{12} myoblasts (34%) and lung epithelial cells (50%)[356]. The findings herein regarding the oxidative profile of bEnd.3s are similar to information gathered on a peripheral EC cell line, HUVECs. HUVECs exhibited a 1.75-fold increase in OCR when stimulated with FCCP, suggesting a low spare capacity for OXPHOS, and around 45% of their basal respiration was being used for ATP synthesis[497]. It is difficult to deduce whether this is due to inherent metabolic and physiological similarities between peripheral and brain ECS, or whether it is because bEnd.3 and HUVEC cells are proliferative cell types and are maximising ATP production in order to create daughter cells.

We also investigated the glycolytic profile of untreated bEnd.3 cells using a Glycolysis Stress Test. Upon the application of 10mM glucose, bEnd.3 cells exhibited a 1.7-fold increase in ECAR, indicating they are able to increase glycolytic flux to produce ATP in the presence of glucose. Peripheral ECs were shown to increase their glycolytic flux by 2.5-fold in response to 10mM glucose, suggesting peripheral ECs are more glycolytic than cerebral ECs. Interestingly, when ATP synthase is inhibited upon oligomycin application, ECAR increases by almost 4-fold compared to basal, indicating bEnd.3 cells have a high ATP drive, but are metabolically flexible. A study investigating the glycolytic capacity of different types of ECs from sprouting vessels found that non-tip cells were significantly more glycolytic than tip cells *in vitro*[498]. Tip cells are described as the leading cells of a sprouting blood vessels and non-tip cells are described as either stalk cells, which directly follow the tip cell. Specifically, upon 10mM glucose application, non-tip cells exhibited a 2.75-fold increase in ECAR, which did not increase further upon oligomycin application, suggesting non-tip cells rely heavily on glycolysis for ATP

synthesis. However, tip cells responded remarkably similar to bEnd.3 cells, where they exhibited a 1.5-fold increase in ECAR following glucose application, and a 2.5-fold increase following ATP synthase inhibition. These data suggest that tip cells are metabolically flexible, relying on both OXPHOS and glycolysis for ATP synthesis. bEnd.3 cells responded in a similar manner, suggesting that brain ECs may be metabolically similar to endothelial tip cells. However, it cannot be ignored that bEnd.3 cells are an immortalised cell line, and this could explain their metabolic flexibility and high ATP drive. Indeed, these intrinsic mechanisms may not be shared between peripheral tip cells and brain ECs in vivo. Furthermore, we did not compare peripheral ECs and brain ECs (bEnd.3 cells) herein, so this would need to be further investigated.

5.3.4 Effects of nutrient excess on mitochondrial bioenergetics in bEnd.3 cells

We modelled nutrient excess in bEnd.3 culture by altering glucose levels in the media (5mM vs. 25mM) and exposing cells to both acute (400µM, 6 hours) and chronic (100µM, 24 hours) palmitate treatments.

It should firstly be noted that sample size was very small for Seahorse experiments. Five replicates per treatment were performed on the same plate in hopes to reduce variability, but unfortunately, inter-plate variability was still present. This makes the data herein difficult to interpret and, to be sure of any genuine results, more experiments would need to be performed to add to the sample size. This issue is discussed in detail in section 5.3.7.

Overall, nutrient excess had very little effect on mitochondrial function in bEnd.3 cells. Basal respiration was significantly increased in cells cultured in HG vs. LG, with no change when exposed to palmitate for 6 hours. Basal respiration is composed of two main mitochondrial processes, ATP-linked respiration and mitochondrial proton leak, and is driven by substrate availability and ATP demand. In the other set of experiments investigating the effects of chronic palmitate exposure, this increase in basal respiration in HG-treated groups was not observed. This is likely due the experimental design being

slightly different between these two sets of experiments. Palmitate exposures are performed by aspirating previous media and adding fresh media that contains palmitate (or control), meaning cells are given fresh glucose in the media as well. This is the most accurate way to add palmitate to the cultures. In acute palmitate experiments fresh media is given 6-7 hours pre-assay, more recently than in chronic palmitate experiments. This particular limitation of experimental design is commented upon further later in this chapter (section 5.3.7.2). The fresh glucose provides the cell with more substrate, presumably in the form of pyruvate that will drive mitochondrial respiration in this proliferating cell line with a high ATP demand, leading to an observed higher basal respiration. In the case of the HG treated group without palmitate, there is a trend toward increased ATP-linked respiration, which is presumably driving the high basal respiration. In the case of the HG treated group with palmitate, the combination of the slightly increased ATP-linked respiration, alongside the palmitate induced trend toward increase in proton leak is driving the higher basal respiration. However, if the availability of nutrients is determining the rate of respiration here, then the addition of palmitate should also result in higher basal respiration compared to cultures without palmitate. This suggests that bEnd.3 cells have a preference for glucose oxidation rather than FAO. It would be interesting to investigate the oxidation of palmitate in the absence of glucose by these cells, by performing a Mito Fuel Flex Test. This test adds different substrate to cultures and measures mitochondrial oxygen consumption in response to substrate, determining the preferred fuel. It would also be useful to investigate fuel preference in normal conditions vs. stress conditions, such as an inflammatory stress or oxidative stress (TNFα or H_20_2).

An interesting outcome was the trend toward increased proton leak in response to palmitate exposure, present with both acute and chronic treatments and in combination with both glucose concentrations. These trends are of a relatively small effect size, but they are consistent across different concentrations and durations of palmitate exposures and are in line with the literature (discussed below). If higher palmitate concentrations were used, there may have been a larger effect size, increasing the likelihood of a significant outcome. However, there is the issue of palmitate induced cell

death in this cell line. Perhaps very low-level chronic treatments whereby the palmitate is in the culture media for upwards 6 days would be a more useful avenue to consider. Chronic, low-level high glucose/palmitate treated cultures could then be treated with an added stressor, such as TNFα or H202, followed by Seahorse analysis. To recap, protons that are pumped across the IMM, generate the protonmotive force. Not all of these protons are used to drive ATP synthesis and some of them leak back across the membrane, dissipating the MMP and thus stimulating ETC activity to compete to maintain MMP[235]. The nature of proton leak is not fully understood, but it is thought that there are two types; basal and inducible proton leak. A small fraction of basal proton leak is attributable to physical leakiness of the lipid bilayer[499], whereas a larger portion is thought to be under control of the adenine nucleotide translocase (ANT), which exchanges ADP for ATP at the IMM[500]. The mechanism of ANT regulated basal proton leak is unknown at this time. A group of anion carriers known as uncoupling proteins (UCP1, 2, 3) partly regulate inducible proton leak. They are activated by fatty acids and may serve as an explanation for why we observed palmitate dependent increases in proton leak herein. The protonophoretic model of FA-mediated UCP activity dictates that protonised FAs carry protons across the bilayer of the IMM from the inter-membrane space (IMS) to the matrix, owing to their ability to flip-flop in the lipid-bilayer. Once the FA has flipped and the proton is released into the matrix, the proton-less FA can no longer readily flop back across the membrane. The proposed role of UCPs is to aid the FA in flopping back across the membrane in order for it to bind another proton from the IMS to carry back to the matrix[501]. Palmitate treatment has previously been reported to increase UCP2 and UCP3 expression[502,503], and thus it would be useful to investigate UCP expression in palmitate treated bEnd.3s, either via Western blot for protein expression or Taqman for mRNA expression. Increased proton leak is linked to mitochondrial uncoupling of respiration to ATP, meaning that potential energy created from substrate oxidation is instead lost as heat rather than ATP generation. Increased flow of electrons through the ETC due to enhanced substrate oxidation (during times of nutrient excess without a parallel increase in ATP demand) increases mROS production and contribute to mitochondrial dysfunction. Uncoupling mitochondrial respiration from ATP synthesis (potentially through increased UCP expression) has been linked to

reduced mROS production and could therefore be a protective mechanism against nutrient excess induced mitochondrial dysfunction.

Another interesting trend was the increase in spare and maximum capacity in HG groups. This was again only observed in the acute experiments and not the chronic experiments due to flaws in the experimental design. As previously mentioned, spare capacity and maximum capacity are calculated from FCCP response. FCCP application to cells uncouples mitochondria, dissipates the proton gradient, and drives OXPHOS to pump protons across the membrane to maintain the gradient. This process is inherently dependent on substrate availability. Mitochondria in HG cultures have more access to substrate, hence the higher spare and maximum capacities. Indeed, there is a starvation step during which cells from all treatment groups are placed in assay medium (Methods section) comprised of the same glucose concentration for one hour prior to the beginning of the assay. However, it is possible that cultures previously treated with HG may still possess more carbon intermediates than those treated with LG and can use these substrates for the TCA cycle and OXPHOS, thus resulting in higher basal respiration. To confirm this, a set of experiments could be undertaken on HG vs. LG cultures to investigate whether, after a one hour starve, HG cultures exhibit a higher pyruvate, malate, succinate, etc. content using basic fluorometric or colorimetric assays for these molecules.

The data we observed herein, whereby nutrient excess does not induce mitochondrial dysfunction in brain ECs, is not in line with the literature on peripheral ECs. A study by Koziel and colleagues investigated the effects of culturing the peripheral EC line EA.hy926, which are derived from HUVECs, at HG (25mM) vs. LG (5mM) on mitochondrial respiration[280]. They measured basal oxygen uptake (substrate = 5mM glucose) after culturing cells in HG for 3, 6, or 9 days and compared this to cells at LG. Culturing cells in HG for 6 days or more significantly reduced basal oxygen uptake. Additionally, maximal oxygen uptake (in response to FCCP) was markedly reduced in ECs exposed to HG compared to LG. These data suggest that exposure of peripheral ECs to HG for 6 or more days induces mitochondrial dysfunction, accompanied by increased

mROS production. We may not have observed similar findings as we utilised a different experimental set up, whereby bEnd.3 cells were constantly maintained in LG or HG for over 2 weeks. This may have allowed cells time to become used to the glucose levels and adapt accordingly. If performing the experiment again, bEnd.3 cells would only be cultured in HG for between 6-10 days, similar to the afore-mentioned study. This experimental set up would perhaps produce similar effects on mitochondrial respiration in bEnd.3 cells. When investigating the effects of chronic palmitate treatment, another study reported that a 6-day incubation with 100µM or 150µM palmitate produced reductions in basal respiration and maximal respiration in EA.hy926 cells. These effects were accompanied by upregulation of ICAM expression and increased mROS and non-mitochondrial ROS production. We did not observe similar findings in bEnd.3 cells with palmitate exposures, but again different experimental designs were used. The experimental design whereby cells are cultured in palmitate chronically for 6 days is more physiological when modelling nutrient excess and is therefore a desired approach. The current study did not attempt this but moving forward this avenue should be considered. A study investigating the effects of LG (5.5mM) vs. HG (25mM) overnight exposure on bovine aortic ECs (BAEs) observed similar findings to the data herein, in that mitochondrial bioenergetics (measured by Seahorse) remained unchanged in response to HG[504]. The authors also reported no change in superoxide production. Although the authors did not investigate palmitate, they incubated BAEs with another saturated FA stearate (150µM, 18 hours) and observed no alterations to mitochondrial function. These data suggest that nutrient excess in BAEs does not induce mitochondrial function. These conflicting data on nutrient excess and ECs suggests strongly that bioenergetic response to nutrient excess is sensitive to different experimental designs and is cell line dependent. Our findings did not align with previous studies investigating nutrient excess in a differentiated immortalised myotube cell line. Nisr and colleagues investigated the effects of glucose (5mM) and palmitate (400µM, 16 hours) alone, or glucose and palmitate together, on mitochondrial function. Glucose and palmitate alone had no effect, but together acted as a nutrient burden and overwhelmed mitochondria, resulting in reduced basal respiration and reduced maximum capacity[278]. Taken together these data suggest that nutrient excess can, in some scenarios, induce

dysfunction in mitochondrial bioenergetics. This may be either due to ROS production or can itself promote ROS production, eventually leading to overall cellular dysfunction. These mechanisms may underlie pathologies associated with metabolic syndrome including ED and skeletal muscle insulin resistance.

5.3.5 Exposure to chronic, but not acute, palmitate upregulates BACE1 mRNA and protein expression

Palmitate exposure has been shown to increase BACE1 expression and activity *in vitro*[306,307,505,506], so we investigated whether acute (400µM, 6 hours) and chronic (100µM, 24 hours) palmitate exposure could influence BACE1 expression (protein and mRNA) in bEnd.3 cells cultured at 25mM glucose. We also investigated the effect of palmitate exposure on APP mRNA levels.

Both acute and chronic palmitate exposure produced a trend toward a slight increase in APP mRNA expression. According to power calculations, a sample size of between 10-20 is required in order to reach statistical significance with these effect sizes. It would be interesting to investigate whether protein expression was also increased in response to palmitate incubation, as previous data from our lab suggests palmitate incubation can increase APP protein expression in a differentiated C_2C_{12} myotube cell line[306]. This could be investigated by performing western blot and probing for APP protein.

Interestingly, in bEnd.3 cells BACE1 mRNA and protein expression was increased in response to chronic exposure to 100µM palmitate, but not by acute exposure to 400µM palmitate, indicating a time-dependent increase in palmitate induced *Bace1* transcription. Indeed, a previous study in differentiated C_2C_{12} cells corroborates this data, reporting that palmitate (750µM) did not increase BACE1 protein levels after 2, 6, and 8-hour incubations and only did so after 16 and 24 hours[306]. BACE1 is in part under transcriptional regulation by NFκB signalling. Indeed, treating cells with an IKK inhibitor, knocking down IKK expression using shRNA, or by overexpression of IκBα attenuated palmitate (100µM, 24 hours) induced increases in BACE1 mRNA and protein levels[505]. This is of particular interest as colleagues in the BACE1 field have noted that there are

few instances where increased transcript levels of Bace1 are detected in response to treatments. As previously mentioned, palmitate activates NFκB pathways in peripheral ECs[494]. It would be interesting to investigate whether palmitate induced BACE1 mRNA and protein expression is dependent on NFκB signalling in bEnd.3 cells using afore-mentioned inhibitor or knockdown methods.

These data also align with our *in vivo* data that show that HFD-feeding in mice increases $A\beta_{42}$ levels in aorta[316]. Although BACE1 has been shown to be present in brain endothelium[319], we ourselves have not investigated whether BACE1 activity or expression is increased upon HFD-feeding in cerebral vasculature. It is important that this avenue is investigated, because brain vasculature and peripheral vasculature might respond differently to HFD in terms of BACE1 expression and activity. However, the fact that we have observed increased BACE1 mRNA and protein expression in bEnd.3 cells is promising. Increased BACE1 expression does not necessarily mean increased activity. To confirm increased BACE1 enzymatic activity in the bEnd.3 cells in response to palmitate, we could perform western blot and probe for sAPPβ, or measure $A\beta_{42}$ levels via ELISA.

5.3.6 The effects of palmitate and $A\beta_{42}$ exposure on mitochondrial respiration in bEnd.3 cells

Palmitate exposure increased BACE1 expression in bEnd.3 cells, indicating that $A\beta_{42}$ is potentially also increased, but this would need further investigation. If $A\beta_{42}$ is increased in bEnd.3 cells in response to palmitate, $A\beta_{42}$ could be secreted and act in a paracrine fashion on neighbouring ECs, or indeed in an autocrine fashion on the EC itself. It is also possible that, *in vivo*, $A\beta_{42}$ derived other sources (HFD-induced increase in BACE1 activity in adipose tissue[307,315], skeletal muscle[307], hypothalamus[308]) can act on endothelium. In support of this, we know that HFD increases plasma $A\beta_{42}$ concentration[316]. Of particular interest when studying the BBB, palmitate has been shown to activate (i.e. increase inflammatory phenotype) of astrocytes, which in turn can upregulate BACE1 levels in neurons by secreting TNFα and IL-1β[507]. Neurons can then secrete Aβ to act on other cell types.

We observed no alterations in mitochondrial function upon nutrient excess in ECs, but perhaps dysfunction that occurs in ECs in metabolic syndromes is dependent on alternative factors such as $A\beta_{42}$ derived from other tissues. Aβ peptides have previously been implicated in the development of mitochondrial dysfunction[306,317,331–335]. For these reasons, we investigated the effects of exogenously applied $A\beta_{42}$ (vs. ScrP control) on mitochondrial bioenergetics using Seahorse in bEnd.3 cells cultured in HG conditions. We also introduced chronic palmitate exposure (100uM, 24 hours) as an additional factor to investigate the cumulative effects of high FA and $A\beta_{42}$ together on EC mitochondria. Once again it should be noted that sample size was also very small for $A\beta_{42}$ Seahorse experiments. Similarly, to other Seahorse experiments, five replicates per treatment were performed on the same plate to reduce variability, but inter-plate variability was still present. The data herein may therefore not reflect what is truly occurring energetically in these cells, but the data do provide a preliminary look.

Overall, exposure of bEnd.3 cells to palmitate, $A\beta_{42}$, or both together did not induce changes to mitochondrial bioenergetics. Consistent with precluding nutrient excess experiments, proton leak was again observed in response to palmitate treatment. Respiratory control ratio also appeared reduced; expectedly by palmitate due to the increase in proton leak, but also by $A\beta_{42}$ alone, suggesting the presence of mitochondrial dysfunction. Due to proton leak not being affected by $A\beta_{42}$ incubation, the observed trend toward reduced respiratory control ratio may be due to a dysfunctional OXPHOS system, potentially due to changes in respiratory complexes[286]. This could be further investigated by measuring protein or mRNA expression of ETC complexes I-V. Indeed, spare and respiratory capacity may also be reduced in $A\beta_{42}$ treated cells, but data are variable and sample size is small. More experiments need to be performed to determine whether these results are genuine.

There is not a vast amount of research into Aβ peptides and mitochondrial bioenergetics, but some studies do indicate a role for increased amyloidogenic APP processing (and reduced non-amyloidogenic processing) in the modulation of mitochondrial function. Accumulation of Aβ in and around the mitochondria has been

observed in both human and murine brain tissue[245,329,330] and APP transgenic mice do exhibit varying parameters of mitochondrial dysfunction including reduced respiration[331,332] due to diminished activity of respiratory complexes[331], reduced MMP[332333], reduced ATP production[332,333]. APP overexpression *in vitro* is also associated with diminished respiratory capacity, reduced MMP, and impaired ATP production, effects that were abolished upon application of a BACE1 inhibitor[334]. BACE1 overexpression in C_2C_{12} myotubes impairs glucose metabolism and reduces mitochondrial oxygen consumption, an effect that can be rescued by BACE1 inhibition[306]. BACE1 overexpression in neuronal SH-SY5Y cells also altered glucose metabolism, by inhibiting glucose oxidation, and compensating by increasing glycolysis[335]. BACE1 overexpressing SH-SY5Ys also exhibited reduced enzymatic activity of alpha-ketoglutarate dehydrogenase, isocitrate dehydrogenase, and pyruvate dehydrogenase indicating lesions in TCA cycle activity. This resulted in reduced substrate delivery to the mitochondria, leading to reduced OXPHOS. Interestingly, $A\beta_{42}$ incubation at 10µM for 3 hours in SH-SY5Ys induced apoptosis, reduced MMP, promoted oxidative stress, and reduced mitochondrial Ca^{2+}[336]. Perhaps most relevant to the study herein is an investigation undertaken by Solesio and colleagues looking at the effects of $A\beta_{40}$-Q22 (a form of Aβ peptide produced with the Dutch mutation) on a human brain EC line, hCMEC/D3. Aβ40-Q22 incubation at 50µM for 3 hours induced apoptosis, reduced MMP, promoted oxidative stress, and reduced mitochondrial Ca^{2+} concentrations[336]. However, this study did not investigate mitochondrial bioenergetics in real-time and the authors utilise a very high concentration of Aβ peptide for a very short incubation time, so it is not particularly physiologically or pathologically relevant. For example, if we are generous and suggest AD patients may exhibit plasma $A\beta_{42}$ concentrations of 0.5ng/ml[508], this equates to ~100pM when a molecular weight of 4514.08g/l is used. Thus, the aforementioned studies use concentrations 100,000-500,000 times the pathophysiological plasma concentrations. For these reasons it is difficult to compare these two studies. It remains unclear at present whether Aβ peptides can induce mitochondrial dysfunction. Our data, suggesting Aβ does not promote mitochondrial dysfunction in brain ECs, does not align with existing literature. The afore-mentioned study does however employ a different brain EC line (which is human), a different form

of Aβ peptide, and their experimental set up uses supraphysiological levels of Aβ. These factors may account for discrepancies between these two investigations.

5.3.7 Limitations associated with the current experimental paradigms

5.3.7.1 Sample size

As mentioned earlier in the chapter, the sample size for Seahorse experiments is very low, resulting in high variability. This made it difficult to interpret the findings. The sample size would have to be increased in order to be certain of any experimental results. In the literature, most studies use a sample size of 6 (6 plates, with technical replicates within each plate), but our power calculations reveal that in some instances a sample size of 10 would be required. Furthermore, these experiments were performed using the Seahorse XF24 analyser, which uses a 24-well culture plate. This allows for five replicates per treatment when four treatments are being investigated, as well as 4 background wells. A far more useful machine for these types of experiments is the Seahorse XF96 analyser, which uses a 96-well culture plate. Agilent, the company that manufacture Seahorse analysers, recommend only 4 background wells still, leaving 92 assay wells that can be used for experimentation. The vast majority of studies in the literature utilise the XF96 for cell cultures because it is a high throughput system and experimenters can perform many technical replicates, leading to more accurate and less varied data sets. However, the XF24 analyser is very useful for tissue explants, as the well size is larger. Where possible, for experiments using cell cultures, the XF96 analyser should be utilised, but unfortunately the School of Medicine at the University of Dundee does not possess one.

5.3.7.2 Immortalised cell lines

The use of immortalised cell lines clearly carries several advantages, such as they are easy to use, cost effective, essentially provide an unlimited supply of experimental material, and researchers do not need ethical approval to use them. The key aspect of immortalised cell lines is they are constantly proliferating, meaning they have a high biosynthetic demand for ATP[356,509]. In retrospect, we believe this makes it particularly

difficult to study nutrient excess in immortalised cell lines, as it may be that any excess substrates will simply be oxidised to meet the ATP demand. This means that nutrient excess isn't acting as a burden on mitochondria. Some studies investigating nutrient excess using immortalised cell lines have bypassed this issue by differentiating their cell lines, thus producing cells that do not proliferate and that possess more specialised functions[278]. It would be more useful to isolate primary differentiated brain ECs. As previously mentioned, this was attempted extensively with mouse brain using CD31+ selection of ECs using magnetic microbead technology. The yield of ECs was pure, but the number of cells obtained was not enough for the experiments we wished to perform. It is possible to purchase human primary brain ECs, which can be cultivated. This may be an option in the future, as well as perhaps attempting to isolate brain ECs from rats, whose brains are larger.

As previously mentioned, bEnd.3 cells have a constitutively active PI3K pathway, due to the manner in which they are immortalised. PI3K signalling, particularly the phosphorylation of PKB, has been linked to increased OXPHOS. Indeed, PTEN$^{-/-}$ (endogenous inhibitor of PKB) immortalised hepatocytes exhibit significantly increased mitochondrial respiration (measured using Seahorse Mito Stress Tests)[510]. The authors report that this is due to PKB-mediated inactivation of GSK3β and subsequent activation of pyruvate dehydrogenase (PDH) through reduced phosphorylation of the E1 α subunit at ser293, a key metabolic enzyme that couples glycolysis to OXPHOS. PTEN$^{-/-}$ cells also exhibited increased ATP synthase activity. Thus, PKB activation enhances mitochondrial electron transfer capacity. A similar mechanism may be present in bEnd.3 cells, but this would have to be investigated by western blotting for phospho-GSKβ at ser9 (inhibitory site) and phospho-PDH (E1 α subunit) at ser293 (inhibitory site) or by investigating PDH activity and ATP synthase activity. If this mechanism is present, it may explain why nutrient excess is not inducing any reductions in mitochondrial respiration, when it does in other EC lines[198,280] as well as other cell types[277,278].

5.3.7.3 Flawed experimental paradigms

The studies herein regarding nutrient excess are limited by the experimental design. As described in Methods (seahorse section), many parameters of extracellular flux analysis are dependent on substrate availability. For many immortalised cells, more substrate = more ATP generation and thus increased OXPHOS. In retrospect we understand that differing substrate availability, due to culturing bEnd.3 cells in 5 vs. 25mM glucose and giving them fresh media 6 hours before the assay (as in acute palmitate exposures), will result in increased OXPHOS and false positives. It may have been useful to perform a glucose starvation step prior to the 45 minutes to an hour degassing step, allowing cells to use up any excess substrate, before reintroducing physiological glucose concentrations for the assay to take place. This could potentially eliminate any false positives, and any observed changes in mitochondrial respiration would be due to the lasting effects of glucose and palmitate incubations (i.e. inflammatory effects, increased BACE1 levels, ROS production etc.)

Another issue with the cell culture experimental set-up is that bEnd.3 cells were sub-cultured at their associated glucose concentrations at all times, 5 and 25mM. Around one month before the Seahorse experiments were performed, cells were transferred into these culturing conditions and kept at these concentrations. Immortalised cell lines are assumed to be able to adapt to their conditions easily since they are essentially cancerous. It is possible that cultures of bend.3 cells have adapted to their respective glucose conditions. It would perhaps be more useful to sub-culture cells in LG levels (5mM) and perform a single incubation in HG vs. LG levels for a set number of days. For example, Koziel and colleagues used a 6-day incubation in HG when they observed mitochondrial dysfunction in a peripheral cell line[280]. Similarly, we did not observe any convincing findings with palmitate exposures, but if we extended the incubation time and sub-cultured cells for 6 days in low palmitate (100-150µM), in line with Broniarek and colleagues[198], the cells may exhibit mitochondrial dysfunction.

5.3.8 Summary

The first aim of this chapter was to develop a suitable cell culture model for brain ECs to investigate endothelial function. Following this, it aimed to investigate the effects of nutrient excess on brain EC mitochondrial function. It also investigated whether incubation with $A\beta_{42}$ in the presence of nutrient excess had any effects on mitochondrial function in the brain EC model. After testing both RBE4 cells and bend.3 cells on their suitability as a model for brain ECs, we opted to use bEnd.3 cells as RBE4s did not express eNOS. bEnd.3 cells were not without their disadvantages however, and we realized that investigating NO bioavailability in the model was not possible. We continued with the bEnd.3 cells and sought to investigate another aspect of EC health – mitochondrial function.

To measure mitochondrial function, we employed the use of extracellular flux analysis, specifically using the Seahorse XF24 to measure oxygen consumption and thus mitochondrial respiration. bEnd.3 cells appeared to have a high ATP demand and exhibited metabolic flexibility, with both oxidative and glycolytic capacities. Their bioenergetic profile appeared similar to peripheral endothelial tip cells. We observed no convincing alterations in mitochondrial respiration in response to HG or palmitate exposures (both acute and chronic) or in response to $A\beta_{42}$ incubations. Trends toward increased proton leak were observed with palmitate exposure (both acute and chronic), which may be attributed to increased activation of UCPs. This would need to be further investigated by blotting for UCP2/3 protein expression or probing for mRNA expression.

The lack of mitochondrial dysfunction upon nutrient excess in these cells, when it has been observed in other cell lines, may be attributed to 1) the flaws in the experimental design herein, 2) the fact that they are an immortalised cell line with a high ATP demand, or 3) the constitutively active PI3K pathway present in these cells. Of course, it may be due to the inherent nature of brain ECs as well, in that they are more robust in order to protect the brain from injury. In hindsight, the experimental paradigm used herein for glucose and palmitate exposures is not the best method. Existing studies in the literature use HG exposures ranging from 8-72 hours to 6-9 days, rather than sub-culturing the cells in HG at all times. Indeed, constantly maintaining the cell line in HG conditions may

allow for metabolic adaptation. Furthermore, short and low-level palmitate exposures may not be enough to induce mitochondrial dysfunction. Previous studies sub-culture peripheral ECs in palmitate for up to 6 days. This take on chronic exposure is more physiological and should be adapted moving forward. Cells with high ATP demand like bEnd.3s may have a high capacity for substrate utilisation, meaning that nutrient excess does not pose a burden nor act as a detriment to mitochondrial function. Furthermore, the constitutively active PI3K pathway observed in bEnd.3 cells may result in decreased GSK3β activity and increased PDH activity. This would lead to increased coupling of glycolysis to OXPHOS, resulting in constant shuttling of pyruvate into the TCA cycle creating substrate for OXPHOS. Activated PKB has also been shown to induce ATP synthase activity, leading to increased ETC activity. This means that no matter the effect of glucose and palmitate on mitochondrial function (i.e. through increase inflammation or ROS production), the ETC will remain active due to constant PKB activity. For these reasons, we conclude that bEnd.3 cells are not a good model for measuring endothelial function or mitochondrial respiration.

However, in this chapter we did manage to confirm our previous data that palmitate can indeed increase BACE1 protein and mRNA expression, and, for the first time, report that palmitate can upregulate ICAM mRNA expression in cultured brain ECs. These data are in line with previously existing *in vivo* studies that suggest a role for nutrient excess in BBB dysfunction.

In summary, these data suggest that nutrient excess may still be a valid avenue to consider when investigating brain EC injury and thus cerebrovascular dysfunction that is present in metabolic disorders. Immediate future directions should focus on seeking a more physiological culture model. As previously mentioned, primary cells that are differentiated with their own specialised functions are the best model when investigating mitochondrial respiration in cultures. Human primary brain ECs are commercially available, but costly. Isolation of primary rat brain ECs is another method to consider. The Seahorse 24XF is also capable of measuring mitochondrial from tissue explants. Moving forward we would consider isolating cerebral vessels such as the

middle cerebral artery for example and measure ex vivo mitochondrial respiration. We would also consider culturing the vessel enriched fraction from the brain (section methods) measuring mitochondrial function ex vivo here. Indeed, using these methods would allow investigation of tissue explants from mice fed HFD, high sugar/fructose diet, high cholesterol diet, mice infused with amyloid, or genetically manipulated models. More long-term future directions should continue investigating nutrient excess and mitochondrial respiration, but with a reevaluated and more physiological experimental design.

Chapter 6

Final discussion

6.1 The role of nutrient excess in the development of endothelial dysfunction

6.1.1 Background summary

Excessive consumption of food that is not complimented by increased energy expenditure can result in numerous adverse health complications, such as obesity, T2D, and CVD. Nutrient excess and sedentary lifestyles are becoming increasingly problematic in the 21st century as the global diet transitions towards refined foods, simple carbohydrates, and high levels of saturated fat. It is imperative that the underlying mechanisms of these diseases are investigated if an effective prevention or treatment strategy is to be developed.

There are several pathologies associated with nutrient excess that are of particular interest to our lab; hyperglycaemia, dyslipidaemia, ED (in both peripheral and central microvasculature), and mitochondrial dysfunction. Hyperglycaemia has been strongly linked to ED in humans[151,158], and *ex vivo* myograph studies[153–155] and multiple *in vitro* studies indicate a role for high glucose levels in inducing peripheral and cerebral EC injury[154,162–164]. Regarding dyslipidaemia, high circulating FFA are a known risk factor for CVD[188], and *in vitro* exposure of peripheral ECs to palmitate has been shown to impair EC health[191–198].

It is widely accepted that nutrient excess in these forms is related to ED, but it is unclear exactly how these pathologies are linked. An attractive mechanism is that of mitochondrial dysfunction. Mitochondrial dysfunction is a common pathology of metabolic and cardiovascular disorders, as well as ageing. Nutrient excess may lead to mitochondrial dysfunction by saturating ETC activity, elevating the MMP, increasing RET, and producing pathological levels of mROS[287]. Oxidative stress is strongly linked to ED, due to its role in eNOS uncoupling, NO inactivity, inflammation, and mitochondrial dysfunction, amongst other pathologies. Furthermore, mitochondria are key to healthy brain EC health, as mitochondrial crisis in brain ECs is linked to BBB opening[127,486].

Aside from impaired respiration, alterations in dynamics may also act as an indicator of unhealthy mitochondria. Indeed, in order for the organelle function properly, mitochondrial morphology must be tightly regulated by fission and fusion processes. Imbalance in the proteins that govern these processes (Mfn1/2, OPA1, Drp1) may lead to reduced ability to produce ATP, heterogenous populations of mitochondria with differing mtDNA distribution, increased mROS, and apoptosis. Nutrient excess has been reported to alter mitochondrial dynamics; the general consensus being that nutrient overload results in increased mitochondrial fission, which may then reduce mitochondrial respiratory function and increases mROS production[278,281–284]

It is presently unclear whether nutrient overload induces alterations in endothelial mitochondrial dynamics, and whether this process is associated with ED, both peripheral and central. To investigate this, we employed the use of two animal models of nutrient excess and measured *in vivo* microvascular function and expression of proteins regulating mitochondrial dynamics in the aorta, VE fraction unit, and hypothalamus. To further elucidate the role of nutrient excess in EC function, an *in vitro* study investigating bEnd.3 cells was initiated whereby cells were exposed to nutrient excess (high glucose and high palmitate alone or in combination) and mitochondrial respiration was measured.

6.1.1 Db/db mice exhibit severe hyperglycaemia and endothelial dysfunction *in vivo*

We report here for the first time that 8-week old female db/db mice exhibit ED *in vivo* as measured by reduced responsiveness in skin perfusion to iontophoresis of the vasoconstrictor PE and the vasodilator ACh. Indeed, the cutaneous microcirculation was already so constricted in db/db mice, that application of PE did not induce vasoconstriction, yet it did in wt/wt and wt/db littermates. Furthermore, ACh application did not result in vasodilation in db/db mice, whereas wt/wt and wt/db mice exhibited increased skin perfusion.

Importantly, we only investigated 8-week old female db/db mice in the study herein and there may be sex and age differences in this model. Other members of the lab have studies underway that are investigating vascular and metabolic parameters in male db/db, db/wt, and wt/wt mice, and at different time points. Preliminary data indicate that male db/db mice at 14 weeks also show reduced ACh response.

Moving forward, it is essential to investigate the mechanism underlying this. It would be important to measure endothelium-independent vasodilation *in vivo* to elucidate whether this is an issue specific to ECs or whether it is a downstream impairment in the VSM. This can be performed by measuring cutaneous microvascular perfusion in response to the endothelium-independent NO donor, SNP. This was not measured herein because following SNP iontophoresis, mice need to be culled immediately after the LDI scan meaning tissue would be harvested without an overnight fast. We decided to prioritise tissue processing in this case, but more db/db mice are available to perform further experiments. Another important aspect to consider is NO bioavailability in db/db mice. This can be investigated by measuring plasma nitrite, as well as phosphorylation and thus activity of eNOS, *eNOS* mRNA, and ET-1 expression in vascular tissues. These are all fairly straight forward measurements, but unfortunately time and financial constraints did not allow for these parameters to be measured herein. Others have however reported decreased eNOS expression, increased eNOS uncoupling[378,379], reduced intracellular NO production[380], increased eNOS mRNA[379], and increased ET-1 expression[381] in db/db mice. Furthermore, impaired VSMC signalling can be investigated using cGMP assays and PKG expression. It should also be noted that in early stage disease, ED is likely to be present in the microcirculation, but not yet present in larger vessels such as the aorta. Therefore, investigating the above signalling molecules in aortic tissue at such an early time point may not be the best option. Studying the microvasculature, such as that in the VE fraction of the brain or in highly vascularised tissues such as lung or kidney, is more physiologically relevant. Harvesting pieces of skin where cutaneous microvasculature is present for IHC or IF is also an option.

It is interesting that db/db mice exhibit such severe impairments in EC responsiveness at such a young age. It has been previously reported that db/db mice exhibit hyperglycaemia at 8 weeks old[372–374], findings corroborated by our study herein (fasting blood glucose 22.1mmol/l). As previously discussed, high blood glucose levels are associated with the onset of ED. It would be of use to measure *in vivo* endothelial function and blood glucose levels at earlier timepoints to decipher when each of these pathologies first appear, and whether high blood glucose precedes ED in this model. This would provide a greater understanding of the development of ED in relation to nutrient excess, allowing for more prevention and treatment options.

The key mediator in this hyperglycaemic ED model is oxidative stress, an aspect we did not measure in our db/db mice. However, measuring ROS in our model is very important moving forward, since others have reported increased superoxide production[379]. mROS production can be measured using MitoSox in fresh tissue[385]. NOX mRNA and protein expression or activity[387] could be investigated, specifically Nox2 in the endothelium. Although we could not successfully investigate Nrf2KO mice herein, using this mouse model is still of interest when considering the role of oxidative stress in the development of ED. Using this model alongside a further stressor such as a dietary intervention or ageing may be useful, or indeed attempt to reduce Nrf2 in a model of severe hyperglycaemia (db/db, STZ). However, perhaps more interesting would be an attempt to relieve oxidative stress in the db/db mouse. This could be done by overexpressing Nrf2 or using Nrf2 activators such as sulforaphane. Another method of increasing Nrf2 is to reduce the expression or activity of an interacting protein Keap1. Keap1 binds to Nrf2 and keeps it in the cytoplasm, making it vulnerable to ubiquitination and degradation. Keap1 KO mice are available and are a model of increased Nrf2 antioxidant activity, which should be considered in this context. Mitoquinone mesylate (MitoQ) is a targeted mitochondrial anti-oxidant with a ubiquinone moiety that has been shown to relieve mitochondrial oxidative stress and protect against metabolic and vascular disorders[511] and AD[512]. Mice can be exposed to MitoQ simply by adding it to drinking water[513]. Another potent antioxidant is the manganese superoxide dismutase (MnSOD or SOD2) that is found in mitochondria. MnSOD neutralises superoxide into the less

reactive H_2O_2. MnSOD overexpressing mice, or Nox2 KO mice, are available and could be crossed with db/db mice to investigate whether endothelial function in db/db mice is completely, or partly, rescued by relieving oxidative stress. Indeed, Thompson et al. have investigated the effects of deletion of Nox1, which is also expressed in ECs as well as VSMCs. They found through ex vivo myograph studies that genetic reduction of Nox1 on a db/db background significantly improved macrovascular function in these mice[514]. However, it would be interesting to repeat similar studies using *in vivo* techniques to measure microvasculature. MnSOD (or SOD2) KO mice are also available, but they exhibit very premature death (3 weeks of age). A heterozygous mouse model of MnSOD deficiency (MnSOD+/-) has been investigated on an ApoE background, to investigate whether increased mROS levels can worsen ED in ApoE mice in both carotid vessels and aorta[515]. In carotid artery, ex vivo responses to acetylcholine were significantly reduced in ApoE mice with MnSOD deficiency compared with ApoE mice with full MnSOD function, suggesting elevated mROS can act as a further detriment in the development of ED. This heterozygous MnSOD mouse, or indeed a tet-inducible/reversible MnSOD knockdown mouse, would be interesting to investigate, either alone or alongside dietary and ageing stressors.

To focus on ECs specifically, a conditional knockout mouse may prove useful. As mentioned, MnSOD KO mice are not suitable herein, but the Cre/loxP system could be utilised in order to create a cell-specific conditional knock out of MnSOD only in ECs. This can be done by crossing a mouse expressing a Cre recombinase under an EC-specific promoter such as VE-Cadherin with a mouse with the MnSOD gene flanked by two loxP sites (floxed), meaning that in cells that express VE-Cadherin the Cre recombinase will cut the gene at the loxP sites, resulting in genetic deletion of MnSOD from EC cells. This would result in high levels of superoxide in the endothelium, and we could use this model to investigate the role of ROS production in ED. Furthermore, this model could be stressed further using dietary intervention or ageing.

Aside from hyperglycaemia, db/db mice are reported to exhibit hyperleptinaemia, likely due to increased fat mass[516]. High leptin levels are thought to adversely affect vascular

health, inducing oxidative stress[517], increasing blood pressure[518], impairing arterial distensibility in humans[519], and inducing vascular permeability[520]. However, chronic leptin treatment has also been shown to reduce atherogenic lesions in leptin deficient atherosclerosis-prone mice (LDLRKO;ob/ob, ApoEKO;ApoB48KO;ob/ob, LDLRKO;ApoB48KO;ob/ob)[521,522], likely mediated by improvements in metabolic parameters. Others report that leptin possesses vasodilatory action, by enhancing NO production through a PI3K-independent PKB/eNOS-dependent mechanism[523]. Leptin clearly plays a role in mediating vascular tone, but it is presently uncertain whether it does so via the leptin receptor or a different receptor entirely. In support of this, isolated mesenteric arteries from ob/ob mice exhibit severely blunted responses to ACh and this was improved upon leptin therapy (14 days minipump infusion)[524]. However, this rescue is likely to be due to improved metabolic status. A synergistic relationship between ACh and leptin action on the endothelium may exist. Indeed, our preliminary data from 14-week old wt/db male mice suggests that mice heterozygous for faulty Ob-Rb may also exhibit reduced ACh responsiveness *in vivo*, independently of any metabolic impairments (data not shown). These data, along with the information from relevant literature cited above, warrant further investigation into leptin and Ob-Rb regulators of endothelial function. Conditional (VE Cadherin-Cre) Ob-Rb KO/mutant models could be utilised to investigate this, as well as using *in vitro* endothelial cultures. EC-specific Ob-R KO exist, but every isoform of the leptin receptor is absent in ECs in these mice[525]. The authors report that EC-specific Ob-R KO mice exhibit impaired vascular remodelling and increased VSMC proliferation, findings similar to that seen in obese, hyperleptinemic WT animals, suggesting obesity induced leptin resistance may influence vascular remodelling. However, the authors did not investigate microvascular perfusion in response to vasodilators and thus this avenue is worth exploring.

6.1.2 A mature adult 10-week HFD model of nutrient excess does not exhibit endothelial dysfunction *in vivo*

Db/db mice are genetically modified and are therefore an imperfect model of nutrient excess. Thus, we fed HFD to a mature adult (6 months old) mice for 10 weeks, in order

to investigate the effects of short-term nutrient excess on endothelial function *in vivo*. We chose this length of diet because we have previously observed reduced endothelial responsiveness to ACh *in vivo* as early as 5 weeks of HFD feeding[316]. However, we did not observe any vascular impairments in HFD-fed mice compared to age-matched NC controls, which was not in line with our previous findings. Indeed, these studies were performed approximately 2 years apart, so the observed discrepancies may be due to batch differences in the diet or genetic variability in the mice. Furthermore, experiments were completed by two separate experimenters, which could account for this variance.

Moving forward, it may be useful to use a more severe diet (65% HFD), an atherogenic diet (Western diet, contains cholesterol), sucrose/fructose in the drinking water, or a longer duration of diet (16-22 weeks). Furthermore, blood samples should be taken at varying time points throughout the study alongside vascular scans to investigate blood glucose, lipid levels, and circulating hormone levels. This method would ensure pathological signs of nutrient excess were present alongside any changes in endothelial responsiveness.

Further to hyperglycaemia and dyslipidaemia, nutrient excess is also associated with increased circulating leptin. As previously mentioned, hyperleptinaemia can enhance oxidative stress and increase vascular permeability, and leptin has also been shown to elevate ET-1 levels[526]. Additionally, *ex* vivo aortae from female protein tyrosine phosphatase 1B (PTP1B) KO mice, which have an increased sensitivity to leptin, display reduced ACh-response compared to WT which is rescued by treatment with the designer leptin receptor antagonist Allo-Aca[527]. Increased circulating leptin is associated with increased sympathetic tone. Indeed, leptin treatment in male mice reduced ACh response in isolated mesenteric arteries, an effect that was abolished by sympathetic denervation[528]. The effect was also abolished by treating mice with a superoxide scavenger. These data suggest that, through increased sympathetic tone, hyperleptinaemia may impair EC function through increased oxidative stress. We did not measure circulating leptin levels in our HFD mature adult model (10 weeks HFD), but others have reported that hyperleptinaemia is present at 16 weeks HFD. Contradictory

to this, aortae from ob/ob mice which are deficient in leptin exhibited enhanced vasoconstriction in response to PE and impaired vasodilation in response to ACh which was rescued when leptin was infused[524]. These data suggest an intricate balance of leptin levels is required for proper endothelial function and responsiveness, and these actions may be mediated both centrally and locally.

Another important hormone when considering nutrient excess and obesity is ghrelin. Ghrelin is primarily released from endocrine cells found in the gastric fundus (upper part of the stomach) and exerts orexigenic effects through the growth hormone secretagogue receptor (GHSR) present on hypothalamic neuronal populations[529]. Circulating ghrelin exists as two forms in the plasma – acylated ghrelin and des-acylated ghrelin. It is acylated ghrelin that is known to be involved in meal initiation. Perhaps paradoxically, obese people exhibit reduced circulating ghrelin[530]. However, obesity is associated with impairments in postprandial reductions in ghrelin, whereby circulating ghrelin is still high after eating, continuing to stimulate orexigenic behaviours[529]. Obesity is also linked with ghrelin resistance. Transport of ghrelin across the BBB is impaired in obese mice[531]. For example, in a 12-week HFD model, central and peripheral injections of ghrelin fail to induce ARC neuronal activity, measured by c-Fos immunoreactivity[532]. Interestingly, ghrelin is reported to be expressed in peripheral ECs, but not brain ECs[533], and has been shown to increase NO production[534,535] as well as protect ECs from apoptosis[536]. Furthermore, whole-body infusion of ghrelin into humans reduces blood pressure[537]. Therefore, reduced circulating ghrelin levels in obesity may contribute to disorders related to CVD. Ghrelin has also been shown to act on cerebral ECs. Ghrelin must pass through the BBB to exert its effects on brain tissue; thus, it can enter ECs and potentiate intracellular effects. However BBB transport of ghrelin does not rely on its signalling receptor GHSR[538] and GHSR protein is not expressed in cerebral vessels[533]. Using *ex vivo* intact middle cerebral arteries, Ku and colleagues observed no dilatory response to acylated ghrelin application (binds GHSR), but increased vasodilation in response to des-acylated ghrelin (does not bind GHSR)[533]. The authors also show that this is a NO-dependent mechanism, which is not present in GHSR knockout mice. Furthermore, des-acylated ghrelin application protected against superoxide production

in MCAs and ghrelin-deficient mice exhibit increased superoxide compared to WT mice. These data suggest that des-acylated ghrelin possesses vasodilatory capacity in cerebral arteries through a receptor that is yet to be identified and is also cardioprotective. However, this peptide did not produce similar effects in systemic arteries[539]. It is clear that ghrelin plays a role in modulating vascular tone and function and, given its role in regulating metabolism, this avenue would be interesting to further investigate in regard to nutrient excess. For example, it may prove useful to investigate *in vivo* endothelial function in the ghrelin deficient mouse with and without oxidative stress relievers (MitoQ, sulforaphane, mild mitochondrial uncoupler), or with and without dietary interventions. Chronically infusing differing forms of ghrelin in to DIO animals or models of atherosclerosis (ApoE KO, LDLR KO), or indeed modulating ghrelin O-acyltransferase (the enzyme responsible for producing acyl-ghrelin), and subsequently studying endothelial function in response to this may also be interesting. Of course, ghrelin resistance occurs in the hypothalamus of DIO models, but ghrelin resistance in vascular tissue requires further investigation.

As previously discussed, ROS production is an important measure to investigate herein. Superoxide production can be measured with MitoSox in fresh tissue (aortic tissue, cutaneous microcirculation), or through investigating activity or protein/mRNA expression of markers associated with ROS production (NOX). Furthermore, enhanced chemiluminescence methods exist for measuring NOX-dependent ROS production *in* vivo, ex *vivo* or *in vitro*. Beyond measuring ROS production in models of nutrient excess, models of increased and reduced oxidative stress (as described earlier in 6.1.1) can be considered in combination with dietary intervention.

6.1.3 Ageing is associated with endothelial dysfunction *in vivo*

We observed reduced endothelial responsiveness to ACh in mature adult mice (6 months old at start of study) vs. young adult mice (3 months old at start of study), suggesting age-related decline in EC function. This is in line with previous literature; increasing age has been associated with reduced eNOS activity[114,360], elevated eNOS

uncoupling[361], reduced NO bioavailability[114,360,361], increased endothelial ROS production[114,360,361], enhanced endothelial activation[114,361], and increased ET-1[360,361]. Similar to our findings herein, human studies have reported that peak response to ACh of forearm skin perfusion progressively declines with age[362–365], and this is a good predictor of CVD risk[366]. Of note is that our 6-month old model is not considered elderly, and rather considered mature adult/borderline middle aged. Indeed, it has been reported that endothelium-dependent vasodilation (response to reactive hyperaemia) begins declining as early as 40 years old in men and 50 years old in women[367].

Ageing is often associated with metabolic dysfunction and increased oxidative stress, so moving forward it would be of use to measure blood glucose levels, ROS production, circulating insulin/leptin/ghrelin in our mature adult mice compared to our young adult mice in association with *in vivo* vascular data.

A useful future study would be to measure endothelial function in WT mice 'longitudinally' over 3-24 months, investigating how EC health declines over this time, when it begins to decline, markers (glucose, lipids, hormones, ROS) it is associated with, and whether it plateaus at a certain age. This would provide more information about the nature of ageing and vascular health. Furthermore, metabolic and oxidative stressors could be introduced. For example, we attempted herein to measure HFD and age as two factors that may affect vascular health. Oxidative stress could also be introduced by using aforementioned models (Nrf2 KO, conditional Nrf2KO, conditional MnSOD KO), or relieved (MnSOD overexpressor, MitoQ, sulforophane, Keap1 KO, conditional Keap1KO, modulate Keap1/Nrf2 binding) and investigating their vascular health as they age.

Many rapid ageing mouse models exist, of which several exhibit impaired cardiovascular phenotypes. It would be interesting to employ the use of one of these models such as the Bub1b deficient mouse which displays reduced aortic ACh response and arterial wall thickening[540], the SAMP8 mouse which exhibits endothelial senescence and cognitive decline[541], or the LMNA mouse which suffers from progressive VSMC dysfunction[542].

Investigating these mice with or without oxidative or dietary interventions would provide useful information on the relationship between healthy and unhealthy ageing, in regard to nutrient excess, oxidative stress, and vascular dysfunction.

6.1.4 Endothelial function *in vivo* is not associated with changes in mitochondrial dynamics proteins

In an attempt to understand how ED develops, proteins governing mitochondrial dynamics were investigated in vascular tissue (peripheral = aorta, central = NVU), as well as tissues that may be vulnerable to BBB breakdown (hypothalamus). The reason for investigating this particular process is dysregulation of mitochondrial dynamics is caused by imbalances in fusion and fission proteins and may result in mitochondrial dysfunction (reduced ATP production and respiration, increased mROS, increased mitophagy, increased apoptosis).

The HFD-fed model and the db/db mice did not exhibit a relationship between nutrient excess and changes in mitochondrial dynamics proteins in any tissue. Furthermore, no association between *in vivo* measurements of endothelial function and expression of mitochondrial dynamics proteins was observed. This was surprising, as nutrient excess has been reported to promote mitochondrial fission previously in several tissues and cell types[274,278,281–284], providing a potential mechanism behind nutrient excess-induced mitochondrial dysfunction. Perhaps no changes were observed herein due to the mild 10-week HFD model not being long enough to induce severe mitochondrial dysfunction. However, db/db mice exhibited endothelial dysfunction *in vivo*, but no alterations in mitochondrial dynamics proteins in aortic or VE fraction tissue, suggesting that the onset of ED may be independent of impairments in mitochondrial dynamics entirely.

In hindsight, probing for proteins involved in mitochondrial dynamics via Western blot is not the most efficient or accurate method. Fission and fusion processes are fleeting. Changes in expression of these proteins is only half the story; cellular localisation is of great importance when considering their activity and functionality. Herein, our lysates contained both cytosolic and mitochondrial fractions due to the nature of sonification

lysis. Moving forward, it would be of use to separate these fractions and measure fission and fusion protein content in each of these fractions in order to gain a better understanding of cellular localisation. Indeed, an increase in mitochondrial fraction expression accompanied by a decrease in cytosolic content may indicate an increase in activity. Cellular localisation could also be investigated using staining immunofluorescence methods in tissues. Ideally, the best method is to visualise mitochondria in tissue using electron microscopy (EM) as this is more accurate and far more coherent. Using this method, the mitochondria can be observed in great detail, and it can be deduced whether mitochondria are more prone to fission (higher presence of fragmented, circular mitochondria) or fusion (hypertubular, elongated mitochondria). Aside from dynamics and morphology, mitochondrial respiration could be taken as a measure of function. Tissues (aorta, cerebral vessels) from our models could be excised and processed as tissue explants, whereby they can be put through a Mito Stress Test protocol using a Seahorse Analyser XF24. Similarly, mitochondria can be isolated from tissues of interest and investigated using Seahorse technology. These avenues should be considered in the future. Furthermore, although mitochondrial dynamic proteins were unchanged in these models, mitochondrial dysfunction may still be present. mROS production should be measured herein, or studies could be initiated where db/db mice are treated with agents to reduce ROS production, or indeed scavenge superoxide, such as sulforaphane, mild mitochondrial uncouplers, or MitoQ.

6.1.5 Exposure to nutrient excess *in vivo* did not induce mitochondrial dysfunction in immortalised brain endothelial cells

As previously discussed, one of the better methods for measuring mitochondrial dysfunction is through extracellular flux analysis using a Seahorse machine. We employed this method to investigate how nutrient excess (glucose, palmitate) could influence mitochondrial respiration in the brain endothelial cell line, bEnd.3s. Others have shown previously that nutrient excess can induce mitochondrial dysfunction (as measured by impaired oxygen uptake) in cultured myotubes[277,278], and peripheral ECs[165,166,194,198,208]. Furthermore, exposure to high glucose has been shown previously to reduce MMP, induce mitochondrial Ca^{2+} overload, increase Drp1 levels, and decrease PGC1-α mRNA expression[173], suggesting mitochondrial dysfunction. This study did not

investigate mitochondrial respiration in real-time however, so we set out to perform these experiments.

We did not observe any changes in mitochondrial respiration in cells exposed to high glucose (25mM) levels vs. normal glucose levels (5mM). Furthermore, acute and chronic exposure to palmitate alongside these two glucose concentrations did not result in any alterations in mitochondrial respiration. One observation was increased mitochondrial oxygen consumption in relation to proton leak upon palmitate exposure. However, sample size for these experiments was small and the effect size was not large enough to produce significance. It was surprising that we did not observe any mitochondrial impairments resulting from nutrient excess. We suggested several reasons for this, highlighted in section 5.3.7.2. It may be because brain ECs are inherently more robust than other cell types, due to their functional barrier properties or their intrinsically higher mitochondrial volume. Brain ECs act as a barrier to protect the brain from systemic insults. Hypothetically, this could mean they are more resilient to stressors such as nutrient excess. It cannot be ignored that immortalised cell lines are not truly physiological models. Immortalised cell lines are cancerous with a very high ATP drive, making it particularly difficult to study the effects of nutrient excess on their functionality. Indeed, excess substrates may simply be oxidised to meet the ATP demand, meaning that nutrient excess does not act as a burden on mitochondria. Additionally, bEnd.3 cells exhibit constantly active PI3K signalling and thus enhanced phosphorylation of PKB, which has been linked to increased OXPHOS. Immortalised hepatocytes that have had PTEN knocked out (an endogenous inhibitor of PKB activity) exhibit significantly increased mitochondrial respiration (measured using Seahorse Mito Stress Tests)[510]. This is due to PKB-dependent inactivation of GSK3β (enhanced phosphorylation at ser9) and subsequent activation of PDH (reduced phosphorylation of the E1 α subunit at ser293). $PTEN^{-/-}$ hepatocytes also exhibited increased ATP synthase activity, indicating that enhanced PKB activity promotes electron transfer capacity and a similar mechanism may be present in bEnd.3 cells with constantly active ATP synthase. If this is true, it may explain why nutrient excess has no effect on

mitochondrial respiration, when it does in other EC lines[198,280] as well as other cell types[277,278].

In retrospect, bEnd.3 cells are not an appropriate model for investigating mitochondrial function due to these downfalls and next steps should focus on developing a working model. The cell line hCMEC/d3 is a human brain EC model utilised mainly for BBB research. This could be an avenue to consider, but it should be noted that these cells are also immortalised using SV40 large T antigen, meaning they likely also have constantly active PI3K signalling. However, it may be that it is not as highly active as in bEnd.3 cells. Ideally, primary brain ECs would be the best avenue to consider. Human primary brain ECs are commercially available, or rodent brain ECs can be isolated in the lab. Another possible model is human iPSCs, which could be differentiated into human brain ECs.

Increased hyperglycaemia and circulating FAs are, as previously mentioned, not the only pathologies associated with nutrient excess. Indeed, systemic inflammation and enhanced circulating cytokines is present in metabolic syndrome[543] as well as increased oxidative stress[544]. These pathologies are strongly associated with the onset of ED. Inflammation can be modelled in cell culture by exposing cultures to inflammatory cytokines (TNFa, interleukins), c-reactive peptide (CRP), LPS, and oxLDL amongst others. It would be interesting to investigate mitochondrial respiration in brain ECs (hCMEC/d3s, primaries) in response to inflammatory stimuli with and without a further nutrient stressor (glucose, palmitate). Similarly, oxidative stress can be induced easily in cultures simply by applying H_2O_2, using hypoxic chambers (stroke model), phorbol-12,13 dibutyrate (PDBu), or angiotensin II amongst others. This may induce impairments in mitochondrial function in cultured brain ECs. After which, the response to palmitate and/or glucose could be investigated – not only as stressors to induce mitochondrial dysfunction but also as a fuel source to study whether brain EC fuel preference changes under stress. This would give further insight into how brain EC mitochondria are affected by several stressors that are associated with metabolic and vascular disease. Indeed, it may be that brain ECs are robust and need to be ‘hit’ several times with multiple stressors in order to become dysfunctional.

6.2 The role of APP processing, BACE1, and Aβ in endothelial dysfunction

6.2.1 Background summary

BACE1 and APP are associated with metabolic[305–307,309–311,317,545] and vascular disorders[320,321,324,466]. The activity of BACE1, and thus amyloidogenic APP processing, is upregulated under a number of cellular stressors, in particular HFD[308,317], hyperglycaemia[546,547], and fatty acid exposure[306,548]. More recently, we have shown that $A\beta_{42}$ is upregulated in aorta and plasma from DIO mice[446], as well as in plasma from T2D humans[545], whilst *Bace1* mRNA is increased in mammary arteries of obese women (manuscript in review). Furthermore, chronic infusion of $A\beta_{42}$ into WT mice on both a NC and HFD background induced ED. These data suggest a role for BACE1 and $A\beta_{42}$ in the development of ED, however the mechanisms by which this occurs are unclear. Furthermore, it is unknown whether BACE1 and $A\beta_{42}$ play a role in ED in brain ECs and thus BBB breakdown. Therefore, part of this PhD project aimed to further confirm the role of BACE1 and $A\beta_{42}$ in the development of ED, whilst investigating the potential mechanism of mitochondrial dysfunction and dysregulated mitochondrial dynamics in vascular tissues (aorta, NVU). Using the bEnd.3 cell line, the effects of $A\beta_{42}$ exposure (with and without palmitate) on mitochondrial respiration were also investigated.

6.2.2 Increased BACE1 activity is associated with the development of endothelial dysfunction

In line with previous data, models of reduced $A\beta_{42}$ (BACE1 KO mice) as well as normalising $A\beta_{42}$ in a model of increased $A\beta_{42}$ (APP23 + M3), exhibited improved endothelial responsiveness *in vivo* compared to their controls, whilst models of increased $A\beta_{42}$ (peripherally and centrally infused, APP23 + vehicle), displayed impaired responsiveness. These data suggest $A\beta_{42}$ plays a role in the development of ED. It is known that HFD upregulates the production of $A\beta_{42}$, meaning this may be a potential link between nutrient excess and the development of vascular disorders.

Importantly, BACE1 possesses substrates other than APP, and it may be that the improved endothelial response in BACE1 KO mice is due to reduced BACE1 interaction with another substrate. Potential identified substrates which may be involved in the improved endothelial response include LRP, a protein involved in lipid metabolism, and IL-1 type II receptor and PSGL-1, proteins that are both involved in inflammatory responses. Furthermore, our collaborators identified the insulin receptor as a potential substrate for BACE1, whereby cleavage of the insulin receptor by BACE1 results in reduced downstream insulin action[300]. Insulin resistance in ECs may be associated with reduced functionality[549]. We have previously considered the use of insulin to investigate vasodilation *in vivo* with iontophoresis. Transdermal iontophoresis of insulin has been shown to be possible, but may prove difficult due to the size of the peptide[550]. Dr Paul Meakin (University of Leeds) continues this work, employing the use of an endothelial-specific BACE1 KO mouse. In relation to this work, our lab and Dr Meakin's lab are currently collaborating to further investigate BACE1s role in EC function using a BACE1-BirA construct that was validated by Dr Jennie Gabriel[354]. This construct is part of what is called a BioID assay. The construct is transiently transfected into cells of interest and cells are loaded with biotin. The BirA protein that is joined to BACE1 will biotinylate any proteins that come into contact with BACE1. A biotin pull-down is then performed followed by proteomics to identify biotinylated proteins. This assay will give insight into the physiological role of BACE1 under normal conditions, and pathophysiological conditions upon application of stressors, in whichever cells are of interest. The current project, funded by Alzheimer's Research UK, attempts to identify differences in the BACE1 interactome in brain ECs vs. peripheral ECs.

We have recently shown that the mechanism behind $A\beta_{42}$ induced ED may be reduced NO bioavailability, with $A\beta_{42}$ infusion resulting in reduced PKB and eNOS phosphorylation, cGMP activity, and PKG expression in the aorta compared to controls. $A\beta_{42}$ infused mice on HFD also exhibited reduced plasma nitrite and enhanced plasma ET-1. We did not measure these parameters herein, but it would be interesting to do so. An aspect we had considered but did not measure in relation to $A\beta_{42}$ induced ED is oxidative stress. $A\beta_{42}$ peptides are strongly linked to the production of ROS and it may

be that this is a key mechanism in this model as well. It would be possible to infuse both $A\beta_{42}$ alongside an oxidative stress-relieving agent, to study whether the adverse vascular effects are rescued. Furthermore, infusing $A\beta_{42}$ into a model of reduced oxidative stress (Nrf2 overexpressor, MnSOD overexpressor, Keap1KO) would be useful. Indeed, the group led by Iadecola have reported topical application of $A\beta_{40}$ onto the cerebrum results in vasoconstriction and reduced resting CBF, but this can be rescued by perfusing superoxide scavengers SOD and MnTBAP[551]. They also corroborated these data in an SOD1 x APP Tg mouse model[552]. It would be interesting to perform similar experiments in regard to peripheral vasculature using $A\beta_{42}$/APP23 mouse and superoxide scavenging.

It has been reported that impaired peripheral microcirculation does indicate impaired cerebral microvasculature[346], but it would be important to investigate the effects of $A\beta_{42}$ on cerebral haemodynamics *in vivo*. This could be done using a laser speckle through the intact skull and can provide information about perfusion of whole cerebrum or certain areas. However perhaps the best approach for investigating CBF in vivo is through the use of 2-/3-photon microscopy. Photon microscopy is a state-of-the-art deep brain imaging tool that is capable of mapping complex angioarchitecture of the brain, whilst also measuring moving RBCs (blood flow) and neurovascular coupling[553]. Dilation capacity of larger vessels could be investigated by isolating cerebral arteries and performing wire myography.

In the study herein, we have only investigated the effects of $A\beta_{42}$, not $A\beta_{40}$, infusion in mice. The reason for this is because when measuring $A\beta_{42}$ and $A\beta_{40}$ levels in response to HFD, only $A\beta_{42}$ was increased in mouse plasma and hypothalamus. Furthermore, we showed that T2D plasma contains a high $A\beta_{42}$ content than controls, but $A\beta_{40}$ was unchanged. More recently however, preliminary data suggest that $A\beta_{40}$ is more strongly associated with impaired vasodilatory responses and arterial stiffness in humans (data not shown). These data are in line with studies investigating $A\beta_{40}$ and cerebral haemodynamics in mice[320,323,466]. We have not yet performed studies in which mice are infused with $A\beta_{40}$ and their vascular responses are measured but moving forward this

must be considered. Additionally, infusing $A\beta_{40}$ and $A\beta_{42}$ together may prove to further exacerbate vascular defects.

6.2.2 Endothelial dysfunction caused by increased BACE1 activity is not associated with alterations in mitochondrial dynamics

We investigated the avenue of the involvement of BACE1 and $A\beta_{42}$ in mitochondrial dysfunction. Indeed, the literature does suggest a role for altered APP processing in certain mitochondrial pathologies including reduced MMP[332–334], increased mROS[334], altered bioenergetics[306,317,331,335], and impaired regulation of mitochondrial dynamics[334]. Particularly, exposure of cultured brain ECs to the Aβ peptide Aβ40-Q22 at a concentration of 50μM resulted in mitochondrial injury[336]. To investigate mitochondrial dysfunction in vascular tissues, we probed for proteins regulating mitochondrial dynamics in aorta from BACE1 KO mice and in NVU from BACE1 and centrally infused $A\beta_{42}$ mice. Minimal alterations in fission and fusion proteins were observed in these models, suggesting the development of $A\beta_{42}$ induced ED is not dependent on a mechanism related to mitochondrial dynamics. Of note was the potential increase in VE fraction expression of Drp1 protein in $A\beta_{42}$ mice compared to controls. Since fusion proteins remained unchanged, this change may indicate an increase in mitochondrial fission in the NVU. This would have to be confirmed by using either EM or fluorescent microscopy (with MitoSox). It would be interesting to investigate this further by isolating which cell type this change may stem from or whether it is a change observed in all cells of the NVU. Drp1 activity has previously been associated with BBB breakdown in response to LPS challenge[414]. The authors observed an increase in brain endothelial activation (ICAM expression), reduction in mitochondrial respiration, increased BBB permeability, and increased cellular ROS production in cultured ECs upon stimulation with LPS, which were all associated with phosphorylation of Drp1 at s616. When cells were treated with LPS in combination with P110 (an inhibitor of Drp1 activity), these effects were abrogated. This suggests a role for Drp1-mediated mitochondrial fission in cerebrovascular dysfunction, and it would be interesting to investigate this further in $A\beta_{42}$ infused mice by measuring Drp1 phosphorylation, as this may be a potential link between nutrient excess, $A\beta_{42,}$ and vascular neurodegeneration.

6.2.3 Exposure of bEnd.3 cells to $A\beta_{42}$ does not alter mitochondrial respiration

To compliment *in vivo* studies, we investigated the effects of $A\beta_{42}$ exposure on mitochondrial respiration in bEnd.3 cells with and without palmitate and observed no changes. The potential issues associated with these cells are described earlier in this chapter.

$A\beta_{42}$ peptides are 'aged' herein; incubated at 37°c for 5 days in order to allow peptides to dimerise and oligomerise. A previous PhD project in the lab completed by Dr Jennie Gabriel optimised this 'ageing' time period and found that $A\beta_{42}$ is present mostly in dimers, with some oligomerisation, after 5 days[354]. Purified Aβ from human CSF has revealed that dimers are indeed associated with neurodegeneration, but oligomers of $A\beta_{42}$ are classically known to be the most toxic[355]. It would be interesting to repeat this study using a longer 'ageing' period with the $A\beta_{42}$ peptides. We unfortunately are not aware of the form (monomers/dimers/oligomers) of the $A\beta_{42}$ that we have detected in the DIO models, as the MSD ELISA does not distinguish between forms. The cells themselves are only exposed to $A\beta_{42}$ dimers for 24 hours, and it may be that this duration is not severe enough. It should be noted however that existing literature on synthetic Aβ peptides and vascular impairments involves vastly supraphysiological concentrations of amyloid (50μM-500μM)[336], whilst we have used a near-physiological concentration of 1nM. This may further explain why we have not observed similar findings to the literature. We should also consider investigating $A\beta_{40,}$ considering this peptide is also involved in neurodegeneration and has indeed been reported to impair cerebral haemodynamics[320,322,323,466]. The reason we did not investigate $A\beta_{40}$ herein is that we did not observe increased plasma $A\beta_{40}$ levels in response to HFD or in plasma from T2Ds compared to controls. It may be that $A\beta_{40}$ and $A\beta_{42}$ need to be present together to exert effects, so this is worth exploring.

In the current study, we studied the effects of $A\beta_{42}$ in association with high glucose levels (25mM) as well as chronic low-level palmitate (100μM 24 hours), but we did not

investigate inflammatory or oxidative stimuli. Since these pathologies are associated with metabolic and vascular dysfunction, as well as neurodegeneration, it would be of interest to investigate the accumulative effects of inflammation, oxidative stress, nutrient excess, and $A\beta_{42}$ on mitochondrial respiration in cells. However, measuring so many parameters may prove difficult, especially with the Seahorse XF24 which only allows 20 wells for experimentation. To investigate as many aspects as this, the XF96 would be far better suited.

Raising BACE1 expression and activity in cells would also be of interest. We have previously been successful in overexpressing BACE1 by transfecting a plasmid into SH-SY5Ys[335], C_2C_{12}s[306], RAW cells and 3T3-L1s (data not published). This was attempted in bEnd.3 cells using several transfection agents (lipofectamine 2000, lipofectamine 3000, FUGENE). Using a GFP-tagged vector as a transfection control, transfection efficiency of these cells was deemed to be very low (< 1%), thus other experiments were prioritised. It would be interesting to further pursue this idea however, perhaps using a different cell line. BACE1-overexpressing endothelial cell cultures could be used to investigate mitochondrial respiration, endothelial activation (inflammation) and monocyte adhesion, ROS production, barrier permeability, and transepithelial resistance, amongst others. Cells could also be used in co-cultures with neurons, astrocytes, and other cell types, to model a functional BBB. For example, BACE1-overexpressing RAW cells (macrophages) may be of interest in investigating how raised BACE1 activity in systemic immune cells (perhaps as a result of nutrient excess, metabolic disorders) may inflict damage on the BBB (inflammation, barrier permeability, migration). Similarly, BACE1-overexpressing neuron-like cells (SH-SY5Ys) could also be considered when investigating raised BACE1 activity and the effects this might have on brain ECs.

6.3 Final comments

The studies presented herein set out to 1) establish whether ED due to nutrient excess was associated with impaired mitochondrial dynamics, 2) further confirm the role of raised BACE1 activity in the development of ED, and 3) develop a cultured EC model with

which mitochondrial respiration could be investigated in real-time. Although the use of the db/db model did indeed strengthen the knowledge that pathologies associated with nutrient excess (obesity, hyperglycaemia) promote the development of ED, the HFD-fed model did not. Furthermore, both these models of nutrient excess did not exhibit changes in vascular mitochondrial dynamic proteins, indicating ED develops independently of this process. The second study was successful in further confirming the role of increased BACE1 activity in the development of ED but did not shed further light on whether ED in the brain endothelium and BBB breakdown is also associated with this protein. However, we did observe that improved EC health in BACE1KO and APP23 + M3 mice, and impaired EC health in $A\beta_{42}$ infused and APP23 mice was not associated with alterations in mitochondrial dynamics proteins. Finally, we report herein that mitochondrial respiration in bEnd.3 cells was not affected by nutrient excess or $A\beta_{42}$ exposure, but also that bEnd.3 cells are not an appropriate model for investigating these parameters. In conclusion, this thesis provides further valuable information about the development of ED in relation to nutrient excess and raised BACE1 activity. Indeed, the findings presented herein, taken together with the existing literature, suggest that it could be useful to repurpose BACE1 inhibitors for the treatment of metabolic and vascular disorders relating to nutrient excess.

Chapter 7

References

1. Belahsen R. Nutrition transition and food sustainability. Proceedings of the Nutrition Society. 2014;73(3):385–8.
2. Mastorci F, Vassalle C, Chatzianagnostou K, Marabotti C, Siddiqui K, Eba A, et al. Undernutrition and overnutrition burden for diseases in developing countries: The role of oxidative stress biomarkers to assess disease risk and interventional strategies. Antioxidants. 2017;6(2):1–10.
3. Yusuf S, Reddy S, Ôunpuu S, Anand S. Clinical Cardiology : New Frontiers Global Burden of Cardiovascular Diseases. Circulation. 2001;104(C):2746–53.
4. Amuna P, Zotor FB. Epidemiological and nutrition transition in developing countries: Impact on human health and development. Proceedings of the Nutrition Society. 2008;67(1):82–90.
5. Poli VFS, Sanches RB, Moraes AS, Fidalgo JPN, Nascimento MA, Bresciani P, et al. The excessive caloric intake and micronutrient deficiencies related to obesity after a long-term interdisciplinary therapy. Nutrition. 2017;
6. Ellulu MS, Patimah I, Khaza'ai H, Rahmat A, Abed Y. Obesity & inflammation: The linking mechanism & the complications. Archives of Medical Science. 2017;13(4):851–63.
7. Jiang SZ, Lu W, Zong XF, Ruan HY, Liu Y. Obesity and hypertension. Experimental and Therapeutic Medicine. 2016;12(4):2395–9.
8. Klop B, Elte JWF, Cabezas MC. Dyslipidemia in Obesity: Mechanisms and Potential Targets. Nutrients. 2013;5(4):1218–40.
9. Martyn JAJ, Kaneki M, Yasuhara S. Obesity-induced insulin resistance and hyperglycemia: Etiologic factors and molecular mechanisms. Anesthesiology. 2008;109(1):137–48.
10. Cook RL, O'Dwyer NJ, Donges CE, Parker HM, Cheng HL, Steinbeck KS, et al. Relationship between Obesity and Cognitive Function in Young Women: The Food, Mood and Mind Study. Journal of Obesity. 2017;2017.
11. Hou Q, Guan Y, Yu W, Liu X, Wu L, Xiao M, et al. Associations between obesity and cognitive impairment in the Chinese elderly: An observational study. Clinical Interventions in Aging. 2019;14:367–73.
12. Zore T, Palafox M, Reue K. Sex differences in obesity, lipid metabolism, and

inflammation—A role for the sex chromosomes? Molecular Metabolism. 2018;15(April):35–44.

13. Arroyo-Johnson C, Mincey KD. Obesity epidemiology trends by race/ethnicity, gender, and education: National Health Interview Survey, 1997-2012. Gastroenterology Clinics of North America. 2016;45(4):571–9.
14. Hruby A, Hu F. The Epidemiology of Obesity: A Big Picture. Pharmacoeconomics. 2015;33(7):673–89.
15. ScottishGovernment. Health of Scotland's Population - Obesity. 2017.
16. Guh DP, Zhang W, Bansback N, Amarsi Z, Birmingham CL, Anis AH. The incidence of co-morbidities related to obesity and overweight: A systematic review and meta-analysis. BioMed Central Public Health. 2009;9:1–20.
17. Pantalone KM, Hobbs TM, Chagin KM, Kong SX, Wells BJ, Kattan MW, et al. Prevalence and recognition of obesity and its associated comorbidities: Cross-sectional analysis of electronic health record data from a large US integrated health system. British Medical Journal Open. 2017;7(11).
18. Ruban A, Stoenchev K, Ashrafian H, Teare J. Current treatments for obesity. Clincal Medicine London. 2019;19(3):205–12.
19. DiabetesUK. Us, diabetes and a lot of facts and stats. 2019.
20. Shoelson SE, Lee J, Goldfine AB, Shoelson SE, Lee J, Goldfine AB. Inflammation and insulin resistance Find the latest version : Review series Inflammation and insulin resistance. Journal of Clinical Investigation. 2006;116(August):1793–801.
21. Chen L, Chen R, Wang H, Liang F. Mechanisms Linking Inflammation to Insulin Resistance. International Journal of Endocrinology. 2015;2015.
22. Mooradian AD. Dyslipidemia in type 2 diabetes mellitus. Nature Reviews Endocrinology. 2009;5(1):150–9.
23. Folli F, Corradi D, Fanti P, Davalli A, Paez A, Giaccari D, et al. The Role of Oxidative Stress in the Pathogenesis of Type 2 Diabetes Mellitus Micro- and Macrovascular Complications: Avenues for a Mechanistic-Based Therapeutic Approach. Current Diabetes Reviews. 2011;7(5):313–24.
24. Lastra G, Syed S, Kurukulasuriya LR, Manrique C, Sowers JR. Type 2 diabetes mellitus and hypertension: An update. Endocrinology and Metabolism Clinics of

North America. 2014;43(1):103–22.

25. Shomali M. Diabetes treatment in 2025: Can scientific advances keep pace with prevalence? Therapeutic Advances in Endocrinology and Metabolism. 2012;3(5):163–73.
26. Siddle K. Signalling by insulin and IGF receptors: Supporting acts and new players. Journal of Molecular Endocrinology. 2011;47(1).
27. Shepherd PR, Kahn BB. Glucose Transporters and Insulin Action — Implications for Insulin Resistance and Diabetes Mellitus. The New England Journal of Medicine. 1999;341(1):248–57.
28. Moll L, Schubert M. The role of insulin and insulin-like growth factor-1/FoxO-mediated transcription for the pathogenesis of obesity-associated dementia. Current Gerontology and Geriatrics Research. 2012;2012.
29. Muniyappa R, Montagnani M, Koh KK, Quon MJ. Cardiovascular actions of insulin. Endocrine Reviews. 2007;28(5):463–91.
30. Ono H. Molecular mechanisms of hypothalamic insulin resistance. International Journal of Molecular Sciences. 2019;20(6).
31. Zhao WQ, Alkon DL. Role of insulin and insulin receptor in learning and memory. Molecular and Cellular Endocrinology. 2001;177(1–2):125–34.
32. Pinti M V., Fink GK, Hathaway QA, Durr AJ, Kunovac A, Hollander JM. Mitochondrial dysfunction in type 2 diabetes mellitus: an organ based analysis. American Journal of Phsyiology: Endocrine and Metabolism. 2019;316(2):268–85.
33. Samuel, Varman T.; Shulman GI. Integrating mechanisms for insulin resistance. Cell. 2012;148(5):852–71.
34. Mozaffarian D, Benjamin EJ, Go AS, Arnett DK, Blaha MJ, Cushman M, et al. Heart disease and stroke statistics-2016 update a report from the American Heart Association. Vol. 133, Circulation. 2016. 38–48 p.
35. Anand SS, Hawkes C, Souza RJD, Mente A, Nugent R, Zulyniak MA, et al. Food consumption and its impact on cardiovascular disease. Journal of the American College of Cardiology. 2016;66(14):1590–614.
36. Artinian NT, Fletcher GF, Mozaffarian D, Kris-Etherton P, Van Horn L, Lichtenstein AH, et al. Interventions to promote physical activity and dietary lifestyle changes

for cardiovascular risk factor reduction in adults: A scientific statement from the american heart association. Circulation. 2010;122(4):406–41.

37. Eilat-Adar S, Sinai T, Yosefy C, Henkin Y. Nutritional recommendations for cardiovascular disease prevention. Vol. 5, Nutrients. 2013. 3646–3683 p.
38. Prince M, Knapp M, Guerchet M, McCrane P, Prina M, Comas-Herrera A, et al. Dementia UK: Update. Alzheimer's Society. 1014;43–4.
39. Prince M, Comas-Herrera A, Knapp M, Guerchet M, Karagiannidou M. World Alzheimer Report 2016 Improving healthcare for people living with dementia. Coverage, Quality and costs now and in the future. Alzheimer's Disease International. 2016;1–140.
40. Yiannopoulou KG, Papageorgiou SG. Current and future treatments for Alzheimer's disease. Therapeutic Advances in Neurological Disorders. 2013;6(1):19–33.
41. Lanctôt KL, Herrmann N, Yau KK, Khan LR, Liu BA, LouLou MM, et al. Efficacy and safety of cholinesterase inhibitors in Alzheimer's disease: A meta-analysis. Canadian Medical Association Journal. 2003;169(6):557–64.
42. Birks J. Cholinesterase inhibitors for Alzheimer's disease. Cochrane Database of Systematic Reviews. 2006;(1).
43. Mcshane R, Areosa Sastre A, Minakaran N. Memantine for dementia. Drug and Therapeutics Bulletin. 2003;41(10):73–6.
44. Robinson DM, Keating GM. Mematine: a review of its use in Alzheimer's disease. Drugs. 2006;66(11):1515–34.
45. Ballard C, Corbett A. Management of neuropsychiatric symptoms in people with dementia. CNS Drugs. 2010;24(9):729–39.
46. Leong C. Antidepressants for depression in patients with dementia: a review of the literature. Consultant Pharmacists. 2014;24(9):254–63.
47. Mehta D, Jackson R, Paul G, Shi J, Sabbagh M. Why do trials for Alzheimer's disease drugs keep failing? A discontinued drug perspective for 2010-2015No Title. Expert Opinion in Investigational Drugs. 2017;26(6):735–9.
48. Chami B, Steel AJ, De La Monte SM, Sutherland GT. The rise and fall of insulin signalling in Alzheimer's disease. Metabolic Brain Disease. 2016;31(3):497–515.

49. Anand R, Gill KD, Mahdi AA. Therapeutics of Alzheimer's disease: past, present and future. Neuopharmacology. 2014;76(1):27–50.
50. Alzheimer's Association . 2019 Alzheimer's disease facts and figures. Alzheimer's Dementia. 2019;15(2019):321–87.
51. Alzheimer A. Üner eine eignartige Erkrankung der Hirnrinde. Allgemeine Zeitschrift fur Psychiatrie und Psychisch-gerichtliche Medizin. 1907;64(1):146–8.
52. Alzheimer A, Steizmann RA, Schnitzlein HN, Murtagh FR. An English translation of Alzheimer's 1907 paper, "Über eine eigenartige Erkrankung der Hirnrinde. Clinical Anatomy. 1995;8(6):429–31.
53. LaFerla FM, Green KM, Oddo S. Intracellular amyloid-beta in Alzheimer's disease. Nature Reviews Neuroscience. 2007;8(7):499–509.
54. Thal DR, Grinberg LT, J. A. Vascular dementia: different forms of vessel disorders contribute to the development of dementia in the elderly brain. Experimental Gerontology. 2013;47(11):816–24.
55. Attems J, Jellinger K, Thal DR, Van Norstrand W. Review: sporadic cerebral amyloid angiopathy. Neuropathology and Applied Neurobiology. 2011;37(1):75–93.
56. Akoudad S, Wolters FJ, Viswanathan A, de Bruijn RF, van der Lugt A, Hofman A, et al. Cerebral microbleeds are associated with cognitive decline and dementia: the Rotterdam Study. Journal of the American Medical Association. 2016;73(8):934–43.
57. Jellinger KA. Pathology and pathogenesis of vascular cognitive impairment-a critical update. Frontiers in Ageing Neuroscience. 2013;5(1):17–20.
58. Gorelick PB, Nilsson PM, Roman GC. Vascular contributions to cognitive impairment and dementia: a statement for healthcare professionals from the American Heart Association/American Stroke Association. Stroke. 2013;42(9):2672–713.
59. Toledo JB, Arnold SE, Raible K, Brettschneider J, Xie SX, Grossman M, et al. Centre, Contribution of cerebrovascular disease in autopsy confirmed neurodegenerative disease cases in the National Alzheimer's Coordinating. Brain. 2013;136(9):2697–706.

60. Schneider JA, Arvanitakis Z, Bang W, Bennett DA. Mixed brain pathologies account for most dementia cases in community-dwelling older persons. Neurology. 2007;69(24):2197–204.

61. Kivipelto M, Ngandu T, Fratiglioni L, Viitanen M, Kåreholt I, Winblad B, et al. Obesity and Vascular Risk Factors at Midlife and the Risk of Dementia and Alzheimer Disease. Archives of Neurology. 2005;62(10):1556–60.

62. Loef M, Walach H. Midlife obesity and dementia: Meta-analysis and adjusted forecast of dementia prevalence in the United States and China. Obesity. 2013;21(1):51–5.

63. Sanz CM, Ruidavets JB, Bongard V, Marquié JC, Hanaire H, Ferrières J, et al. Relationship between markers of insulin resistance, markers of adiposity, HbA1c, and cognitive functions in a middle-aged population-based sample: The MONA LISA study. Diabetes Care. 2013;36(6):1512–21.

64. Alford S, Patel D, Perakakis N, Mantzoros CS. Obesity as a risk factor for Alzheimer's disease: weighing the evidence. Obesity Reviews. 2018;19(2):269–80.

65. de la Monte SM, Wands JR. Alzheimer's disease is type 3 diabetes-evidence reviewed. Journal of Diabetes Science and Technology. 2008;2(6):1101–13.

66. Ott A, Stolk RP, Hofman A, van Harskamp F, Grobbee DE, Breteler MN. Association of diabetes mellitus and dementia: the Rotterdam Study. Diabetologia. 1996;39(11):1392–7.

67. Ott A, Stolk RP, van Harskamp F, Pols P, Hofman A, Breteler MN. Diabetes mellitus and the risk of dementia: the Rotterdam Study. Neurology. 1999;53(9):1937–43.

68. Janson J, Laedtke T, Parisi JE, O'Brien P, Petersen RC, Butler PC. Increased Risk of Type 2 Diabetes in Alzheimer Disease. Diabetes. 2004;53(2):474–81.

69. Arvanitakis Z, Wilson RS, Bienias JL, Evans DA, Bennett DA. Diabetes Mellitus and Risk of Alzheimer Disease and Decline in Cognitive Function. Archives of Neurology. 2004;61(5):661–6.

70. Biessels GJ, Stakenborg S, Brunner E, Brayne C, Scheltens P. Risk of dementia in diabetes mellitus: a systematic review. The Lancet Neurology. 2006;5(1):64–74.

71. Ahtiluoto S, Polvikoski T, Peltonen M, Solomon A, Tuomilehto J, Winblad B, et al.

Diabetes, Alzheimer disease, and vascular dementia:a population-based neuropathologic study. Neurology. 2010;54(13):1195–202.

72. Profenno A, Porsteinsson AP, Faraone S V. Meta-analysis of Alzheimer's disease risk with obesity, diabetes, and related disorders. Biological Psychiatry. 2010;67(6):505–12.
73. De Feice FG, Lourenco M V., Ferreira ST. How does brain insulin resistance develop in Alzheimer's disease? Alzheimers Dementia. 2014;10(1):26–32.
74. Zhao WQ, Townsend M. Insulin resistance and amyloidogenesis as common molecular foundation for type 2 diabetes and Alzheimer's disease. Biochimica et Biophysica Acta. 2009;1792(5):482–96.
75. Li L, Hölscher C. Common pathological processes in Alzheimer disease and type 2 diabetes: A review. Brain Research Reviews. 2007;56(2):384–402.
76. Dolan H, Crain B, Troncoso J, Resnick SM, Zonderman AB, Obrien RJ. Atherosclerosis, Dementia, and Alzheimer's Disease in the BLSA Cohort. Annals of Neurology. 2011;68(2):231–40.
77. Ritz K, Denswil NP, Stam OCG, Van Lieshout JJ, Daemen MJAP. Cause and mechanisms of intracranial atherosclerosis. Circulation. 2014;130(16):1407–14.
78. VanderLaan PA, Reardon CA, Getz GS. Site Specificity of Atherosclerosis: Site-Selective Responses to Atherosclerotic Modulators. Arteriosclerosis, Thrombosis, and Vascular Biology. 2004;24(1):12–22.
79. Torres N, Guevara-Cruz M, Velázquez-Villegas LA, Tovar AR. Nutrition and Atherosclerosis. Archives of Medical Research. 2015;46(5):408–26.
80. Mathieu P, Pibarot P, Després JP. Metabolic syndrome: The danger signal in atherosclerosis. Vascular Health and Risk Management. 2006;2(3):285–302.
81. Siasos G, Tsigkou V, Kokkou E, Oikonomou E, Vavuranakis M, Vlachopoulos C, et al. Smoking and Atherosclerosis: Mechanisms of Disease and New Therapeutic Approaches. Current Medicinal Chemistry. 2014;21(34):3936–48.
82. Zaheer M, Chrysostomou P, Papademetriou V. Hypertension and Atherosclerosis: Pathophysiology, Mechanisms and Benefits of BP Control. Hypertension and Cardiovascular Disease. 2016. 201–216 p.
83. Kovacic S, Bakran M. Genetic susceptibility to atherosclerosis. Stroke Research

and Treatment. 2012;2012:4–9.

84. Dede DS, Yavuz B, Yavuz BB, Cankurtaran M, Halil M, Ulger Z, et al. Assessment of endothelial function in Alzheimer's disease: Is Alzheimer's disease a vascular disease? Journal of the American Geriatrics Society. 2007;55(10):1613–7.
85. Iadecola C. Hypertension and dementia. Hypertension. 2014;64(1):3–5.
86. Zhao Y, Vanhoutte PM, Leung SWS. Vascular nitric oxide: Beyond eNOS. Journal of Pharmacological Sciences.. 2015;129(2):83–94.
87. Michel T, Vanhoutte PM. Cellular signaling and NO production. Pflugers Archiv European Journal of Physiology. 2010;459(6):807–16.
88. Zhou J, Li Y, Chien S. Shear stress-initiated signaling and its regulation of endothelial function. Arteriosclerosis, Thrombosis, and Vascular Biology. 2014;34(10):2191–8.
89. Brozovich F V., Nicholson CJ, Degen C V., Gao YZ, Aggarwal M, Morgan KG. Mechanisms of vascular smooth muscle contraction and the basis for pharmacologic treatment of smooth muscle disorders. Pharmacological Reviews. 2016;68(2):476–532.
90. Engin A. Endothelial Dysfunction in Obesity. Obesity and Liptoxicity. 2017. 345–379 p.
91. Doerries C, Grote K, Hilfiker-Kleiner D, Luchtefeld M, Schaefer A, Holland SM, et al. Critical role of the NAD(P)H oxidase subunit p47phox for left ventricular remodeling/dysfunction and survival after myocardial infarction. Circulation Research. 2007;100(6):894–903.
92. Wenzel P, Schuhmacher S, Kienhöfer J, Müller J, Hortmann M, Oelze M, et al. Manganese superoxide dismutase and aldehyde dehydrogenase deficiency increase mitochondrial oxidative stress and aggravate age-dependent vascular dysfunction. Cardiovascular Research. 2008;80(2):280–9.
93. Gryglewski RJ, Palmer RMJ, Moncada S. Superoxide anion is involved in the breakdown of endothelium-derived vascular relaxing factor. Nature. 1986;320(6061):454–6.
94. Gimbrone MA, Garcia-Cardena G. Endothelial Cell Dysfunction and the Pathobiology of Atherosclerosis. Circulation Research. 2016;118(4):620–36.

95. Zhang C, Hein TW, Wang W, Miller MW, Fossum TW, McDonald MM, et al. Upregulation of vascular arginase in hypertension decreases nitric oxide-mediated dilation of coronary arterioles. Hypertension. 2004;44(6):935–43.

96. Romero MJ, Platt DH, Tawfik HE, Labazi M, El-Remessy AB, Bartoli M, et al. Diabetes-induced Coronary Vascular Dysfunction Involves Increased Arginase Activity. Circulation Research. 2008;102(1):95–102.

97. Frey RS, Rahman A, Kefer JC, Minshall RD, Malik AB. PKCζ regulates TNF-α-induced activation of NADPH oxidase in endothelial cells. Circulation Research. 2002;90(9):1012–9.

98. Buckley DA, Cheng A, Kiely PA, Tremblay ML, O'Connor R. Regulation of Insulin-Like Growth Factor Type I (IGF-I) Receptor Kinase Activity by Protein Tyrosine Phosphatase 1B (PTP-1B) and Enhanced IGF-I-Mediated Suppression of Apoptosis and Motility in PTP-1B-Deficient Fibroblasts. Molecular and Cellular Biology. 2002;22(7):1998–2010.

99. Moreno JM, Gomez IR, Wangensteen R, Duarte J, Osuna A, Vargas F, et al. Mechanisms of Hydrogen Peroxide-Induced Vasoconstriction. 2010;(24):325–32.

100. Ruiz-Gines JA, Lopez-Ongil S, Gonzalez-Rubio M, Gonzalez-Santiago L, Rodriguez-Puyol M, Rodriguez-Puyol D. Reactive Oxygen Species Induce Proliferation of Bovine Aortic Endothelial Cells. 1999. p. 109–13.

101. Stauffer BL, Westby CM, DeSouza CA. Endotheln-1, aging, and hypertension. Current Opinion in Cardiology. 2008;23(4):350–5.

102. Liao JK. Linking endothelial dysfunction with endothelial cell activation Find the latest version : Linking endothelial dysfunction with endothelial cell activation. 2013;123(2):540–1.

103. Scalia R, Appel JZ, Lefer AM. Leukocyte-Endothelium Interaction During the Early Stages of Hypercholesterolemia in the Rabbit: Role of P-Selectin, ICAM-1, and VCAM-1. Arteriosclerosis, Thrombosis, and Vascular Biology. 1998;18(7):1093–100.

104. Naim Abu Nabah Y, Mateo T, Cerdá-Nicolás M, Álvarez Á, Martinez M, Issekutz AC, et al. L-NAME induces direct arteriolar leukocytes adhesion, which is mainly mediated by angiotensin-II. Microcirculation. 2005;12(5):443–53.

105. Qian J, Fulton DJR. Exogenous, but not endogenous nitric oxide inhibits adhesion molecule expression in human endothelial cells. Frontiers in Physiology. 2012;3 JAN(January):1–7.

106. Warboys CM, Amini N, De Luca A, Evans PC. The role of blood flow in determining the sites of atherosclerotic plaques. F1000 Medicine Reports. 2011;3(1):1–8.

107. Ponnuswamy P, Schröttle A, Ostermeier E, Grüner S, Huang PL, Ertl G, et al. ENOS protects from atherosclerosis despite relevant superoxide production by the enzyme in apoE -/- mice. PLoS ONE. 2012;7(1).

108. Reese TS, Karnovsky MJ. Fine structural localization of a blood-brain barrier to exogenous peroxidase. The Journal of cell biology. 1967;34(1):207–17.

109. Daneman R, Prat A. The Blood-Brain Barrier. Cold Spring Harbor Perspectives in Biology. 2015;7:a020412.

110. Chauhan B, Thaker G. The blood brain barrier and the cerebral blood flow: From basics to the bedside. Neurology Review Article. 2016;268–77.

111. Varatharaj A, Galea I. The blood-brain barrier in systemic inflammation. Brain, Behaviour, and Immunity. 2017;60(2):1–12.

112. Riddle DR, Sonntag WE, Lichtenwalner RJ. Mirovascular plasticity in aging. Ageing Research Reviews. 2003;2(2):149–68.

113. Gröschel K, Terborg C, Schnaudigel S, Ringer T, Riecker A, Witte OW, et al. Effects of physiological aging and cerebrovascular risk factors on the hemodynamic response to brain activation: A functional transcranial Doppler study. European Journal of Neurology. 2007;14(2):125–31.

114. Toda N. Age-related changes in endothelial function and blood flow regulation. Pharmacology & Therapeutics. 2012;133(2):159–76.

115. Davidson TL, Monnot A, Neal AU, Martin AA, Horton JJ, Zheng W. The effects of a high-energy diet on hippocampal-dependent discrimination performance and blood–brain barrier integrity differ for diet-induced obese and diet-resistant rats. Physiology & Behaviour. 2012;107(1):26–33.

116. Chehade JM, Haas MJ, Mooradian AD. Diabetes-related changes in rat cerebral occludin and zonula occludens-1 (ZO-1) expression. Neurochem Res. 2002;27(3):249–52.

117. Argaw AT, Gurfein BT, Zhang Y, Zameer A, John GR. VEGF-mediated disruption of endothelial CLN-5 promotes blood-brain barrier breakdown. Proceedings of the National Academy of Sciences of the United States of America. 2009;106(6):1977–82.

118. Sajja RK, Prasad S, Cucullo L. Impact of altered glycaemia on blood-brain barrier endothelium: An in vitro study using the hCMEC/D3 cell line. Fluids and Barriers of the CNS. 2014;11(1):1–14.

119. Yoo DY, Yim HS, Jung HY, Nam SM, Kim JW, Choi JH, et al. Chronic type 2 diabetes reduces the integrity of the blood-brain barrier by reducing tight junction proteins in the hippocampus. Journal of Veterinary Medical Science. 2016;78(6):957–62.

120. Xu Z, Zeng W, Sun J, Chen W, Zhang R, Yang Z, et al. The quantification of blood-brain barrier disruption using dynamic contrast-enhanced magnetic resonance imaging in aging rhesus monkeys with spontaneous type 2 diabetes mellitus. NeuroImage. 2017;158(1):480–7.

121. Hawkins BT, Lundeen TF, Norwood KM, Brooks HL, Egleton RD. Increased blood-brain barrier permeability and altered tight junctions in experimental diabetes in the rat: Contribution of hyperglycaemia and matrix metalloproteinases. Diabetologia. 2007;50(1):202–11.

122. Fujihara R, Chiba Y, Nakagawa T, Nishi N, Murakami R, Matsumoto K, et al. Albumin microvascular leakage in brains with diabetes mellitus. Microscopy research and technique. 2016;79(9):833–7.

123. Janeldize S, Hertze J, Nagga K, Nilsson K, Nilsson C, Wennstrom M, et al. Increased blood-brain barrier permeability is associated with dementia and diabetes but not amyloid pathology or APOE genotype. Neurobiol Aging. 2017;51(1):104–12.

124. Roy S, Bae E, Amin S, Kim D. Extracellular matrix, gap junctions, and retinal vascular homeostasis in daibetic retinopathy. Experimental Eye Research. 2015;133(1):58–68.

125. Roy S, Ha J, Trudeau K, Beglova E. Vascular Basement Membrane Thickening in Diabetic Retinopathy. Current Eye Research. 2010;35(12):1045–56.

126. Chronopoulos A, Trudeau L, Roy S, Haung H, Vinores SA, Roy S. High Glucose-induced Altered Basement Membrane Composition and Structure Increases

Trans-endothelial Permeability: Implications for Diabetic Retinopathy. Current Eye Research. 2011;36(8):747–53.

127. Doll DN, Hu H, Sun J, Lewis SE, Simpkins JW, Ren X. Mitochondrial Crisis in Cerebrovascular Endothelial Cells Opens the Blood-Brain Barrier. Stroke. 2015;46(6):1681–9.
128. Lobato NS, Filgueira FP, Akamine EH, Tostes RC, Carvalho MHC, Fortes ZB. Mechanisms of endothelial dysfunction in obesity-associated hypertension. Brazilian Journal of Medical and Biological Research. 2012;45(5):392–400.
129. De Boer MP, Meijer RI, Wijnstok NJ, Jonk AM, Houben AJ, Stehouwer CD, et al. Microvascular Dysfunction: A Potential Mechanism in the Pathogenesis of Obesity-associated Insulin Resistance and Hypertension. Microcirculation. 2012;19(1):5–18.
130. De Jongh RT, Serné EH, Ijzerman RG, De Vries G, Stehouwer CDA. Impaired microvascular function in obesity: Implications for obesity-associated microangiopathy, hypertension, and insulin resistance. Circulation. 2004;109(21):2529–35.
131. Agapitov A V., Correia MLG, Sinkey CA, Dopp JM, Haynes WG. Impaired skeletal muscle and skin microcirculatory function in human obesity. Journal of Hypertension. 2002;20(7):1401–5.
132. Yang J, Park Y, Zhang H, Xu X, Laine GA, Dellsperger KC, et al. Feed-forward signaling of TNF-α and NF-κB via IKK-β pathway contributes to insulin resistance and coronary arteriolar dysfunction in type 2 diabetic mice. American Journal of Physiology: Heart and Circulatory Physiology. 2009;296(6):1850–8.
133. Woodman RJ, Watts GF, Playford DA, Best JD, Chan CC. Oxidized LDL and small LDL particle size are independently predictive of a selective defect in microcirculatory endothelial function in type 2 diabetes. Diabetes, Obesity and Metabolism. 2005;7(5):612–7.
134. Okon EB, Chung AWY, Rauniyar P, Padilla E, Tejerina T, McManus BM, et al. Compromised arterial function in human type 2 diabetic patients. Diabetes. 2005;54(8):2415–23.
135. Di Carli MF, Janisse J, Grunberger G, Ager J. Role of chronic hyperglycemia in the

pathogenesis of coronary microvascular dysfunction in diabetes. Journal of the American College of Cardiology. 2003;41(8):1387–93.

136. Khalil Z, LoGiudice D, Khodr B, Maruff P, Masters C. Impaired Peripheral Endothelial Microvascular Responsiveness in Alzheimer's Disease. Journal of Alzheimer's Disease. 2007;11(1):25–32.
137. Borroni B, Volpi R, Martini G, Del Bono R, Archetti S, Colciaghi F, et al. Peripheral Blood Abnormalities in Alzheimer Disease: Evidence for Early Endothelial Dysfunction. Alzheimer Disease & Associated Disorders. 2002;16(3):150–5.
138. Noronha BT, Li J, Wheatcroft SB, Shah AM, Kearney MT. on Vascular and Metabolic Function in Obesity. Diabetes. 2005;54(1):1–8.
139. Sena CM, Pereira A, Fernandes R, Letra L, Seiça RM. Adiponectin improves endothelial function in mesenteric arteries of rats fed a high-fat diet: role of perivascular adipose tissue. British Journal of Pharmacology. 2017;174(20):3514–26.
140. Oishi JC, Castro CA, Silva KA, Fabricio V, Cárnio EC, Phillips SA, et al. Endothelial dysfunction and inflammation precedes elevations in blood pressure induced by a high-fat diet. Arquivos Brasileiros de Cardiologia. 2018;110(6):558–67.
141. Madkhali H. Morin attenuates high-fat diet induced-obesity related vascular endothelial dysfunction in Wistar albino rats. Saudi Pharmaceutical Journal. 2020;6(1):1–8.
142. Meakin PJ, Coull BM, Tuharska Z, McCaffery C, Akoumianakis I, Antoniades C, et al. Elevated circulating amyloid concentrations in obesity and diabetes promote vascular dysfunction. Journal of Clinical Investigation. 2020;
143. Wang CY, Liao JK. A mouse model of diet-induced obesity and insulin resistance. Methods in Molecular Biology. 2012;821(1):421–33.
144. Da Silva Rocha V, Goncąlves Claudio ER, Da Silva VL, Cordeiro JP, Domingos LF, Da Cunha MRH, et al. High-fat diet-induced obesity model does not promote endothelial dysfunction via increasing leptin/Akt/eNOS signaling. Frontiers in Physiology. 2019;10(1):1–10.
145. Belch JJF, Akbar N, Alapati V, Petrie J, Arthur S, Khan F. Longitidinal assessment of endothelial function in the microvasculature of mice in-vivo. Microvascular

Research. 2013;85:86/92.

146. Zuloaga KL, Johnson LA, Roese NE, Marzulla T, Zhang W, Nie X, et al. High fat diet-induced diabetes in mice exacerbates cognitive deficit due to chronic hypoperfusion. Journal of Cerebral Blood Flow and Metabolism. 2016;36(7):1257–70.

147. Bracko O, Vinarcsik LK, Cruz Hernández JC, Ruiz-Uribe NE, Haft-Javaherian M, Falkenhain K, et al. High fat diet worsens Alzheimer's disease-related behavioral abnormalities and neuropathology in APP/PS1 mice, but not by synergistically decreasing cerebral blood flow. Scientific Reports. 2020;10(1):1–16.

148. Haley MJ, Krishnan S, Burrows D, de Hoog L, Thakrar J, Schiessl I, et al. Acute high-fat feeding leads to disruptions in glucose homeostasis and worsens stroke outcome. Journal of Cerebral Blood Flow and Metabolism. 2019;39(6):1026–37.

149. Pétrault O, Pétrault M, Ouk T, Bordet R, Bérézowski V, Bastide M. Visceral adiposity links cerebrovascular dysfunction to cognitive impairment in middle-aged mice. Neurobiology of Disease. 2019;130(June):104536.

150. Tong XK, Trigiani LJ, Hamel E. High cholesterol triggers white matter alterations and cognitive deficits in a mouse model of cerebrovascular disease: benefits of simvastatin. Cell Death and Disease. 2019;10(2).

151. McGill HC, McMahan CA, Zieske AW, Malcom GT, Tracy RE, Strong JP. Effects of nonlipid risk factors on atherosclerosis in youth with a favorable lipoprotein profile. Circulation. 2001;103(11):1546–50.

152. Van Golen LW, Huisman MC, Ijzerman RG, Hoetjes NJ, Schwarte LA, Lammertsma AA, et al. Cerebral blood flow and glucose metabolism measured with positron emission tomography are decreased in human type 1 diabetes. Diabetes. 2013;62(8):2898–904.

153. Nacci C, Tarquinio M, De Benedictis L, Mauro A, Zigrino A, Carratù MR. J, et al. Endothelial Dysfunction in Mice with Streptozotocin-induced Type 1 Diabetes Is Opposed by Compensatory Overexpression of Cyclooxygenase-2 in the Vasculature. Endocrinology. 2009;150(2):849–61.

154. Xin R, An D, Li Y, Fu J, Huang F, Zhu Q. Fenofibrate improves vascular endothelial function in diabetic mice. Biomedicine and Pharmacotherapy.

2019;112(1):108722.

155. Ding H, Hashem M, Wiehler WB, Lau W, Martin J, Reid J, et al. Endothelial dysfunction in the streptozotocin-induced diabetic apoE-deficient mouse. British Journal of Pharmacology. 2005;146(8):1110–8.

156. Zhou C, Pridgen B, King N, Xu J, Breslow JL. Hyperglycemic Ins2AkitaLdlr-/- mice show severely elevated lipid levels and increased atherosclerosis: A model of type 1 diabetic macrovascular disease. Journal of Lipid Research. 2011;52(8):1483–93.

157. Awasthi H, Tota S., Hanif K, Chaniswar N, Shukla R. Protective effect of curcumin against intracerebral streptozotocin induced impairment in memory and cerebral blood flow. Life Sciences. 2010;86(3–4):87–94.

158. Nathan DM, Cleary PA, Backlund YC, Genuth SM, Lachin JM, Orchard TJ, et al. Intensive Diabetes Treatment and Cardiovascular Disease in Patients with Type 1 Diabetes. New England Journal of Medicine. 2005;353(25):2643–53.

159. Holman RR, Paul SK, Bethel MA, Matthews DR, Neil AW. 10-Year Follow-up of Intensive Glucose Control in Type 2 Diabetes. The New England Journal of Medicine. 2008;399(1):1577–89.

160. Patel A, MacMahon S, Chalmers J, Neal B, Billot L, Woodward M, et al. Intensive Blood Glucose Control and Vascular Outcomes in Patients with Type 2 Diabetes. The New England Journal of Medicine. 2008;358(1):2560–72.

161. C. HG, Miller ME, Byington R., Goff DC, Bigger JT, Buse JB, et al. Effects of Intensive Glucose Lowering in Type 2 Diabetes. The New England Journal of Medicine. 2008;358(24):2545–59.

162. Lee CH, Shieh YS, Hsiao FC, Kuo FC, Lin CY, Hsieh CH, et al. High glucose induces human endothelial dysfunction through an Axl-dependent mechanism. Cardiovascular Diabetology. 2014;13(1):1–13.

163. Chen YH, Lin SJ, Lin FY, Wu TC, Tsao CR, Huang PH, et al. High glucose impairs early and late endothelial progenitor cells by modifying nitric oxide-related but not oxidative stress-mediated mechanisms. Diabetes. 2007;56(6):1559–68.

164. Chen X, Duong MN, Psaltis PJ, Bursill CA, Nicholls SJ. High-density lipoproteins attenuate high glucose-impaired endothelial cell signaling and functions: Potential implications for improved vascular repair in diabetes. Cardiovascular

Diabetology. 2017;16(1):1–9.

165. Li G, Xu Y, Sheng X, Liu H, Guo J, Wang J, et al. Naringin Protects Against High Glucose-Induced Human Endothelial Cell Injury Via Antioxidation and CX3CL1 Downregulation. Cellular Physiology and Biochemistry. 2017;42(6):2540–51.
166. Joshi MS, Williams D, Horlock D, Samarasinghe T, Andrews KL, Jefferis AM, et al. Role of mitochondrial dysfunction in hyperglycaemia-induced coronary microvascular dysfunction: Protective role of resveratrol. Diabetes and Vascular Disease Research. 2015;12(3):208–16.
167. Han J, Mandal AK, Hiebert LM. Endothelial cell injury by high glucose and heparanase is prevented by insulin, heparin and basic fibroblast growth factor. Cardiovascular Diabetology. 2005;4:1–12.
168. Ho FM, Liu SH, Liau CS, Huang PJ, Lin-Shiau SY. High glucose-induced apoptosis in human endothelial cells is mediated by sequential activations of c-JUN NH2-terminal kinase and caspase-3. Circulation. 2000;101(22):2618–24.
169. Hempel A, Maasch C, Heintze U, Lindshcau C, Dietz R, Luft RC, et al. High Glucose Concentrations Increase Endothelial Cell Permeability via Activation of Protein Kinase Cα. Circulation Research. 1997;81(3):363–71.
170. Maeda M, Hayashi T, Mizuno N, Hattori Y, Kuzuya M. Intermittent high glucose implements stress-induced senescence in human vascular endothelial cells: Role of superoxide production by NADPH oxidase. PLoS ONE. 2015;10(4):1–14.
171. Shao B, Bayraktutan U. Hyperglycaemia promotes human brain microvascular endothelial cell apoptosis via induction of protein kinase C-βI and prooxidant enzyme NADPH oxidase. Redox Biology. 2014;2(1):694–701.
172. Li W, Maloney RE, Aw TY. High glucose, glucose fluctuation and carbonyl stress enhance brain microvascular endothelial barrier dysfunction: Implications for diabetic cerebral microvasculature. Redox Biology. 2015;5:80–90.
173. Jin H, Zhu Y, Li Y, Ding X, Ma W, Han X, et al. BDNF-mediated mitophagy alleviates high-glucose-induced brain microvascular endothelial cell injury. Apoptosis. 2019;24(5):511–28.
174. Rossi F, Grzeskowiak M, Della Bianca V, Sbarbati A. De novo synthesis of diacylglyverol from glucose. The Journal of Biological Chemistry.

1991;266(13):8034–8.

175. Koya D, King GL. Protein Kinase C Activation and the Development of Diabetic Complications. Diabetes. 1998;47(1):1998.

176. Cantero A, Portero-Otín M, Ayala V, Auge N, Sanson M, Elbaz M, et al. Methylglyoxal induces advanced glycation end product (AGEs) formation and dysfunction of PDGF receptor-β: implications for diabetic atherosclerosis. The FASEB Journal. 2007;21(12):3096–106.

177. Yan SD, Schmidt AM, Anderson GM, Zhang J, Brett J, Zou YS, et al. Enhanced Cellular Oxidant Stress by the Interaction of Advanced Glycation End Products with Their Receptors/Binding Proteins. Journal of Biological Chemistry. 1994;269(13):9889–97.

178. Ren X, Ren L, Wei Q, Shao H, Chen L, Liu . Advanced glycation end-products decreases expression of endothelial nitric oxide synthase through oxidative stress in human coronary artery endothelial cells. Cardiovascular Diabetology. 2017;16(1):1–12.

179. Tan KCB, Chow WS, Ai VHG, Metz C, Bucala R, Lam KSL. Advanced glycation end products and endothelial dysfunction in type 2 diabetes. Diabetes Care. 2002;25(6):1055–9.

180. da Costa RM, da Silva JF, Alves J V., Dias TB, Rassi DM, Garcia L V., et al. Increased O-GlcNAcylation of endothelial nitric oxide synthase compromises the anti-contractile properties of perivascular adipose tissue in metabolic syndrome. Frontiers in Physiology. 2018;9(APR):1–16.

181. Rajapakse AG, Ming XF, Carvas JM, Yang Z. O-linked β-N-acetylglucosamine during hyperglycemia exerts both anti-inflammatory and pro-oxidative properties in the endothelial system. Oxidative Medicine and Cellular Longevity. 2009;2(3):172–5.

182. Buse MG. Hexosamines, insulin resistance, and the complications of diabetes: Current status. American Journal of Physiology - Endocrinology and Metabolism. 2006;290(1):1–15.

183. Demiot C, Tartas M, Fromy B, Abraham . L., Sigaudo-Roussel D. Aldose reductase pathway inhibition improved vascular and C-fiber functions, allowing for pressure-induced vasodilation restoration during severe diabetic neuropathy.

Diabetes. 2006;55(5):1478–83.

184. Huang Z, Hong Q, Zhang X, Xiao W, Wang L, Cui S, et al. Aldose reductase mediates endothelial cell dysfunction induced by high uric acid concentrations. Cell Communication and Signaling. 2017;15(1):1–13.

185. Marchetti V, Menghini R, Rizza S, Vivanti A, Feccia T, Lauro D, et al. Benfotiamine counteracts glucose toxicity effects on endothelial progenitor cell differentiation via Akt/FoxO signaling. Diabetes. 2006;55(8):2231–7.

186. Bruce R, Godsland I, Walton C, Crook D, Wynn V. Associations between insulin sensitivity, and free fatty acid and triglyceride metabolism independent of uncomplicated obesity. Metabolism. 1994;43(1):1275–81.

187. Boden G. Obesity and FFAs. Endocrinology and Metabolism Clinics of North America. 2008;37(3):635.

188. Steinberg HO, Tarshoby M, Monestel R, Hook G, Cronin J, Johnson A, et al. Elevated circulating free fatty acid levels impair endothelium-dependent vasodilation. Journal of Clinical Investigation. 1997;100(5):1230–9.

189. Vaag A, Skott P, Damsbo P, Gall MA, Richter EA, Beck-Nielsen H. Effect of the antilipolytic nicotinic acid analogue acipimox on whole-body and skeletal muscle glucose metabolism in patients with non-insulin-dependent diabetes mellitus. Journal of Clinical Investigation. 1991;88(4):1282–90.

190. Oliviera AF, Cunha DA, Ladriere L, Igoillo-Esteve M, Bugliani M, Marchetti P, et al. In vitro use of free fatty acids bound to albumin: A comparison of protocols. BioFeedback. 2015;58(5):228–33.

191. Maloney E, Sweet IR, Hockenbery DM, Pham M, Rizzo NO, Tateya S, et al. Activation of NF-κB by Palmitate in Endothelial Cells: A Key Role for NADPH Oxidase-Derived Superoxide in Response to TLR4 Activation. Arteriosclerosis, Thrombosis, and Vascular Biology. 2009;29(9):1370–5.

192. Lee DM, Sevits KJ, Battson ML, Wei Y, Cox-York KA, Gentile CL. Monounsaturated fatty acids protect against palmitate-induced lipoapoptosis in human umbilical vein endothelial cells. PLoS ONE. 2019;14(12):1–18.

193. Kim JE, Kim YW, Lee IK, Kim JY, Kang YJ, Park SY. AMP-activated protein kinase activation by 5-aminoimidazole-4-carboxamide-1-beta-D-ribofuranoside (AICAR)

inhibits palmitate-induced endothelial cell apoptosis through reactive oxygen species suppression. Journal of Pharmacological Sciences. 2008;106(3):394–403.

194. Li X, Fang P, Li Y, Kuo YM, Andrews AJ, Nanayakkara G, et al. Mitochondrial reactive oxygen species mediate lysophosphatidylcholine-induced endothelial cell activation. Arteriosclerosis, Thrombosis, and Vascular Biology. 2016;36(6):1090–100.
195. Dymkowska D, Kawalec M, Wyszomirski T, Zablocki K. Mild palmitate treatment increases mitochondrial mass but does not affect EA.hy926 endothelial cells viability. Archives of Biochemistry and Biophysics. 2017;634(15):88–95.
196. Yamagishi S, Okamato T, Amano S, Inagaki Y, Koga K, Koga M, et al. Palmitate-Induced Apoptosis of Microvascular Endothelial Cells and Pericytes. Molecular Medicine. 2002;8(4):179–84.
197. Pillon NJ, Azizi PM, Li YE, Liu J, Wang C, Chan KL, et al. Palmitate-induced inflammatory pathways in human adipose microvascular endothelial cells promote monocyte adhesion and impair insulin transcytosis. American Journal of Physiology - Endocrinology and Metabolism. 2015;309(1):E35–44.
198. Broniarek I, Koziel A, Jarmuszkiewicz W. The effect of chronic exposure to high palmitic acid concentrations on the aerobic metabolism of human endothelial EA.hy926 cells. Pflugers Archiv European Journal of Physiology. 2016;468(9):1541–54.
199. Zhou H, Liu X, Liu L, Yang Z, Zhang S, Tang M, et al. Oxidative stress and apoptosis of human brain microvascular endothelial cells induced by free fatty acids. Journal of International Medical Research. 2009;37(6):1897–903.
200. Seppo L, Lähteenmäki T, Tikkanen MJ, Vanhanen H, Korpela R, Vapaatalo H. Effects of vitamin E on the toxicity of oxidized LDL on endothelial cells in vitro in smokers vs nonsmokers on diets rich in fish. European Journal of Clinical Nutrition. 2005;59(11):1282–90.
201. Magalhaes A, Matias I, Palmela I, Brito MA, Dias S. LDL-cholesterol increases the transcytosis of molecules through endothelial monolayers. PLoS ONE. 2016;11(10):1–11.
202. Alderson LM, Endemann G, Lindsey S, Pronczuk A, Hoover RL, Hayes KC. LDL

enhances monocyte adhesion to endothelial cells in vitro. American Journal of Pathology. 1986;123(2):334–42.

203. Xavier HT, Parra Abdalla DS, Da Rocha Martinez TL, Franchini Ramires JA, De Toledo Gagliardi AR. Effects of oxidized LDL on in vitro proliferation and spontaneous motility of human coronary artery endothelial cells. Arquivos Brasileiros de Cardiologia. 2004;83(6):488–97.
204. Oh ST, Park H, Yoon HJ, Yang SY. Long-Term Treatment of Native LDL Induces Senescence of Cultured Human Endothelial Cells. Oxidative Medicine and Cellular Longevity. 2017;2017.
205. Artwohl M, Graier WF, Roden M, Bischof M, Freudenthaler A, Waldhäus W, et al. Diabetic LDL triggers apoptosis in vascular endothelial cells. Diabetes. 2003;52(5):1240–7.
206. Chen M, Ren L, Meng Y, Shi L, Chen L, Yu B, et al. The protease inhibitor E64d improves ox-LDL-induced endothelial dysfunction in human aortic endothelial cells. Canadian Journal of Physiology and Pharmacology. 2018;96(2):120–7.
207. Zhong X, Zhang L, Li Y, Li P, Li J, Cheng G. Kaempferol alleviates ox-LDL-induced apoptosis by up-regulation of miR-26a-5p via inhibiting TLR4/NF-κB pathway in human endothelial cells. Biomedicine and Pharmacotherapy. 2018;108(July):1783–9.
208. Li S, Sun Y, Han Z, Bu X, Yu W, Wang J. Cytoprotective effects of euxanthone against ox-LDL-induced endothelial cell injury is mediated via Nrf2. Life Sciences. 2019;223(1):174–84.
209. Su Q, Sun Y, Ye Z, Yang H, Kong B, Li L. Pinocembrin protects endothelial cells from oxidized LDL-induced injury. Cytokine. 2018;111(1):475–80.
210. Cai L, Zhang X, Hou M, Gao F. Natural flavone tricetin suppresses oxidized LDL-induced endothelial inflammation mediated by Egr-1. International Immunopharmacology. 2020;80(2):106224.
211. Gonnissen S, Ptok J, Goy C, Jander K, Jakobs P, Eckermann O, et al. High concentration of low-density lipoprotein results in disturbances in mitochondrial transcription and functionality in endothelial cells. Oxidative Medicine and Cellular Longevity. 2019;2019.

212. Wang X, Mao R, Chen W. FSD-C10 shows therapeutic effects in suppressing oxidized low-density lipoprotein (Ox-LDL)-induced human brain microvascular endothelial cells apoptosis via rho-associated coiled-coil kinase (ROCK)/mitogen-activated protein kinase (MAPK) signaling. Medical Science Monitor. 2018;24:5509–16.

213. Pan Q, Liao X, Liu H, Wang Y, Chen Y, Zhao B, et al. MicroRNA-125a-5p alleviates the deleterious effects of ox-LDL on multiple functions of human brain microvessel endothelial cells. American Journal of Physiology - Cell Physiology. 2016;312(2):119–30.

214. Zhang Q, Liu C, Li Q, Li J, Wu Y, Liu J. MicroRNA-25–5p counteracts oxidized LDL-induced pathological changes by targeting neuronal growth regulator 1 (NEGR1) in human brain micro-vessel endothelial cells. Biochimie. 2019;165(1):141–9.

215. Liu S, Pan S, Tan J, Zhao W, Liu F. Oxytocin inhibits ox-LDL-induced adhesion of monocytic THP-1 cells to human brain microvascular endothelial cells. Toxicology and Applied Pharmacology. 2017;337(1):104–10.

216. Krützfeldt A, Sphar R, Mertens S, Siegmund B, Piper HM. Metabolism of exogenous substrates by coronary endothelial cells in culture. Journal of Molecular and Cellular Cardiology. 1990;22(12):1393–404.

217. Grynberg A, Demaison L. Fatty acid oxidation in the heart. Journal of Cardiovascular Pharmacology. 1996;28(1):11–7.

218. De Bock K, Georgiadou M, Schoors S, Kuchnio A, Wong BW, Cantelmo AR, et al. Role of PFKFB3-driven glycolysis in vessel sprouting. Cell. 2013;154(3):651–63.

219. Blouin A, Bolender RP, Weibel ER. Distribution of organelles and membranes between hepatocytes and nonhepatocytes in the rat liver parenchyma. A stereological study. Journal of Cell Biology. 1977;72(2):441–55.

220. Quintero M, Colombo SL, Godfrey A, Moncada S. Mitochondria as signaling organelles in the vascular endothelium. Proceedings of the National Academy of Sciences of the United States of America. 2006;103(14):5379–84.

221. Craige SM, Kant S, Keaney JF. Reactive Oxygen Species in Endothelial Function: From Disease to Adaptation. Circulation Journal. 2015;79(6):1145–55.

222. Hunt TK, Aslam RS, Beckert S, Wagner S, Ghani QP, Hussain MZ, et al. Aerobically

derived lactate stimulates revascularization and tissue repair via redox mechanisms. Antioxidants and Redox Signaling. 2007;9(8):1115–24.

223. Ruan GX, Kazlauskas A. Lactate engages receptor tyrosine kinases Axl, Tie2, and vascular endothelial growth factor receptor 2 to activate phosphoinositide 3-kinase/AKT and promote angiogenesis. Journal of Biological Chemistry. 2013;288(29):21161–72.
224. Parra-Bonilla G, Alvarez DF, Al-Mehdi A., Stevens T. Critical role for lactate dehydrogenase A in aerobic glycolysis that sustains pulmonary microvascular endothelial cell proliferation. American Journal of Physiology - Lung Cellular and Molecular Physiology. 2010;299(4):513–22.
225. Villegas JC, Broadwell RD. Transcytosis of protein through the mammalian cerebral epithelium and endothelium. II. Adsorptive transcytosis of WGA-HRP and the blood-brain and brain-blood barriers. Journal of Neurocytology. 1993;22(1):67–80.
226. Yu Q, Tao H, Wang X, Li M. Targeting brain microvascular endothelial cells: a therapeutic approach to neuroprotection against stroke. Neural Regeneration Research. 2015;10(11):1882–91.
227. Oldendorf WH, Cornford ME, Brown J. The large apparent work capability of the blood-brain barrier: A study of the mitochondrial content of capillary endothelial cells in brain and other tissues of the rat. Annals of Neurology. 1977;1(5):409–17.
228. Wang L, Fan H, He J, Wang L, Tian Z, Wang C. Protective effects of omega-3 fatty acids against Alzheimer's disease in rat brain endothelial cells. Brain and Behaviour. 2018;8(11):1–9.
229. Betley JN, Cao ZFH, Ritola KD, Sternson SM. Parallel, redundant circuit organization for homeostatic control of feeding behavior. Cell. 2013;155(6):1337–50.
230. Shi YC, Lau J, Lin Z, Zhang H, Zhai L, Sperk G, et al. Arcuate NPY controls sympathetic output and BAT function via a relay of tyrosine hydroxylase neurons in the PVN. Cell Metabolism. 2013;17(2):236–48.
231. Kim K, Choe HK. Role of hypothalamus in aging and its underlying cellular mechanisms. Mechanisms of Ageing and Development. 2019;177(April 2018):74–

9.

232. Mullier A, Bouret SG, Prevot V, Dehouck B. Differential distribution of tight junction proteins suggests a role for tanycytes in blood-hypothalamus barrier regulation in the adult mouse brain. J Comp Neurol. 2010;518(7):943/062.
233. Bennett L, Yang M, Enikolopov G, Iacovitti L. Circumventricular organs: A novel site of neural stem cells in the adult brain. Molecular and Cellular Neuroscience. 2009;41(3):337–47.
234. Kikusato M, Furukawa K, Toyomizu M. Roles of mitochondrial oxidative phosphorylation and reactive oxygen species generation in the metabolic modification of avian skeletal muscle Roles of mitochondrial oxidative phosphorylation and reactive oxygen species generation in the metabolic modific. Proceedings of the Japan Society for Animal Nutrition and Metabolism. 2016;60(2):57–67.
235. Jastroch M, Divakaruni AS, Mookerjee S, Treberg JR, Brand MD. Mitochondrial proton and electron leaks. Essays in Biochemistry. 2010;47:53–67.
236. Busiello RA, Savarese S, Lombardi A. Mitochondrial uncoupling proteins and energy metabolism. Frontiers in Physiology. 2015;6(36).
237. Gray MW. Mitochondrial evolution. Cold Spring Harbor Perspectives in Biology. 2012;4(9):1476–82.
238. Herst PM, Rowe MR, Carson GM, Berridge MV. Functional mitochondria in health and disease. Frontiers in Endocrinology. 2017;8(NOV).
239. Chan DC. Fusion and Fission: Interlinked Processes Critical for Mitochondrial Health. Annual Review of Genetics. 2012;46(1):265–87.
240. Ploumi C, Daskalaki I, Tavernarakis N. Mitochondrial biogenesis and clearance: a balancing act. FEBS Journal. 2017;284(2):183–95.
241. Srivastava S. The mitochondrial basis of aging and age-related disorders. Genes. 2017;8(12).
242. Breitzig MT, Alleyn MD, Lockey RF, Kolliputi N. A mitochondrial delicacy: dynamin-related protein 1 and mitochondrial dynamics. American Journal of Physiology - Cell Physiology. 2018;315(1):80–90.
243. Smirnova E, Griparic L, Shurland D-L, Van Der Bliek AM. Drp1 Is Required for

Mitochondrial Division in Mammalian Cells. Molecular Biology of the Cell. 2001;12(August):2245–56.

244. Fahrner JA, Liu R, Perry MS, Klein J, Chan DC. A Novel de novo Dominant Negative Mutation in DNM1L Impairs Mitochondrial Fission and Presents as Childhood Epileptic Encephalopathy. American Journal of Medical Genetics. 2016;170(8):2002–11.
245. Manczak M, Anekonda TS, Henson E, Park BS, Quinn J, Reddy PH. Mitochondria are a direct site of Aβ accumulation in Alzheimer's disease neurons: Implications for free radical generation and oxidative damage in disease progression. Human Molecular Genetics. 2006;15(9):1437–49.
246. Basu K, Lajoie D, Aumentado-Armstrong T, Chen J, Koning RI, Bossy B, et al. Molecular mechanism of DRP1 assembly studied in vitro by cryo-electron microscopy. PLoS ONE. 2017;12(6):1–21.
247. Del Dotto V, Mishra P, Vidoni S, Fogazza M, Maresca A, Caporali L, et al. OPA1 Isoforms in the Hierarchical Organization of Mitochondrial Functions. Cell Reports. 2017;19(12):2557–71.
248. Eura Y, Ishihara N, Yokota S, Mihara K. Two Mitofusin Proteins, Mammalian Homologues of FZO, with Distinct Functions Are Both Required for Mitochondrial Fusion. The Journal of Biochemistry. 2003;134(3).
249. Ishihara N, Eura Y, Mihara K. Mitofusin 1 and 2 play distinct roles in mitochondrial fusion reactions via GTPase activity. Journal of Cell Science. 2004;117(26):6535–46.
250. Z. S, Ghochani M, McCaffery JM, Frey TG, Chan DC. Mitofusins and OPA1 mediate sequential steps in mitochondrial membrane fusion. Molecular Biology of the Cell. 2009;20(15):3535–3532.
251. Liu X, Weaver D, Shirihai O, Hajnóczky G. Mitochondrial kiss-and-run: Interplay between mitochondrial motility and fusion-fission dynamics. EMBO Journal. 2009;28(20):3074–89.
252. Chen H, Chomyn A, Chan DC. Disruption of fusion results in mitochondrial heterogeneity and dysfunction. Journal of Biological Chemistry. 2005;280(28):26185–92.

253. Chen H, Vermulst M, Wang YE, Chomyn A, Prolla TA, McCaffery JM, et al. Mitochondrial fusion is required for mtdna stability in skeletal muscle and tolerance of mtDNA mutations. Cell. 2010;141(2):280–9.

254. Wanagat J, Cao Z, Pathare P, Aiken JM. Mitochondrial DNA deletion mutations colocalize with segmental electron transport system abnormalities, muscle fiber atrophy, fiber splitting, and oxidative damage in sarcopenia. FASEB Journal. 2001;15(2):322–32.

255. Chen H, McCaffery JM, Chan DC. Mitochondrial fusion protects against neurodegeneration in the cerebellum. Cell. 2007;130(1):548–62.

256. Chen Y, Liu Y, Dorn GWI. Mitochondrial fusion is essential for organelle function and cardiac homeostasis. Circulation Research. 2011;109(12):1327–31.

257. Frank S, Gaume B, Bergmann-Leitner ES, Leitner WW, Robert EG, Catez F, et al. The Role of Dynamin-Related Protein 1, a Mediator of Mitochondrial Fission, in Apoptosis. Developmental Cell. 2001;1(4):515–25.

258. Cassidy-Stone A, Chipuk JE, Ingerman E, Song C, Yoo C, Kuwana T, et al. Chemical Inhibition of the Mitochondrial Division Dynamin Reveals Its Role in Bax/Bak-Dependent Mitochondrial Outer Membrane Permeabilization. Developmental Cell. 2008;14(2):193–204.

259. Germain M, Mathai JP, McBride HM, Shore GC. Endoplasmic reticulum BIK initiates DRP1-regulated remodelling of mitochondrial cristae during apoptosis. EMBO Journal. 2005;24(8):1546–56.

260. Sugioka R, Shimizu S, Tsujimoto Y. Fzo1, a protein involved in mitochondrial fusion, inhibits apoptosis. Journal of Biological Chemistry. 2004;279(50):52726–34.

261. Shen T, Zheng M, Cao C, Chen C, Tang J, Zhang W, et al. Mitofusin-2 is a major determinant of oxidative stress-mediated heart muscle cell apoptosis. Journal of Biological Chemistry. 2007;282(32):23354–61.

262. Ishihara N, Nomura M, Jofuku A, Kato H, Suzuki SO, Masuda K, et al. Mitochondrial fission factor Drp1 is essential for embryonic development and synapse formation in mice. Nature Cell Biology. 2009;11(1):958–66.

263. Estaquier J, Arnoult D. Inhibiting Drp1-mediated mitochondrial fission selectively

prevents the release of cytochrome c during apoptosis. Cell Death and Differentiation. 2007;14(6):1086–94.

264. Parone PA, James DI, Da Cruz S, Mattenberger Y, Donze O, Barja F, et al. Inhibiting the Mitochondrial Fission Machinery Does Not Prevent Bax/Bak-Dependent Apoptosis. Molecular and Cellular Biology. 2006;26(20):7397–408.
265. Galgani JE, Moro C, Ravussin E. Metabolic flexibility and insulin resistance. American Journal of Physiology - Endocrinology and Metabolism. 2008;295(5):1009–17.
266. Kelley DE, Mandarino LJ. Fuel selection in human skeletal muscle in insulin resistance: A reexamination. Diabetes. 2000;49(5):677–83.
267. Wellen KE, Thompson CB. Cellular Metabolic Stress: Considering How Cells Respond to Nutrient Excess. Molecular Cell. 2010;40(2):323–32.
268. Boulange CL, Claus SP, Chou CJ, Collino S, Montoliu I, Kochhar S, et al. Early Metabolic Adaptation in C57BL/6 Mice Resistant to High Fat Diet Induced Weight Gain Involves an Activation of Mitochondrial Oxidative Pathways. Journal of Proteome Research. 2013;12(3):1956–68.
269. Kim H, Kim JH, Noh S, Hur HJ, Sung MJ, Hwang J, et al. Metabolomic Analysis of Livers and Serum from High-Fat Diet Induced Obese Mice. Journal of Proteome Research. 2011;10(2):722–31.
270. Penke M, Larsen PS, Schuster S, Dall M, Jensen BAH, Gorski T, et al. Hepatic NAD salvage pathway is enhanced in mice on a high-fat diet. 2015. 412AD;1(65–72).
271. Cantó C, Houtkooper RH, Pirinen E, Youn DY, Oosterveer MH, Cen Y, et al. The NAD+ precursor nicotinamide riboside enhances oxidative metabolism and protects against high-fat diet-induced obesity. Cell Metabolism. 2012;15(6):838–47.
272. Mollica MP, Iossa S, Liverini G, Soboll S. Steady state changes in mitochondrial electrical potential and proton gradient in perfused liver from rats fed a high fat diet. Molecular and Cellular Biochemistry. 1998;172(1–2):213–7.
273. Ruiz-Ramírez A, Chavez-Salgado M, Peñeda-Flores JA, Zapata E, Masso F, El-Hafidi M. High-sucrose diet increases ROS generation, FFA accumulation, UCP2 level, and proton leak in liver mitochondria. American Journal of Physiology -

Endocrinology and Metabolism. 2011;301(6):1198–207.

274. Zhu X, Xiao Z, Xu Y, Zhao X, Cheng P, Cui N, et al. Differential Impacts of Soybean and Fish Oils on Hepatocyte Lipid Droplet Accumulation and Endoplasmic Reticulum Stress in Primary Rabbit Hepatocytes. Gastroenterology Research and Practice. 2016;2016(Ld).

275. Bhaskaran S, Unnikrishnan A, Ranjit R, Qaiser R, Pharoah G, Matyi S, et al. A fish oil diet induces mitochondrial uncoupling and mitochondrial unfolded protein response in epididymal white adipose tissue of mice. Free Radical Biology and Medicine. 2017;108(1):704–14.

276. Lionetti L, Mollica MP, Donizzetti I, Gifuni G, Sica R, Pignalosa A, et al. High-lard and high-fish-oil diets differ in their effects on function and dynamic behaviour of rat hepatic mitochondria. PLoS ONE. 2014;9(3).

277. Nisr RB, Affourtit C. Palmitate-induced changes in energy demand cause reallocation of ATP supply in rat and human skeletal muscle cells. Biochimica et Biophysica Acta - Bioenergetics. 2016;1857(9):1403–11.

278. Nisr RB, Shah DS, Ganley IG, Hundal HS. Proinflammatory NFkB signalling promotes mitochondrial dysfunction in skeletal muscle in response to cellular fuel overloading. Cellular and Molecular Life Sciences. 2019;76(24):4887–

279. Sergi D, Morris AC, Kahn DE, McLean FH, Hay EA, MacKenzie A, et al. Palmitic acid triggers inflammatory responses in N42 cultured hypothalamic cells partially via ceramide synthesis but not via TLR4. Nutritional Neuroscience. 2020;23(4):321–34.

280. Koziel A, Woyda-Ploszczyca A, Kicinska A, Jarmuszkiewicz W. The influence of high glucose on the aerobic metabolism of endothelial EA.hy926 cells. Pflugers Archiv European Journal of Physiology. 2012;464(6):657–69.

281. Gomes LC, Benedetto GD, Scorrano L. During autophagy mitochondria elongate, are spared from degradation and sustain cell viability. Nature Cell Biology. 2011;13(5):589–98.

282. Molina AJA, Wikstrom JD, Stiles L, Las G, Mohamed H, Elorza A, et al. Mitochondrial networking protects β-cells from nutrient-induced apoptosis. Diabetes. 2009;58(10):2303–15.

283. Jheng HF, Tsai PJ, Guo SM, Kuo LH, Chang CS, Su IJ, et al. Mitochondrial Fission Contributes to Mitochondrial Dysfunction and Insulin Resistance in Skeletal Muscle. Molecular and Cellular Biology. 2012;32(2):309–19.

284. Smith ME, Tippetts TS, Brassfield ES, Tucker BJ, Ockey A, Swensen AC, et al. Mitochondrial fission mediates ceramide-induced metabolic disruption in skeletal muscle. Biochemical Journal. 2013;456(3):427–39.

285. Murphy MP. How mitochondria produce reactive oxygen species. Biochemical Journal. 2009;417(1):1–13.

286. Brand MD, Affourtit C, Esteves TC, Green K, Lambert AJ, Miwa S, et al. Mitochondrial superoxide: Production, biological effects, and activation of uncoupling proteins. Free Radical Biology and Medicine. 2004;37(6):755–67.

287. Scialò F, Fernández-Ayala DJ, Sanz A. Role of mitochondrial reverse electron transport in ROS signaling: Potential roles in health and disease. Frontiers in Physiology. 2017;8:1–7.

288. Cadenas S. Mitochondrial uncoupling, ROS generation and cardioprotection. Biochimica et Biophysica Acta - Bioenergetics. 2018;1859(9):940–50.

289. Dikalov SI, Nazarewicz RR, Bikineyeva A, Hilenski L, Lassègue B, Griendling KK, et al. Nox2-Induced production of mitochondrial Superoxide in Angiotensin ii-mediated endothelial oxidative stress and hypertension. Antioxidants and Redox Signaling. 2014;20(2):281–94.

290. Balteau M, Tajeddine N, De Meester C, Ginion A, Des Rosiers C, Brady NR, et al. NADPH oxidase activation by hyperglycaemia in cardiomyocytes is independent of glucose metabolism but requires SGLT1. Cardiovascular Research. 2011;92(2):237–46.

291. Vassar R, Bennett BD, Babu-Khan S, Kahn S, Mendiaz EA, Denis P, et al. β-Secretase cleavage of Alzheimer's amyloid precursor protein by the transmembrane aspartic protease BACE. Science. 1999;286(5440):735–41.

292. Vassar R, Kovacs DM, Yan R, Wong PC. The β-secretase enzyme BACE in health and Alzheimer's disease: Regulation, cell biology, function, and therapeutic potential. Journal of Neuroscience. 2009;29(41):12787–94.

293. Capell A, Steiner H, Willem M, Kaiser H, Meyer C, Walter J, et al. Maturation and

pro-peptide cleavage of β-secretase. Journal of Biological Chemistry. 2000;275(40):30849–54.

294. Hemming ML, Elias JE, Gygi SP, Selkoe DJ. Identification of β-secretase (BACE1) substrates using quantitative proteomics. PLoS ONE. 2009;4(12).
295. Von Arnim CAF, Kinoshita A, Peltan ID, Tangredi MM, Herl L, Lee BM, et al. The low density lipoprotein receptor-related protein (LRP) is a novel β-secretase (BACE1) substrate. Journal of Biological Chemistry. 2005;280(18):17777–85.
296. Hu X, Hicks CW, He W, Wong P, MacKlin WB, Trapp BD, et al. Bace1 modulates myelination in the central and peripheral nervous system. Nature Neuroscience. 2006;9(12):1520–5.
297. Lichtenthaler SF, Dominguez DI, Westmeyer GG, Reiss K, Haass C, Saftig P, et al. The cell adhesion protein P-selectin glycoprotein ligand-1 is a substrate for the aspartyl protease BACE1. Journal of Biological Chemistry. 2003;278(49):48713–9.
298. Wong HK, Sakurai T, Oyama F, Kaneko K, Wada K, Miyazaki H, et al. β subunits of voltage-gated sodium channels are novel substrates of β-site amyloid precursor protein-cleaving enzyme (BACE1) and γ-secretase. Journal of Biological Chemistry. 2005;280(24):23009–17.
299. Kuhn PH, Marjaux E, Imhof A, De Strooper B, Haass C, Lichtenthaler SF. Regulated intramembrane proteolysis of the interleukin-1 receptor II by α-, β-, and γ-secretase. Journal of Biological Chemistry. 2007;282(16):11982–95.
300. Meakin PJ, Mezzapesa A, Benabou E, Haas ME, Bonardo B, Grino M, et al. The beta secretase BACE1 regulates the expression of insulin receptor in the liver. Nature Communications. 2018;9(1306).
301. Zhang YW, Thompson R, Zhang H, Xu H. APP processing in Alzheimer's disease. Molecular Brain. 2011;4(1):3.
302. Jawhar S, Wirths O, Bayer TA. Pyroglutamate amyloid-β (Aβ): A hatchet man in alzheimer disease. Journal of Biological Chemistry. 2011;286(45):38825–32.
303. Mori H, Takio K, Ogawara M, Selkoe DJ. Mass spectrometry of purified amyloid β protein in Alzheimer's disease. Journal of Biological Chemistry. 1992;267(24):17082–6.
304. Fukumoto H, Rosene DL, Moss MB, Raju S, Hyman BT, Irizarry MC. β-Secretase

Activity Increases with Aging in Human, Monkey, and Mouse Brain. American Journal of Pathology. 2004;164(2):719–25.

305. Meakin PJ, Jalicy SM, Montagut G, Allsop DJP, Cavellini DL, Irvine SW, et al. Bace1-dependent amyloid processing regulates hypothalamic leptin sensitivity in obese mice. Scientific Reports. 2018;8(1).
306. Hamilton DL, Findlay JA, Montagut G, Meakin PJ, Bestow D, Jalicy SM, et al. Altered amyloid precursor protein processing regulates glucose uptake and oxidation in cultured rodent myotubes. Diabetologia. 2014;57(8):1684–92.
307. Botteri G, Salvado L, Guma A, Hamilton DL, Meakin PJ, Montagut G, et al. The BACE1 product sAPPβ induces ER stress and inflammation and impairs insulin signaling. Metabolism. 2018;85(1):59–75.
308. Meakin PJ, Jalicy SM, Montagut G, Allsop DJP, Cavellini DL, Irvine SW, et al. Bace1-dependent amyloid processing regulates hypothalamic leptin sensitivity in obese mice. Scientific Report. 2018;8(1):1–16.
309. Plucińska K, Dekeryte R, Koss D, Shearer K, Mody N, Whitfield PD, et al. Neuronal human BACE1 knockin induces systemic diabetes in mice. Diabetologia. 2016;59(7):1513–23.
310. Mody N, Agouni A, Mcilroy GD, Platt B, Delibegovic M. Susceptibility to diet-induced obesity and glucose intolerance in the APPSWE/PSEN1A246E mouse model of Alzheimer's disease is associated with increased brain levels of protein tyrosine phosphatase 1B (PTP1B) and retinol-binding protein 4 (RBP4), and basal. Diabetologia. 2011;54(8):2143–51.
311. Dekeryte R, Hull C, Plucinska K, Khan S, Kamli-Salino S, Mody N, et al. Effects of Liraglutide and Fenretinide treatments on the diabetic phenotype of neuronal human BACE1 knock-in mice. Biochemical Pharmacology. 2019;166(1):222–30.
312. Muche A, Arendt T, Schliebs R. Oxidative stress affects processing of amyloid precursor protein in vascular endothelial cells. PLoS ONE. 2017;12(6):1–15.
313. Salminen A, Kauppinen A, Kaarniranta K. Hypoxia/ischemia activate processing of Amyloid Precursor Protein: impact of vascular dysfunction in the pathogenesis of Alzheimer's disease. Journal of Neurochemistry. 2017;140(4):536–49.
314. Chami L, Checler F. BACE1 is at the crossroad of a toxic vicious cycle involving

cellular stress and β-amyloid production in Alzheimer's disease. Molecular neurodegeneration. 2012;7:1–15.

315. Jalicy SM. "The hypothalamic role of BACE1 in energy homeostasis." 2016.
316. Meakin PJ, Coull BM, Tuharska Z, McCaffery C, Akoumianakis I, Antoniades C, et al. Elevated circulating amyloid concentrations in obesity and diabetes promote vascular dysfunction. Journal of Clinical Investigation. 2020;In-Press P.
317. Meakin PJ, Harper AJ, Hamilton DL, Gallagher J, McNeilly AD, Burgess LA, et al. Reduction in BACE1 decreases body weight, protects against diet-induced obesity and enhances insulin sensitivity in mice. Biochemical Journal. 2012;441(1):285–95.
318. Sun R, He T, Pan Y, Katusic ZS. Effects of senescence and angiotensin II on expression and processing of amyloid precursor protein in human cerebral microvascular endothelial cells. Aging. 2018;10(1):100–14.
319. Devraj K, Poznanovic S, Spahn C, Schwall G, Harter PN, Mittelbronn M, et al. BACE-1 is expressed in the blood-brain barrier endothelium and is upregulated in a murine model of Alzheimer's disease. Journal of Cerebral Blood Flow and Metabolism. 2016;36(7):1281–94.
320. Niwa K, Younkin L, Ebeling C, Turner SK, Westaway D, Younkin S, et al. Aβ1-40-related reduction in functional hyperemia in mouse neocortex during somatosensory activation. Proceedings of the National Academy of Sciences of the United States of America. 2000;97(17):9735–40.
321. Niwa K, Porter VA, Kazama K, Cornfield D, Carlson GA, Iadecola C. Aβ-peptides enhance vasoconstriction in cerebral circulation. American Journal of Physiology - Heart and Circulatory Physiology. 2001;281(6):2417–24.
322. Park L, Anrather J, Zhou P, Frys K, Pitstick R, Younkin S, et al. NADPH oxidase-derived reactive oxygen species mediate the cerebrovascular dysfunction induced by the amyloid β peptide. Journal of Neuroscience. 2005;25(7):1769–77.
323. Niwa K, Kazama K, Younkin SG, Carlson GA, Iadecola C. Alterations in Cerebral Blood Flow and Glucose Utilization in Mice Overexpressing the Amyloid Precursor Protein. Neurobiology of Disease. 2002;9(1):61–8.
324. Park L, Koizumi K, El Jamal S, Zhou P, Preveti ML, Van Nostrand WE, et al. Age-

Dependent Neurovascular Dysfunction and Damage in a Mouse Model of Cerebral Amyloid Angiopathy. Stroke. 2014;45(6):1815–21.

325. Austin SA, Santhanam A V., Hinton DJ, Choi DS, Katusic ZS. Endothelial nitric oxide deficiency promotes Alzheimer's disease pathology. Journal of Neurochemistry. 2013;127(5):691–700.
326. Mouton-Liger F, Paquet C, Dumurgier J, Bouras C, Pradier L, Gray F, et al. Oxidative stress increases BACE1 protein levels through activation of the PKR-eIF2α pathway. Biochimica et Biophysica Acta - Molecular Basis of Disease. 2012;1822(6):885–96.
327. Ali MI, Chen X, Didion SP. Heterozygous eNOS deficiency is associated with oxidative stress and endothelial dysfunction in diet-induced obesity. Physiological Reports. 2015;3(12):1–13.
328. Suvorava T, Nagy N, Pick S, Lieven O, Rüther U, Dao VTV, et al. Impact of eNOS-Dependent Oxidative Stress on Endothelial Function and Neointima Formation. Antioxidants and Redox Signaling. 2015;23(9):711–23.
329. Devi L, Prabhu BM, Galati DF, Avadhani NG, Anandatheerthavarada HK. Accumulation of amyloid precursor protein in the mitochondrial import channels of human Alzheimer's disease brain is associated with mitochondrial dysfunction. Journal of Neuroscience. 2006;26(35):9057–68.
330. Lustbader JW, Cirilli M, Lin C, Xu HW, Takuma K, Wang N, et al. ABAD Directly Links Aβ to Mitochondrial Toxicity in Alzheimer's Disease. Science. 2004;304(5669):448–52.
331. Caspersen C, Wang N, Yao J, Sosunov A, Chen X, Lustbader JW, et al. Mitochondrial Aβ: a potential focal point for neuronal metabolic dysfunction in Alzheimer's disease. The FASEB Journal. 2005;19(14):2040–1.
332. Hauptmann S, Scherping I, Drose S, Brandt U, Schulz KL, Jendrach M, et al. Mitochondrial dysfunction: An early event in Alzheimer pathology accumulates with age in AD transgenic mice. Neurobiology of Aging. 2009;30(10):1574–86.
333. Keil U, Bonert A, Marques CA, Scherping I, Weyermann J, Strosznajder JB, et al. Amyloid β-induced changes in nitric oxide production and mitochondrial activity lead to apoptosis. Journal of Biological Chemistry. 2004;279(48):50310–20.

334. Wang X, Su B, Siedlak SL, Moreira PI, Fujioka H, Wang Y, et al. Amyloid-β overproduction causes abnormal mitochondrial dynamics via differential modulation of mitochondrial fission/fusion proteins. Proceedings of the National Academy of Sciences of the United States of America. 2008;105(49):19318–23.

335. Findlay JA, Hamilton DL, Ashford MLJ. BACE1 activity impairs neuronal glucose oxidation: Rescue by beta-hydroxybutyrate and lipoic acid. Frontiers in Cellular Neuroscience. 2015;9(OCT):1–14.

336. Solesio ME, Peixoto PM, Debure L, Madamba SM, de Leon MJ, Wisniewski T, et al. Carbonic anhydrase inhibition selectively prevents amyloid β neurovascular mitochondrial toxicity. Aging Cell. 2018;17(4).

337. Lenth R V. Post Hoc Power : Tables and Commentary. Department of Statistics and Actuarial Science. 2007;Technical Report No. 378.

338. Harrison SM, Harper AJ, Hawkins J, Duddy G, Grau E, Pugh PL, et al. BACE1 (beta-secretase) transgenic neurochernical deficits ind knockout mice: identification of and behavioral changes. Molecular and Cellular Neuroscience. 2003;24(3):646–55.

339. Hummel KP, Dickie MM, Coleman DL. Diabetes, a New Mutafton in the Mouse. Science. 1966;153(3740):1127–8.

340. Peng BY, Wang Q, Luo YH, He JF, Tan T, Zhu H. A novel and quick PCR-based method to genotype mice with a leptin receptor mutation (db/db mice). Acta Pharmacologica Sinica. 2018;39(1):117–23.

341. Van Dam D, D'Hooge R, Staufenbiel M, Van Ginneken C, Van Mier F, De Deyn PP. Age-dependent cognitive decline in the APP23 model precedes amyloid deposition. European Journal of Neuroscience. 2003;17(2):388–96.

342. Hickman DL, Swan M. Use of a body condition score technique to assess health status in a rat model of polycystic kidney disease. Journal of the American Association for Laboratory Animal Science. 2010;49(2):155–9.

343. Levy BI, Ambrosio G, Pries AR, Struijker-Boudier HAJ. Microcirculation in hypertension: A new target for treatment? Circulation. 2001;104(6):735–40.

344. Barstow TJ, Wong BJ. Commentary on Viewpoint: The human cutaneous circulation as a model of generalized microvascular function. Journal of Applied

Physiology. 2008;105(1):376.

345. Abularrage CJ, Sidawy AN, Aidinian G, Singh N, Weiswasser JM, Arora S. Evaluation of the microcirculation in vascular disease. Journal of Vascular Surgery. 2005;42(3):574–81.

346. Feng W, Liu S, Zhang C, Xia Q, Yu T, Zhu D. Comparison of cerebral and cutaneous microvascular dysfunction with the development of type 1 diabetes. Theranostics. 2019;9(20):5854–68.

347. Emanuel AL, van Duinkerken E, Wattjes MP, Klein M, Barkhof F, Snoek FJ, et al. The presence of cerebral white matter lesions and lower skin microvascular perfusion predicts lower cognitive performance in type 1 diabetes patients with retinopathy but not in healthy controls—A longitudinal study. Microcirculation. 2019;26(3):1–10.

348. Akbar N, Nanda S, Belch J, Cohen P, Khan F. An important role for A20-binding inhibitor of nuclear factor-kB-1 (ABIN1) in inflammation-mediated endothelial dysfunction: An in vivo study in ABIN1 (D485N) mice. Arthritis Research and Therapy. 2015;17(1):1–10.

349. Yousif S, Marie-Claire C, Roux F, Scherrmann JM, Declèves X. Expression of drug transporters at the blood-brain barrier using an optimized isolated rat brain microvessel strategy. Brain Research. 2007;1134(1):1–11.

350. Uhlen, M., Oksvold, P., Fagerbeg, L., Lundberg, E., Jonasson, K,. Forsberg, M., Zwaheln, M., Kampf, C., Wester, K., Hober, S., Wernerus, H., Björling, L., Ponten, F. Towards a knowledge-based Human Protein Atlas. Nature Biotechnology. 2010;28;1248-1250.

351. Regina A, Roux F, Revest PA. Glucose transport in immortalized rat brain capillary endothelial cells in vitro: Transport activity and GLUT1 expression. Biochimica et Biophysica Acta - General Subjects. 1997;1335(1–2):135–43.

352. Montesano R, Pepper MS, Möhle-Steinlein U, Risau W, Wagner F, Orci L. Increased Proteolytic Activity Is Responsible for the Aberrant Morphogenetic Behavior of Endothelial Cells Expressing the Middle T Oncogene. Cell. 1990;62(10):435–45.

353. Schmidt JA, Rinaldi S, Scalbert A, Ferrari P, Achaintre D, Gunter MJ, et al. Plasma

concentrations and intakes of amino acids in male meat-eaters, fish-eaters, vegetarians and vegans: A cross-sectional analysis in the EPIC-Oxford cohort. European Journal of Clinical Nutrition. 2016;70(3):306–12.

354. Gabriel J. Investigating the physiological function of BACE1 and its role in metabolism. 2020.
355. Haass C, Selkoe DJ. Soluble protein oligomers in neurodegeneration: Lessons from the Alzheimer's amyloid β-peptide. Nature Reviews Molecular Cell Biology. 2007;8(2):101–12.
356. Divakaruni AS, Paradyse A, Ferrick DA, Murphy AN, Jastroch M. Analysis and interpretation of microplate-based oxygen consumption and pH data. 1st ed. Vol. 547, Methods in Enzymology. Elsevier Inc.; 2014. 309–354 p.
357. Higashi Y, Maruhashi T, Noma K, Kihara Y. Oxidative stress and endothelial dysfunction: Clinical evidence and therapeutic implications. Trends in Cardiovascular Medicine. 2014;24(4):165–9.
358. Kuk JK, Saunders TJ, Davidson LE, Ross R. Age-related changes in total and regional fat distribution. Ageing Research Reviews. 2009;8(4):339–48.
359. Lutz W, Sanderson W, Scherbov S. The coming acceleration of global population ageing. Nature Letters. 2008;451(1):716–9.
360. Matz RL, Andriantsitohaina R. Age-related endothelial dysfunction: potential implications for pharmacotherapy. Drugs Aging. 2003;20(7):527–50.
361. Seals DR, Jablonski KL, Donato AJ. Aging and vascular endothelial function in humans. Clinical Science London. 120AD;9(357–375).
362. Taddei S, Virdis A, Mattei P, Ghiadoni L, Gennari A, Fasolo CB, et al. Aging and Endothelial Function in Normotensive Subjects and Patients With Essential Hypertension. Circulation. 1995;91(7):1981–7.
363. Taddei S, Virdis A, Ghiadoni L, Mattei P, Sudano I, Bernini G, et al. Menopause is associated with endothelial dysfunction in women. Circulation. 1996;28(4):576–82.
364. Gerhard M, Roddy M, Creager SJ, Creager MA. Aging Progressively Impairs Endothelium-Dependent Vasodilation in Forearm Resistance Vessels of Humans. Hypertension. 1996;27(4):849–53.

365. DeSouza CA, Shapiro LF, Clevenger CM, Dinenno FA, Monahan KD, Tanaka H, et al. Regular Aerobic Exercise Prevents and Restores Age-Related Declines in Endothelium-Dependent Vasodilation in Healthy Men. Circulatio. 2000;102(12):1351–7.

366. Fichtlscherer S, Breuer S, Zeiher AM. Prognostic Value of Systemic Endothelial Dysfunction in Patients With Acute Coronary Syndromes. Circulation. 2004;110(14):1926–32.

367. Celermajer DS, Sorensen KE, Spiegelhalter DJ, Georgakopoulos D, Robinson J, Deanfield JE. Aging is associated with endothelial dysfunction in healthy men years before the age-related decline in women. Journal of the American College of Cardiology. 1994;24(2):471–6.

368. Ma Q. Role of Nrf2 in oxidative stress and toxicity. Annual Review of Pharmacology and Toxicology. 2013;53(1):401–26.

369. Alfieri A, Srivastava S, Siow RCM, Modo M, Fraser PA, Mann GE. Targeting the Nrf2-Keap1 antioxidant defence pathway for neurovascular protection in stroke. Journal of Physiology. 2011;589(17):4125–36.

370. Kong X, Thimmulappa R, Craciun F, Harvey C, Singh A, Kombairaju P, et al. Enhancing Nrf2 pathway by disruption of Keap1 in myeloid leukocytes protects against sepsis. American Journal of Respiratory and Critical Care Medicine. 2011;184(8):928–38.

371. Della Vedova MC, Muñoz MD, Santillan LD, Plateo-Pignatari MG, Germanó MJ, Rinaldi Tosi ME, et al. A mouse model of diet-induced obesity resembling most features of human metabolic syndrome. Nutrition and Metabolic Insights. 2016;9:93–102.

372. Kobayashi K, Forte TM, Taniguchi S, Ishida BY, Oka K, Chan L. The db/db mouse, a model for diabetic dyslipidemia: Molecular characterization and effects of western diet feeding. Metabolism. 2000;49(1):22–31.

373. Bogdanov P, Corraliza L, Villena JA, Carvalho AR, Garcia-Arumí J, Ramos D, et al. The db/db mouse: A useful model for the study of diabetic retinal neurodegeneration. PLoS ONE. 2014;9(5).

374. Nguyen Dinh Cat A, Callera GE, Friederich-Persson M, Sanchez A, Dulak-Lis M,

Tsiropoulou S, et al. Vascular dysfunction in obese diabetic db/db mice involves the interplay between aldosterone/mineralocorticoid receptor and Rho kinase signaling. Scientific Reports. 2018;8(1):1–11. Available from: http://dx.doi.org/10.1038/s41598-018-21087-5

375. Kamper AM, de Craen AJM, Westendorp RGJ, Blauw GJ. Endothelium-dependent NO-mediated vasodilation in humans is attenuated by peripheral alpa1-adrenoceptor activation. Vascular health and risk management. 2005;1(3):251–6.
376. Kolluru GK, Bir SC, Kevil CG. Endothelial dysfunction and diabetes: Effects on angiogenesis, vascular remodeling, and wound healing. International Journal of Vascular Medicine. 2012;2012(Figure 1).
377. Böhm F, Pernow J. The importance of endothelin-1 for vascular dysfunction in cardiovascular disease. Cardiovascular Research. 2007;76(1):8–18.
378. Ge Z, Li Y, Qiao S, Bai X, Wartltier DC, Kersten JR, et al. Failure of isoflurane cardiac preconditioning in obese type 2 diabetic mice involves aberrant regulation of microRNA-21, endothelial nitric oxide synthase, and mitochondrial complex I Zhi-Dong. Anesth. 2018;128(1):117–29.
379. Solini A, Rossi C, Duranti E, Taddei S, Natali A, Virdis A. Saxagliptin prevents vascular remodeling and oxidative stress in db/db mice. Role of endothelial nitric oxide synthase uncoupling and cyclooxygenase. Vascular Pharmacology. 2015;76:62–71.
380. Han X, Tao Y, Deng Y, Yu J, Sun Y, Jiang G. Metformin accelerates wound healing in type 2 diabetic db/db mice. Molecular Medicine Reports. 2017;16(6):8691–8.
381. Lee AS, Lee YJ, Lee SM, Yoon JJ, Kim JS, Kang DG, et al. Portulaca oleracea ameliorates diabetic vascular inflammation and endothelial dysfunction in db/db mice. Evidence-based Complementary and Alternative Medicine. 2012;2012:1–9.
382. Dikalov SI, Harrison DG. Methods for detection of mitochondrial and cellular reactive oxygen species. Antioxidants and Redox Signaling. 2014;20(2):372–82.
383. Zhao H, Kalivendi S, Zhang H, Joseph J, Nithipatikom K, Vásquez-Vivar J, et al. Superoxide reacts with hydroethidine but forms a fluorescent product that is distinctly different from ethidium: Potential implications in intracellular

fluorescence detection of superoxide. Free Radical Biology and Medicine. 2003;34(11):1359–68.

384. Hayyan M, Hashim MA, Alnashef IM. Superoxide Ion: Generation and Chemical Implications. Chemical Reviews. 2016;116(5):3029–85.
385. Wang Q, Zou MH. Measurement of reactive oxygen species (ROS) and mitochondrial ROS in AMPK knockout mice blood vessels. Methods in Molecular Biology. 2018;1732:507–17.
386. Kauffman M, Kauffman M, Traore K, Zhu H, Trush M, Jia Z, et al. MitoSOX-Based Flow Cytometry for Detecting Mitochondrial ROS. Reactive Oxygen Species. 2016;2(5):361–70.
387. Amanso A, Lyle AN, Griendling KK. NADPH Oxidases and Measurement of Reactive Oxygen Species. Hypertension0. 2017;1527:219–32.
388. Grisham MB. Methods to detect hydrogen peroxide in living cells: Possibilities and pitfalls. Comparative Biochemistry and Physiology - A Molecular and Integrative Physiology. 2013;165(4):429–38.
389. Altun I, Oz F, Arkaya SC, Altun I, Bilge AK, Umman B, et al. Effect of Statins on Endothelial Function in Patients With Acute Coronary Syndrome: A Prospective Study Using Adhesion Molecules and Flow-Mediated Dilatation. Journal of Clinical Medicine Research. 2014;6(5):354–61.
390. Getz GS, Reardon CA. Do the Apoe-/- and the Ldlr-/- mice yield the same insight on atherogenesis? Arteriosclerosis, Thrombosis, and Vascular Biology. 2016;36(9):1734–41.
391. Constantinides C, Mean R, Janssen BJ. Effects of Isoflurane Anesthesia on the Cardiovascular Function of the C57BL/6 Mouse Christakis. ILAR Journal. 2011;52(1):e21–31.
392. Senador D, Kanakamedala K, Irigoyen MC, Morris M, Elased KM. Cardiovascular and autonomic phenotype of db/db diabetic mice. Experimental Physiology. 2009;94(6):648–58.
393. Son JM, Sarsour EH, Kakkerla Balaraju A, Fussell J, Kalen AL, Wagner BA, et al. Mitofusin 1 and optic atrophy 1 shift metabolism to mitochondrial respiration during aging. Aging Cell. 2017;16(5):1136–45.

394. Marzetti E, Calvani R, Cesari M, Buford TW, Lorenzi M, Behnke BJ, et al. Mitochondrial dysfunction and sarcopenia of aging: from signaling pathways to clinical trials. International Journal of Biochemistry and Cell Biology. 2013;45(10):2288–301.

395. Tezze C, Romanello V, Debats MA, Fadini GP, Albiero M, Favaro G, et al. Age-Associated Loss of OPA1 in Muscle Impacts Muscle Mass, Metabolic Homeostasis, Systemic Inflammation, and Epithelial Senescence. Cell Metabolism. 2017;25(6):1374–89.

396. Crane JD, Devries MC, Safdar A, Hamadeh MJ, Tarnopolsky MA. The effect of aging on human skeletal muscle mitochondrial and intramyocellular lipid ultrastructure. Journals of Gerontology - Series A Biological Sciences and Medical Sciences. 2010;65(2):119–28.

397. Sebastián D, Sorianello E, Segalés J, Irazoki A, Ruiz-Bonilla V, Sala D, et al. Mfn2 deficiency links age-related sarcopenia and impaired autophagy to activation of an adaptive mitophagy pathway. The EMBO Journal. 2016;35(15):1677–93.

398. Thai PN, Seidlmayer LK, Miller C, Ferrero M, Dorn GW, Schaefer S, et al. Mitochondrial quality control in aging and heart failure: Influence of ketone bodies and mitofusin-stabilizing peptides. Frontiers in Physiology. 2019;10(APR).

399. Lacroix S, Cantin J, Nigam A. Contemporary issues regarding nutrition in cardiovascular rehabilitation. Annals of Physical and Rehabilitation Medicine. 2017.

400. Leduc-Gaudet JP, Reynaud O, Chabot F, Mercier J, Andrich DE, St-Pierre DH, et al. The impact of a short-term high-fat diet on mitochondrial respiration, reactive oxygen species production, and dynamics in oxidative and glycolytic skeletal muscles of young rats. Physiological Reports. 2018;6(4).

401. Chen D, Li X, Zhang LT, Zhu M, Gao L. A high-fat diet impairs mitochondrial biogenesis, mitochondrial dynamics, and the respiratory chain complex in rat myocardial tissues. Journal of Cellular Biochemistry. 2018;119(11):9602.

402. Ruan XH, Ma T, Fan Y. Ablation of TMEM126B protects against heart injury via improving mitochondrial function in high fat diet (HFD)-induced mice. Biochemical and Biophysical Research Communications. 2019;515(4):636–43.

Available from:

403. Liesa M, Shirihai OS. Mitochondrial dynamics in the regulation of nutrient utilization and energy expenditure. Cell Metabolism. 2013;17(4):491–506.
404. Chang CR, Blackstone C. Dynamic regulation of mitochondrial fission through modification of the dynamin-related protein Drp1. Annals of the New York Academy of Sciences. 2010;1201:34–9.
405. Ko AR, Hyun HW, Min SJ, Kim JE. The differential DRP1 phosphorylation and mitochondrial dynamics in the regional specific astroglial death induced by status Epilepticus. Frontiers in Cellular Neuroscience. 2016;10(MAY):1–18.
406. Wang W, Wang Y, Long J, Wang J, Haudek SB, Overbeek P, et al. Mitochondrial fission triggered by hyperglycemia is mediated by ROCK1 activation in podocytes and endothelial cells. Cell Metabolism. 2012;15(2):186–200.
407. Han XJ, Lu YF, Li SA, Kaitsuka T, Sato Y, Tomizawa K, et al. CaM kinase Iα-induced phosphorylation of Drp1 regulates mitochondrial morphology. Journal of Cell Biology. 2008;182(3):573–85.
408. Kim H, Scimia MC, Wilkinson D, Trelles RD, Wood MR, Bowtell D, et al. Fine-Tuning of Drp1/Fis1 Availability by AKAP121/Siah2 Regulates Mitochondrial Adaptation to Hypoxia. Molecular Cell. 2011;44(4):532–44.
409. Zaja I, Bai X, Liu Y, Kikuchi C, Dosenovic S, Yan Y, et al. Cdk1, PKCδ and calcineurin-mediated Drp1 pathway contributes to mitochondrial fission-induced cardiomyocyte death. Biochemical and Biophysical Research Communications. 2014;453(4):710–21.
410. Hu Q, Zhang H, Gutiérrez Cortés N, Wu D, Wang P, Zhang J, et al. Increased Drp1 Acetylation by Lipid Overload Induces Cardiomyocyte Death and Heart Dysfunction. Circulation Research. 2020;126(4):456–70.
411. Del Dotto V, Fogazza M, Carelli V, Rugolo M, Zanna C. Eight human OPA1 isoforms, long and short: What are they for? Biochimica et Biophysica Acta - Bioenergetics. 2018;1859(4):263–9.
412. Liu R, Jin P, Yu L, Wang Y, Han L, Shi T, et al. Impaired mitochondrial dynamics and bioenergetics in diabetic skeletal muscle. PLoS ONE. 2014;9(3):1–8.
413. Cheng J, Nayakkara G, Shao Y, Cueto R, Wang L, Yang WY, et al. Mitochondrial

Proton Leak Plays a Critical Role in Pathogenesis of Cardiovascular Diseases Jiali. Advanced in Experimental Medicine and Biology. 2017;982(1):359–70.

414. Haileselassie B, Joshi AU, Minhas PS, Mukherjee R, Andreasson KI, Mochly-Rosen D. Mitochondrial dysfunction mediated through dynamin-related protein 1 (Drp1) propagates impairment in blood brain barrier in septic encephalopathy. Journal of Neuroinflammation. 2020;17(1):1–11.
415. Zhang T, Xu S, Wu P, Zhou K, Wu L, Xie Z, et al. Mitoquinone attenuates blood-brain barrier disruption through Nrf2/PHB2/OPA1 pathway after subarachnoid hemorrhage in rats. Experimental Neurology . 2019;317(December 2018):1–9.
416. Zhang T, Wu P, Zhang JH, Li Y, Xu S, Wang C, et al. Docosahexaenoic Acid Alleviates Oxidative Stress-Based Apoptosis Via Improving Mitochondrial Dynamics in Early Brain Injury After Subarachnoid Hemorrhage. Cellular and Molecular Neurobiology. 2018;38(7):1413–23.
417. Yang SB, Tien AC, Boddupalli G, Xu AW, Jan YN, Jan LY. Rapamycin ameliorates age-dependent obesity associated with increased mTOR signaling in hypothalamic POMC neurons. Neuron. 2012;75(3):425–36.
418. Li G, Zhang Y, Wilsey JT, Scarpace PJ. Hypothalamic pro-opiomelanocortin gene delivery ameliorates obesity and glucose intolerance in aged rats. Diabetologia. 2005;48(11):2376–85.
419. Kowalsi C, Micheau J, Corder R, Gaillard R, Conte-Devolx B. Age-related changes in cortico-releasing factor, somatostatin, neuropeptide Y, methionine enkephalin and β-endorphin in specific rat brain areas. Brain Research. 1992;582(1):38–46.
420. Wolden-Hanson T, Marck BT, Matsumoto AM. Blunted hypothalamic neuropeptide gene expression in response to fasting, but preservation of feeding responses to AgRP in aging male Brown Norway rats. American Journal of Physiology - Regulatory Integrative and Comparative Physiology. 2004;287(1 56-1):138–46.
421. Ma W, Yuan L, Yu H, Xi Y, Xiao R. Mitochondrial dysfunction and oxidative damage in the brain of diet-induced obese rats but not in diet-resistant rats. Life Sciences. 2014;110(2):53–60.
422. Diano S, Liu Z, Jeong JK, Dietrich MO, Ruan H, Kim E, et al. Peroxisome

proliferation–associated control of reactive oxygen species sets melanocortin tone and feeding in diet-induced obesity. Nature Medicine. 2011;17(1):1121–7.

423. Diano S. Role of Reactive Oxygen Species in Hypothalamic Regulation of Energy Metabolism. Endocrinology and Metabolism. 2013;28(1):3.
424. Andrews ZB, Liu ZW, Walllingford N, Erion DM, Borok E, Friedman JM, et al. UCP2 mediates ghrelin's action on NPY/AgRP neurons by lowering free radicals. Nature. 2008;454(7206):846–51.
425. Haissaguerre M, Ferrière A, Simon V, Saucisse N, Dupuy N, André C, et al. mTORC1-dependent increase in oxidative metabolism in POMC neurons regulates food intake and action of leptin. Molecular Metabolism-2018;12(April):98–106.
426. Schneeberger M, Dietrich MO, Sebastián D, Imbernón M, Castaño C, Garcia A, et al. Mitofusin 2 in POMC neurons connects ER stress with leptin resistance and energy imbalance. Cell. 2013;155(1):172–87.
427. Dietrich MO, Liu ZW, Horvath TL. XMitochondrial dynamics controlled by mitofusins regulate agrp neuronal activity and diet-induced obesity. Cell. 2013;155(1):188.
428. Chhabria K, Chakravarthy VS. Modulation of neural firing through intracellular ATP dynamics governed by energy feedback from the vascular system. BMC Neuroscience. 2015;16(S1):1–2.
429. Erion KA, Corkey BE. Hyperinsulinemia: a Cause of Obesity? Current obesity reports. 2017;6(2):178–86.
430. Myers MG, Leibel RL, Seeley RJ, Schwartz MW. Obesity and leptin resistance: Distinguishing cause from effect. Trends in Endocrinology and Metabolism. 2010;21(11):643–51.
431. Shiiya T, Nakazato M, Mizuta M, Date Y, Mondal MS, Tanaka M, et al. Plasma ghrelin levels in lean and obese humans and the effect of glucose on ghrelin secretion. Journal of Clinical Endocrinology and Metabolism. 2002;87(1):240–4.
432. Varela L, Horvath TL. Leptin and insulin pathways in POMC and AgRP neurons that modulate energy balance and glucose homeostasis. EMBO Reports.2012;13(12):1079–86.

433. Lin H V., Plum L, Ono H, Gutiérrez-Juárez R, Shanabrough M, Borok E, et al. Divergent regulation of energy expenditure and hepatic glucose production by insulin receptor in agouti-related protein and POMC neurons. Diabetes. 2010;59(2):337–46.

434. Cowley MA, Smith RG, Diano S, Tschöp M, Pronchuk N, Grove KL, et al. The distribution and mechanism of action of ghrelin in the CNS demonstrates a novel hypothalamic circuit regulating energy homeostasis. Neuron. 2003;37(4):649–61.

435. Zhang Z, Wakabayashi N, Wakabayashi J, Tamura Y, Song WJ, Sereda S, et al. The dynamin-related GTPase Opa1 is required for glucose-stimulated ATP production in pancreatic beta cells. Molecular Biology of the Cell. 2011;22(13):2235–45.

436. Millet AMC, Bertholet AM, Daloyau M, Reynier P, Galinier A, Devin A, et al. Loss of functional OPA1 unbalances redox state: Implications in dominant optic atrophy pathogenesis. Annals of Clinical and Translational Neurology. 2016;3(6):408–21.

437. Yu T, Sheu S, Robotham J, Yoon Y. Mitochondrial fission mediates high glucose-induced cell death through elevated production of reactive oxygen species. Cardiovascular Research. 2008;79(2):341–51.

438. Yu T, Robotham JL, Yoon Y. Increased production of reactive oxygen species in hyperglycemic conditions requires dynamic change of mitochondrial morphology. Proceedings of the National Academy of Sciences of the United States of America. 2006;103(8):2653–8.

439. Huang S, Wang Y, Gan X, Fang D, Zhong C, Wu L, et al. Drp1-mediated mitochondrial abnormalities link to synaptic injury in diabetes model. Diabetes. 2015;64(5):1728–42.

440. Douglass JD, Dorfman MD, Thaler JP. Glia: silent partners in energy homeostasis and obesity pathogenesis. Diabetologia. 2017;60(2):226–36.

441. Song W, Zhang CL, Gou L, He L, Gong YY, Qu D, et al. Endothelial TFEB (Transcription Factor EB) Restrains IKK (IκB Kinase)-p65 Pathway to Attenuate Vascular Inflammation in Diabetic db/db Mice. Arteriosclerosis, thrombosis, and vascular biology. 2019;39(4):719–30.

442. Li W, Ma N, Liu M xin, Ye B jie, Li Y jun, Hu H yao, et al. C1q/TNF-related protein-

9 attenuates retinal inflammation and protects blood–retinal barrier in db/db mice. European Journal of Pharmacology. 2019;853(December 2018):289–98.

443. Xu YH, Gao CL, Guo HL, Zhang WQ, Huang W, Tang SS, et al. Sodium butyrate supplementation ameliorates diabetic inflammation in db/db mice. Journal of Endocrinology. 2018;238(3):231–44.

444. Maffei M, Fei H, Lee G, Danit C, Leroyt P, Zhang Y, et al. Increased expression in adipocytes of ob RNA in mice with lesions of the hypothalamus and with mutations at the db locus. Proceedings of the National Academy of Sciences of the United States of America. 1995;92(7):6957–60.

445. Toshinai K, Mondal MS, Nakazato M, Date Y, Murakami N, Kojima M, et al. Upregulation of ghrelin expression in the stomach upon fasting, insulin-induced hypoglycemia, and leptin administration. Biochemical and Biophysical Research Communications. 2001;281(5):1220–5.

446. Meakin PJ, McCaffery C, Tuharksa Z, Khan F, Ashford MLJ. Beta-amyloid promotes diabetes-likevascular dysfunction in mice. Diabetes Medicine: Abstracts of the Diabetes UK Professional Conference. 2017;34(1):84–84.

447. Schuler B, Rettich A, Vogel J, Gassmann M, Arras M. Optimized surgical techniques and postoperative care improve survival rates and permit accurate telemetric recording in exercising mice. BMC Veterinary Research. 2009;5.

448. McGowan E, Pickford F, Kim J, Onstead L, Eriksen J, Yu C, et al. McGowan et al., 2005 NIH Aβ42 Is Essential for Parenchymal and Vascular Amyloid Deposition in Mice.pdf. Neuron. 2006;47(2):191–9.

449. Wirths O, Breyhan H, Cynis H, Schilling S, Demuth HU, Bayer TA. Intraneuronal pyroglutamate-Abeta 3-42 triggers neurodegeneration and lethal neurological deficits in a transgenic mouse model. Acta Neuropathologica. 2009;118(4):487–96.

450. Camandola S. Astrocytes, emerging stars of energy homeostasis. Cell Stress. 2018;2(10):246–52.

451. Sheng Y, Zhu L. The crosstalk between autonomic nervous system and blood vessels. International journal of physiology, pathophysiology and pharmacology. 2018;10(1):17–28.

452. Balligand JL, Kelly RA, Marsden PA, Smith TW, Michel T. Control of cardiac muscle cell function by an endogenous nitric oxide signaling system. Proceedings of the National Academy of Sciences of the United States of America. 1993;90(1):347–51.

453. Ferro A, Queen LR, Priest RM, Xu B, Ritter JM, Poston L, et al. Activation of nitric oxide synthase by β2-adrenoceptors in human umbilical vein endothelium in vitro. British Journal of Pharmacology. 1999;126(8):1872–80.

454. Balligand JL. Regulation of cardiac β-adrenergic response by nitric oxide. Cardiovascular Research. 1999;43(3):607–20.

455. Muszkat M, Kurnik D, Sofowora GG, Wood AJJ, Stein M. Independent regulation of α1 and α2 adrenergic receptor-mediated vasoconstriction in vivo. Journal of Hypertension. 2012;29(2):251–6.

456. Morris SJ, Shore AC. Skin blood flow responses to the iontophoresis of acetylcholine and sodium nitroprusside in man: Possible mechanisms. Journal of Physiology. 1996;496(2):531–42.

457. Deane R, Bell R, Sagare A, Zlokovic B. Clearance of amyloid-B peptide across the blood-brain barrier: implication for therapies in Alzheimers disease. CNS & Neurological Disorders - Drug Targets. 2009;8(1):16–30.

458. Iwata N, Higuchi M, Saido TC. Metabolism of amyloid-β peptide and Alzheimer's disease. Pharmacology and Therapeutics. 2005;108(2):129–48.

459. Gentile MT, Vecchione C, Maffei A, Aretini A, Marino G, Poulet R, et al. Mechanisms of soluble β-amyloid impairment of endothelial function. Journal of Biological Chemistry. 2004;279(46):48135–42.

460. Suhara T, Magrané J, Rosen K, Christensen R, Kim HS, Zheng B, et al. Aβ42 generation is toxic to endothelial cells and inhibits eNOS function through an Akt/GSK-3β signaling-dependent mechanism. Neurobiology of Aging. 2003;24(3):437–51.

461. Lamoke F, Mazzone V, Persichini T, Maraschi A, Harris BM, Venema RC, et al. Amyloid β peptide-induced inhibition of endothelial nitric oxide production involves oxidative stress-mediated constitutive eNOS/HSP90 interaction and disruption of agonist-mediated Akt activation. Journal of Neuroinflammation.

2015;12(1):1–14.

462. Sigfridsson E, Marangoni M, Johnson JA, Hardingham GE, Fowler JH, Horsburgh K. Astrocyte-specific overexpression of Nrf2 protects against optic tract damage and behavioural alterations in a mouse model of cerebral hypoperfusion. Scientific Reports. 2018;8(1):1–14.

463. Aubdool AA, Kodji X, Abdul-Kader N, Heads R, Fernandes ES, Bevan S, et al. TRPA1 activation leads to neurogenic vasodilatation: involvement of reactive oxygen nitrogen species in addition to CGRP and NO. British Journal of Pharmacology. 2016;(2):2419–33.

464. Sturchler-Pierrat C, Abramowski D, Duke M, Wiederhold KH, Mistl C, Rothacher S, et al. Two amyloid precursor protein transgenic mouse models with Alzheimer disease-like pathology. Proceedings of the National Academy of Sciences of the United States of America. 1997;94(24):13287–92.

465. Maia LF, Keeser SA, Reichwald J, Hruscha M, Martus P, Staufenbiel M, et al. Changes in amyloid-β and Tau in the cerebrospinal fluid of transgenic mice overexpressing amyloid precursor protein. Science Translational Medicine. 2013;5(194):194re2.

466. Park L, Zhou P, Koizumi K, El Jamal S, Previti M Lou, Van Nostrand WE, et al. Brain and circulating levels of Aβ1-40 differentially contribute to vasomotor dysfunction in the mouse brain. Stroke. 2013;44(1):198–204.

467. Dietrich HH, Xiang C, Han BH, Zipfel GJ, Holtzman DM. Soluble amyloid-β, effect on cerebral arteriolar regulation and vascular cells. Molecular Neurodegeneration. 2010;5(1):17–9.

468. Thomas T, Thomas G, McLendon C, Sutton T, Mullan M. β-Amyloid-mediated vasoactivity and vascular endothelial damage. Nature. 1996;380(6570):168–71.

469. Palmer JC, Barker R, Kehoe PG, Love S. Endothelin-1 is Elevated in Alzheimer's Disease and Upregulated by Amyloid-β. Journal of Alzheimer's Disease. 2012;29(4):853–61.

470. Palmer JC, Tayler HM, Love S. Endothelin-Converting Enzyme-1 Activity, Endothelin-1 Production, and Free Radical-Dependent Vasoconstriction in Alzheimer's Disease. Journal of Alzheimer's Disease. 2013;36(3):577–87.

471. Rybka V, Suzuki YJ, Gavrish AS, Dibrova VA, Gychka SG, Shults N V. Transmission electron microscopy study of mitochondria in aging brain synapses. Antioxidants. 2019;8(6).

472. Sorvina A, Bader CA, Darby JRT, Lock MC, Soo JY, Johnson IRD, et al. Mitochondrial imaging in live or fixed tissues using a luminescent iridium complex. Scientific Reports. 2018;8(1):1–8.

473. Lo KK. Luminescent Rhenium(I) and Iridium(III) Polypyridine Complexes as Biological Probes, Imaging Reagents, and Photocytotoxic Agents. Accounts of Chemical Research. 2015;48(12):2985–95.

474. Jendrach M, Mai S, Pohl S, Vöth M, Bereiter-Hahn J. Short- and long-term alterations of mitochondrial morphology, dynamics and mtDNA after transient oxidative stress. Mitochondrion. 2008;8(4):293–304.

475. Paltauf-Doburzynska J, Malli R, Graier WF. Hyperglycemic conditions affect shape and Ca2+ homeostasis of mitochondria in endothelial cells. Journal of Cardiovascular Pharmacology. 2004;44(4):423–36.

476. Shenouda SM, Widlansky ME, Chen K, Xu G, Holbrook M, Tabit CE, et al. Altered mitochondrial dynamics contributes to endothelial dysfunction in diabetes mellitus. Circulation. 2011;124(4):444–53.

477. Giedt RJ, Yang C, Zweier JL, Matzavinos A, Alevriadou BR. Mitochondrial fission in endothelial cells after simulated ischemia/reperfusion: Role of nitric oxide and reactive oxygen species. Free Radical Biology and Medicine. 2012;52(2):348–56.

478. Lugus JJ, Ngoh GA, Bachschmid MM, Walsh K. Mitofusins are required for angiogenic function and modulate different signaling pathways in cultured endothelial cells. Journal of Molecular and Cellular Cardiology. 2011;51(6):885–93.

479. Paul M Carvey, Bill Hendey AJM. The Blood Brain Barrier in Neurodegenerative Disease: A. Journal Neurochemistry. 2009;111(2):291–314.

480. Kis B, Szabó CA, Pataricza J, Krizbai IA, Mezei Z, Gecse Á, et al. Vasoactive substances produced by cultured rat brain endothelial cells. European Journal of Pharmacology. 1999;368(1):35–42.

481. Niwa K, Younkin L, Ebeling C, Turner SK, Westaway D, Younkin S, et al. Aβ1-40-

related reduction in functional hyperemia in mouse neocortex during somatosensory activation. Proceedings of the National Academy of Sciences of the United States of America. 2000;97(17):9735–40.

482. Bevers LM, Braam B, Post JA, Van Zonneveld AJ, Rabelink TJ, Koomans HA, et al. Tetrahydrobiopterin, but not L-arginine, decreases NO synthase uncoupling in cells expressing high levels of endothelial NO synthase. Hypertension. 2006;47(1):87–94.

483. Correia SC, Santos RX, Cardoso SM, Santos MS, Oliveira CR, Moreira PI. Cyanide preconditioning protects brain endothelial and NT2 neuron-like cells against glucotoxicity: Role of mitochondrial reactive oxygen species and HIF-1α. Neurobiology of Disease. 2012;45(1):206–18.

484. Ku JM, Taher M, Chin KY, Grace M, McIntyre P, Miller AA. Characterisation of a mouse cerebral microvascular endothelial cell line (bEnd.3) after oxygen glucose deprivation and reoxygenation. Clinical Experimental Pharmacology and Physiology. 2016;43:777–86.

485. Watanabe T, Dohgu S, Takata F, Nishioku T, Nakashima A, Futagami K, et al. Paracellular barrier and tight junction protein expression in the immortalized brain endothelial cell lines bend.3, bend.5 and mouse brain endothelial cell 4. Biological and Pharmaceutical Bulletin. 2013;36(3):492–5.

486. Hu H, N. Doll D, Sun J, E. Lewis S, H. Wimsatt J, J. Kessler M, et al. Mitochondrial Impairment in Cerebrovascular Endothelial Cells is Involved in the Correlation between Body Temperature and Stroke Severity. Aging and Disease. 2016;7(1):14.

487. Sanadgol N, Mostafaie A, Mansouri K, Bahrami G. Effect of palmitic acid and linoleic acid on expression of ICAM-1 and VCAM-1 in human bone marrow endothelial cells (HBMECs). Archives of Medical Science. 2012;8(2):192–8.

488. Sathanoori R, Swärd K, Olde B, Erlinge D. The ATP receptors P2X7 and P2X4 modulate high glucose and palmitate-induced inflammatory responses in endothelial cells. PLoS ONE. 2015;10(5):1–24.

489. Johnson RH, Kho DT, O'Carroll SJ, Angel CE, Graham ES. The functional and inflammatory response of brain endothelial cells to Toll-Like Receptor agonists.

Scientific Reports. 2018;8(1):1–12.

490. Chai Q, He WQ, Zhou M, Lu H, Fu ZF. Enhancement of Blood-Brain Barrier Permeability and Reduction of Tight Junction Protein Expression Are Modulated by Chemokines/Cytokines Induced by Rabies Virus Infection. Journal of Virology. 2014;88(9):4698–710.
491. Yilmaz G, Granger DN. Leukocyte Recruitment and Ischemic Brain Injury Gokhan. Neuromolecular Medicine. 2010;12(2):193–204.
492. Senn JJ. Toll-like receptor-2 is essential for the development of palmitate-induced insulin resistance in myotubes. Journal of Biological Chemistry. 2006;281(37):26865–75.
493. Green CJ, Macrae K, Fogarty S, Hardie G, Sakamoto K, Hundal HS. Counter-modulation of fatty acid-induced pro-inflammatory nuclear factor κB signalling in rat skeletal muscle cells by AMP-activated protein kinase. Biochemical Journal. 2011;435(2):463–74.
494. Maloney E, Sweet IR. Activation of NF-κB by Palmitate in Endothelial Cells: A Key Role for NADPH Oxidase-Derived Superoxide in Response to TLR4 Activation Ezekiel. Bone. 2010;23(1):1–7.
495. Håversen L, Danielsson KN, Fogelstrand L, Wiklund O. Induction of proinflammatory cytokines by long-chain saturated fatty acids in human macrophages. Atherosclerosis. 2009;202(2):382–93.
496. Arciuch VGA, Elguero ME, Poderoso JJ, Carreras MC. Mitochondrial regulation of cell cycle and proliferation. Antioxidants and Redox Signaling. 2012;16(10):1150–80.
497. Chang Y, Li Y, Ye N, Guo X, Li Z, Sun G, et al. Atorvastatin protects the proliferative ability of human umbilical vein endothelial cells inhibited by angiotensin II by changing mitochondrial energy metabolism. International Journal of Molecular Medicine. 2018;41(1):33–42.
498. Yetkin-Arik B, Vogels IMC, Neyazi N, van Duinen V, Houtkooper RH, van Noorden CJF, et al. Endothelial tip cells in vitro are less glycolytic and have a more flexible response to metabolic stress than non-tip cells. Scientific Reports. 2019;9(1):1–17.

499. Brookes PS, Rolfe DFS, Brand MD. The Proton Permeability of Liposomes Made from Mitochondrial Inner Membrane Phospholipids: Comparison with Isolated Mitochondria. The Journal of Membrane Biology. 1997;155(1):167–74.

500. Brand MD, Pakay JL, Ocloo A, Kokoszka J, Wallace DC, Brookes PS, et al. The basal proton conductance of mitochondria depends on adenine nucleotide translocase content. Biochemical Journal. 2005;392(2):353–62.

501. Berardi MJ, Chou JJ. Fatty acid flippase activity of UCP2 is essential for its proton transport in mitochondria. Cell Metabolism. 2014;20(3):541–52.

502. Lou J, Wang Y, Wang X, Jiang Y. Uncoupling Protein 2 Regulates Palmitic Acid-Induced Hepatoma Cell Autophagy. BioMed Research International. 2014;2014.

503. Ma S, Yang D, Li D, Tan Y, Tang B, Yang Y. Inhibition of uncoupling protein 2 with genipin exacerbates palmitate-induced hepatic steatosis. Lipids in Health and Disease. 2012;11:1–6.

504. Fink BD, Herlein JA, O'Malley Y, Sivitz WI. Endothelial cell and platelet Bioenergetics: Effect of glucose and nutrient composition. PLoS ONE. 2012;7(6).

505. Marwarha G, Schommer J, Lund J, Schommer T, Ghribi O. Palmitate-induced C/EBP homologous protein activation leads to NF-κB-mediated increase in BACE1 activity and amyloid beta genesis. Journal of Neurochemistry. 2018;144(6):761–79.

506. Marwarha G, Rostad S, Lilek J, Kleinjan M, Schommer J, Ghribi O. Palmitate Increases β-site AβPP-Cleavage Enzyme 1 Activity and Amyloid-β Genesis by Evoking Endoplasmic Reticulum Stress and Subsequent C/EBP Homologous Protein Activation. Journal of Alzheimer's Disease. 2017;57(3):907–25.

507. Liu L, Martin R, Chan C. Palmitate-activated astrocytes via serine palmitoyltransferase increase BACE1 in primary neurons by sphingomyelinases. Neurobiology of Aging. 2013;34(2):540–50.

508. Song F, Poljak A, Valenzuela M, Mayeux R, Smythe GA, Sachdev PS. Meta-analysis of plasma amyloid-β levels in alzheimer's disease. Journal of Alzheimer's Disease. 2011;26(2):365–75.

509. Vazquez A, Oltvai ZN. Molecular crowding defines a common origin for the warburg effect in proliferating cells and the lactate threshold in muscle

physiology. PLoS ONE. 2011;6(4):1–9.

510. Li C, Li Y, He L, Agarwal A, Zeng N, Cadenas E, et al. PI3K/AKT Signaling Regulates Bioenergetics in Immortalized Hepatocytes. Free Radical Biology and Medicine. 2013;60(1):29–40.
511. Mercer JR, Yu E, Figg N, Chen K, Prime TA, Griffin JL, et al. The mitochondria-targeted antioxidant MitoQ decreases features of the metabolic syndrome in ATM+/-/ApoE-/- mice. Free Radical Biology and Medicine. 2012;52(5):841–9.
512. Manczak M, Maoa P, Calkinsa M, Corneaa A, Arubalaa RP, Murphy MP, et al. Mitochondria-targeted antioxidants protect against Abeta toxicity in Alzheimer's disease neurons. Journal of Alzheimer's Disease. 2010;20(Suppl 2):S609–31.
513. Sukjamnong S, Chan YL, Zakarya R, Nguyen LT, Anwer AG, Zaky AA, et al. MitoQ supplementation prevent long-term impact of maternal smoking on renal development, oxidative stress and mitochondrial density in male mice offspring. Scientific Reports. 2018;8(1):1–10.
514. Thompson JA, Larion S, Mintz JD, Chantemele EJ, Fulton D, Stepp DW. Genetic Deletion of NADPH Oxidase 1 Rescues Microvascular Function in Mice with Metabolic Disease. Circulation Research. 2017;121(5):502–11.
515. Ohashi M, Runge MS, Faraci FM, Heistad DD. MnSOD deficiency increases endothelial dysfunction in ApoE-deficient mice. Arteriosclerosis, Thrombosis, and Vascular Biology. 2006;26(10):2331–6.
516. Wang W, Poole B, Mitra A, Falk S, Fantuzzi G, Lucia S, et al. Role of Leptin Deficiency in Early Acute Renal Failure during Endotoxemia in ob/ob Mice. Journal of the American Society of Nephrology. 2004;15(3):645–9.
517. Bouloumié A, Marumo T, Lafontan M, Busse R. Leptin induces oxidative stress in human endothelial cells. The FASEB Journal. 1999;13(10):1231–8.
518. Haynes WG, Sivitz WI, Morgan DA, Walsh SA, Mark AL. Sympathetic and Cardiorenal Actions of Leptin. Hypertension. 1997;30(3):619–23.
519. Singhal A, Farooqi S, Cole TJ, O'Rahilly S, Fewtrell M, Kattenhorn M, et al. Influence of leptin on arterial distensibility: A novel link between obesity and cardiovascular disease? Circulation. 2002;106(15):1919–24.
520. Cao R, Brakenhielm E, Wahlestedt C, Thyberg J, Cao Y. Leptin induces vascular

permeability and synergistically stimulates angiogenesis with FGF-2 and VEGF. Proceedings of the National Academy of Sciences of the United States of America. 2001;98(11):6390–5.

521. Hoffmann A, Ebert T, Klöting N, Dokas J, Jeromin F, Jessnitzer B, et al. Leptin dose-dependently decreases atherosclerosis by attenuation of hypercholesterolemia and induction of adiponectin. Biochimica et Biophysica Acta - Molecular Basis of Disease. 2016;1862(1):113–20.
522. Lloyd DJ, McCormick J, Helmering J, Kim KW, Wang M, Fordstrom P, et al. Generation and characterization of two novel mouse models exhibiting the phenotypes of the metabolic syndrome: Apob48-/-Lepob/ob mice devoid of ApoE or Ldlr. American Journal of Physiology - Endocrinology and Metabolism. 2008;294(3):496–505.
523. Vecchione C, Maffei A, Colella S, Aretini A, Poulet R, Frati G, et al. Leptin effect on endothelial nitric oxide is mediated through Akt-endothelial nitric oxide synthase phosphorylation pathway. Diabetes. 2002;51(1):168–73.
524. Winters B, Mo Z, Brooks-Asplund E, Kim S, Shoukas A, Li D, et al. Reduction of obesity, as induced by leptin, reverses endothelial dysfunction in obese (Lep(ob)) mice. Journal of Applied Physiology. 2000;89(6):2382–90.
525. Hubert A, Bochenek ML, Schütz E, Gogiraju R, Münzel T, Schäfer K. Selective Deletion of Leptin Signaling in Endothelial Cells Enhances Neointima Formation and Phenocopies the Vascular Effects of Diet-Induced Obesity in Mice. Arteriosclerosis, Thrombosis, and Vascular Biology. 2017;37(9):1683–97.
526. Quehenberger P, Exner M, Sunder-Plassmann R, Ruzicka K, Bieglmayer C, Endler G, et al. Leptin induces endothelin-1 in endothelial cells in vitro. Circulation Research. 2002;90(6):711–8.
527. Huby A, Otvos L, Belin de Chantemèle EJ. Leptin Induces Hypertension and Endothelial Dysfunction via Aldosterone-Dependent Mechanisms in Obese Female Mice. Hypertension. 2016;67(5):1020–8.
528. Wang J, Wang H, Luo W, Guo C, Wang J, Chen YE, et al. Leptin-Induced endothelial dysfunction is mediated by sympathetic nervous system activity. Journal of the American Heart Association. 2013;2(5):1–7.

529. Makris MC, Alexandrou A, Papatsoutsos EG, Malietzis G, Tsilimigras DI, Guerron AD, et al. Ghrelin and obesity: Identifying gaps and dispelling myths. A reappraisal. In Vivo. 2017;31(6):1047–50.

530. Tschöp M, Weyer C, Tataranni PA, Devanarayan V, Ravussin E, Heiman ML. Circulating ghrelin levels are decreased in human obesity. Diabetes. 2001;50(4):707–9.

531. Banks WA, Burney BO, Robinson SM. Effects of triglycerides, obesity, and starvation on ghrelin transport across the blood-brain barrier. Peptides. 2008;29(11):2061–5.

532. Briggs DI, Enriori PJ, Lemus MB, Cowley MA, Andrews ZB. Diet-induced obesity causes ghrelin resistance in arcuate NPY/AgRP neurons. Endocrinology. 2010;151(10):4745–55.

533. Ku JM, Andrews ZB, Barsby T, Reichenbach A, Lemus MB, Drummond GR, et al. Ghrelin-related peptides exert protective effects in the cerebral circulation of male mice through a nonclassical ghrelin receptor(s). Endocrinology. 2015;156(1):280–90.

534. Xu X, Jhun BS, Ha CH, Jin Z. Molecular Mechanisms of Ghrelin-Mediated Endothelial Nitric Oxide Synthase Activation. Endocrinology. 2008;149(8):4183–92.

535. Iantorno M, Chen H, Kim JA, Tesauro M, Lauro D, Cardillo C, et al. Ghrelin has novel vascular actions that mimic PI 3-kinase-dependent actions of insulin to stimulate production of NO from endothelial cells. American Journal of Physiology - Endocrinology and Metabolism. 2007;292(3):756–64.

536. Li P, Liu Y, Xiang Y, Lin M, Gao J. Ghrelin protects human umbilical vein endothelial cells against advanced glycation end products-induced apoptosis via NO/cGMP signaling. International Journal of Clinical and Experimental Medicine. 2015;8(9):15269–75.

537. Nagaya N, Kojima M, Uematsu M, Yamagishi M, Hosoda H, Oya H, et al. Hemodynamic and hormonal effects of human ghrelin in healthy volunteers. American Journal of Physiology - Regulatory Integrative and Comparative Physiology. 2001;280(5 49-5):1483–7.

538. Rhea EM, Salameh TS, Gray S, Niu J, Banks WA, Tong J. Ghrelin transport across the blood–brain barrier can occur independently of the growth hormone secretagogue receptor. Molecular Metabolism. 2018;18(September):88–96.

539. Ku JM, Sleeman MW, Sobey CG, Andrews ZB, Miller AA. Ghrelin-related peptides do not modulate vasodilator nitric oxide production or superoxide levels in mouse systemic arteries. Clinical and Experimental Pharmacology and Physiology. 2016;43(4):468–75.

540. Matsumoto T, Baker DJ, D'Uscio L V., Mozammel G, Katusic ZS, Van Deursen JM. Aging-associated vascular phenotype in mutant mice with low levels of BubR1. Stroke. 2007;38(3):1050–6.

541. Ota H, Akishita M, Akiyoshi T, Kahyo T, Setou M, Ogawa S, et al. Testosterone deficiency accelerates neuronal and vascular aging of samp8 mice: Protective role of enos and sirt1. PLoS ONE. 2012;7(1):1–10.

542. Varga R, Eriksson M, Erdos MR, Olive M, Harten I, Kolodgie F, et al. Progressive vascular smooth muscle cell defects in a mouse model of Hutchinson-Gilford progeria syndrome. Proceedings of the National Academy of Sciences of the United States of America. 2006;103(9):3250–5.

543. Willerson JT, Ridker PM. Inflammation as a cardiovascular risk factor. Circulation. 2004;109(21 SUPPL.):2–10.

544. Marseglia L, Manti S, D'Angelo G, Nicotera A, Parisi E, Di Rosa G, et al. Oxidative stress in obesity: A critical component in human diseases. International Journal of Molecular Sciences. 2015;16(1):378–400.

545. Meakin PJ, Tuharska Z, Gooding KM, Casanova F, Shore AC, Ashford MLJ, et al. Association between b-amyloid, diabetesand endothelial function in human s. Diabetic Medicine: Abstracts of the Diabetes UK Professional Conference. 2018;35(1):87–87.

546. Macauley-Rambach S, Stanley M, Yamada S, Caesar E, Raichle M, Perez R, et al. Hyperglycemia modulates extracellular amyloid-beta levels and neuronal activity in vivo. Neurodegenerative Diseases. 2015;15:570.

547. Lee HJ, Ryu JM, Jung YH, Lee SJ, Kim JY, Lee SH, et al. High glucose upregulates BACE1-mediated Aβ production through ROS-dependent HIF-1α and

LXRα/ABCA1-regulated lipid raft reorganization in SK-N-MC cells. Scientific Reports. 2016;6(October):1–15.

548. Kim JY, Lee HJ, Lee SJ, Jung YH, Yoo DY, Hwang IK, et al. Palmitic Acid-BSA enhances Amyloid-β production through GPR40-mediated dual pathways in neuronal cells: Involvement of the Akt/mTOR/HIF-1α and Akt/NF-κB pathways. Scientific Reports. 2017;7(1):1–16.
549. Janus A, Szahidewicz-Krupska E, Mazur G, Doroszko A. Insulin resistance and endothelial dysfunction constitute a common therapeutic target in cardiometabolic disorders. Mediators of Inflammation. 2016;2016.
550. Pillai O, Nair V, Panchagnula R. Transdermal iontophoresis of insulin: IV. Influence of chemical enhancers. International Journal of Pharmacology. 2004;269(1):109–20.
551. Niwa K, Carlson GA, Iadecola C. Exogenous Aβ1-40 reproduces cerebrovascular alterations resulting from amyloid precursor protein overexpression in mice. Journal of Cerebral Blood Flow and Metabolism. 2000;20(12):1659–68.
552. Iadecola C, Zhang F, Niwa K, Eckman C, Turner SK, Fischer E, et al. SOD1 rescues cerebral endothelial dysfunction in mice overexpressing amyloid precursor protein. Nature Neuroscience. 1999;2(2):157–61.
553. Shih AY, Driscoll JD, Drew PJ, Nishimura N, Schaffer CB, Kleinfeld D. Two-photon microscopy as a tool to study blood flow and neurovascular coupling in the rodent brain. Journal of Cerebral Blood Flow and Metabolism. 2012;32(7):1277–309.
554. ENSG00000090339-ICAM1.The Human Protein Atlas. URL: https://www.proteinatlas.org/ENSG00000090339-ICAM1/tissue

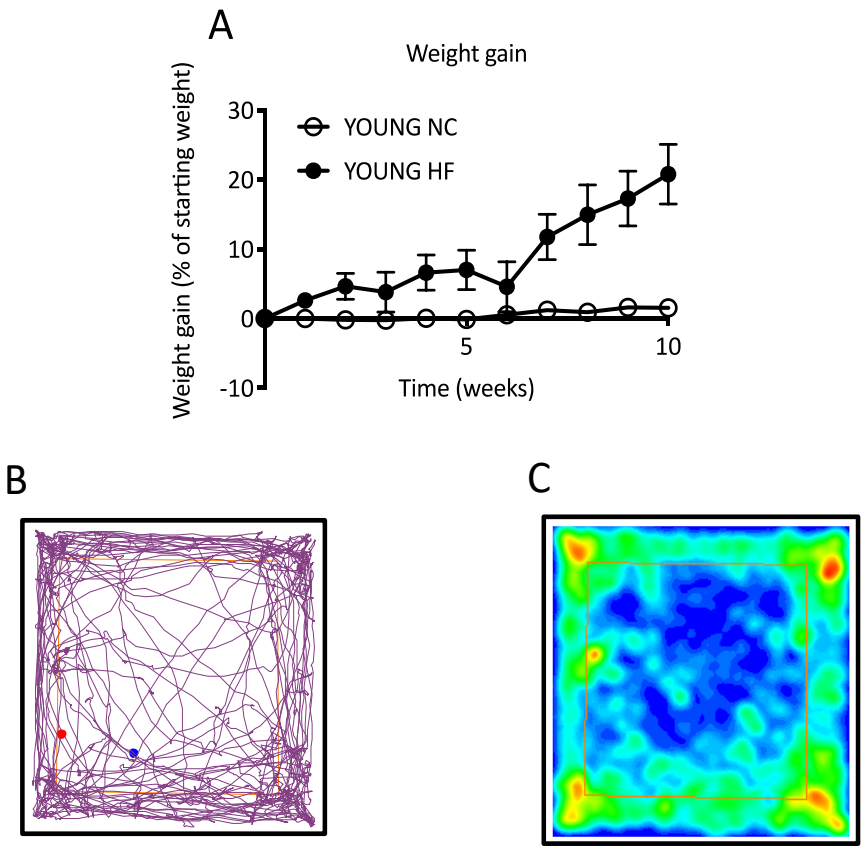

Appendix S1 Weight gain trajectory and open-field phenotype of YOUNG HF mice

(A) 12-week old male mice were placed on NC or HFD for 10 weeks and their body weights were measured weekly. Weights are expressed as % weight gain from starting weight. Representative trace (B) and heat map (C) images from an open-field anxiety test in YOUNG HF mice. YOUNG HF mice exhibit an anxious phenotype as evidenced by the mouse keeping to the outside of the box, close to the sides and rarely venturing into the middle.

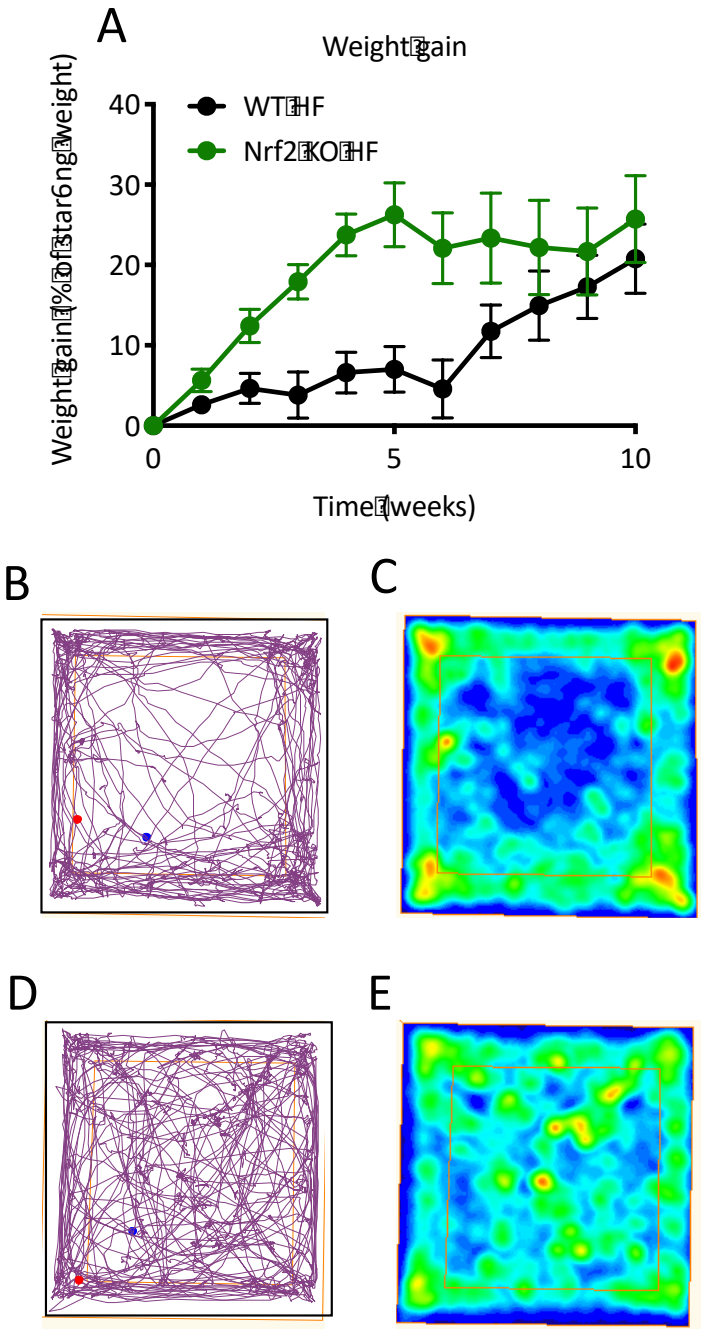

Appendix S2 Weight trajectories and open-field phenotype tests of WT HF and Nrf2 KO HF mice

(A) 12-week old male WT and Nrf2 KO mice were placed on HFD for 10 weeks and weighed weekly. Weights are expressed as % weight gain from starting weight. Representative traces (B, D) and heat-map images (C, E) of open-field anxiety tests from WT mice and Nrf2KO mice respectively. Nrf2KO mice are less anxious than WT mice and exhibit an exploratory phenotype, evidenced by their frequent ventures into the middle of the box.

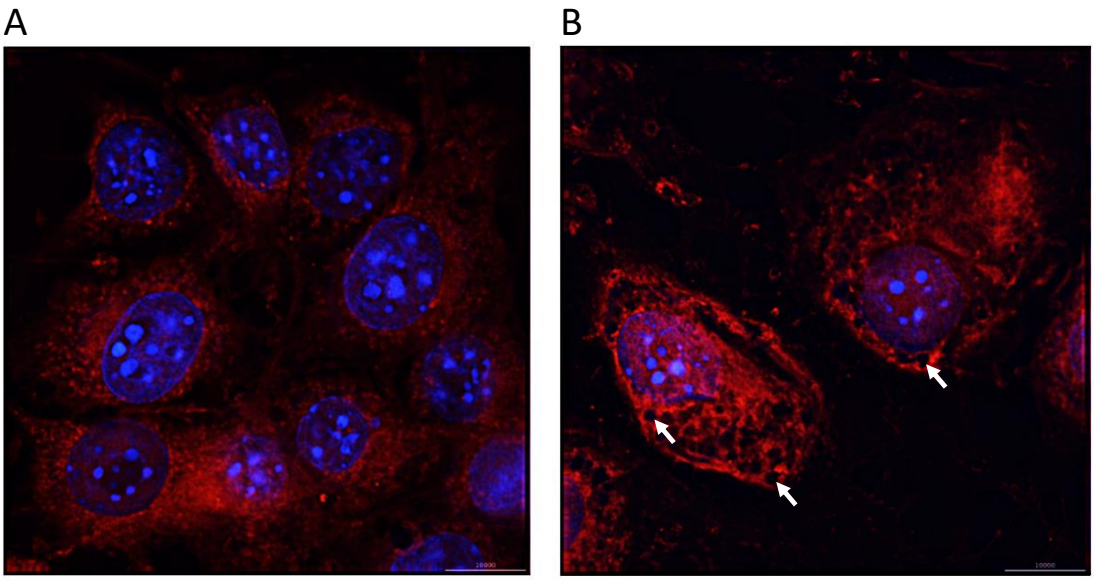

Appendix S3 bEnd.3 cells exposed to palmitate exhibit large cellular vesicles that may be lipid droplets

bEnd.3 cells were exposed to control (A) or 100µM palmitate for 24 hours. Mitochondria (red) were stained using MitoTracker (Methods section 2.8), cells were fixed using formalin, and then nuclei (blue) were stained using DAPI. Slides were imaged by Dr Iain Porter using a DeltaVision Widefield Fluorescent microscope. White arrows depict potential lipid droplets.